Solute rejection
in multicomponent systems
during ultrafiltration

Carien van Oers
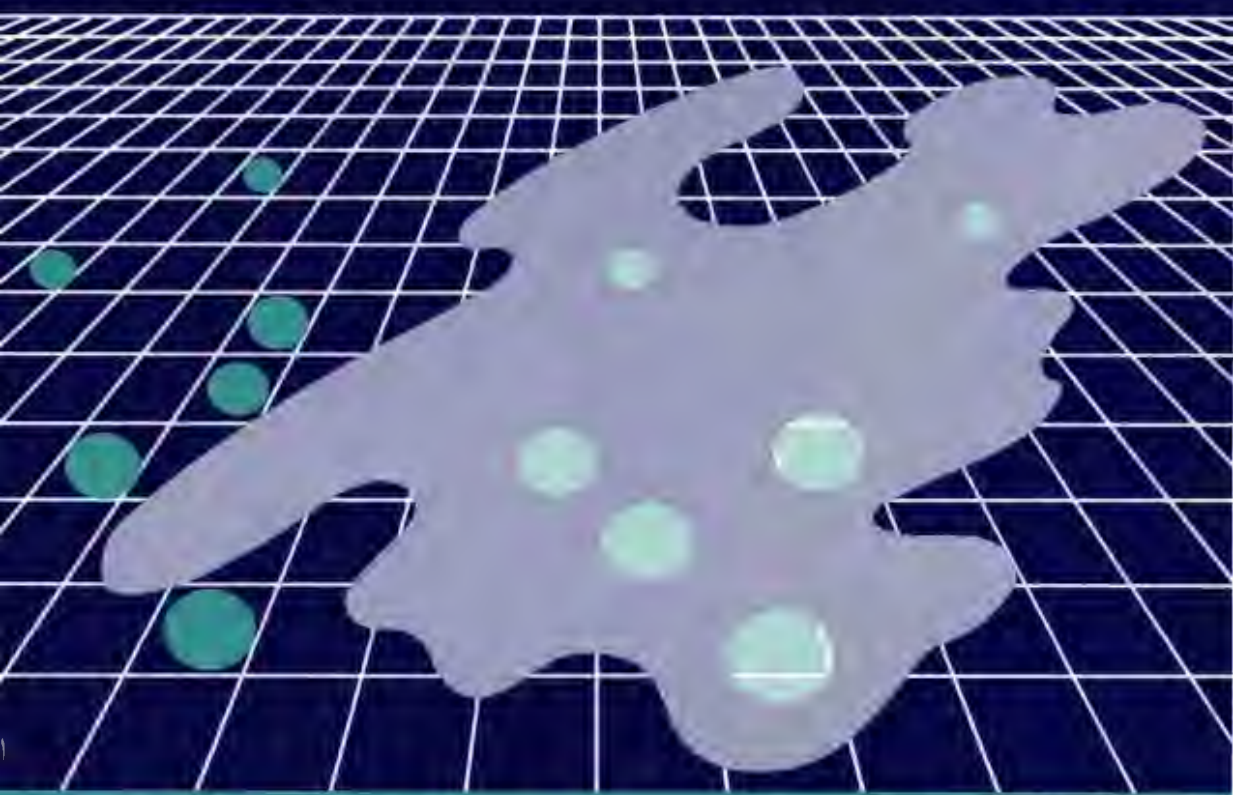
Solute Rejection in Multicomponent Systems during Ultrafiltration

PROEFSCHRIFT

ter verkrijging van de graad van doctor aan de
Technische Universiteit Eindhoven, op gezag van
de Rector Magnificus, prof.dr. J.H. van Lint,
voor een commissie aangewezen door het College
van Dekanen in het openbaar te verdedigen op
dinsdag 22 maart 1994 om 16.00 uur

door

CATHARINA WILHELMINA VAN OERS

Geboren te Eindhoven

Dit proefschrift is goedgekeurd
door de promotoren
prof.dr.ir. P.J.A.M. Kerkhof
en
prof.ir. J.A. Wesselingh

voor Eric,
voor mijn ouders

DANKWOORD

Veel mensen hebben bijgedragen aan de totstandkoming van dit proefschrift. Mijn dnak gaat uit naar alle collega's van de vakgroep Chemische Proceskunde voor hun advies en steun in de afgelopen jaren, in het bijzonder:

Piet Kerkhof, bedankt voor de aan mij geboden kansen en de grote vrijheid in het onderzoek. Ik heb veel van deze promotie geleerd.

Marius Vorstman, ik kijk met veel plezier terug op de vele discussies en je waardevolle opmerkingen m.b.t. het onderzoek. Verder bedankt voor je steun op alle fronten, je was er altijd op het juiste moment.

Pim Muijselaar, Rob v.d. Hout, Marc Defesche, Richard Kuijpers, Richard v. Lijssel, Frensly Panneflek, Karin Meeuwsen, Li Rong Xu en Will Kaethoven, jullie hebben met een geweldige inzet een grote bijdrage aan dit proefschrift geleverd. Ik heb met veel plezier met jullie samengewerkt. Verder wil ik ook de researchpraktikanten bedanken voor hun bijdrage in het onderzoek en Bair Cluitmans voor de analyses.

Johan Wijers, ondanks de soms hoge barrières in de vorm van stapels papier was de communicatie altijd prima. Bedankt voor je steun en adviezen.

De technici, bedankt voor jullie ondersteuning bij het ontwerpen en bouwen van experimentele opstellingen.

Verder wil ik nog enkele mensen buiten de vakgroep bedanken voor hun bijdrage:

De betrokkenheid van de gebruikerscommissie bij het onderzoek en de levendige discussies tijdens de vergaderingen heb ik als zeer stimulerend ervaren.

Eric Nies ben ik veel dank verschuldigd voor zijn hulp bij het modelleren van het thermodynamische gedrag in ternaire systemen.

The molecular weight distribution measurements and the useful comments of dr. Andreas Pfennig of the University of Darmstadt are very much appreciated.

Pieter Vonk wil ik bedanken voor zijn hulp bij het opstellen van een computerprogramma voor het oplossen van de Stefan-Maxwell vergelijkingen.

Henk Claessens en Marion van Straten hebben een grote bijdrage geleverd aan het oplossen van problemen met de HPLC.

Mijn familie en vrienden wil ik bedanken voor de morele steun in de afgelopen jaren. En dan natuurlijk Eric: jouw bijdrage als cateraar, corrector, schouder en luisterend oor is van onschatbare waarde geweest.

<div align="right">Carien van Oers</div>

ABSTRACT

Ultrafiltration is a pressure-driven membrane filtration technique, which is used for the concentration of solutions and size-selective separations of large molecules and colloids from low molecular weight species. The major applications of ultrafiltration are found in food processing, downstream separations in biotechnology, waste-water treatment, and the pharmaceutical industry. The filtering solutions are often complex multicomponent mixtures.

This thesis describes various phenomena which may alter the filtration behaviour in multicomponent systems in comparison with binary systems. The study has been focussed on the characterization of the rejection of a component and how this is influenced by the presence of other components in multicomponent systems.

Several model systems have been investigated consisting of one component with a small molecular size, which is only partly rejected by the membrane, and a second almost totally rejected component. The smaller component used in these studies was the non-ionic polyethylene glycol (PEG). Three types of larger components were selected with each exhibiting a different type of behaviour during filtration.
Filtration experiments were performed in a stirred cell and a tubular membrane module.

The mass transport during ultrafiltration has been modelled by applying the Stefan-Maxwell equations for the transport in both the polarization layer and the membrane. The mass-transfer coefficient for the stirred cell, in which most of the experiments have been performed, has been determined by heat transfer and electrochemical measurements. The local mass transfer coefficient was found to increase with the distance from the centre of the membrane. This has been confirmed by filtration experiments with separate collection of the permeate streams from the inner circle of the membrane and the outer ring.

The filtration behaviour of PEG has been studied on several membranes for two types of membrane modules. The partially rejected PEG showed a maximum in the observed rejection due to concentration polarization. The flux was lowered as a result of

osmotic pressure. In most cases an almost linear relationship between the flux and the pressure was observed. At the highest fluxes a more than proportional increase in flux was measured, which was ascribed to limitation of the PEG concentration at the membrane surface at high permeate fluxes.

The Stefan-Maxwell model has been used to simultaneously describe the flux and rejection behaviour during PEG filtration. To obtain a good description the diffusion coefficient of PEG and water with the membrane, the exclusion coefficient and the pre-factor of the Sherwood relation have been fitted to the experimental flux and rejection data. A good fit of both rejection and flux could be achieved for a set of experiments with a particular solute and membrane. A strong correlation was found between the two diffusion coefficients and the exclusion coefficient, which resulted in a physically unrealistic dependence on the membrane and solute properties. The introduction of the thermodynamic activities in the equations had only a minor effect on the calculated flux and rejection.

To evaluate the possible formation of a gel layer on the membrane surface during filtration, the unsteady flux behaviour and the response of the flux to a sudden pressure change have been studied. From the combined interpretation of these phenomena it was clear that the filtration of dextran is determined by the osmotic pressure, whereas the decrease in flux during silica filtration is caused by gel formation. Although no unsteady flux behaviour was observed for BSA the response of the flux to a pressure change indicated that at low pressure the flux was determined by the osmotic pressure, while at higher pressures it was also influenced by the formation of a deposit layer.

In this study it has been shown that major changes in the solute rejection can indeed occur, when the solute is part of a multicomponent system instead of a binary system. The effect of changes in the thermodynamic activity of the solute on its rejection has been studied by the combined filtration of PEG and dextran. The thermodynamic activities of PEG and dextran have been modelled with the UNIQUAC model and a Linearized Quasi-Chemical Approxmation. Rejection measurements showed a decrease in the observed PEG rejection when dextran was added to the solution, under conditions where the dextran was mainly retained by the membrane. At high dextran concentrations and low fluxes the PEG rejection even became strongly negative, indicating a higher PEG concentration in the permeate than in the bulk solution. The

elevated transport of PEG through the membrane in the presence of dextran was ascribed to the additional driving force (besides the pressure difference) due to the increased thermodynamic activity of PEG at the retentate side of the membrane. For a more open membrane the PEG rejection was found to increase in the presence of dextran.

The change in solute rejection due to the presence of an open gel layer on the membrane surface has been evaluated using silica sols in combination with PEG or dextran. In the presence of a silica gel layer a decrease in the solute rejection was observed. The thicker the gel layer, the stronger decrease in rejection was found. A thick, open silica gel layer showing no exclusion for the permeating solutes caused the observed solute rejection to drop to zero. By means of a model it was proven that due to the thickness of the gel layer the diffusion back to the bulk solution strongly diminishes, which resulted in a total permeation of the normally partly rejected bulk solution through the membrane.

The solute rejection in the presence of proteins has been studied using PEG and BSA as model solutes. BSA adsorption, by simply soaking the regenerated cellulose membrane in the protein solution, was so low that the solute rejection was not affected. Filtration of BSA caused protein deposition on the membrane surface at higher pressures, which resulted in an increase in the observed PEG rejection. The rejection increased with increasing pressure indicating the compressibility of the deposit layer. Rejection measurements at different pH values showed that the most compact BSA deposit was formed close to the isoelectric point.

Summarizing, the introduction of other components in the filtration solution may completely alter the separation behaviour compared to binary systems. The insights gained in this thesis can be used to interpret the rejection behaviour in multicomponent systems. Some interesting possibilities are shown to use these multicomponent phenomena to improve the separation characteristics.

SAMENVATTING

Ultrafiltratie is een membraanfiltratie techniek met de druk als drijvende kracht. Deze techniek wordt gebruikt voor het concentreren van oplossingen en de scheiding van hoog en laag moleculaire stoffen op basis van de molecuulgrootte. De belangrijkste toepassingen van ultrafiltratie liggen in de bereiding van voedingsmiddelen, in de biotechnologie, afvalwaterreiniging en de farmaceutische industrie. De oplossingen, die worden gefiltreerd, zijn vaak complexe multicomponent systemen.

Dit proefschrift beschrijft verschillende verschijnselen, die het filtratiegedrag in multicomponent systemen kunnen veranderen in vergelijking met binaire systemen. De studie is toegespitst op de karakterisering van de retentie van een component en hoe deze wordt beïnvloed door de aanwezigheid van de andere componenten in het systeem. Diverse modelsystemen zijn onderzocht, elk bestaande uit één component met een kleine molecuulgrootte, die slechts gedeeltelijk door het membraan wordt tegengehouden, en een tweede bijna volledig tegengehouden component. Als kleinere component is gekozen voor het niet-geladen polyethyleen glycol (PEG). Drie verschillende grotere componenten werden geselecteerd met elk een specifieke gedrag tijdens filtratie. De filtratie experimenten zijn uitgevoerd in een geroerde cel en een buismembraanmodule.

Het stoftransport tijdens ultrafiltratie is gemodelleerd door de Stefan-Maxwell vergelijkingen toe te passen voor het transport in de polarisatielaag en in het membraan. De stofoverdrachtscoëfficiënt voor de geroerde cel, waarin de meeste experimenten zijn uitgevoerd, is bepaald door warmteoverdrachts- en electrochemische metingen. De lokale stofoverdrachtscoëfficiënt bleek groter te worden naarmate de afstand ten opzichte van het centrum van het membraan toenam. Dit is bevestigd door filtratie experimenten met gescheiden opvang van het permeaat van de binnencirkel van het membraan en de buitenring.

Het filtratiegedrag van PEG is bestudeerd op verschillende membranen en voor twee typen membraanmodules. Het gedeeltelijk tegengehouden PEG vertoonde een maximum in de schijnbare retentie ten gevolge van de optredende concentratie polarisatie. De flux tijdens PEG filtratie nam af als gevolg van de osmotische druk. In

de meeste gevallen werd een vrijwel lineair verloop van de flux met de druk waargenomen. Bij hogere fluxen werd echter een meer dan proportionele toename in de flux gemeten, die wordt toegeschreven aan de limitering van de PEG concentratie op het membraanoppervlak.

Met behulp van het Stefan-Maxwell model werd de flux en de retentie tijdens PEG filtratie gelijktijdig gemodelleerd. Om een goede beschrijving te verkrijgen zijn de diffusiecoëfficiënten van PEG en water in het membraan, de exclusiefactor en de préfactor van de Sherwood relatie gefit. Op die manier kon een goede fit worden verkregen voor een set experimenten voor een bepaalde opgeloste component en een bepaald type membraan. Er bestond een sterke correlatie tussen de twee diffusiecoëfficiënten en de exclusie factor, wat resulteerde in een fysisch onrealistische afhankelijkheid van de eigenschappen van het membraan en de opgeloste component.
De introductie van de thermodynamische activiteit van PEG in de vergelijkingen had slechts een gering effect op de berekende flux en retentie.

Om de mogelijke vorming van een gellaag op het membraanoppervlak na te gaan is het instationaire fluxgedrag en de respons van de flux op een plotselinge drukverandering bestudeerd. Uit de gecombineerde interpretatie van deze verschijnselen kan duidelijk worden geconcludeerd dat de filtratie van dextran wordt bepaald door de osmotische druk, terwijl de daling in de flux tijdens silica filtratie wordt veroorzaakt door gelvorming. Alhoewel geen instationair flux gedrag werd waargenomen tijdens BSA filtratie wijst de respons van de flux op een verandering van de druk op de vorming van een depositielaag. Bij lage drukken werd de flux alleen bepaald door de heersende osmotische druk, bij hoge drukken werd de flux tevens beïnvloed door de aanwezigheid van een depositielaag.

Uit het onderzoek is gebleken dat er inderdaad grote veranderingen in de retentie van een opgeloste component optreden, wanneer deze zich in een multicomponent systeem in plaats van een binair systeem bevindt. D.m.v. de gecombineerd filtratie van PEG en dextran is het effect van een verandering in de thermodynamische activiteit van een opgeloste component op zijn retentie onderzocht. De thermodynamische activiteiten van PEG en dextran zijn gemodelleerd met het UNIQUAC model en een gelineariseerde Quasi-Chemische benadering. De retentiemetingen vertoonden een daling in de PEG retentie, wanneer dextran werd toegevoegd aan de oplossing. Bij hoge dextran

concentraties en lage fluxen werd de PEG retentie zelfs sterk negatief, wat een hogere PEG concentratie in het permeaat dan in de bulk inhoudt. Het verhoogde PEG transport door het membraan in aanwezigheid van dextran wordt toegeschreven aan de extra drijvende kracht (naast het drukverschil) t.g.v. de verhoogde thermodynamische activiteit van PEG aan de retentaatzijde van het membraan.

In het geval van een membraan met een hogere permeabiliteit trad een duidelijke toename in de PEG retentie op in aanwezigheid van dextran.

De verandering in de retentie van een opgeloste component t.g.v. de aanwezigheid van een open gellaag op het membraanoppervlak is onderzocht m.b.v. silicadeeltjes in combinatie met PEG of dextran. In aanwezigheid van een silica gellaag trad een daling op in de retentie van de opgeloste component. Deze daling was sterker naarmate de gellaag dikker was. Een voldoende dikke, open gellaag veroorzaakte een daling in de retentie naar nul. M.b.v. een model werd aangetoond dat t.g.v. de dikte van de gellaag de terugdiffusie naar de bulk oplossing sterk vermindert, hetgeen resulteert in een vrijwel totale permeatie van een component, die op een schoon membraan gedeeltelijk wordt tegengehouden.

De retentie van opgeloste componenten in aanwezigheid van eiwitten is bestudeerd door het gebruik van PEG en BSA als modelstoffen. De adsorptie van BSA door het geregenereerde cellulose acetaat membraan eenvoudigweg onder te dompelen in een eiwitoplossing was zo gering dat de retentie van PEG niet merkbaar werd beïnvloed. De filtratie van BSA veroorzaakte een depositie van eiwit op het membraanoppervlak bij hogere drukken, wat resulteerde in een toename van de PEG retentie. De sterke toename van de PEG retentie bij hogere drukken duidde op de vorming van een compressibele depositielaag. Uit retentiemetingen onder verschillende pH condities kon worden geconcludeerd dat de meest compacte BSA laag wordt gevormd in de buurt van het iso-electrisch punt.

Samenvattend, de introductie van andere componenten in de filtratie oplossing kan het scheidingsgedrag totaal veranderen in vergelijking met binaire systemen. De verkregen inzichten kunnen worden gebruikt om het retentiegedrag in multicomponent systemen te interpreteren. Enkele interessante mogelijkheden worden aangedragen om deze multicomponent verschijnselen aan te wenden voor de verbetering van de scheidings-karakteristieken.

CONTENTS

1. INTRODUCTION

1.1 General introduction

Ultrafiltration is a pressure-driven membrane filtration technique, which is used for the concentration and size-selective separations of large molecules and colloids from low molecular weight species. Ultrafiltration membranes are porous filters with pore sizes in the range of 1 to 200 nm. Other pressure-driven membrane processes are hyperfiltration (reverse osmosis) and microfiltration in lower and higher pore size regions, respectively.

The major applications of ultrafiltration are found in food processing, downstream separations in biotechnology, waste-water treatment, and the pharmaceutical industry. Some applications are the recovery of proteins from cheese whey, the concentration of egg products for use in the bakery industry, the clarification of fruit juices, the recovery of beer from yeast suspension, the recovery of raw material from waste water in the corn starch industry, the recovery of paint from waste water in the textile industry, the purification of waste water in the production of PVC, the treatment of oil/water wastes, and the concentration of blood plasma for plasma powder [Lonsdale, 1982; Stork Friesland]. This list of applications shows that the filtering solutions are often complex multicomponent mixtures.

Two important characteristics of ultrafiltration are the filtrate flux and the rejection of solutes by the membrane. The rejection represents a measure of the amount of solute retained by the membrane. The consequence of partial or total rejection of species by the membrane is an accumulation of that species in the boundary layer adjacent to the membrane surface. This phenomenon is referred to as 'concentration polarization'; the boundary layer is called the 'polarization layer'. The extent of concentration polarization is determined by the convective transport towards the membrane and the diffusion away from the membrane back into the bulk solution. The latter is a function of the mass transfer coefficient in the boundary layer.
Concentration polarization may cause a lowering in flux due to an increase in osmotic pressure difference across the membrane [Kozinski, 1972; Goldsmith, 1971]. In some cases the concentration at the membrane can exceed the gel concentration, which results in a gel layer formation on the membrane surface [Blatt, 1970]. The hydraulic

resistance of the gel layer may considerably lower the flux.

Another phenomenon which may influence the flux is adsorption of a species on the external membrane surface and/or internal pore surface [Fane, 1983a]. Due to pore constriction and/or pore blockage the hydraulic resistance of the membrane increases. Especially the filtration of protein can be influenced considerably by this phenomenon depending on the type of protein and membrane used for filtration [Nilsson, 1990]. Besides adsorption, also irreversible deposition of protein on the membrane surface can occur [Opong, 1991b]. These phenomena are often referred to as fouling.

Since process streams in ultrafiltration often contain a variety of components, the above mentioned phenomena may not only affect the flux, but also the rejection of the other components in the solution. Although Strathmann already mentioned in 1973 the possible increase in rejection of other components in the presence of a deposit of a fully rejected component, relatively few data are available on the solute rejection in multicomponent systems. Nakao [1982] and Kimura [1985] both observed an increase in low molecular weight solute rejection by ovalbumin and polyvinyl alcohol layers during ultrafiltration. During the filtration of enzymes Kerkhof [1988] observed an increase in rejection of a colour component with pressure, which was ascribed to the formation of a secondary membrane. In two recent studies Mochizuki separately investigated the effect of BSA adsorption [1992a] and BSA deposition [1993a] on the rejection of a polydisperse mixture of dextrans for open microfiltration membranes. The adsorption of BSA occurred preferentially in the largest pores causing a rise in dextran rejection compared to that of the clean membrane. The protein deposit also increased the dextran rejection depending on solution pH, ionic strength, and salt composition. Meireles [1991] studied the effect of protein fouling on the rejection characteristics of low molecular weight cut-off ultrafiltration membranes. For 10 kDa membranes the dextran rejection coefficients were not affected, but a significant increase in rejection was found for the 40 kDa membranes. Besides adsorption and gel layer formation, other effects can influence the rejection in a multicomponent system. Papamichael [1987] observed for the combined filtration of PEG and BSA, besides an increase in PEG rejection, also a decrease in PEG rejection compared to the rejection on a clean membrane. They suggest that this might be explained by the interaction of PEG and BSA. According to Busby [1980] protein-protein interactions can interfere with the attempts to separate proteins by ultrafiltration. Tam [1991] has shown that solute-solute interference in the solution can also occur using data for the rejection

characteristics for a five-component mixture of polyethylene glycols versus that for a single component solution. The higher rejection of a component in the mixture was ascribed to the hindered movement of the smaller solutes caused by the presence of the larger solutes. Bozzano [1991] found that the permeation of proteins was lowered in the presence of polyacrylic acid due to a complexation reaction.

1.2 Outline of the thesis

The objective of this thesis is to investigate phenomena which occur during the ultrafiltration of multicomponent systems. This study has been focussed on the characterization of the influence of other components on the rejection of the different components in these multicomponent systems. Several model systems were chosen consisting of one component with a small molecular size, which is only partly rejected by the membrane and a second almost totally rejected component. The smaller component used in these studies was the non-ionic polyethylene glycol (PEG) to avoid electrostatic interactions. Three types of larger components were selected with each exhibiting a different type of behaviour during filtration; this is discussed in more detail in the subsequent overview of the contents of each chapter. This thesis mainly covers the influence of the presence of each of the larger components on the rejection of the smaller component PEG. None of these components showed complexation with PEG.

First, the transport of multicomponent systems based on the Stefan-Maxwell equations will be presented in chapter 2. This chapter will also discuss the hydrodynamic models of hindered transport inside a membrane, which will be used for comparison with the Stefan-Maxwell equations in chapter 5. To interpret the results and to be able to perform quantitative calculations, a number of physical properties have to be evaluated. A review has been given in chapter 3. Many of these physical properties have been taken directly from literature. More extensive studies have been performed to characterize the thermodynamic activities in ternary systems and the mass transfer in one of the modules used for the ultrafiltration experiments.

In chapter 4 the unsteady-state flux behaviour of totally rejected components is discussed. It is shown how unsteady-state flux behaviour can be used to interpret whether or not a gel layer is formed on the membrane.

The flux and rejection of PEG in the binary system will be extensively evaluated in chapter 5. This chapter provides some of the insights necessary to understand the change in filtration behaviour observed when other components are added to the PEG

solution. The combination of the flux and the rejection of PEG have been modelled with the Stefan-Maxwell equations.

In chapters 6, 7 and 8 the influence of the addition of various components will be discussed. Chapter 6 describes the flux and rejection for PEG/dextran systems. Dextran does not form a gel layer on the membrane, but PEG and dextran are known to mutually alter their thermodynamic activity. Chapter 7 deals with the presence of an open silica gel layer on the membrane surface and how it affects the rejection of PEG and dextran. In chapter 8 the influence of the protein BSA on the PEG rejection is studied. This is the most complex model system, because BSA may alter PEG transport by adsorption, deposition, and/or a change in the thermodynamic activity of the PEG. Chapter 9 will end this thesis with a comparison of the different effects of additional components on the rejection of a solute and its consequences in the practice of the filtration of multicomponent solutions.

2. TRANSPORT MODELS

This chapter describes the generalized Stefan-Maxwell equations for multicomponent transport, followed by the form of these equations as specialized for ultrafiltration. Subsequently, the hydrodynamic model of hindered transport is presented. A comparison will be made between these types of transport models.

2.1 Generalized Stefan-Maxwell theory

The multicomponent transport phenomena are described using the generalized Stefan-Maxwell equations. In these equations transport is described in terms of intermolecular friction. The driving force exerted on a species is counteracted by the friction with all of the other species, present in the system.

The generalized driving force can be expressed as follows [Lightfoot, 1974]:

$$d_j = \frac{x_j}{RT} \nabla_{T,P}\, \mu_j + \frac{(\phi_j - \omega_j)}{c_t RT} \nabla P + \frac{x_j Z_j F}{RT} \nabla \Phi - \frac{\rho_j}{c_t RT}\left[g_j - \sum_{k=1}^{n_{comp}} \omega_k g_k \right] \quad (2.1)$$

d_j = total driving force on component j $[m^{-1}]$
x_j = mole fraction of component j $[mol.mol^{-1}]$
R = molar gas constant $[J.mol^{-1}.K^{-1}]$
T = temperature $[K]$
μ_j = chemical potential $[J.mol^{-1}]$
ϕ_j = volume fraction of component j $[m^3.m^{-3}]$
ω_j = mass fraction of component j $[kg.kg^{-1}]$
c_t = total molar concentration $[mol.m^{-3}]$
P = pressure $[Pa]$
Z_j = number of charges on component j
F = Faraday's constant (= $9,6\cdot10^4$ $C.mol^{-1}$)
Φ = electrical potential $[V]$
ρ_j = mass concentration of component j $[kg.m^{-3}]$
g_j = total body force per mass of component j $[N.kg^{-1}]$
n_{comp} = number of components

The total body force per unit mass of the component g_j represents all external forces acting on the species except the pressure and electrical potential.

The factor $(\phi_j\text{-}\omega_j)$ in front of the pressure gradient indicates that only when the volume fraction differs from the mass fraction (i.e. when the components differ in density)

will the pressure gradient be able to cause a relative motion between the species.

All of the species also experience a frictional force due to interactions with the other components. The friction between two species is assumed to be proportional to their relative amounts and to the differences in velocities. The total friction a species is exposed to can be expressed by the following equation [Lightfoot, 1974]:

$$r_j = \sum_{\substack{k=1 \\ k \neq j}}^{n_{comp}} \frac{x_j x_k (u_k - u_j)}{D_{j,k}^{sm}} \qquad (2.2)$$

r_j = total friction force on component j $[m^{-1}]$
$D_{j,k}^{sm}$ = Stefan-Maxwell diffusion coefficient $[m^2.s^{-1}]$
u_j = specific velocity of component j $[m.s^{-1}]$

If the molar flux (N_j) with respect to stationary coordinates is defined as follows:

$$N_j = x_j c_t u_j \qquad (2.3)$$

substitution of equation (2.3) will convert equation (2.2) into [Standart et al., 1979]:

$$r_j = \sum_{\substack{k=1 \\ k \neq j}}^{n_{comp}} \frac{x_j N_k - x_k N_j}{c_t D_{j,k}^{sm}} \qquad (2.4)$$

The generalized Stefan-Maxwell equations for a multicomponent system thus have the following form $(d_j = r_j)$:

$$\frac{x_j}{RT} \nabla_{T,P} \mu_j + \frac{(\phi_j - \omega_j)}{c_t RT} \nabla P + \frac{x_j Z_j F}{RT} \nabla \Phi - \frac{\rho_j}{c_t RT} \left[g_j - \sum_{k=1}^{n_{comp}} \omega_k g_k \right] = \sum_{\substack{k=1 \\ j \neq k}}^{n_{comp}} \frac{x_j N_k - x_k N_j}{c_t D_{j,k}^{sm}} \qquad (2.5)$$

The same type of relationship has been found by Mason and Viehland [1978] based on statistical-mechanical principles.

2.2 Stefan-Maxwell model applied to ultrafiltration

Several authors have derived the Stefan-Maxwell equations for membrane filtration [Jackson, 1977; Mason et al., 1978; Krishna, 1987a,b]. A detailed derivation of both the homogeneous and heterogeneous description will be presented here since inconsis-

tencies seem to occur in the texts as a result of the unclear definitions of the concentrations, fluxes and velocities.

2.2.1 Definitions

To avoid confusion about the definition of the mole fractions, concentrations and fluxes, a clear distinction is made by introducing different symbols for these properties outside and inside the membrane. Moreover, a distinction is made between homogeneously and heterogenously defined mole fractions, concentrations, and fluxes inside the membrane.

Outside the membrane, i.e. in retentate and permeate, the total molar concentration c_t is defined as mole (solution) per volume (solution) and the molar concentration of component j, c_j, is defined as mole component j per volume (solution). The mole fraction x_j is equal to c_j/c_t. The molar flux N_j is based on the cross-sectional membrane area.

For the *homogeneous* description inside the membrane the total molar concentration c_t' is defined as mole (solution + membrane) per volume (solution + membrane) and the molar concentration of component j, c_j', is defined as mole component j per volume (solution + membrane). The mole fraction x_j' is equal to c_j'/c_t'. The molar flux N_j' is based on the cross-sectional membrane area.

For the *heterogeneous* description inside the membrane the total molar concentration c_t'' is evaluated in the pore liquid and is thus defined as mole (solution) per volume (solution). The molar concentration of component j, c_j'', is defined as mole component j per volume (solution). The mole fraction x_j'' is equal to c_j''/c_t''. The molar flux N_j'' is now based on the cross-sectional <u>pore</u> area.

2.2.2 Assumptions considering ultrafiltration

Before the Stefan-Maxwell model is presented for the description of transport during ultrafiltration, first some assumptions will be given:

1 - The chemical potential and the pressure are the only important driving forces.

2 - The membrane is considered as a separate component ($n_{comp} + 1$). In the homogeneous description the membrane is seen as the so-called 'dust' species, analogous to the treatment in the Dusty Gas model [Jackson, 1977; Mason et al., 1983; Krishna, 1987]. These dust species are giant molecules with an infinite molecular weight which are uniformly distributed in space.

According to this assumption the total molar concentration c'_t defined as mole (solution + membrane) per volume (solution + membrane) is equal to mole (solution) per volume (solution + membrane). This implies that the mole fraction x'_j is defined as mole component j per mole (solution). The mole fraction of the membrane, x'_m, is not set to zero, because otherwise the term which describes the interaction with the membrane would vanish in the transport equations. Instead a species-membrane diffusion coefficient $(D_{j,m})$ is defined:

$$\frac{x'_m}{D^{sm}_{j,m}} = \frac{1}{D_{j,m}} \tag{2.6}$$

In the heterogeneous description the Stefan-Maxwell equations are defined inside the pore. To be able to describe species-membrane interactions an extra term is added. Analogous to the homogeneous description a species-membrane diffusion coefficient is defined. In principle the interactions between species and membrane only take place at the pore wall. It may be more convenient to consider x''_m as a fictitious mole fraction of the pore wall. Since x'_m and x''_m are incorporated in the species-membrane diffusion coefficients, their different definitions have no consequences for the ultimate form of the Stefan-Maxwell equations for the homogeneous and heterogeneous description.

3 - The specific molar velocity of the membrane (u'_m) is equal to zero because it is mechanically constrained. According to equation (2.3) the flux (N'_m) is also equal to zero.

4 - In order to relate the fluxes inside the membrane to the experimentally measurable fluxes outside the membrane the flux must be corrected by the tortuosity of the membrane τ. The tortuosity is a measure of the difference in path length and cross-sectional area with respect to a pore perpendicular to the membrane surface.

5 - The transport of a component through a membrane occurs both by diffusive transport and viscous flow. Viscous flow is due to the fact that the fluid is constrained by the walls of the porous medium. The diffusive transport is separative, the viscous flow non-separative. It is assumed that the total flux of component j is the sum of the viscous and diffusive contributions [Jackson, 1977; Mason, 1983 and 1985; Bearman, 1958].

6 - The binary diffusion coefficients $D_{j,k}^{sm}$ and $D_{k,j}^{sm}$ are equal. This assumption is based on Onsager's reciprocity postulate [Lightfoot, 1974].

2.2.3 Stefan-Maxwell equations in the polarization layer

In the polarization layer the number of components is equal to n_{comp}; there is no question of interaction with the membrane. The Stefan-Maxwell equations for the polarization layer can be written in a simplified form.

$$\frac{(\phi_j - \omega_j)}{c_t RT} \nabla P - \frac{\rho_j}{c_t RT} \left[g_j - \sum_{k=1}^{n_{comp}} \omega_k g_k \right] = \frac{x_j V_j}{RT} \left[1 - \frac{\rho_j}{\rho_{tot}} \right] \nabla P \qquad (2.7)$$

$\quad V_j \quad$ = partial molar volume component j $[m^3.mol^{-1}]$
$\quad \rho_j \quad$ = mass concentration component j $[kg.m^{-3}]$

where the total density ρ_{tot} is defined as:

$$\rho_{tot} = \sum_{k=1}^{n_{comp}} \omega_k \rho_k \qquad (2.8)$$

For a binary system the gradient of the chemical potential can be expressed as a term representing the non-ideality of the system multiplied by the gradient of the mole fraction:

$$\frac{x_j}{RT} \nabla_{T,P} \mu_j = x_j \nabla \ln a_j = \left[1 + x_j \frac{\partial \ln \gamma_j}{\partial x_j} \right] \nabla x_j \qquad (2.9)$$

$\quad a_j \quad$ = activity component j
$\quad \gamma_j \quad$ = activity coefficient component j

The factor between brackets in front of the gradient in x_j is called the thermodynamic factor. In the case of ideal behaviour this factor is equal to one.

Substitution of equation (2.7) in equation (2.5) gives the following relation for component j in the polarization layer:

$$\frac{x_j}{RT} \nabla_{T,P} \mu_j + \frac{x_j V_j}{RT} \left[1 - \frac{\rho_j}{\rho_{tot}} \right] \nabla P = \sum_{\substack{k=1 \\ k \neq j}}^{n_{comp}} \frac{x_j N_k - x_k N_j}{c_t D_{j,k}^{sm}} \qquad (2.10)$$

If the solution is fluid throughout the entire polarization layer the pressure gradient is

equal to zero. If, however, one of the species forms a gel or precipitate adjacent to the membrane, a force is transmitted from the membrane to this species and a hydrodynamic pressure gradient will develop within the concentrated layer [Lightfoot, 1974]. In our calculations we have assumed that the solution remains fluid throughout the polarization layer so that the equation $\nabla P = 0$ is solved simultaneously with equation (2.10).

For binary systems, eqn. (2.10) is equivalent to Fick's Law, in which the flux is expressed as a function of the concentration gradient and the Fick diffusion coefficient. The Fick diffusion coefficient is equal to the thermodynamic factor multiplied by the Stefan-Maxwell diffusion coefficient [Lightfoot, 1974]. In chap. 4 the description according to Fick's Law has been used to derive an analytical relationship for the flux based on concentration polarization.

2.2.4 Stefan-Maxwell equations within the membrane

Homogeneous description
In accordance with the Stefan-Maxwell equation in the polarization layer a simplification can be introduced in the term which describes the driving force as a result of the pressure gradient.

$$\frac{(\phi_j' - \omega_j')}{c_t' RT} \nabla P - \frac{\rho_j'}{c_t' RT} \left[g_j - \sum_{k=1}^{n_{comp}+1} \omega_k' g_k \right] = \frac{x_j' V_j}{RT} \nabla P \qquad (2.11)$$

The difference between equations (2.11) and (2.7) is due to the fact that the membrane is mechanically constrained.

For binary systems the term for the gradient of the chemical potential can be also rearranged according to equation (2.9). Combining eqn. (2.11) and the fact that the flux of the membrane (N_m') is equal to zero the following Stefan-Maxwell relation within the membrane can be obtained:

$$\frac{x_j'}{RT} \nabla_{T,P} \mu_j' + x_j' \left[\frac{V_j}{RT} \right] \nabla P = \sum_{\substack{k=1 \\ k \neq j}}^{n_{comp}} \frac{x_j' N_k'^d - x_k' N_j'^d}{c_t' D_{j,k}^{sm} \frac{1}{\tau}} - \frac{N_j'^d}{c_t' D_{j,m} \frac{1}{\tau}} \qquad (2.12)$$

in which superscript d represents the diffusive contribution to the flux.
The first term on the righthand side of the equation describes the friction in the

solution, the second term represents the friction with the membrane. The friction in the solution has the same form as in the free solution. The friction between component j and the membrane is based on the difference between N'_m (=0) and the diffusive flux N'^d_j. This can be understood by realizing that at the membrane surface, where the interaction takes place, the local viscous velocity is zero. This implies that the flux difference between the membrane and component j is only determined by the diffusive flux at the surface of the membrane, which is assumed to be equal to the radially averaged flux N'_j minus the radially averaged viscous flux N'^v_j.

As stated in § 2.2.2, the total flux is the sum of the viscous flux and the diffusive flux:

$$N'_j = N'^v_j + N'^d_j \tag{2.13}$$

N'^v_j = viscous flux [mol.m^{-2}.s^{-1}]

For viscous flow D'Arcy's law applies:

$$N'^v_j = -\frac{x'_j c'_t B_o}{\tau \eta} \nabla P \tag{2.14}$$

η = viscosity of the solution [Pa.s]
B_o = permeability [m^2]

In equations (2.12) and (2.14) the membrane is included in the definitions for the mole fractions and concentrations. It is convenient to convert these quantities into quantities which refer only to the liquid phase. The mole fraction x'_j is equal to x''_j, because the membrane is considered as a component with infinite molecular weight (see section 2.2.2). The relationship between γ'_j and γ''_j can be understood if the situation of no pressure gradient and total permeability for solute j is considered. In that case $\gamma'_j x'_j$ is equal to $\gamma''_j x''_j$. Since $x'_j = x''_j$, γ'_j and γ''_j have the same value. The total molar concentration c'_t is equal to $\varepsilon c''_t$, where ε represents the membrane porosity. The homogeneous flux N'_j inside the membrane is equal to the flux N_j outside the membrane, both per cross-sectional membrane area.

Substitution of equations (2.13) and (2.14) in equation (2.12) together with the definitions for the mole fractions and concentrations provides the following Stefan-Maxwell equation in the membrane for component j:

$$\frac{x_j^{//}}{RT}\nabla_{T,P}\mu_j^{//} + x_j^{//}\left[\frac{V_j}{RT} + \frac{B_o}{D_{j,m}\eta}\right]\nabla P = \sum_{\substack{k=1 \\ k\neq j}}^{n_{comp}}\frac{x_j^{//}N_k - x_k^{//}N_j}{c_t^{//}D_{j,k}^{sm}\frac{\varepsilon}{\tau}} - \frac{N_j}{c_t^{//}D_{j,m}\frac{\varepsilon}{\tau}} \qquad (2.15)$$

Heterogeneous description

In the heterogeneous description the Stefan-Maxwell equations are defined inside the pores. The membrane is considered as pore walls which cause friction with the fluid inside the pore. This representation is in contrast with the homogeneous description where the membrane is considered as a uniformly distributed component.

In accordance with the homogeneous description a simplification can be introduced in the term which describes the driving force as a result of the pressure gradient.

$$\frac{(\phi_j^{//} - \omega_j^{//})}{c_t^{//}RT}\nabla P - \frac{\rho_j^{//}}{c_t^{//}RT}\left[g_j - \sum_{k=1}^{n_{comp}}\omega_k^{//}g_k\right] = \frac{x_j^{//}V_j}{RT}\nabla P \qquad (2.16)$$

The difference between equation (2.17) and (2.7) is due to the body force acting on the pore fluid through the mechanically constrained pore walls.

The following Stefan-Maxwell equation inside the pore can be derived (similar to eq. (2.12)):

$$\frac{x_j^{//}}{RT}\nabla_{T,P}\mu_j^{//} + x_j^{//}\left[\frac{V_j}{RT}\right]\nabla P = \sum_{\substack{k=1 \\ k\neq j}}^{n_{comp}}\frac{x_j^{//}N_k^{//d} - x_k^{//}N_j^{//d}}{c_t^{//}D_{j,k}^{sm}\frac{1}{\tau}} - \frac{N_j^{//d}}{c_t^{//}D_{j,m}\frac{1}{\tau}} \qquad (2.17)$$

The first term on the right-hand side of the equation represents friction between the components in the pore fluid itself. The second term on the right-hand side describes the friction between the solution and the pore wall. A fictitious pore wall mole fraction is incorporated in the species-membrane diffusion coefficient $D_{j,m}$ (see section 2.2.2). The flux difference, which has to be taken into account for the friction between the membrane and the solute and solvent molecules, is equal to the diffusive flux $N_j^{//d}$, because the local viscous flow at the pore wall is equal to zero. The diffusive flux $N_j^{//d}$ is assumed to be equal to the radially averaged flux $N_j^{//}$ minus the radially averaged viscous flux $N_j^{//v}$. This assumption seems reasonable for the small solvent molecules, but might introduce some error for the larger solute molecules.

Due to geometrical exclusion the solute molecules are only able to approach the pore wall as near as their radii. This implies that the solute molecules at the wall still experience the influence of the viscous flow profile in the pore. The radial variations in velocity have been incorporated in the hydrodynamic models for hindered transport [Deen, 1987].

Equations (2.13) to (2.14) also hold for the heterogeneous description if $'$ is replaced by $''$. The total molar flux N_j outside the membrane per cross-sectional membrane area is equal to the total molar flux N_j'' inside the pore divided by ε. This leads to the following Stefan-Maxwell equation in the membrane for component j:

$$\frac{x_j''}{RT}\nabla_{T,P}\mu_j'' + x_j''\left[\frac{V_j}{RT} + \frac{B_0}{D_{j,m}\eta}\right]\nabla P = \sum_{\substack{k=1 \\ k \neq j}}^{n_{comp}} \frac{x_j''N_k - x_k''N_j}{c_t''D_{j,k}^{sm}\frac{\varepsilon}{\tau}} - \frac{N_j}{c_t''D_{j,m}\frac{\varepsilon}{\tau}} \quad (2.18)$$

Equation (2.18) is equal to equation (2.15) derived for the homogeneous description.

According to Poiseuille the permeability B_0 is

$$B_0 = \frac{r_p^2}{8} \quad (2.19)$$

for cylindrical pores of radius r_p.

As already mentioned, a detailed derivation of the governing equations for the homogeneous and heterogeneous membrane descriptions has been given here, because in the various texts of Jackson [1977], Mason and Viehland [1978] and Krishna [1987] inconsistencies seem to occur as a result of unclear definitions of the concentrations, fluxes, and velocities. The Stefan-Maxwell equations derived in those articles are only analogous to equations (2.18) and (2.15) if the concentrations are defined without incorporating the membrane, the fluxes are based on the cross-sectional membrane area, and ε/τ is incorporated in B_0.

2.2.5 Boundary condition

The following boundary condition at the permeate side of the membrane is used: the flux of component j, N_j, is equal to x_j^P multiplied by the total permeate flux N_{per}. In other words, the ratio of the molar fluxes of the various components is equal to the

ratio of their mole fractions in the permeate:

$$\frac{N_j}{N_k} = \frac{x_j^P}{x_k^P} \tag{2.20}$$

x_j^P = mole fraction component j in the permeate

The number of bootstrap relations depends on the number of components, and equals $n_{comp}-1$.

2.2.6 Interphase equilibria

After the definition of the Stefan-Maxwell transport equations in the polarization layer and the membrane, it is necessary to formulate a link between the polarization layer and the membrane [Lightfoot, 1974]. The interfacial region is very small and the difference in chemical potential will be negligible. Therefore interfacial equilibrium is assumed. This assumption implies that d_j is equal to zero. Since pressure gradients can develop only as a result of the mechanical restraint on the membrane matrix, the proper expression for d_j is

$$\frac{x_j}{RT}\nabla_{T,P}\mu_j + \frac{x_j V_j}{RT}\nabla P = 0 \tag{2.21}$$

Integration of this expression with $\mu_{j,(T,P)} = RT\ln a_{j,(T,P)}$ from the external phase to the membrane phase gives

$$\ln\left[\frac{a_j}{a_j'}\right]_{T,P} + \frac{V_j}{RT}\left(P-P'\right) = 0 \tag{2.22}$$

where P' and a_j' are defined inside the membrane. Equation (2.21) can be used for both interfaces. The interface between the polarization layer and membrane will be referred to with subscript 0, the interface between the membrane and permeate will be indicated by subscript L. From here the solvent w (water) and the solute s (representing all solutes in the multicomponent mixture) are given a non-parallel treatment. First the solvent will be discussed.

By means of equation (2.21) it is possible to relate the internal and external compositi-

ons and pressures:

$$P_0' - P_L' + \frac{RT}{V_w} \ln \left[\frac{a_{w0}}{a_{wL}} \right]_{T,P}' = P_0 - P_L + \frac{RT}{V_w} \ln \left[\frac{a_{w0}}{a_{wL}} \right]_{T,P} \qquad (2.23)$$

Since

$$\Pi = -\frac{RT}{V_w} \ln a_w \qquad (2.24)$$

the right-hand side of the equation can be written in the more familiar form ΔP_e-$\Delta \Pi_e$, where e means external phase. This difference between the external applied pressure and the external osmotic pressure is used as the driving force in the osmotic pressure model [see chap. 4].

Our interest concerning the solute is to find a relationship between the mole fraction of the solute inside and outside the membrane. Using $a_j = \gamma_j x_j$, we can write equation (2.21) as

$$\frac{x_s}{x_s'} = K_{eq}' = \frac{\gamma_s'}{\gamma_s} e^{(P-P')Vs/RT} \qquad (2.25)$$

The equilibrium partition coefficient K_{eq} between the membrane and the external phase depends on the pressure difference at the interface as well as on the activity coefficients.

For the special case of purely steric interactions between the solute and pore wall Giddings [1968] has derived the following equation for K_{eq} based on statistical thermodynamic arguments:

$$K_{eq} = \frac{c_s}{c_s''} = (1 - \lambda)^2 \qquad (2.26)$$

in which λ is the quotient of the solute radius and the pore radius. The same equation has been found by Renkin using geometric arguments [1954].

In fig. 2.1 the concentration and pressure profiles in the polarization layer and membrane are depicted as described by the Stefan-Maxwell equations and the interphase equilibria. At both interfaces a sudden change in concentration and pressure occurs.
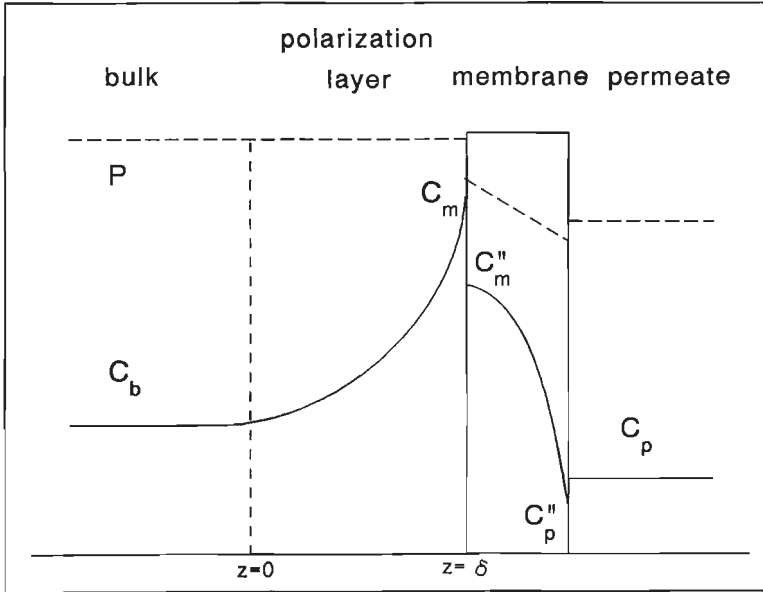
Figure 2.1 *Concentration (——) and pressure profiles (- -) in polarization layer and membrane.*

2.2.7 Stefan-Maxwell model for pure solvent

The ultrafiltration of pure solvent can be used to obtain information about the various membrane related parameters in the Stefan-Maxwell model. Therefore the Stefan-Maxwell equations for pure solvent are presented here. First of all, no relevant equation can be formulated for the polarization layer, since there is no friction with other components ($r_j = 0$) and there are no activity and pressure gradients ($d_j = 0$). In the membrane, on the other hand, friction with the membrane does occur and a pressure gradient over the membrane is present. Since $\nabla_{T,P} \, \mu_j$ is equal to zero, this leads to the following equation:

$$\left[\frac{B_o}{D_{j,m}\eta} + \frac{V_j}{RT} \right] \nabla P = \frac{-N_j}{c_t'' D_{j,m}\frac{\varepsilon}{\tau}} \qquad (2.27)$$

This differential equation has the following boundary conditions:

$$z = 0 \quad : \quad P = P_{ret}$$

$$z = L \quad : \quad P = P_{per}$$

P_{ret} = pressure at retentate side [Pa]
P_{per} = pressure at permeate side [Pa]

From eqn. (2.27) and the boundary conditions the following expression for the pure solvent flux can be derived ($c_t'' = 1/V_j$):

$$N_j = \frac{\varepsilon}{\tau} \left[\frac{c_t'' B_o}{\eta} + \frac{D_{j,m}}{RT} \right] \frac{\Delta P}{L} \qquad (2.28)$$

The terms between brackets represent the viscous component of the flux and the pressure diffusion term proportional to $D_{j,m}$. Pressure diffusion phenomena can be quite prominent in gaseous systems, but they generally do not play a significant role in the case of liquids.

From the experimentally measured pure solvent fluxes a membrane resistance can be calculated according to $\Delta P / \eta v_{per}$ with $v_{per} = N_j V_j$. For the membrane resistance R_m the following expression can be derived ($c_t'' = 1/V_j$):

$$\frac{1}{R_m} = \frac{\eta N_j V_j}{\Delta P} = \frac{\frac{\varepsilon}{\tau} \eta D_{j,m}}{L} \left[\frac{B_o}{D_{j,m}\eta} + \frac{V_j}{RT} \right] \qquad (2.29)$$

Equation (2.29) provides an expression that can be used to check the calculated membrane resistance with the experimentally determined membrane resistance, using the fitted values for the diffusion coefficient of solvent in the membrane, $D_{j,m}$, and the quotient of the porosity and the tortuosity. Another possibility is substitution of equation (2.29), including the experimentally determined value for the membrane resistance, in the Stefan-Maxwell model. In that case the quotient of porosity and

tortuosity becomes a function of the diffusion coefficient between solvent and membrane.

2.2.8 Mass transfer in the polarization layer

Mass transfer in the polarization layer is considered according to the stagnant film model. In that case the mass transfer coefficient is defined as:

$$k_{j,k} = \frac{D_{j,k}}{\delta_{pol}} \tag{2.30}$$

The mass transfer coefficients according to the Sherwood relation (see chap. 3) have been used to evaluate the thickness of the boundary layer. Since the mass transfer coefficient is proportional to $D_{j,k}^{0.67}$, the boundary thickness is a function of the diffusion coefficient of the component according to $D_{j,k}^{0.33}$. This implies that in multicomponent systems the boundary layer thickness of the various components can be different. This can be circumvented by defining a dimensionless distance coordinate in the polarization layer z^*, which is equal to z/δ_{pol} [Krishna et al., 1976]. δ_{pol} represents the thickness of the polarization layer. The diffusion coefficients are then replaced, using eqn. (2.30). It is questionable whether this treatment can account for the partial overlap between the boundary layers of the various components.

2.2.9 Numerical solution of the Stefan-Maxwell equations

To be able to calculate flux and rejection, the concentration and pressure profile in the polarization layer and membrane should be known. The Stefan-Maxwell equations have been solved by a discretization and linearization of the differential equations. A Jacobian matrix was formulated. The solution of the set of equations was found by iteratively determining the zero-point with the Newton-Raphson method [Press, 1983]. The variation of the viscosity, the diffusion coefficient, and the activity coefficient with concentration (see chap. 3) has been incorporated in the solution by calculation of these parameters on each grid point in the polarization layer and membrane. The variation in the Stefan-Maxwell diffusion coefficient with concentration has been derived from the measured Fick diffusion coefficient and the thermodynamic factor calculated with the activity models (see chap. 5).

The Stefan-Maxwell equations contain various unknown parameters. These parameters have been fitted to both the experimental flux and rejection data by means of the least-square Levenberg-Marquardt fitting procedure [Press, 1983]. The following objective

function has been used:

$$\chi^2(a) = \sum_{i=1}^{Ndata} \left(\frac{y_i - y(x_i;a)}{\sigma_i \, y_{Ndata}} \right)^2 \tag{2.31}$$

in which y_i is the experimental value of flux or rejection, $y(x_i;a)$ is the calculated value, a is a vector of the fit parameters, x_i an experimental condition (pressure, stirrer speed, circulation velocity), and σ_i is the standard deviation for data point i. The language used for the computer program is Turbo Pascal.

The set-up for the solution of the Stefan-Maxwell equations and the fit procedure have been adopted from a computer program developed by Vonk (Rijksuniversiteit Gronin-gen).

2.3 Hydrodynamic models of hindered transport

One of the major difficulties of the Stefan-Maxwell model is the absence of much experimental and/or theoretical data for the Stefan-Maxwell diffusion coefficients. A lot of work, however, has been done on the modelling of hindered transport in liquid-filled pores using a hydrodynamic type of description [Deen, 1987]. In this section, first the hydrodynamic description will be presented and the Stefan-Maxwell model will then be translated in terms of the hydrodynamic model in order to be able to compare the parameters in both models.

In contrast with the Stefan-Maxwell model, which is based on the principals of irreversible thermodynamics, the hydrodynamic model gives an expression for the flux and the rejection of the solute by solving the hydrodynamic equations. The solute flux inside the pore can be written in the following form [Deen, 1987]:

$$N_s'' = K_c v'' c_s'' - K_d D_\infty \frac{\partial c_s''}{\partial z} \tag{2.32}$$

N_s'' = radially averaged molar flux of solute through pore [mol.m^{-2}.s^{-1}]

v'' = radially averaged axial solution velocity inside pore [m.s^{-1}]

c_s'' = radially averaged solute concentration inside pore [mol.m^{-3}]

D_∞ = diffusion coefficient of solute in free solution [m^2.s^{-1}]

K_c = hindrance factor for convection

K_d = hindrance factor for diffusion

The boundary conditions for this differential equation (2.32) are:

$$z = 0 \; : \; c_s'' = c_{s0}''$$
$$z = L \; : \; c_s'' = c_{sL}''$$

c_{s0}'' = solute concentration inside the membrane at the pore entrance [mol.m^{-3}]

c_{sL}'' = solute concentration inside the membrane at the pore exit [mol.m^{-3}]

L = membrane thickness [m]

The terms K_c and K_d in equation (2.32) are correction factors for convection and diffusion, respectively. They both account for the effects of finite pore size (in an unbounded fluid, $K_c = K_d = 1$). K_d corrects for the extra friction of the solute with the solvent molecules, which are forced to move in opposite direction of the solute due to the finite pore size. K_c corrects for the parabolic velocity profile and the drag of the solute compared to the fluid velocity. Due to the larger dimensions of the solute particles compared to the solvent molecules, the solute particles are present in that part of the pore where the higher fluid velocities occur. This results in a solute velocity higher than the radially averaged fluid velocity. The evaluation of the hindrance factors will be discussed later.

If we assume long pores, the concentrations just within the pores are essentially at equilibrium with the corresponding external concentrations (see Interphase equilibria) and a solute equilibrium partition coefficient ϕ can be defined:

$$\phi = \frac{c_{s0}''}{c_s^m} = \frac{c_{sL}''}{c_s^p} \tag{2.33}$$

c_s^m = solute concentration at upper surface of the membrane [mol.m^{-3}]

c_s^p = solute concentration in the permeate [mol.m^{-3}]

Integration of equation (2.32) and substitution of equation (2.33) leads to the following expression for the solute flux through the membrane (N_s''):

$$N''_s = \phi K_c v'' c_s^m \frac{\left[1 - \dfrac{c_s^p}{c_s^m} e^{-Pe_m}\right]}{\left(1 - e^{-Pe_m}\right)} \tag{2.34}$$

The Peclet number (Pe_m) is defined as follows:

$$Pe_m = \frac{\phi K_c v'' L}{\phi K_d D_\infty} \tag{2.35}$$

For large Pe_m numbers $(Pe_m \gg 1)$, at which convection is predominant, equation (2.34) reduces to:

$$N''_s = \phi K_c v'' c_s^m \tag{2.36}$$

If the transport is predominated by diffusion $(Pe_m \ll 1)$, equation (2.34) converts into:

$$N''_s = \frac{\phi K_d D_\infty}{L} (c_s^m - c_s^p) \tag{2.37}$$

If the solute flux N''_s can be neglected compared to the solvent flux N''_s is equal to $v'' c_p$ and equation (2.34) can be converted into an expression for the actual 'sieving' coefficient S_a.

This coefficient indicates the degree to which the solute migrates through the membrane:

$$S_a = 1 - R_a = \frac{c_s^p}{c_s^m} = \frac{S_\infty e^{Pe_m}}{S_\infty + e^{Pe_m} - 1} \tag{2.38}$$

R_a = actual rejection

S_∞ is the value for the actual sieving coefficient at large Pe_m numbers and can be evaluated from eq. (2.36) as follows:

$$S_\infty = \phi K_c \tag{2.39}$$

The observed rejection R_0 follows from the combination of eqn. (2.38) with the relationship derived for concentration polarization (eqn. (4.4)).

In a review article by Deen [1987] several theoretically derived equations are presented for the hydrodynamic factors K_c and K_d. Bungay and Brenner [1973] have formulated an analytical relationship for spherical particles in cylindrical pores using the centreline approximation, which is valid for all values of the ratio of the solute to pore diameters λ ($0 \le \lambda < 1$). The centre line approximation implies that the centre of the sphere inside the pore is considered on the central axis of the pore. The hindrance factors have been expressed as follows:

$$K_d = \frac{6\pi}{K_t} \tag{2.40}$$

$$K_c = \frac{(2-\phi)K_s}{2K_t} \tag{2.41}$$

K_t and K_s can be written as a function of λ and the hydrodynamic expansion coefficients a_i and b_i:

$$\begin{bmatrix} K_t \\ K_s \end{bmatrix} = \frac{9}{4}\pi^2\sqrt{2}\,(1-\lambda)^{-5/2} \left[1 + \sum_{n=1}^{2} \begin{bmatrix} a_n \\ b_n \end{bmatrix} (1-\lambda)^n \right] + \sum_{n=0}^{4} \begin{bmatrix} a_{n+3} \\ b_{n+3} \end{bmatrix} \lambda^n \tag{2.42}$$

Subscript n	a_n	b_n
1	-73/60	7/60
2	77293/50400	-2227/50400
3	-22.5083	4.0180
4	-5.6177	-3.9788
5	-0.3363	-1.9215
6	-1.216	4.392
7	1.647	5.006

Table 2.1: *Expansion coefficients for the hydrodynamic functions K_t and K_s in eqn. (2.1).*

In equation (2.41) the solute equilibrium partition coefficient ϕ is defined as follows:

$$\phi = (1-\lambda)^2 \tag{2.43}$$

Equation (2.43) has been derived by several authors, using either geometric [Renkin, 1954] or statistical thermodynamic arguments [Giddings, 1968] for the special case of purely steric interactions between the solute and pore wall.

The hydrodynamic factors ΦK_c and ΦK_d are given in figure 2.2 as a function of λ.

For the transport of a spherical solute in slit-shaped pores a centre line approximation was obtained by Happel and Brenner [1983]:

$$K_d = 1 - 1.004\lambda + 0.418\lambda^3 + 0.21\lambda^4 - 0.169\lambda^5 + O(\lambda^6) \tag{2.44}$$

$$K_c = \frac{3-\Phi^2}{2}\left(1 - \frac{\lambda^2}{3} + O(\lambda^3)\right) \tag{2.45}$$

where λ is equal to the ratio of the solute diameter to the slit width. In this case, the partition coefficient Φ is equal to $1-\lambda$.
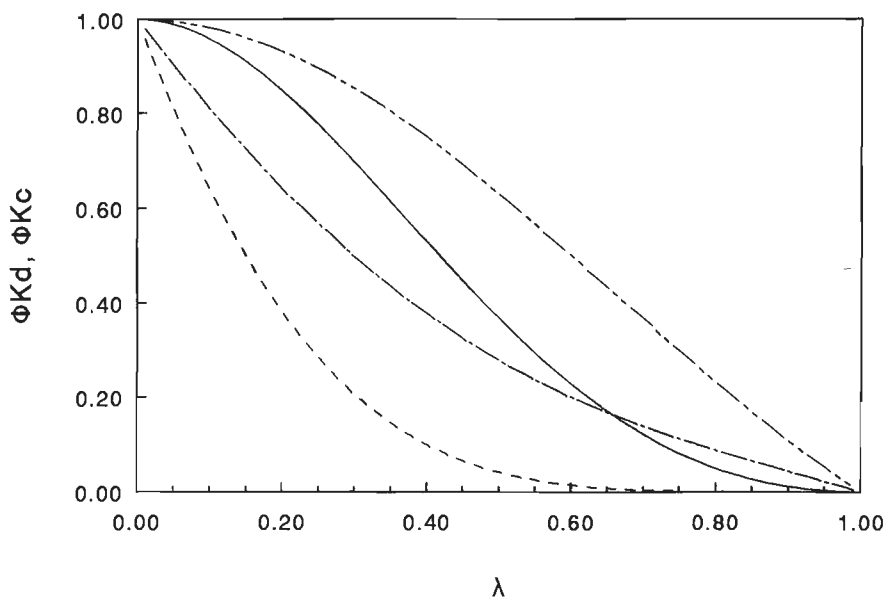
Figure 2.2 *Hydrodynamic factors for spherical solutes in slit and cylindrical pores. Cylindrical: ϕK_c (——) and ϕK_d (———); slit pores: ϕK_c (—··—) and ϕK_d (—·—).*

The values for the hindrance factors ΦK_c and ΦK_d have been depicted in fig. 2.2, showing that the hindrance factors for the cylindrical pores are much smaller than those for slit-shaped pores, due to the greater interaction with the pore walls in the cylindrical geometry.

To extend the description of Bungay and Brenner for spheres in cylindrical pores to non-spherical particles in pores of arbitrary geometry, Opong [1991a] and Mochizuki [1992b] used a model developed by Giddings [1968]. It describes the partitioning of rigid solutes in a porous network formed by random intersecting parallel planes. Giddings showed that the partitioning behaviour of a wide range of solutes in different pore geometries was governed primarily by the quantity

$$\lambda^* = \frac{r_s^*}{2s} \tag{2.46}$$

where r_s^* is the mean projected solute radius ($r_s^* = r_s$ for a sphere) and s is the reciprocal specific area of the pore, equal to the pore volume (V_{pore}) divided by the pore surface area (S_{pore}). The partition coefficient is given by

$$\phi = e^{-2\lambda^*} \tag{2.47}$$

This model implicitly accounts for the presence of a pore size distribution through the evaluation of λ^*. Opong and Mochizuki calculated the specific surface area of the pores (s) from the permeability of the membrane L_p ($=1/R_m$) using the Kozeny-Carman equation:

$$s = \left(\frac{2LL_p}{\varepsilon}\right)^{1/2} \tag{2.48}$$

where L is the membrane thickness and ε the porosity.

Using the partition coefficient ϕ defined by eqn. (2.45), an effective size ratio λ_{eff} for an equivalent spherical solute in a cylindrical pore can be calcaluted from equation (2.43). λ_{eff} can be substituted in the model of Bungay and Brenner in order to calculate K_d and K_c.

2.4 Comparison of Stefan-Maxwell model with hindered transport model

In this section a comparison will be made between the Stefan-Maxwell model and the hindered-transport model. The hindered-transport model has been derived for a very dilute, binary solution. In order to compare the hindered-transport model with the

Stefan-Maxwell model an analytical solution for the Stefan-Maxwell model is used. This analytical solution for a binary, ideally behaving system has been derived by Robertson and Zydney [1988]. The Stefan-Maxwell equations used for the derivation have a somewhat different form than the equations presented in section 2.2. The viscous flow was not considered separately as it is in section 2.2, but was incorporated in the diffusion coefficients [Mason, 1985]. Therefore these diffusion coefficients deviate from the diffusion coefficients introduced in section 2.2 and consequently they will be represented by the symbol E instead of D. Besides viscous flow terms, E also contains the tortuosity of the membrane.

The one-dimensional Stefan-Maxwell equations for the solute (s) and the solvent (w) have the following form [Robertson et al., 1988]:

$$\frac{V_s}{RT}\frac{dP}{dz} + \frac{d}{dz}\ln(x_s''\gamma_s) = \frac{1}{c_s''E_{s,w}}(x_s''N_w'' - x_w''N_s'') - \frac{1}{c_s''E_{s,m}}N_s'' \quad (2.49)$$

$$\frac{V_w}{RT}\frac{dP}{dz} + \frac{d}{dz}\ln(x_w''\gamma_w) = \frac{1}{c_w''E_{s,w}}(x_w''N_s'' - x_s''N_w'') - \frac{1}{c_w''E_{w,m}}N_w'' \quad (2.50)$$

$E_{s,m}$ = diffusion coefficient of solute in the membrane [$m^2.s^{-1}$]
$E_{w,m}$ = diffusion coefficient of water in the membrane [$m^2.s^{-1}$]
$E_{s,w}$ = diffusion coefficient solute-water [$m^2.s^{-1}$]

These differential equations have the following boundary conditions:

$$z = 0 \ : \ P = P_{ret} \ , \ x_s'' = x_{s0}'' \ , \ x_w'' = x_{w0}''$$
$$z = L \ : \ P = P_{per} \ , \ x_s'' = x_{sL}'' \ , \ x_w'' = x_{wL}''$$

P_{ret} = pressure at retentate side [Pa]
P_{per} = pressure at permeate side [Pa]
x_{s0}'' = solute mole fraction at pore entrance [mol/mol]
x_{w0}'' = water mole fraction at pore entrance [mol/mol]
x_{sL}'' = solute mole fraction at pore exit [mol/mol]
x_{wL}'' = water mole fraction at pore exit [mol/mol]

If the flux equations are rewritten in terms of ultrafiltrate velocity v'':

$$v'' = V_s N_s'' + V_w N_w''$$ (2.51)

the following equations can be derived for the ultrafiltrate velocity v'' and the molar solute flux inside the pore N_s'' in the dilute solution limit [Robertson et al., 1988]:

$$v = \frac{E_{w,m}}{c_t'' RT} \left[\frac{dP}{dz} - c_t'' RT \left[1 - \frac{D_2}{D_1} \right] \frac{d}{dz} \ln(x_w'' \gamma_w) \right]$$ (2.52)

$$N_s'' = \frac{D_2}{D_1} x_s'' c_t'' v - D_2 c_t'' x_s'' \frac{d}{dz} \ln(x_s'' \gamma_s)$$ (2.53)

The diffusion coefficients D_1 and D_2 are defined as follows:

$$\frac{1}{D_1} = \frac{1}{E_{s,w}} + \frac{c_t'' V_s}{E_{w,m}}$$ (2.54)

$$\frac{1}{D_2} = \frac{x_w''}{E_{s,w}} + \frac{1}{E_{s,m}}$$ (2.55)

The boundary conditions belonging to these differential equations are analogous to the boundary conditions given for equation (2.49) and (2.50).

If ideal-solution behaviour is assumed, equation (2.53) can be written as:

$$\frac{dx_s''}{dz} = \frac{1}{D_1} x_s'' v'' - \frac{1}{c_t'' D_2} N_s''$$ (2.56)

Using equation (2.33) as an expression for the solute equilibrium partition coefficient ϕ, the integration of equation (2.56) leads to:

$$x_s^p \frac{D_1}{D_2} - \left[\phi x_s^m - \frac{D_1}{D_2} x_s^p \right] e^{-\frac{L}{D_1} v} = \phi x_s^p$$ (2.57)

x_s^m = solute mole fraction at upper membrane surface
x_s^p = solute mole fraction in permeate

Since for dilute solutions $N_s'' = v'' \cdot c_s^P$, equation (2.57) can be rewritten into the following expression for the actual sieving coefficient S_a:

$$S_a = \frac{\phi \dfrac{D_2}{D_1} e^{-\frac{L}{D_1}v}}{\phi \dfrac{D_2}{D_1} - 1 + e^{-\frac{L}{D_1}v}} \qquad (2.58)$$

By combining equations (2.35), (2.38), (2.39) and (2.58) the Stefan-Maxwell model of Robertson and Zydney [1988] can be expressed in the hydrodynamic factors K_c and K_d:

$$K_c = \frac{D_2}{D_1} \qquad K_d = \frac{D_2}{D_\infty} \qquad (2.59)$$

As discussed before, the main difference between the Stefan-Maxwell model derived by Robertson and Zydney and the Stefan-Maxwell model, presented in section 2.2, is the way in which the viscous flow inside the pores is taken into account. In section 2.2 it is considered separately and here the viscous flow term is concealed in the diffusion coefficients E. It is possible to convert these approaches into each other. For this purpose Mason and del Castillo [1985] have derived an equation for the diffusion coefficient of the components inside the membrane $E_{j,m}$ and the diffusion coefficient of the solute in the solution $E_{s,w}$:

$$E_{s,m} = \frac{D_{s,m}}{\tau}(1+\beta) \qquad E_{w,m} = \frac{D_{w,m}}{\tau}(1+\beta) \qquad (2.60)$$

$$\frac{1}{E_{s,w}} = \frac{\tau}{D_{s,w}} + \frac{\tau D_m}{D_{s,m} D_{w,m}}\left[\frac{\beta}{1+\beta}\right] \qquad (2.61)$$

where:

$$\frac{1}{\overline{D}_m} = \sum_{j=1}^{NComp} \frac{x_j^{//}}{D_{j,m}} \qquad (2.62)$$

$$\beta = \frac{c_t^{//} R T B_o}{\eta \overline{D}_m} \qquad (2.63)$$

It should be pointed out that equations (2.60) and (2.61) contain the tortuosity τ in contrast with the equations presented by Mason and del Castillo [1985]. This is due to the fact that they incorporate the deviation of the porous medium from straight pores perpendicular to the membrane surface into their diffusion coefficients $D_{j,k}$.
Substitution of equations (2.60) and (2.61) in equation (2.59), by making use of equations (2.54) and (2.55), leads to the following expressions for K_c and K_d:

$$K_d = \frac{D_{s,m} D_{w,m}(1+\beta)}{x_w^{//} D_{s,m} D_{w,m}(1+\beta) + x_w^{//} \overline{D}_m D_{s,w}\beta + D_{s,w} D_{w,m}} \qquad (2.64)$$

$$K_c = \frac{D_{s,m} D_{w,m}(1+\beta) + \overline{D}_m D_{s,w}\beta + c_t^{//} V_s D_{s,m} D_{s,w}}{x_w^{//} D_{s,m} D_{w,m}(1+\beta) + x_w^{//} \overline{D}_m D_{s,w}\beta + D_{s,w} D_{w,m}} \qquad (2.65)$$

It should be emphasized that the free-solution diffusion coefficient D_∞ in equation (2.59) is equal to $D_{s,w}^{sm}$ instead of $E_{s,w}$, because in $E_{s,w}$ the viscous flow term is incorporated. Several authors [Spiegler, 1966; Anderson, 1974] have mistaken $E_{s,w}$ for $D_{s,w}^{sm}$, which leads to an erroneous description as shown by Mason et al. [1985].
The combination of the relationships for K_d and K_c from Bungay and Brenner for cylindrical pores (eqns. (2.40) and (2.41)) or those from Happel and Brenner for slit pores (eqns. (2.44) and (2.45)) with eqns. (2.64) and (2.65) provides the possibility to compare the Stefan-Maxwell model with the hindered-transport model. The results of this comparison will be treated in chap. 5.

3 PHYSICAL PROPERTIES OF THE MODEL SYSTEMS

3.1 Introduction

To interpret the experimental results and to be able to perform quantitative calculations a number of physical properties must be known. Part of the physical properties has been derived directly from literature. The osmotic pressure data for the various solutes will be presented here, other physical data like diffusivity, viscosity and particle diameters are listed in an appendix at the end of this chapter. More extensive study has been performed to characterize the thermodynamic activity in ternary PEG/dextran/water systems. The results will be discussed in section 3.3. Subsequently, experimental correlations will be presented to describe the mass transfer in the membrane modules. By electrochemical and heat transfer measurements we have characterized the overall and local mass transfer in the stirred cell. The mass transfer in the tubular membrane module has been taken from literature.

3.2 Osmotic pressure

Polyethylene glycol

Binary polyethylene glycol (PEG)/water systems show non-ideal behaviour, which implies that the osmotic pressure is higher than expected by Van 't Hoff's Law. Van der Linden [1973] has measured the osmotic pressure for several types of PEG by determining the vapour-pressure for various concentrations. In fig. 3.1 the osmotic pressure is presented as a function of the PEG concentration for PEG1000 and PEG3400 at 298 K. The following relationships correspond to the curves drawn through the data points [Van der Linden, 1973]:

$$\text{PEG1000:} \quad \Pi = \frac{RTM_w}{1000\,V_w}\, m_{PEG}(0.970 + 3.183\,m_{PEG} + 2.09\,m_{PEG}^2) \quad (3.1)$$

$$\text{PEG3400:} \quad \Pi = \frac{RTM_w}{1000\,V_w}\, m_{PEG}(0.940 + 0.0126\,C_{PEG}) \quad (3.2)$$

The molality m_{PEG} is expressed in [mol.(kg solvent)$^{-1}$]. Eqn. (3.1) is valid for C_{PEG} below 100 kg.m^{-3} and eqn. (3.2) for $C_{PEG} < 70$ kg.m^{-3}. The osmotic pressure of PEG3400 is higher than that for PEG1000. Due to the increase in excluded volume at

higher molecular weights, the mutual interactions between the polymer molecules are already noticeable at lower concentrations.
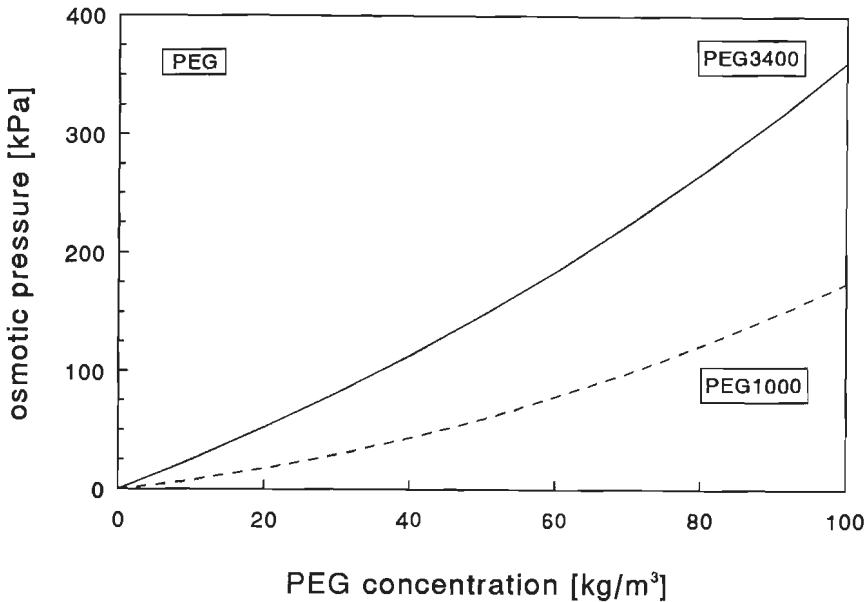
Figure 3.1 *Osmotic pressure of PEG1000 and PEG3400 as a function of the concentration.*

Dextran

Several authors have presented osmotic pressure data for dextran of different molecular weights [Wijmans et al., 1985; de Balmann et al., 1989; Ogsten et al., 1979]. Figure 3.2 shows the osmotic pressure versus solute concentration. When we compare the various osmotic pressure data it can be seen that there is little influence of the molecular weight. Therefore, the osmotic pressure data for dextran T70 of Wijmans et al. [1985] have been used to model the osmotic pressure for dextranT40, dextranT70 and dextranT250:

$$\Pi = 37.5C + 0.752C^2 + 76.4 \cdot 10^{-4} C^3 \tag{3.3}$$

This relationship is valid for $C_{dex} < 260$ kg.m^{-3} at 298 K.

The measurements have been carried out with a high pressure osmometer with Sartorius 'allerfeinst' membranes.
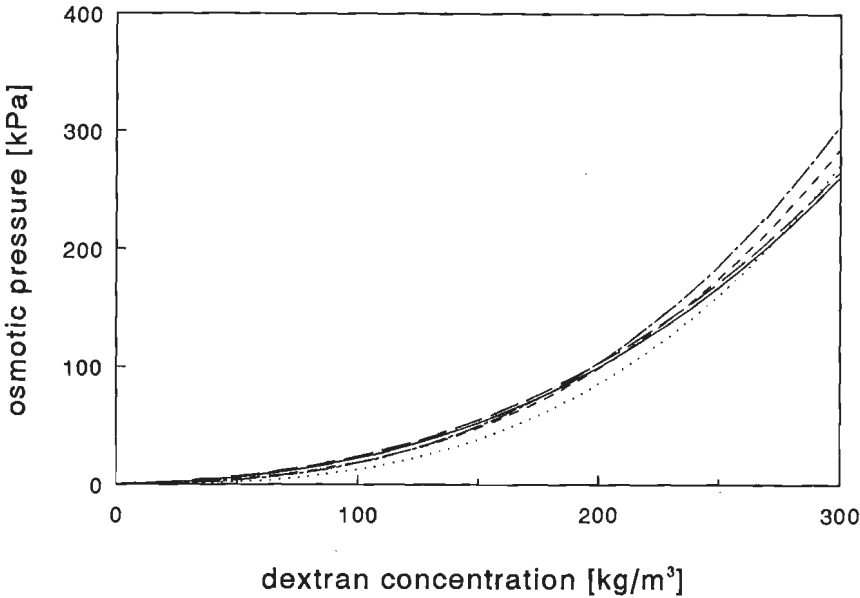
Figure 3.2 *Osmotic pressure for dextran of different molecular weight.* (——) *T52.5 [Ogston];* (——) *T70 [Wijmans]; (- -) T70 [Balmann]; (—·—·) T500 [Ogston]; (···) T500 [Wijmans].*

Bovine Serum Albumine

Vilker et al. [1984] have measured the osmotic pressure of Bovine Serum Albumine (BSA) for various pH values at an ionic strength of 0.15 M NaCl. The measurements were performed in a high-pressure membrane osmometer of which one side was filled with the BSA solution and the other side with the 0.15 M saline solvent. The rejection of BSA by the membrane was larger than 0.99, the rejection for saline was less than 2×10^{-4}. In fig. 3.3 the osmotic pressure is presented for the two pH values which are relevant for this study: pH=7.4 and pH=4.5. The latter pH value is close to the isoelectric point, which is equal to 4.7. The relationships for the osmotic pressure are as follows:

pH=7.4:

$$\Pi = \frac{1000\,RT}{M_{BSA}} [C - 1.09 \cdot 10^{-2} C^2 + 1.24 \cdot 10^{-4} C^3 + 20.4 (C^2 + 1.03 \cdot 10^6)^{0.5} - 2.07 \cdot 10^4] \qquad (3.4)$$

pH=4.5:

$$\Pi = \frac{1000\,RT}{M_{BSA}}[C-2.39\cdot10^{-3}C^2+2.83\cdot10^{-5}C^3+4.49(C^2+2.12\cdot10^7)^{0.5}-2.07\cdot10^4] \qquad (3.5)$$

M_{BSA} is the molecular weight of BSA, and the BSA concentration, C, is expressed in kg.m^{-3}. Both relationships are valid for BSA concentrations from 0 to 500 kg.m^{-3}. The osmotic pressures for pH=7.4 are considerably higher than the values found for pH=4.5.
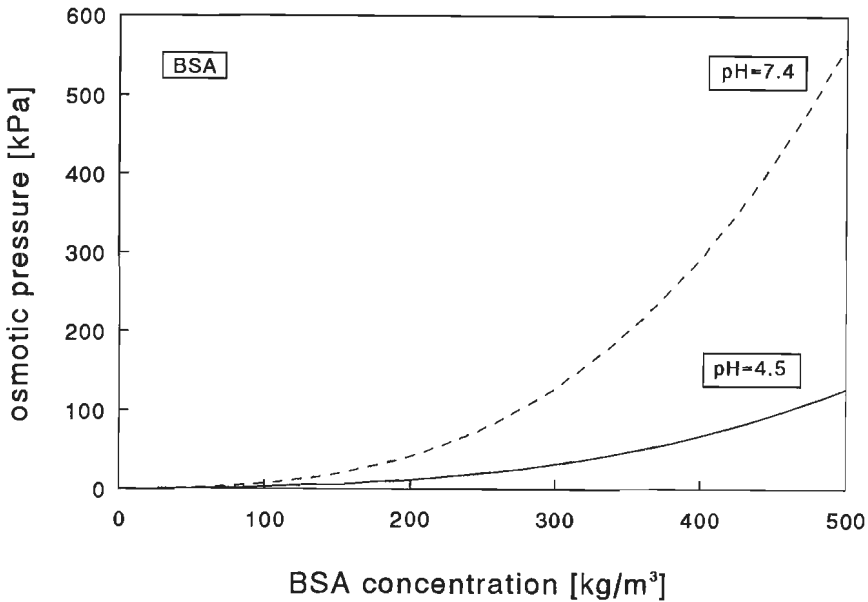
Figure 3.3 *Osmotic pressure of BSA as a function of the concentration for pH=7.4 and 4.5.*

3.3 Thermodynamic activity of components in polymer solutions

In this section two models will be presented for the calculation of the thermodynamic activity of components in multicomponent solutions. First a general description of the models is given. Subsequently, the models are applied to the PEG/dextran/water system.

3.3.1 UNIQUAC-model.

The UNIQUAC-model has been derived by Abrams and Prausnitz [1975]. This model has been used by Kang and Sandler [1988a] to predict demixing curves for PEG/dextran/water systems. Our interest is not to predict the demixing curve but is instead to

describe the thermodynamic activity in the homogeneous solution. The model presented here is a simplified model which does not take molecular weight distribution of the polymers into account. For the extended model with molecular weight distribution, see Kang and Sandler [1988b].

The UNIQUAC-model is composed of two parts: a combinatorial contribution and a part which describes the intermolecular forces responsible for the Gibbs free energy of mixing.

The activity of component j in a n component system can be represented in terms of the mass fractions by the following relationship:

$$
\ln a_j = \ln \phi_j' + \frac{z}{2} M_j q_j' \ln \frac{\theta_j'}{\phi_j'} + M_j l_j' - M_j \frac{\phi_j'}{w_j} \sum_{k=1}^{n} l_k' w_k
$$

$$
+ M_j q_j' \left[1 - \ln \sum_{k=1}^{n} \theta_k' \tau_{kj} - \sum_{k=1}^{n} \frac{\theta_k' \tau_{jk}}{\sum_{m=1}^{n} \theta_m' \tau_{mk}} \right]
$$

(3.6)

in which the various quantities are defined as follows:

$$
\phi_j' = \frac{r_j' w_j}{\sum_{k=1}^{n} r_k' w_k} \qquad\qquad \theta_j' = \frac{q_j' w_j}{\sum_{k=1}^{n} q_k' w_k}
$$

(3.7)

$$
l_j' = \frac{z}{2}(r_j' - q_j') - (r_j' - \frac{1}{M_j})
$$

(3.8)

$$
\tau_{jk} = \exp\left[\frac{-A_{jk}}{T} \right] \qquad\qquad A_{jk} = \frac{(u_{jk} - u_{jj})}{R}
$$

(3.9)

A_{jk} = interaction parameter between components i and j [K]
M_j = molecular weight [g.mol^{-1}]
q_j' = surface area parameter [mol.g^{-1}]
r_j' = volume parameter [mol.g^{-1}]
R = gas constant [J.mol^{-1}.K^{-1}]
T = absolute temperature [K]
u_{jk} = interaction energy [J.mol^{-1}]
w_j = mass fraction [kg.kg^{-1}]
z = coordination number (z = 10)
θ_j' = surface area fraction [m$^2\cdot$m^{-2}]
ϕ_j' = volume fraction [m$^3\cdot$m^{-3}]

The parameters r_j' and q_j' for the various components can be calculated as shown by Fredenslund et al. [1977].

The activity coefficients may be evaluated based on the mass fractions: $\gamma_j^{wt}=a_j/w_j$ [kg.kg^{-1}] or on the mole fractions: $\gamma_j=a_j/x_j$ [mol.mol^{-1}]. The last expression has been used in the Stefan-Maxwell equations in chapter 2. The activity coefficients in this chapter are all based on mass fractions.

For the activity coefficients the following conventions will be used (for a ternary system):

polymer : $\gamma_1^{wt} = 1$ for $w_1 \rightarrow 0$

               $\gamma_2^{wt} = 1$ for $w_2 \rightarrow 0$

solvent : $\gamma_3^{wt} = 1$ for $w_3 \rightarrow 1$

This requires that the activity for the polymers calculated by eqn. (3.6) be corrected for the activity coefficient found at infinite dilution.

In order to determine the six interaction parameters A_{jk} for the ternary system are determined using the experimental demixing data and osmotic pressure data. The polymer-water interaction parameters are determined from osmotic pressure data for the binary systems. The osmotic pressure is equal to

$$\Pi = -\frac{RT}{V_w}\ln(a_w) \tag{3.10}$$

By adjusting the polymer-water interaction parameters A_{j3} and A_{3j}, the water activity according to the UNIQUAC-model can be fitted to the water activity derived from experimental osmotic pressure data for binary systems using eqn. (3.10).

The polymer-polymer interaction parameters are fitted to experimental demixing data. For two phases in equilibrium, the chemical potentials of each component are equal in both phases: $\mu_j{}^I = \mu_j{}^{II}$. If for several mixtures the mass fractions of the components of two coexisting phases are known, the polymer-polymer interaction parameters A_{12} and A_{21} can be determined using this condition. The polymer-water interaction parameters derived from binary data are assumed to be valid in the ternary system.

3.3.2 LQCA-model.

The UNIQUAC-model, which is based on a lattice model, assumes that six interaction parameters are necessary to describe a ternary system. In cases in which only interaction energies between nearest neighbours are relevant and no steric interactions take place, no more than three independent interaction parameters can be defined in a lattice model for a ternary system [Madden, 1990]. Kang and Sandler [1987] indeed reported a strong correlation between the polymer-polymer interaction parameters A_{jk} and A_{ji}. According to our calculations for the UNIQUAC-model, the polymer-water interaction parameters A_{jk} and A_{kj} are also correlated. Therefore an alternative model is considered, which assumes that the interaction between each pair of components can be described by one interaction parameter instead of two. This model, the Linearized Quasi-Chemical Approximation (LQCA), consists of three parts [Guggenheim, 1952]. The first part represents the combinatorial contribution. The second part is an entropic nearest segment connectivity correction. This statistical correction accounts for the fact that polymer segments are connected to each other and cannot be located independently of each other on an arbitrary site in the solution. The last part describes of the intermolecular forces which are responsible for the mixing enthalpy. The Gibbs free energy per mol lattice sites of a polymer solution can be written as follows:

$$\frac{\Delta G}{n_\varphi RT} = FH + HOG + EN \qquad (3.11)$$

$$FH = \frac{\phi_1}{m_1}\ln\phi_1 + \frac{\phi_2}{m_2}\ln\phi_2 + \frac{\phi_3}{m_3}\ln\phi_3 \qquad (3.12)$$

$$\begin{aligned} HOG = &\frac{\phi_1(1-\alpha_1)}{\gamma}\ln(1-\alpha_1) + \frac{\phi_2(1-\alpha_2)}{\gamma}\ln(1-\alpha_2) \\ &- \frac{(1-\phi_1\alpha_1-\phi_2\alpha_2)}{\gamma}\ln(1-\phi_1\alpha_1-\phi_2\alpha_2) \end{aligned} \qquad (3.13)$$

$$EN = \frac{1}{(1-\phi_1\alpha_1-\phi_2\alpha_2)}(\phi_1\phi_2 g_{12}+\phi_1\phi_3 g_{13}+\phi_2\phi_3 g_{23}) \qquad (3.14)$$

in which the various quantities are defined as follows:

$$g_{ij} = \frac{b_{ij}}{T} \qquad\qquad m_j = \frac{M_j \nu_j}{1000\,V_3}$$

$$\alpha_j = \frac{2}{z}(1-\frac{1}{m_j}) \qquad\qquad \phi_j = \frac{w_j \nu_j}{\sum\limits_{k=1}^{n} w_j \nu_j} \qquad (3.15)$$

FH is the entropic contribution, which has been derived by Flory and Huggins. HOG is a term for the connectivity correction derived by Huggins, Orr and Guggenheim [1952]. EN is the expression for the Gibbs free energy of mixing.

The symbols have the following meaning:

b_{jk} = interaction parameter [K]
ΔG = Gibbs free energy [J.mol^{-1}]
m_j = relative chain length compared to solvent
n_φ = total number lattice sites
V_3 = partial molar volume solvent [m^3.mol^{-1}]
z = coordination number (z = 12)
α_j = correction term for connectivity
ν_j = specific volume of component i [m^3.kg^{-1}]
ϕ_j = volume fraction [m^3.m^{-3}]

The activity of the solvent (component 3) is equal to:

$$\ln a_3 = \frac{\Delta G}{n_\varphi RT} - \phi_1\frac{\partial(\frac{\Delta G}{n_\varphi RT})}{\partial\phi_1} - \phi_2\frac{\partial(\frac{\Delta G}{n_\varphi RT})}{\partial\phi_2} \qquad (3.16)$$

the activities of the dissolved components are given as:

$$\frac{1}{m_1}\ln a_1 = \frac{\Delta G}{n_\varphi RT} + (1-\phi_1)\frac{\partial(\frac{\Delta G}{n_\varphi RT})}{\partial\phi_1} - \phi_2\frac{\partial(\frac{\Delta G}{n_\varphi RT})}{\partial\phi_2} \qquad (3.17)$$

$$\frac{1}{m_2}\ln a_2 = \frac{\Delta G}{n_\varphi RT} + (1-\phi_2)\frac{\partial(\frac{\Delta G}{n_\varphi RT})}{\partial\phi_2} - \phi_1\frac{\partial(\frac{\Delta G}{n_\varphi RT})}{\partial\phi_1} \qquad (3.18)$$

The activity coefficients for the LQCA-model are defined according to the same conventions as used for the UNIQUAC-model.

By means of the LQCA-model liquid-liquid equilibria of aqueous polymer solutions can be modelled. The three interaction parameters b_{jk} for the ternary system are fitted to experimental demixing data and osmotic pressure data according to the procedure described for the UNIQUAC-model.

3.3.3 Thermodynamic activities in a PEG/dextran/water system

The thermodynamic activities in a PEG/dextran/water system have been modelled with both the UNIQUAC-model and the LQCA-model. First the results of the UNIQUAC-model are presented.

UNIQUAC-model

In table 3.1 the values for the volume parameters r_j' and the surface area parameters q_j' for PEG, dextran and water are given as provided by Kang and Sandler [1988a].

parameter	PEG1000 PEG3400	DextranT70	Water
r_j' [mol.g^{-1}]	0,0387	0,0272	0,0511
q_j' [mol.g^{-1}]	0,0257	0,0196	0,0778

Table 3.1 *Volume and surface area parameters.*

For the ternary PEG/dextran/water system six interaction parameters should be fitted to experimental data. The polymer-water interaction parameters are determined from osmotic pressure data for the binary systems (see section 3.2). As a first approach it is assumed that the fitted polymer-water interaction parameters are also valid for concentrations higher than those for which osmotic pressure data are available. This assumption is necessary to be able to calculate the activities for the highly concentra-

ted demixing phases.

The polymer-polymer interaction parameters have been fitted to experimental de-
mixing data for the PEG3400/dextranT70/water system [King et al., 1988]. Since the
interaction parameters in the UNIQUAC-model are based on a unit area of interacting
surface, these parameters should apply for all polyethylene glycols and dextrans,
providing the molecules are linear and their conformations are equal to those for the
PEG3400/dextranT70/water system. According to Kang and Sandler [1988a], low-
molecular-weight PEG molecules ($M_n < 1.0 \times 10^4$) are likely to be similar in structure.
Although dextran is not stretched out in solution but behaves almost like an ideal coil,
it may suffice that dextran has the same conformation in both systems. In that case the
statistical weights of contact sites along the chain may be similar. Based on these
assumptions the polymer-polymer interaction parameters for PEG1000 and dextranT70
have been taken to be equal to the interaction parameters for PEG3400 and dex-
tranT70, since no experimental demixing data are available for the PEG1000/dex-
tranT70/water system.

In table 3.2 the fitted interaction parameters are given for PEG1000, PEG3400,
dextranT70 and water. Their values will be discussed later. The experimental and
fitted osmotic pressures of PEG3400 and dextranT70 are depicted in figs. 3.4 and 3.5,
respectively.

Component j	Component k			
	PEG1000	PEG3400	DextranT70	Water
PEG1000	0	-	-8,18	-308,9
PEG3400	-	0	-8,18	-261,4
DextranT70	123	123	0	-215,3
Water	139,7	-105,6	13,06	0

Table 3.2 *Interaction parameters A_{jk} [Kelvin] for the UNIQUAC-model.*

Figures 3.4 and 3.5 show that the description for PEG3400 is excellent, while the
osmotic pressure of dextranT70 is somewhat underestimated at the highest mass
fractions.
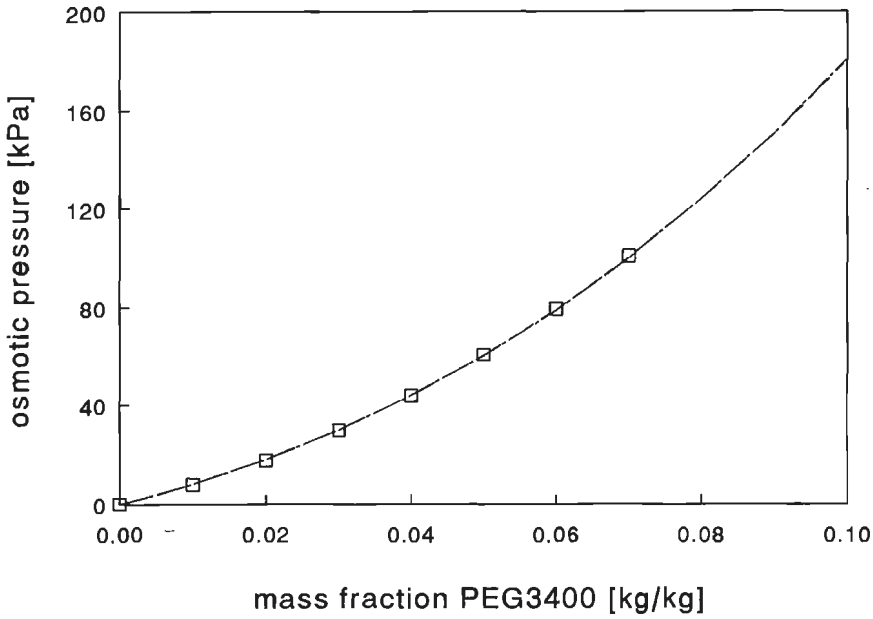
Figure 3.4 *Comparison between the experimental osmotic pressure data for PEG3400 (□) and the model fit according to UNIQUAC (—·—·) and LQCA (- -).*
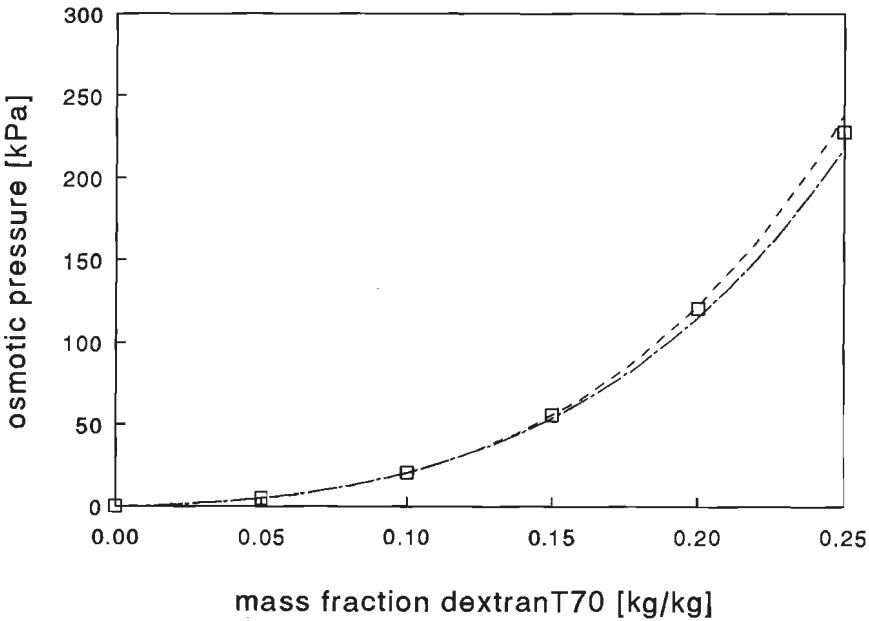
Figure 3.5 *Comparison between the experimental osmotic pressure data for dextranT70 (□) and the model fit according to UNIQUAC (—·—·) and LQCA (- -).*

The interaction parameters $A_{water,PEG}$ for PEG1000 and PEG3400 in table 3.2 seem inconsistent. Their sign is opposite, whereas these interaction parameters are expected to be equal according to the same considerations as presented above for the polymer-polymer interaction parameters. This is the result of a strong correlation between the parameters A_{jk} and A_{ji}. A range of combinations between these parameters for every set of components results in almost identical values for the activities of the three components. Illustrative in this respect is the fact that although the water-polymer interaction parameters for PEG3400 and PEG1000 are totally different, the osmotic pressure of PEG1000 can be predicted very well by means of the polymer-water interaction parameters of PEG3400.

In figs. 3.6 and 3.7 the calculated activity coefficients of PEG3400 and dextranT70 in the binary systems are presented as a function of the mass fraction. The activity coefficients have been calculated relative to the values for the natural logarithm of the activity coefficients at infinite dilution: -966.68 for dextranT70 and -93.73 for PEG-3400. In the relevant concentration ranges $\ln(\gamma_{PEG}^{wt})$ is a linear function of the mass fraction, whereas $\ln(\gamma_{dex}^{wt})$ shows a more than linear increase with mass fraction. The mutual influence of PEG and dextran on the activity coefficients will be discussed in chap. 6.
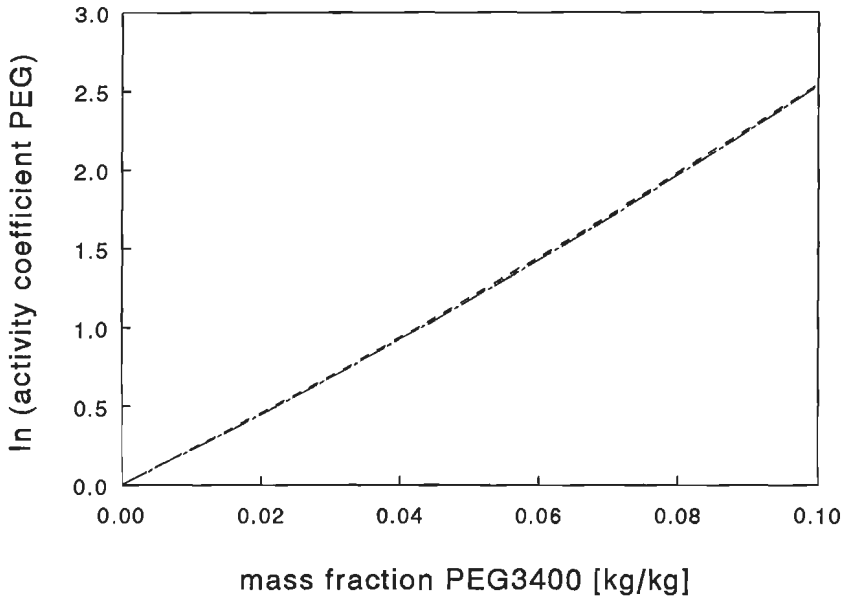
Figure 3.6 *Activity coefficient of PEG3400 as a function of the mass fraction calculated by UNIQUAC (—·—·) and LQCA model (- -).*
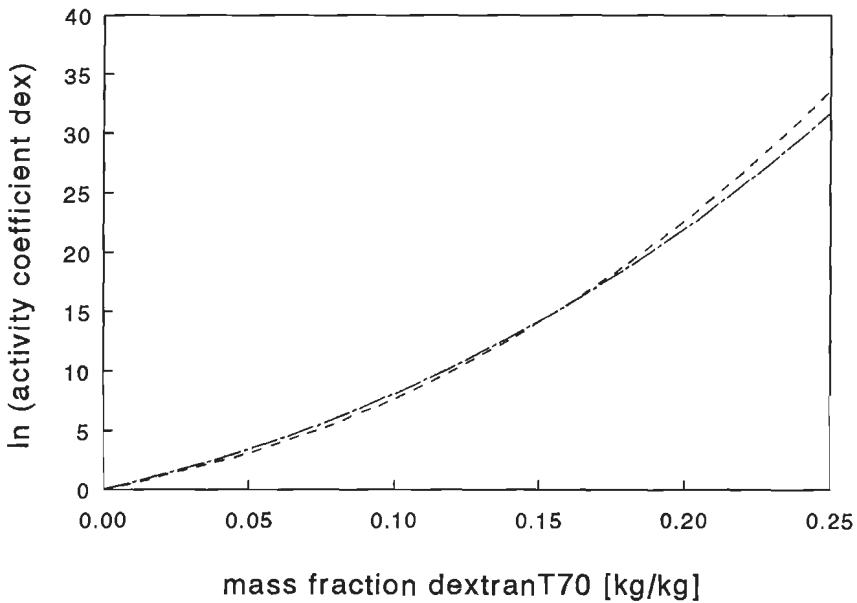
Figure 3.7 *Activity coefficient of dextranT70 as a function of the mass fraction calculated by UNIQUAC (—·—·) and LQCA model (- -).*

LQCA-model

As mentioned in § 3.3.2, the LQCA-model contains only three interaction parameters b_{jk}, which are independent of each other. The polymer-water interaction parameters are again fitted to the binary osmotic pressure data with the polymer-polymer interaction parameters determined from experimental demixing data (Table 3.3). The experimental and fitted osmotic pressures are presented in figs. 3.4 and 3.5 together with the results for the UNIQUAC model. The LQCA model provides the same excellent description of the PEG osmotic pressure as was seen with the UNIQUAC model. A small deviation was found for high mass fractions in the case of dextranT70.

Component j	Component k			
	PEG1000	PEG3400	DextranT70	Water
PEG1000	0	-	*	*
PEG3400	-	0	9,487	117,60
DextranT70	-	-	0	143,46
Water	-	-	-	0

*not determined

Table 3.3 *Interaction parameters b_{jk} [Kelvin] for the LQCA-model.*

The interaction parameter for PEG-water is found to be lower than the interaction parameter for dextran-water. This means that the polymer-water interaction for PEG is stronger than for dextran.

The PEG3400 and dextranT70 activity coefficients are depicted in figs. 3.6 and 3.7, respectively, together with the activities according to the UNIQUAC model. Comparison between both models shows that they both predict a similar relationship between the activity coefficient and the mass fraction. The description of the PEG activity is equivalent for both models. At low mass fractions the activity coefficient of dextran according to the LQCA model is slightly lower than that for the UNIQUAC model; at higher mass fractions the situation is reversed. In view of the mass transport modelling our interest is in the gradient in the activity, $\partial \ln(a)/\partial \ln(x)$, which is equal to the thermodynamic factor as defined in eqn. (2.9) in chapter 2.
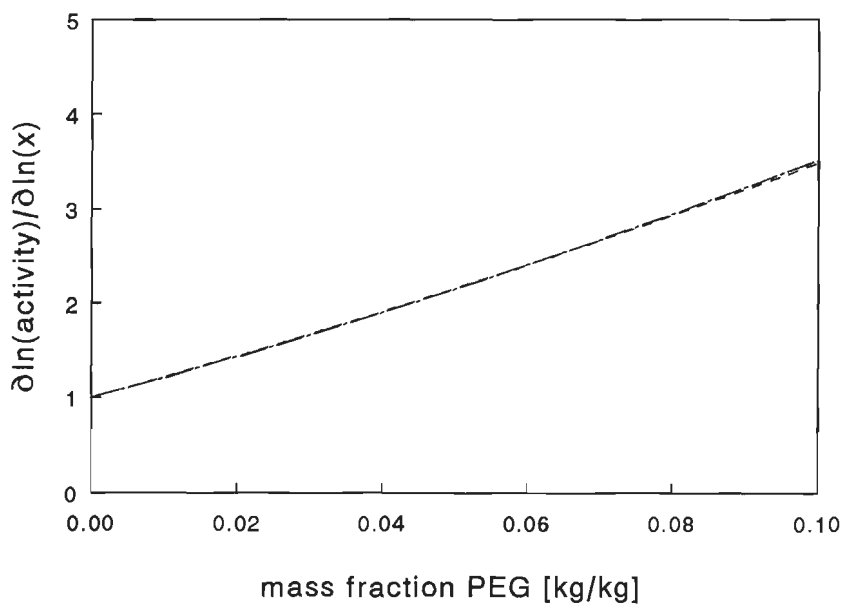
Figure 3.8 *The thermodynamic factor ∂lna/∂lnx for PEG3400 as a function of the mass fraction calculated by UNIQUAC (—·—·) and LQCA model (- -).*
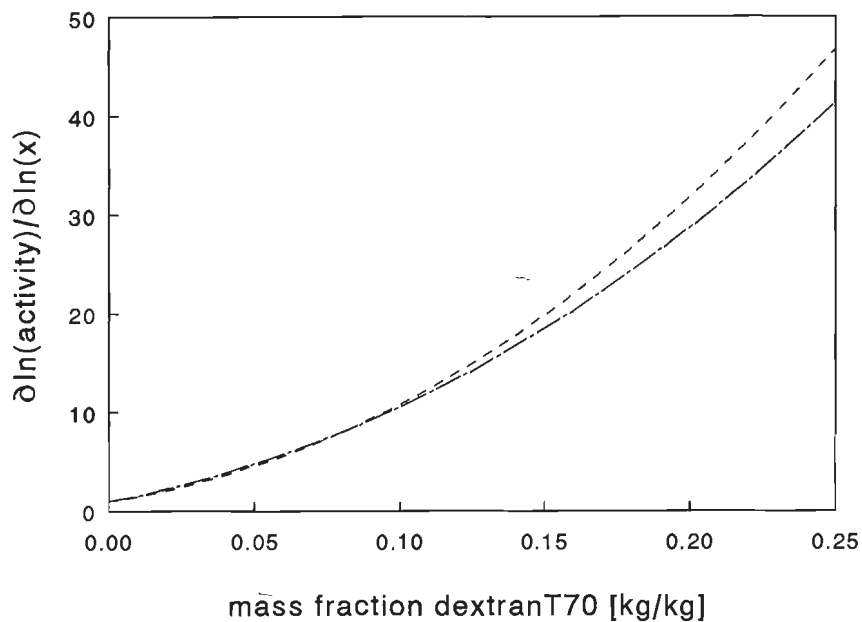
Figure 3.9 *The thermodynamic factor ∂lna/∂lnx for dextranT70 as a function of the mass fraction calculated by UNIQUAC (—·—·) and LQCA model (- -).*

According to figs. 3.8 and 3.9 no difference in gradient for both models is found for PEG3400. A difference of 13% is calculated for dextranT70 at a mass fraction of 0.25.

3.3.4 Conclusions

The thermodynamic activities in a PEG/dextran/water system have been modelled using two types of models: the UNIQUAC-model and the Linearized Quasi-Chemical Approximation (LQCA). The interaction parameters in the models have been fitted to experimental osmotic pressures for the binary systems and the experimental demixing data for the ternary system. Both models provide a reasonable description of the experimental data. Comparing the thermodynamic factor, which characterizes the influence of the thermodynamic activity on the mass transport, it is found that both models predict the same values for PEG3400 and the UNIQUAC-model predicts at most a 13% lower value for dextranT70 in the concentration range used for the filtration experiments.

3.4 Mass transfer in the polarization layer

The mass transfer in the polarization layer is an important factor in the filtration behaviour. Therefore reliable information is needed on the mass transfer coefficient as a function of the experimental conditions in the membrane module. First the mass transfer in the stirred cell will be discussed, subsequently the mass transfer coefficient in the tubular module will be presented.

3.4.1 Stirred cell

Experimental correlations for mass transfer in stirred cells have previously been determined by Marangozis et al. [1962], Kaufmann et al. [1968], Smith et al. [1968; 1972], Colton et al. [1972], Malone et al. [1977] and Mitchell et al. [1986]. All correlations have been written or can be rewritten, in the following form:

$$Sh = A \, Re^P Sc^{0.33}$$

$$Sh = \frac{k_m d_c}{D} \qquad Re = \frac{\rho_b n d_s^2}{\eta_b} \qquad Sc = \frac{\eta_b}{\rho_b D}$$

(3.19)

k_m = mass transfer coefficient [m.s^{-1}]
d_c = diameter cell [m]
D = diffusion coefficient [m^2.s^{-1}]
ρ_b = bulk density [kg.m^{-3}]
n = stirrer speed [s^{-1}]
d_s = diameter stirrer [m]
η_b = bulk viscosity [Pa.s]

Various definitions of the Reynolds number, Re, and Sherwood number, Sh, have been used in literature, but the values of the coefficients presented below have been translated according to the definitions given here (table 3.4). Marangozis et al. have derived a correlation using various types of interfacial transport data, e.g. dissolution of suspended pellets, rotating cylinders, and flat surfaces and electrochemically induced transport. Kaufmann and Leonard studied the mass transfer by dialysis of aqueous sugar solutions. They used a Wilson plot to derive the mass transfer coefficients and obtained a value of 0.390 for A and 0.68 for p (in their case the exponent of Sc was 0.32). However, these coefficients correspond to a line that was different than the one depicted as the best fit in their graph. Therefore we have estimated the coefficients from the line given in their plot and obtained 0.14 for A and 0.75 for p. The value of 0.75 is more in accordance with the powers presented by Kaufmann and Leonard for separate experiments.

Colton and Smith [1972] have determined the mass transfer coefficients by replacing the membrane by an aluminium plate, which contained inserts of compressed benzoic acid at various distances from the centre of the plate. The local mass transfer coefficients were derived from the rate of benzoic acid dissolution by measuring the depth of the benzoic inserts. They found a considerable decrease in mass transfer coefficient going from the edge of the bottom towards the centre in the laminar boundary layer region at Reynolds numbers below 16,560. At higher Reynolds numbers only a decrease in mass transfer coefficient occured at the edge of the bottom, little variation in mass transfer coefficient was found towards the centre. The overall mass transfer coefficient in the laminar region was correlated by A equal to 0.828 and the exponent p of 0.567. In the turbulent region A is equal to 0.145 and p is 0.746. Colton and Smith have compared their results with those of Kaufmann and Leonard, but an error slipped into the translation of Re and Sh. The values obtained from the plot of Kaufmann and Leonard coincide very well with those found by Colton and Smith in the turbulent region, although they have also measured below the transition point from laminar to turbulent.

Anderson and Malone [1977] have determined the overall mass transfer coefficient by evaluating the diffusion rates of potassium chloride. They have found the same dependence on the stirrer speed as Colton and Smith in the laminar region, but the mass transfer coefficients were a factor three lower than those calculated by Colton and Smith. Anderson and Malone suggested that the low porosity of their membranes might affect the mass transfer coefficient. Instead of the cell diameter they used the diameter of the active membrane surface, 16 mm, which was less than the impeller diameter, 25 mm. This might explain part of the large discrepancy with the values obtained by Colton and Smith. Mitchell and Deen [1986] used the oxidation of $Fe(CN)_6^{4-}$ to $Fe(CN)_6^{3-}$ at the surface of a platinum sheet electrode, which replaced the membrane, to evaluate the average mass transfer coefficient. The power of the Reynolds number, 0.537, was in good agreement with that of Colton and Smith in the laminar region, although part of the measurements were carried out at Reynolds numbers, which, according to Colton and Smith, belong to the turbulent region.

regime	pre-factor A	exponent Re	author
$100 < Re < 100,000$ $386 < Sc < 4.8 \times 10^6$	0.635	0.70	Marangozis
$3740 < Re < 70,000$ $387 < Sc < 1622$	0.390 0.14	0.68 0.75	Kaufmann Kaufmann cor.
$16,560 < Re < 42,435$	0.145	0.746	Colton
$4140 < Re < 16,560$	0.828	0.567	Colton
$152 < Re < 1015^a$	0.225	0.58	Anderson
-	*	0.537	Mitchell

* stirrer diameter not available
^{a} characteristic diameter is membrane diameter instead of the cell diameter

Table 3.4 *Coefficients of empirical Sherwood relations taken from literature. The exponent of Sc is 0.33, except for Kaufmann who found 0.32. Upper section for turbulent regime, lower section for laminar regime.*

According to the above mentioned studies two regions exist, which differ in the dependence of the mass transfer coefficient on the Reynolds number. However, the

transition point between the laminar and turbulent regime does not seem to be determined simply by the Reynolds number.

Except for Marangozis, whose correlation deviates considerably from the ones found by Kaufmann and Leonard and by Colton and Smith, the above studies have been performed in stirred cells which are considerably smaller (diameters of 0.02 to 0.076 m) with different types of stirrers (four-bladed paddle and cylindrical bar) than that in the Amicon 2000A cell used in our case: a cell diameter of 0.14 m and a rectangular bar impeller. The Amicon cell was equipped with inserts to support the stirrer axis. Therefore we have decided to characterize the local and surface-averaged mass transfer coefficient using the reduction of ferricyanide, $Fe(CN)_6^{3-}$, to ferrocyanide, $Fe(CN)_6^{4-}$, at the surface of nickel electrodes [Selman, 1978]. The surface-averaged mass transfer coefficient has also been evaluated by heat transfer measurements.

Method

Heat transfer
The heat transfer in a cell can be expressed by the same type of relationship as eqn. (3.19), if Sc is replaced by the Prandtl number, $Pr = \eta c_{heat}/\lambda_{therm}$, and Sh by the Nusselt number, $Nu = \alpha D/\lambda_{therm}$, in which c_{heat} is the specific heat, λ_{therm} is the thermal conductivity and α is the heat transfer coefficient.
In order to determine the heat transfer coefficient, the membrane was replaced by a copper plate in which three thermocouples were installed at various radial distances from the centre to measure the temperature. In the cell two electrical heating elements were placed in order to heat the solution. An identical cell with stirrer was situated beneath the cell through which cooling water was pumped. In that way a temperature difference could be created between the bulk solution and the surface of the plate. Water and an 80 wt% glycerol-water solution were used as bulk liquids. Under steady-state conditions the heat transfer coefficient can be calculated as follows:

$$\alpha = \frac{P_{heat}}{S(T_{bulk} - T_{plate})} \qquad (3.20)$$

in which P_{heat} is the power of the electrical heaters and S is the surface of the bottom. To account for the viscosity difference between the bulk solution and the solution at the plate arising from the temperature differences, the Nusselt relation was multiplied

by $(\eta_b/\eta_w)^q$.

The coefficient for the Prandtl number, Pr, was set to 0.33. The power of the Reynolds number (p) and the viscosity correction (q), and pre-factor, A, were evaluated by double regression of two double logarithmic plots: $Nu/(Pr^{0.33}\cdot(\eta_b/\eta_w)^q)$ vs. Re and secondly, $Nu/(Pr^{0.33}\cdot Re^p)$ vs. $(\eta_b/\eta_w)^q$. The slope of the first plot is equal to the exponent of the Re number, the slope of the second plot provides the value of the exponent of (η_b/η_w). The intersections of both plots at $\log(Re)=0$ and $\log(\eta_b/\eta_w)$ yield the logarithm of the pre-factor.

Electrochemical method

The mass transfer measurements are based on the following electrochemical reactions [Selman et al., 1978]:

$$
\begin{array}{llll}
\text{cathode:} & Fe(CN)_6^{3-} + e^- & \rightarrow \quad Fe(CN)_6^{4-} & E_0 = 0.36V \\
\text{anode:} & Fe(CN)_6^{4-} & \rightarrow \quad Fe(CN)_6^{3-} + e^- & E_0 = 0.36V
\end{array} \tag{3.21}
$$
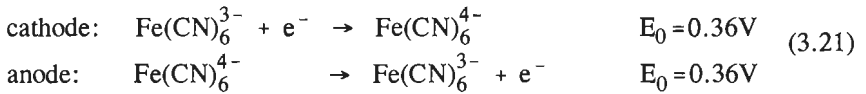
To avoid side reactions the cell was darkened and nitrogen was led over the solution. The mass transfer coefficient was derived from the limiting current condition at which the reaction rate is totally determined by the diffusive transport towards the electrode. In that case the concentration at the electrode surface was virtually zero and the following relationship between the mass transfer coefficient and the limiting current was valid assuming stagnant diffusion:

$$
k_m = \frac{I_{lim}}{n_e F S c_{bulk}} \tag{3.22}
$$

$$
\begin{array}{lll}
k_m & = & \text{mass transfer coefficient } [m.s^{-1}] \\
I_{lim} & = & \text{limiting current } [A] \\
n_e & = & \text{number of electrons } [-] \\
F & = & \text{Faraday's constant } [C.mol^{-1}] \\
S & = & \text{electrode surface } [m^2]
\end{array}
$$

In order to study the variation of the mass transfer coefficient over the membrane surface, the membrane was replaced by a Perspex (polymethylmethacrylate) bottom containing seven concentric nickel rings as nickel electrodes, separated from each other by 2.5 mm Perspex. Moreover, the mass transfer coefficient was evaluated with the bottom containing two nickel electrodes: an outer ring and an inner circle with a

surface area of 72.4×10^{-4} m^2 and 75.4×10^{-4} m^2, separated by 4 mm Perspex. The nickel electrodes in the bottom served as a cathode, while a nickel gauze, placed at the wall above the stirrer, served as the anode. The potential of the working electrode with respect to a calomel reference electrode was kept at a value of -0.4 V by a potentiostat. The solution consisted of 0.01 M ferricyanide, 0.05 M ferrocyanide and 1 M KOH. In order to accurately measure the mass transfer coefficient at low Reynolds numbers, carboxymethylcellulose (CMC) was added to the solution (max. 0.3 wt%) to increase the viscosity. In that case KOH was replaced by K_2CO_3 to prevent CMC from degrading.

Several experiments have been performed in which the distance between the bottom and the stirrer was varied and the volume of the solution in the cell was changed. The mass transfer coefficients derived from the limiting current measurements under the various conditions have been expressed in a Sherwood relation of the form presented in eqn. (3.19). The exponent for the Schmidt number, Sc, was set to 0.33, because it is commonly found for this type of relationships in literature [see above-mentioned articles]. The power of the Reynolds number, p, and pre-factor, A, have been evaluated from the double logarithmic plot of Sh/Sc$^{0.33}$ vs. Re and are equal to the slope and the intercept at log(Re)=0, respectively.

Results

In figs. 3.10 and 3.11 the heat transfer measurements have been depicted in the double logarithmic plots: Nu/(Pr$^{0.33} \cdot (\eta_b/\eta_w)^q$) vs. Re and Nu/(Pr$^{0.33} \cdot$Re^p) vs. $(\eta_b/\eta_w)^q$. Fig. 3.10 shows a linear relationship with log(Re), except at Reynolds numbers below 3000. This deviation at lower Reynolds numbers indicates a transition. The exact nature of this transition is not clear since the slope is higher in the low Reynolds region, which is in contrast with the lower exponent of Re found in literature for the laminar region. The transition point occurs at a value for Re distinctly lower than observed by Colton and Smith, who found a value of 16,560. No indication of a transition was found in that region. The data for Re < 3000 have not been depicted in fig. 3.11. In that case a linear relationship was also obtained. From the double regression the exponent of the Reynolds number was evaluated as 0.66, the pre-factor was 0.36 and the exponent of the viscosity factor was equal to 0.14. These coefficients describe the heat (or mass) transfer coefficient averaged over the total surface of the bottom of the cell. The measurements have been performed for $5 < Pr < 740$.
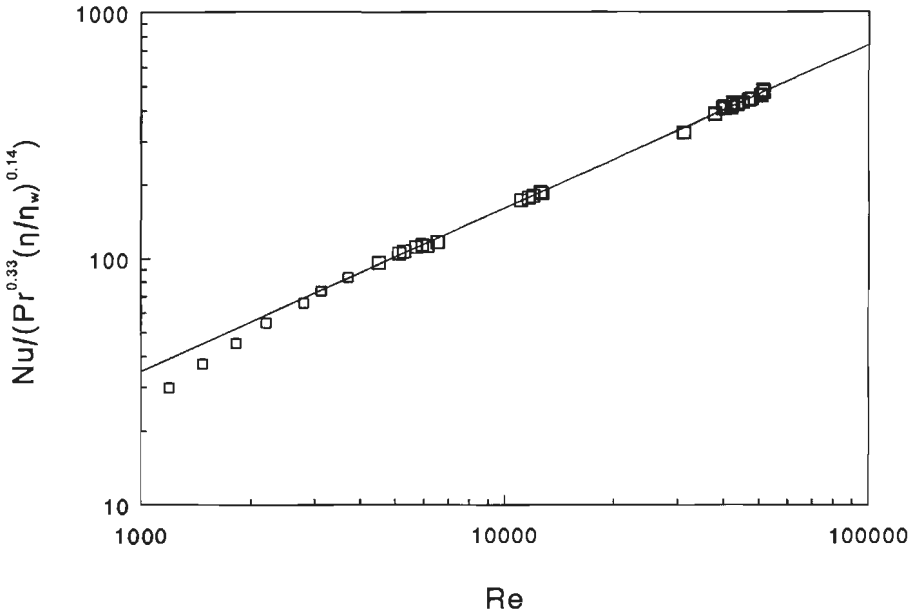
Figure 3.10 *Experimental data and correlation for the surface-averaged heat transfer in the stirred cell as a function of Re determined by heat transfer measurements.*
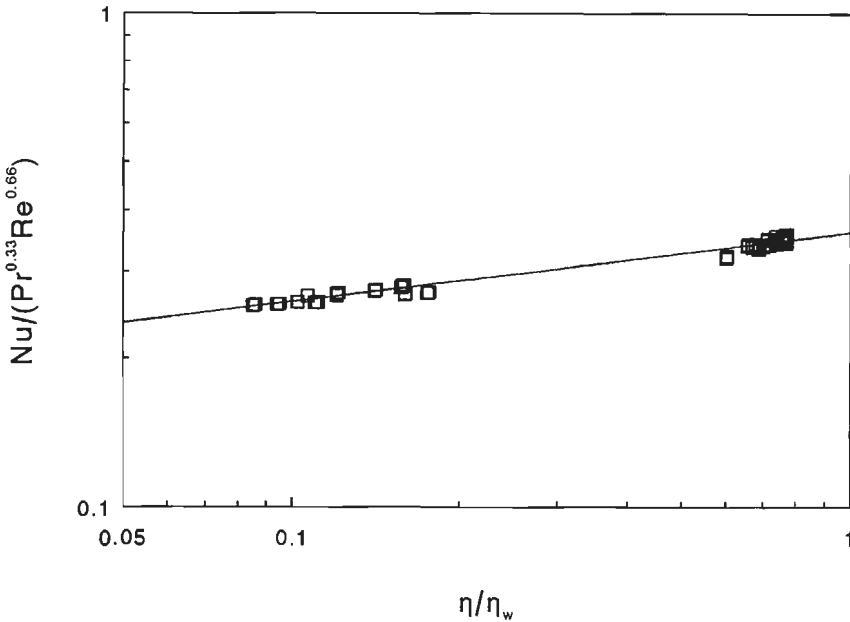
Figure 3.11 *Experimental data and correlation for the surface-averaged heat transfer at the bottom of the stirred cell as a function of (η/η_w).*

The local mass transfer coefficients have been determined by the electrochemical measurements. To illustrate the dependence of the local mass transfer coefficient on the distance to the centre of the cell, $Sh/Sc^{0.33}$ is depicted versus the dimensionless radial distance for various values of Re (fig. 3.12). The limiting current of one ring was evaluated while the same potential was applied to the other rings. The mass transfer coefficient has its lowest value in the center of the cell and increases with increasing radial distance. From a radial distance of about 0.5 of the vessel radius the mass transfer coefficient hardly rises anymore, except near the wall of the cell. The increase near the wall has also been found by Colton and Smith. They reported a more constant value of the mass transfer below a radial distance of 0.8 in a turbulent region at Reynolds numbers between 17,000 and 40,000; the maximum variation in the local mass transfer coefficient was between two and threefold.
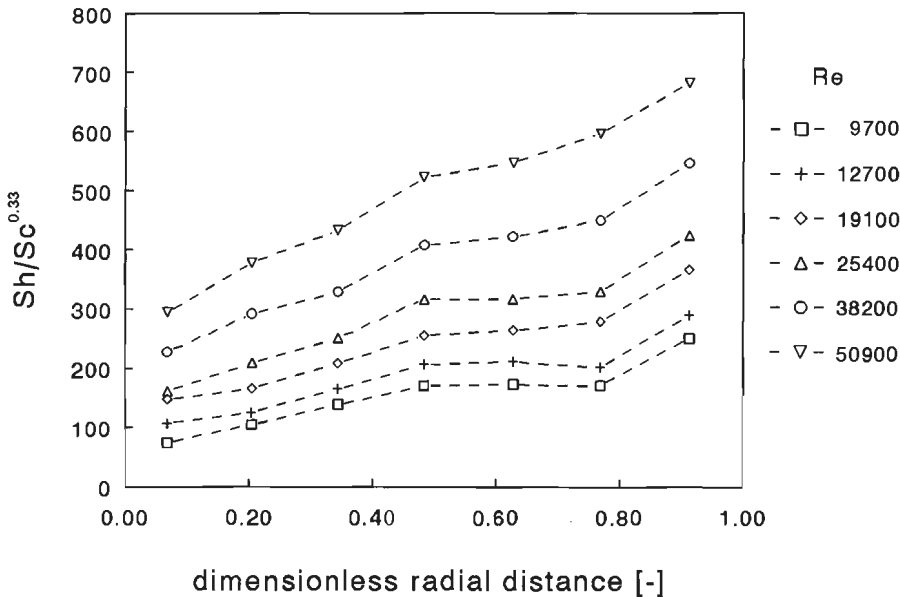
Figure 3.12 *Local mass transfer as a function of the dimensionless radial distance at the bottom of the stirred cell for various Reynolds numbers.*

In order to investigate the consequences of the variation in local mass transfer on the filtration behaviour, a special membrane cell was constructed in which the permeate can be collected in two separate streams: one from the centre part of the cell and the other from the outer ring (discussed in more detail in chaps. 4 and 5). The mass transfer coefficient for both sections has been measured using the bottom with the two

nickel electrodes.

First, the flow pattern in the cell will be considered. According to Colton and Smith spiral-like flow patterns occur below the stirrer in the cell. Thin momentum boundary layers are formed on the impeller, the base and the cylindrical side wall. All radial flow occurs within the boundary layers; fluid flows radially outward in the boundary layer on the impeller, where the effect of centrifugal force is larger than that of the radial pressure gradient. On the base, where the tangential velocity is slowed down, the radial pressure gradient dominates, and the fluid flows inward (see fig. 3.13). Continuity demands an axial upflow. Colton and Smith observed these patterns in flow visualization studies.
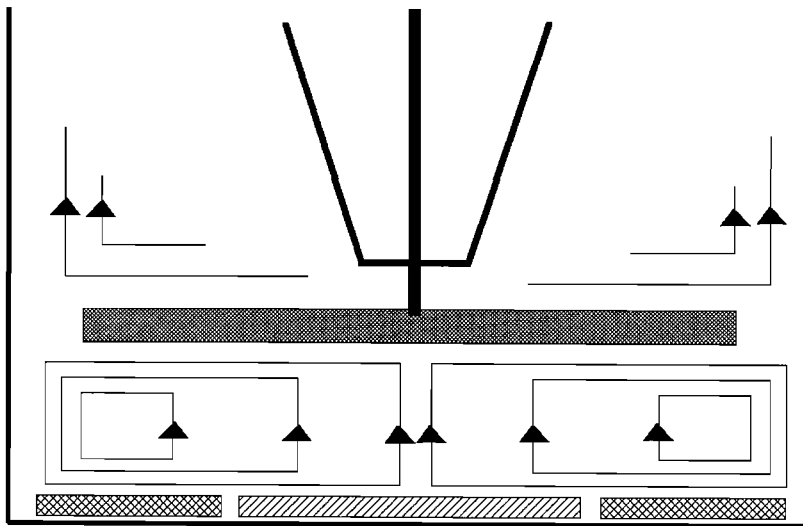
Figure 3.13 *Flow pattern near bottom of the stirred cell.*

To confirm the existence of such flow patterns in our cell we have measured the mass transfer coefficient at the bottom with two nickel electrodes for several situations. First, the mass transfer to each single electrode was evaluated without the other electrode being connected to the potentiostat. The current measurements of each single electrode were repeated with the other electrode connected and the overall mass transfer coefficient for the total bottom was also determined. The results are presented

in fig. 3.14. I represents the inner section, II the outer section. The label 'on' indicates that the other electrode was connected, 'out' means the opposite.
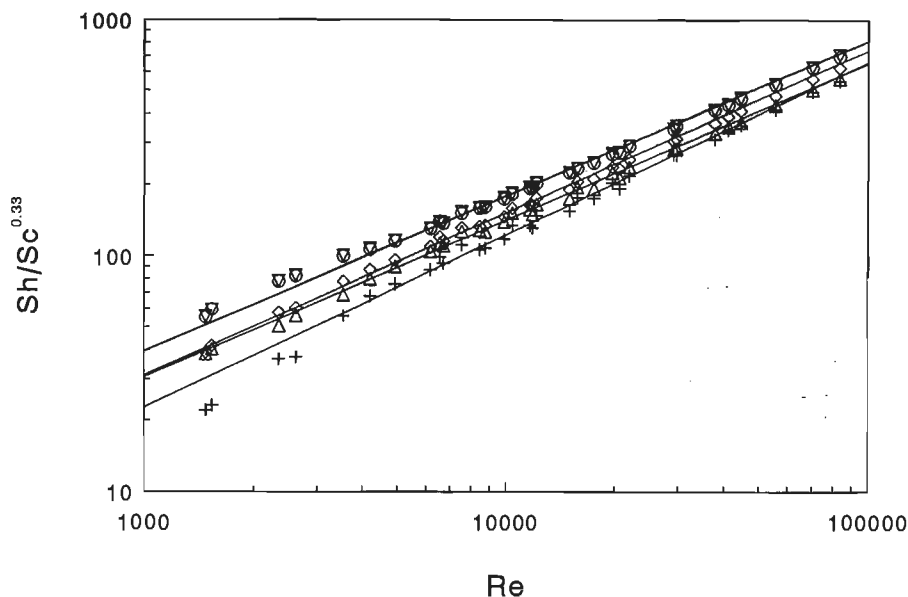
Figure 3.14 *Mass transfer as a function of Re for section I and II. The influence of the presence of a potential in the other section. Section I: II on (+) and II out ($\triangle$); section II: I on ($\bigcirc$) and II out ($\triangledown$); total based on both sections ($\diamond$).*

The measurements show that the mass transfer in the outer section II was not affected, whether electrode I was connected or not. However, the mass transfer in section I lowered considerable when electrode II was connected. This behaviour can be understood if the spiral-like flow pattern is considered. As described above, the radial flow at the base of the cell is inward. If electrode II is connected, part of ferricyanide reacts to ferrocyanide in that region, which implies that less ferricyanide is available in section I. This is in agreement with the lower current and therefore lower mass transfer coefficient in section I compared to the situation with a disconnected electrode II. The inward flow direction is also confirmed by the fact that the mass transfer in section II is not affected by the reaction of ferricyanide in section I. The overall mass transfer is similar to that found for electrode I with disconnected electrode II.

In the same Reynolds region in which a transition was seen in the heat transfer measurements a transition point was also found in section I when the other electrode

was connected. These values for Re were obtained for stirrer speeds below 60 rpm, which might cause insufficient mixing of the bulk solution. This was also suggested by temperature differences in the bulk solution during the heat transfer measurements at such low stirrer speeds. However, the low Reynolds numbers in fig. 3.10 were reached at a stirrer speed of 350 rpm.

Variation of the gap between the bottom and the stirrer from 5 mm to 20 mm slightly influenced the mass transfer coefficients in both sections. In general, the mass transfer coefficient decreased with increasing distance between the bottom and the stirrer (see figs. 3.15a and 3.12b). Since the volume of the solution in the cell decreases during filtration experiments, the influence of a variation in volume from 2.0×10^{-3} to 0.5×10^{-3} m^3 was also studied. The amount of solution has a considerable effect on the mass transfer especially at lower Reynolds numbers. In that region the mass transfer increased with decreasing volume in the cell (figs. 3.16a and 3.16b).

The electrochemical measurements presented above are recent measurements over a large Reynolds number range due to the addition of CMC to the solution. The Sherwood relations used for the calculations in the following chapters were based on previous measurements without CMC. In fig. 3.17 both measurements have been depicted for a gap width of 5 mm and a volume of 2.0×10^{-3} m^3. For clarity only the Reynolds region is shown in which the first measurements (exp. 1) have been performed. For section I the lines match well with a maximum deviation of 6%, in section II the deviation varies from 1% at Re=10,000 to 17% at Re=75,000. The coefficients for both sections and the mass transfer coefficient for the total surface are presented in table 3.5.

	Electrochemical (1)			Electrochemical (2)			Heat
	I	II	total	I	II	total	total
A	0.14	0.29	0.23	0.14	0.42	0.27	0.36
p	0.73	0.70	0.71	0.73	0.66	0.69	0.66

Table 3.5 *The coefficients for the Sherwood relation determined by electrochemical and heat transfer measurements. Electro(1): water; electro(2) water and CMC solutions. I: inner section; II: outer section; total: based on both sections.*
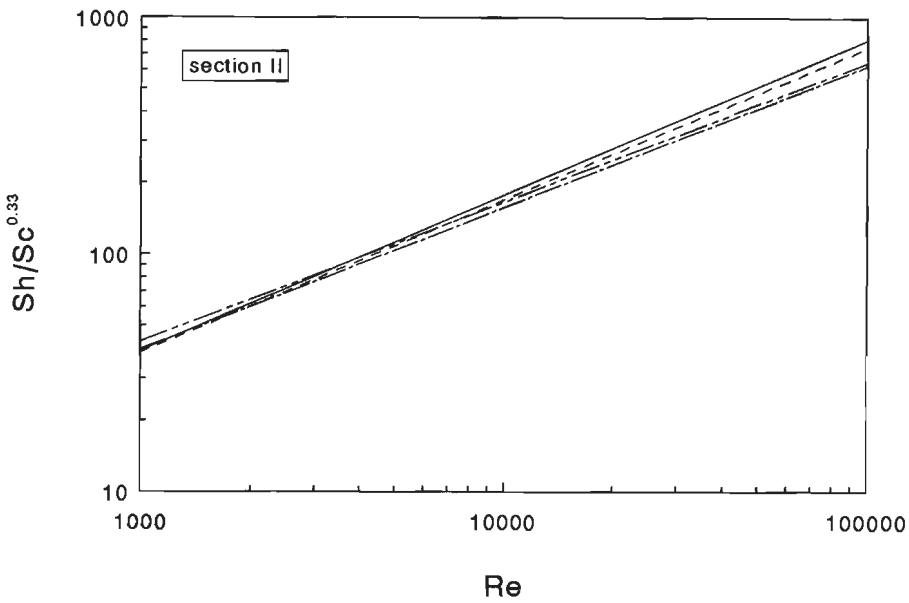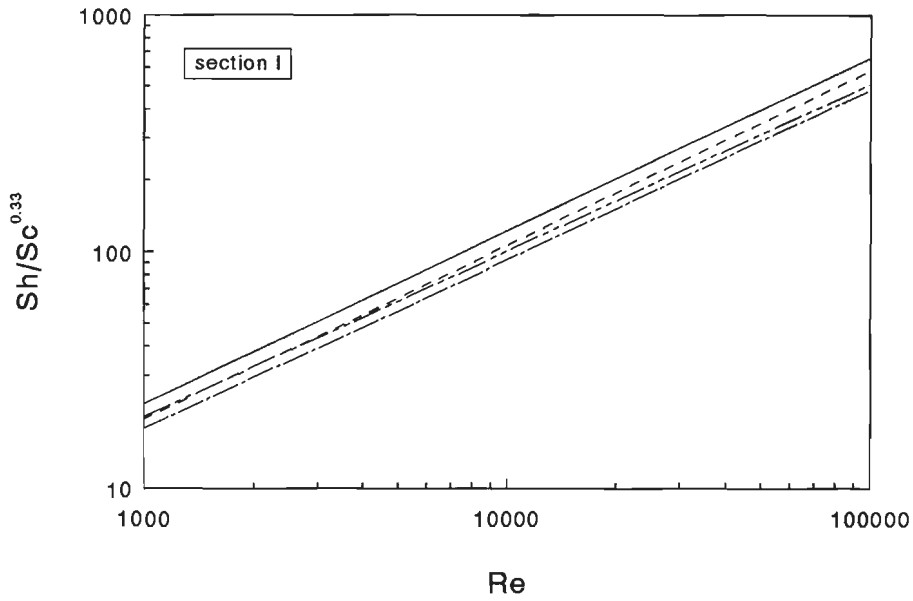
Figure 3.15a *Mass transfer correlations as a function of Re for section I. The influence of the variation in gap width between stirrer and bottom. Gap width: 5 mm (——), 10 mm (- -), 15 mm (—··—) and 20 mm (—·—).*

Figure 3.15b *Idem for section II.*
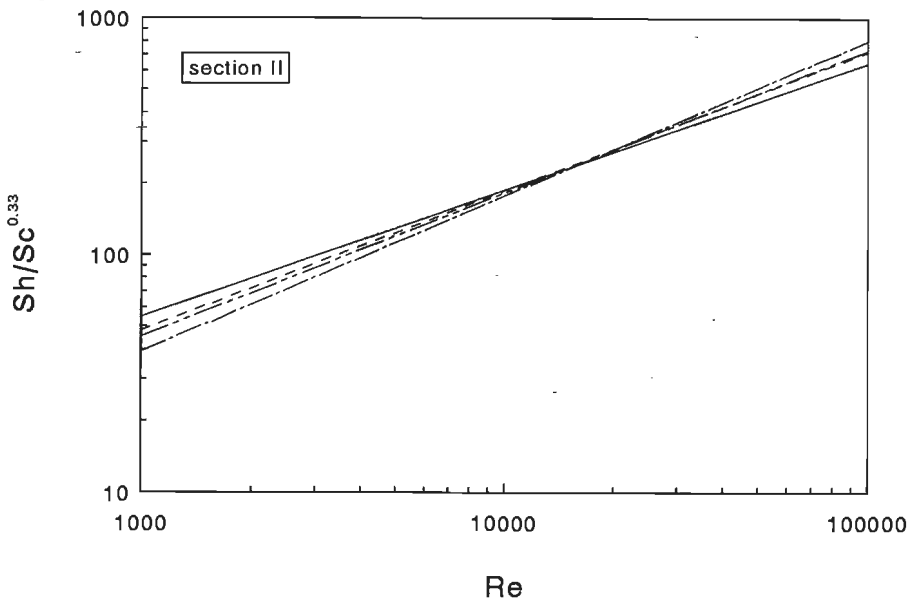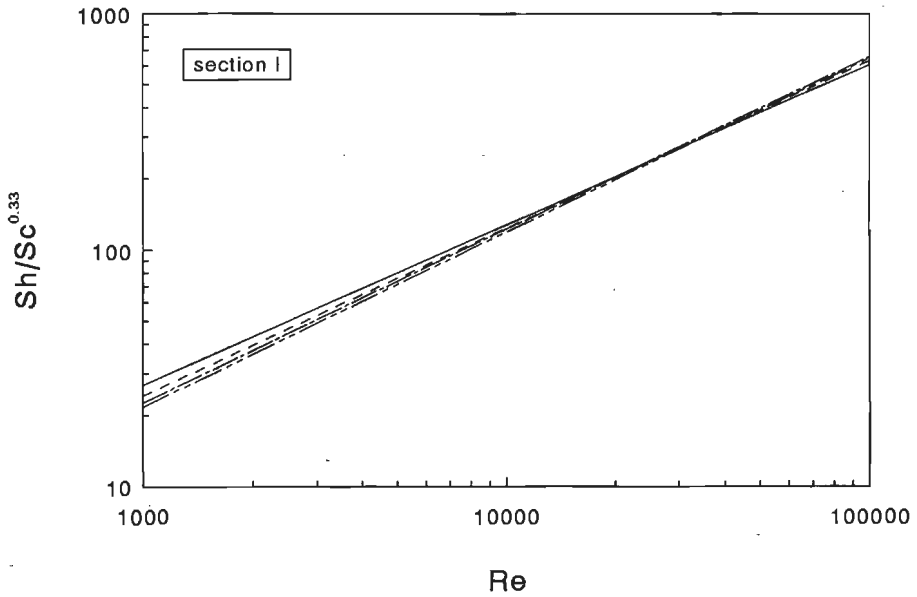
Figure 3.16a *Mass transfer correlations as a function of Re for section I. The influence of the variation in volume of the solution in the cell. Volume: 0.5×10^{-3} m^3 (——), 1.0×10^{-3} m^3 (- -), 1.5×10^{-3} m^3 (—··—) and 2.0×10^{-3} m^3 (—·—).*

Figure 3.16b *Idem for section II.*
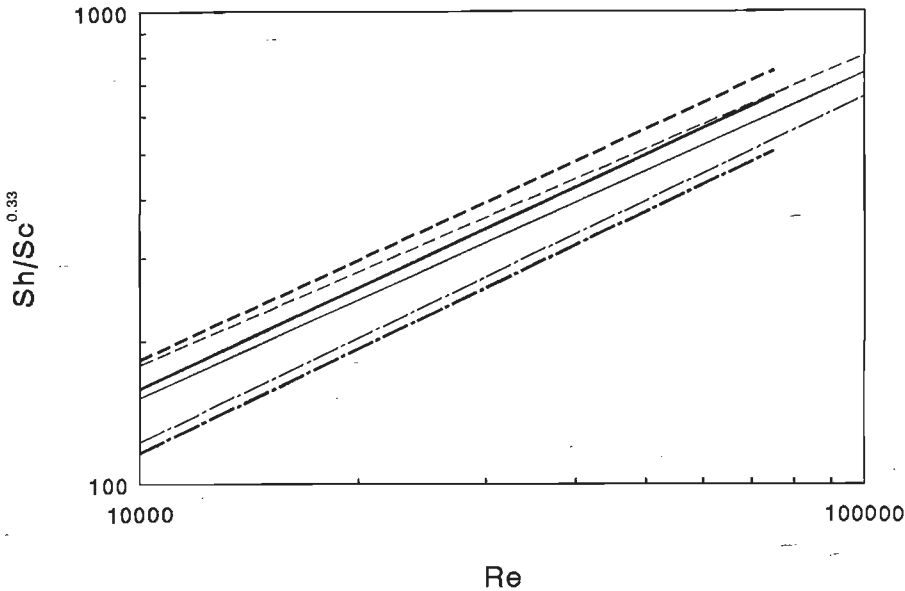
Figure 3.17 *Comparison between mass transfer correlations for two sets of experiments. Section I: (—·—·); section II: (- -); total based on both sections: (——). Thick lines for exp(1): water; thin lines for exp(2): water and CMC solutions.*

In fig. 3.18 the mass transfer relationships obtained in this study are compared with those found in literature for the entire bottom. Although the configurations of the cell and the impeller are not identical, the agreement with the corrected results of Kaufmann and the values from Colton in the turbulent regime is rather good, especially for the second set of electrochemical measurements. The variation in the slope of the lines, equivalent to the exponent of Re, is compensated for by the change in the prefactors. The heat transfer measurements appear to correspond closely to the mass transfer measurements. However, electrochemical measurements have shown that the installation of the heating elements in the cell caused a 35-40% decrease in the mass transfer coefficient. This means that without electrical heaters the heat transfer coefficients are distinctly higher than the electrochemically measured mass transfer coefficients. It is not clear whether this could be attributed partially to the much smaller value of Pr compared to that for Sc.

Except for Kaufmann and Leonard, who used a permeable membrane, all measurements have been performed with non-permeable surfaces with a constant surface

concentration over the entire bottom. Smith [1968] and Colton [1972] have shown that the mass transfer coefficient increases with decreasing mass transfer coefficient in the membrane to a maximum of 26% for the laminar region. They have not evaluated the effect in the turbulent regime, but they expect a smaller dependence on the mass transfer coefficient in the membrane.
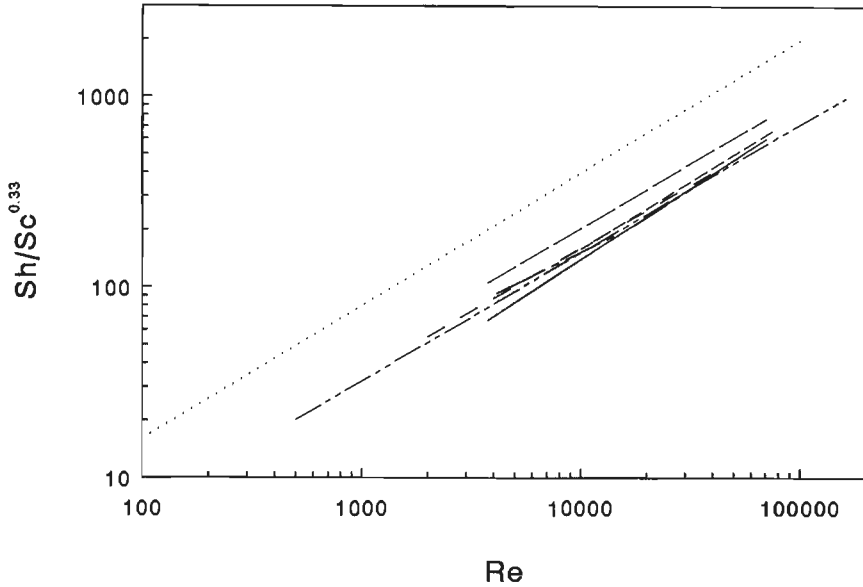
Figure 3.18 *Comparison of the surface-averaged mass transfer correlations with empirical mass transfer correlations from literature. Electrochemical (1): (- -); electrochemical (2): (—··—); heat: (— —); Marangozis: (···); Kaufmann: (——); Kaufmann, corrected: (——); Colton: (—·—).*

Summarizing, the heat transfer coefficients in the stirred cell were higher than the electrochemically measured mass transfer coefficients. In the higher Reynolds number region the mass transfer coefficients agree well with the empirical correlations of Colton and Kaufmann. The slope of the correlations differs from the results found by Colton for low Reynolds numbers. Considerable decrease in local mass transfer rate was found starting from the edge of the bottom of the vessel to the centre, which provided a motivation to divide the filtration cell into two different permeate sections. Due to the inward flow near the base of the vessel the mass transfer in the center is influenced by the situation in the outer section. The extent of the influence is different for the electrochemical measurements and the filtration measurements on the membra-

ne, since in the latter case the surface concentration is not constant. The mass transfer coefficients during membrane filtration are probably somewhat higher than those determined electrochemically.

3.4.2 Tubular membrane

The mass transfer coefficient in the tubular membrane has been described by the experimental correlation derived by Sieder-Tate [1936] for heat transfer in pipe-flow. Translated to the mass transfer situation the correlation has the following form:

$$Sh = 0.023 Re^{0.8} Sc^{0.33} (\eta/\eta_w)^{0.14} \tag{3.23}$$

The Reynolds number Re has been defined as $\rho_b u_{circ} d_h/\eta_b$. This relationship is valid for $Re > 10^4$ and $Sc > 0.5$. For the pre-factor a value of 0.027 has also been reported.

Appendix: Physical properties

Viscosity

Polyethylene glycol (PEG)
The viscosity of PEG solutions has been described with the following relationship [Thomas et al., 1960]:

$$\frac{\eta_{sp}}{C} = [\eta] + k'[\eta]^2 C \qquad (A.1)$$

η_{sp} = specific viscosity of solution [-]
C   = solute concentration [g.dl^{-1}]
$[\eta]$ = intrinsic viscosity [dl.g^{-1}]
k'   = constant (= 0.33 for most polymers)

The specific viscosity η_{sp} is equal to:

$$\eta_{sp} = \frac{\eta - \eta_{water}}{\eta_{water}} \qquad (A.2)$$

η = viscosity of solution [Pa.s]
η_w = viscosity of water [Pa.s]

The intrinsic viscosity can be expressed as follows [Amu, 1982]:

$$[\eta] = 6.04 \cdot 10^{-5} M_n^{0.90} \qquad (A.3)$$

M_n = number-averaged molecular weight [g.mol^{-1}]

Dextran
The viscosity of dextranT70 as a function of concentration and temperature is represented by the following expressions [René et al., 1991]:

$$\ln \eta = a + b \ln T \qquad (A.5)$$

η = viscosity of solution [Pa.s]
T   = temperature [°C]
in which:

$$a = -5,078 + 3,428 \cdot 10^{-2}C - 1,133 \cdot 10^{-4}C^2 + 2,298 \cdot 10^{-7}C^3$$
$$b = -5,972 \cdot 10^{-1} - 2,409 \cdot 10^{-3}C + 1,583 \cdot 10^{-5}C^2 - 4,279 \cdot 10^{-8}C^3 \tag{A.6}$$

This relationship is valid for $0 \leq C \leq 300$ kg.m^{-3} and $20 \leq T \leq 40$ °C.

Bovine Serum Albumine (BSA)

Kozinski et al. [1972] have derived the following relationship for the viscosity of BSA in [Pa.s] as a function of the concentration:

$$\frac{1}{1000\eta} = 1.11 - 0.00542C + 6.71 \cdot 10^{-6}C^2 \tag{A.7}$$

The maximum concentration is 500 kg.m^{-3}.

Diffusivity

Polyethylene glycol (PEG)

Van der Linden [1973] has determined the mutual (Fick) diffusion coefficients of PEG in a Killmann diffusion cell [Killmann, 1964] using a Rayleigh interferometer [Svensson, 1950] for a range of molecular weights from 62 to 3400. The diffusion coefficient of PEG1000 was found to be constant in the concentration range up to 70 kg.m^{-3} and was equal to 2.61×10^{-10} m^2.s^{-1}. The diffusion coefficient of PEG3400 was a linear function of the mass fraction:

$$D_{Fick} = \left(5w_{PEG} + 1.37\right) \cdot 10^{-10} \qquad w_{PEG} < 0.07 \text{ kg.kg}^{-1} \tag{A.8}$$

In order to estimate the diffusion coefficient of PEG6000 use was made of the relationship between the diffusion coefficient of PEG at infinite dilution and the molecular weight for $62 < M < 3400$: $8.6 \times 10^{-9} \cdot M^{-0.5}$ (factor derived from figure). According to equation A.8 the diffusion coefficient at infinite dilution is equal to 1.11×10^{-10} m^2.s^{-1}. The increase of the diffusion coefficient of PEG6000 with the mass fraction will be stronger than the one reported for PEG3400.

Dextran

The Fick diffusion coefficient of dextranT70 as a function of the concentration has been determined by Clifton [1982]:

$$D_{Fick} = 5.96 \cdot 10^{-11} + 2.12 \cdot 10^{-11} \tanh(0.0284C - 1.491) \qquad (A.9)$$

The maximum concentration was equal to 200 kg.m^{-3}. The diffusion data obtained by Wijmans [1985] using the boundary layer broadening method coincided very well with this relationship.

Bovine Serum Albumine (BSA)

Phillies [1976] measured mutual diffusion coefficients with quasi-elastic light scattering spectroscopy. Tirmizi [1990] described the diffusion data for pH=4.6-5.0 in a phosphate buffer of 0.3 M and an acetate buffer of 0.25 M with the following linear relationship:

$$D_{Fick} = (6.1 - 0.0475C) \cdot 10^{-11} \qquad (A.10)$$

The diffusion coefficients derived from ultrafiltration experiments by Probstein [1979] had a similar decrease with the concentration for a 0.1 M acetate buffer. Diffusion data obtained by Keller [1971] in a diaphragm cell indicated a much stronger decrease with concentration.

The diffusion data from Phillies for pH=7.2-7.4 in a 0.15 M NaCl solution showed considerable scattering. The diffusion coefficient was approximated up to a concentration of 50 kg.m^{-3} by the following equation :

$$D_{Fick} = (5.2 + 0.022C) \cdot 10^{-11} \qquad (A.11)$$

At this pH the diffusion coefficient increases with concentration in contrast to the results for the diffusion coefficient near the isoelectric point pH=4.7.

For additional data: see next page.

Additional data

	PEG1000	PEG3400	PEG6000	dextran T70	BSA
M_w [g.mol^{-1}]	1,023	3,600	7,250	98,000	69,000
M_w/M_n	1.13	1.18	1.27	1.9	-
ρ [kg.m^{-3}]	1,200	1,204	1,125	1,600	1,340
V [mol.m^{-3}]	8.33×10^{-4}	2.82×10^{-3}	5.33×10^{-3}	4.56×10^{-2}	5.15×10^{-2}
d_{par} [nm]	1.62[a]; 1.95[b]	3.10[a]; 3.56[b]	4.41[a]	12.0[c]	4×4×14[d]

a Tremblay [1992]
b van der Linden [1973]
c Granath [1967]
d Cooney [1976]; mean projected diameter = 8.06 nm

The molecular weight measurements have been performed in the laboratory of Pfennig and Gaube, Technische Hochschule Darmstadt. The experimental set-up and method used for these measurements were described by Connemann [1992].

4. UNSTEADY-STATE FLUX BEHAVIOUR IN RELATION TO THE PRESENCE OF A GEL LAYER

4.1 Introduction

Several models are available to describe the flux behaviour during ultrafiltration. The osmotic pressure model [Kozinski et al., 1972; Goldsmith, 1971] and the boundary layer resistance model [Wijmans et al., 1985] are based on the formation of a polarization layer. According to the gel-polarization model [Blatt et al., 1970] also a gel layer is formed at the membrane surface.

The question which of the models is 'correct' has caused years of discussion [Jonsson, 1984; Fane, 1983]. Nowadays most researchers seem to recognize that the gel layer model and the osmotic pressure model describe two different physical phenomena.

For our study of the interactions of solutes near the membrane surface it is important to know whether a gel layer is present or only a polarization layer. A gel layer can be several times thicker than a polarization layer. It is expected that solutes experience more hindrance if a gel layer of a rejected component is permeated than in the case a polarization layer of a rejected component is passed. Information may be obtained about the amount of solute present near the membrane surface by studying the flux behaviour of solutions in which only the rejected component is present.

As shown by Wijmans the three models mentioned above predict almost equivalent permeate fluxes under steady-state conditions, especially at higher concentrations [Wijmans et al., 1984 and 1985]. For this reason it is very difficult to conclude from experimental steady flux data which mechanism is valid. Trettin and Doshi [1981] showed that flux measurements in an unstirred cell at various pressures can be used to determine whether the pressure independent ultrafiltration is gel-limited or osmotic pressure limited. The concentration at the membrane surface is pressure independent in the gel-limited case, whereas in the osmotic pressure limited case the concentration at the membrane surface is a function of pressure. However, especially when the osmotic pressure is a strong function of the concentration the pressure range must be carefully chosen in order to find a discernable change in the concentration at the membrane surface.

Since the polarization layer and the gel layer can differ considerably in layer thickness we expect a difference in flux behaviour in a stirred cell under unsteady-state conditions as a result of the time needed to build up the layers. The amount of solute transported to the membrane surface for the formation of a gel layer can be several

times larger. Therefore the formation of the gel layer will take longer than the build-up of the polarization layer. This leads to a different flux behaviour during the period that the layers are build up and the steady-state flux is not yet reached.

In this paper we will describe the unsteady-state behaviour of two model components: dextran and silica. Silica is known to form a gel layer under certain conditions [Stakic et al., 1989; Frolov et al., 1978]. Dextran solutions cause considerable osmotic pressures and their filtration is likely to be osmotic pressure limited [Wijmans et al., 1985; Jonsson, 1984]. Experimental fluxes under unsteady-state conditions will be compared with fluxes predicted by the gel-polarization and the osmotic pressure model. Since according to Wijmans et al. [1985] the boundary layer resistance model is equivalent to the osmotic pressure model, it is not considered separately. An attempt will be made to discriminate between gel-limited and osmotic pressure limited filtration based on the unsteady-state flux measurements.

4.2 Theory

Concentration polarization

Both the osmotic pressure model and the gel-polarization model incorporate the phenomenon of concentration polarization (fig. 4.1) [van den Berg, 1988]. Based upon the film theory the formation of a polarization layer can be described with the following equation:

$$\frac{\partial C}{\partial t} = -v\frac{\partial C}{\partial z} + D\frac{\partial^2 C}{\partial z^2} \tag{4.1}$$

Initial and boundary conditions:

$t=0 : 0 \leq z \leq \delta_{pol}$ $C = C_b$

$t>0 : z = 0$ $C = C_b$

       $z = \delta_{pol}$ $v{\cdot}C_m = D\,(\partial C/\partial z)_{z=\delta pol} + v{\cdot}C_p$

The diffusion coefficient D is taken constant.
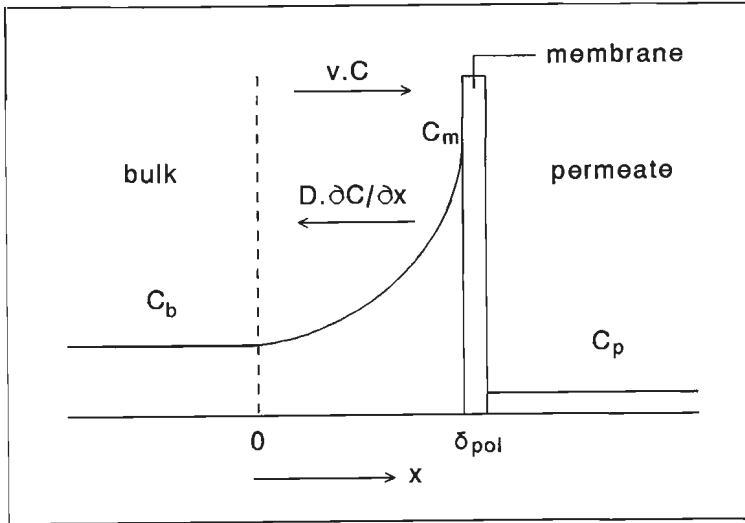
Figure 4.1 *Concentration polarization.*

Osmotic pressure model

To describe the permeate flux the osmotic pressure caused by the enhanced concentration at the membrane surface is taken into account [Goldsmith, 1971]. The permeate flux is given by

$$v = \frac{\Delta P - \sigma \Delta \Pi}{\eta_p R_m} \qquad (4.2)$$

$\Delta\Pi$ is the osmotic pressure at the high-pressure side of the membrane minus the osmotic pressure at the permeate side of the membrane. If the solutes used are nearly completely rejected the osmotic pressure at the permeate side can be neglected and the osmotic reflection coefficient can be set equal to one. $\Delta\Pi$ can be expressed as a function of the concentration at the membrane surface C_m [Flory, 1953]:

$$\Delta\Pi = A_1 C_m + A_2 C_m^2 + A_3 C_m^3 \qquad (4.3)$$

A_1, A_2 and A_3 are the virial coefficients.

Solving equations (4.1)-(4.3) the ultrafiltration flux can be calculated as a function of time. After the polarization layer has been built up the equation for steady flux is used instead of eqn. (4.1):

$$v = k_m \ln\frac{C_m - C_p}{C_b - C_p} \tag{4.4}$$

where $k_m = D/\delta_{pol}$ is the mass transfer coefficient in absence of a net flux. The change in the bulk concentration due to the batch filtration is taken into account.

Gel-polarization model

In the gel-polarization model the flux decline with increasing bulk concentration during ultrafiltration is explained by the formation of a gel layer [Blatt et al., 1970]. The gel-polarization model is based on the assumption that the concentration at the membrane surface can not exceed a certain value, the gel concentration C_g. Starting a filtration first the formation of a polarization layer takes place. After the gel concentration has been reached the net solute flux does not lead to a further increase of the concentration at the membrane surface but to an increasing thickness of the gel layer, δ_g:

$$\rho_g \frac{\partial \delta_g}{\partial t} = v \cdot C - D\frac{\partial C}{\partial z} - v \cdot C_p \tag{4.5}$$

Although the concentration at the membrane surface does not change during the build-up of the gel layer the concentration profile in the polarization layer still changes due to a decrease in flux. We assume that the amount of solute necessary for the accumulation of the concentration in the polarization layer is negligible compared with the material needed to build up the gel layer. The influence of the change of the concentration profile on the back-diffusion due to the decrease in flux is taken into account in the model calculations. Integration of eqn. (4.5) with respect to x at given t with the boundary conditions $x=0$, $C=C_b$ and $x=\delta_{pol}$, $C=C_g$ provides a relationship for the net solute flux at each permeate flux v:

$$\rho_g \frac{\partial \delta_g}{\partial t} = v \frac{e^\alpha C_b - C_g}{e^\alpha - 1} - v \cdot C_p \tag{4.6}$$

where $\alpha = v \cdot \delta_{pol}/D$ and $\delta_{pol} = D/k_m$.

Taking the resistance of the gel layer into account the flux is expressed by the following equation:

$$v = \frac{\Delta P - \sigma \Delta \Pi}{\eta_p (R_m + R_g)} \qquad (4.7)$$

If the gel layer is considered as a packed bed of solute particles or molecules the resistance R can be calculated by [Kerkhof et al., 1988]:

$$R_g = \frac{170(1-\varepsilon)^2}{\varepsilon^3 d_{par}^2} \delta_g \qquad (4.8)$$

Equations (4.1) and (4.2) are used to calculate the time needed to reach C_g. The flux during the formation of the gel layer is found by solving eqns. (4.6)-(4.8). Besides the increase in the bulk concentration due to the permeation of solvent also changes in bulk concentration through the formation of the gel layer are taken into account. Part of the solute is located in the gel layer and does not participate in the bulk concentration. For the calculations of the bulk concentration only the amount of solute actually present in the bulk solution is used.

4.3 Experimental

Materials

Dextrans of different molecular weights were used for the ultrafiltration experiments: dextran T250 (MW=266,000 Da, ICN chemicals), dextranT70 (MW=73,500 Da, Sigma Chemical) and dextranT40 (MW=39,000 Da, Sigma Chemical). Silica particles (Aerosil 200, primary particle diameter=12 nm) were obtained from Degussa.

The dead-end ultrafiltration experiments were performed with asymmetric YM5 and YM10 membranes having a MW cut-off of 5000 Da and 10000 Da respectively (regenerated cellulose acetate, Amicon). The rejection of the solutes/particles was > 99%

Apparatus and procedure

Flux measurements with dextran were carried out in a stirred batch cell (Amicon, type 2000A). The diameter of the cell was 14×10^{-2} m. The bar-like stirrer had a diameter of 12×10^{-2} m. The effective area of the circular membrane was 144×10^{-4} m^2 .

The experiments with silica were performed in a similar cell with the possibility to collect the permeate in two separate streams (fig. 4.2). The membrane area connected with the inner permeate section was 67×10^{-4} m^2, the area connected with the outer

section was 75×10^{-4} m^2.

Both cells were pressurized with nitrogen gas and the temperature was controlled with a thermostate. The amount of permeate was determined gravimetrically. The bulk volume at the start of each experiment was 2×10^{-3} m^3.

Before and after each ultrafiltration experiment the pure water flux (PWF) was measured in order to determine the membrane resistance. Both dextran and silica were found not to effect the PWF of the membranes used. Therefore it can be assumed that the flux measurements were not affected by adsorption. Before filtration silica suspended in water was placed in an ultrasonic bath for two hours in order to break up silica agglomerates (except experiment Sil6, which was treated only one hour).The bulk concentration at the start of all experiments was 7 kg/m^3, except for Sil1 where a concentration of 2.5 kg/m^3 was used.
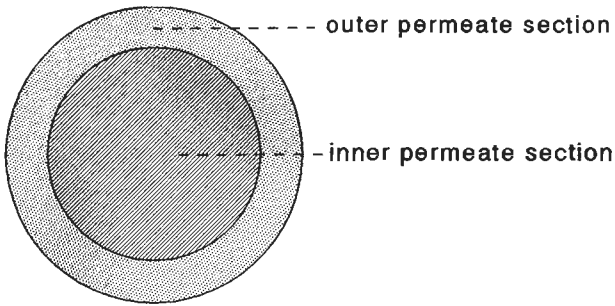
Figure 4.2 *Permeate collection in two separate streams*

4.4 Model parameters

In this section the values for the parameters used for the model calculations are given; first for dextran, next for silica.

Dextran

Osmotic pressure

Several authors present osmotic pressure data for dextran of different molecular weights [Wijmans et al., 1985; de Balmann et al., 1989; Ogsten et al.; 1979]. Figure 4.3 shows the osmotic pressure versus the solute concentration. Comparing the various osmotic pressure data it can be seen that there is not much influence of the molecular weight.
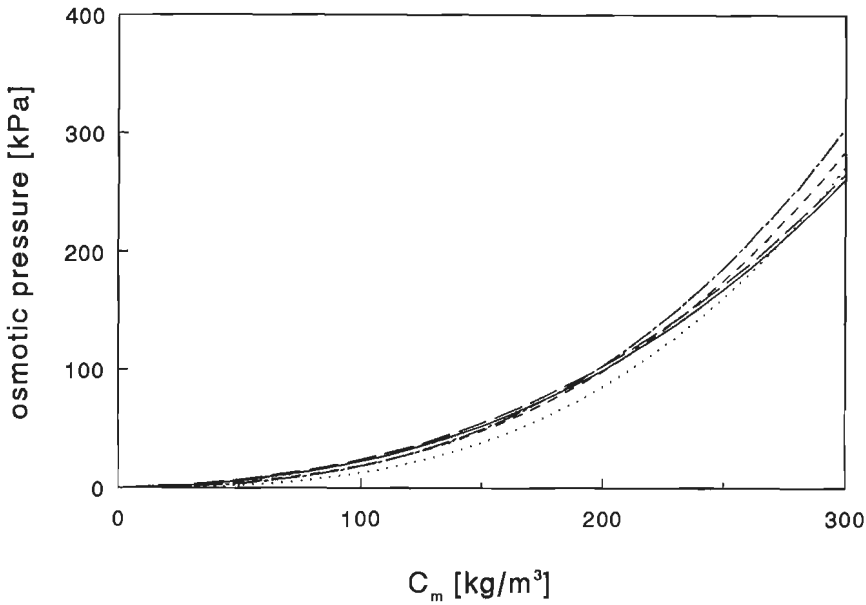
Figure 4.3 *Osmotic pressure for dextran of different molecular weight. (——) T52.5 [Ogston]; (————) T70 [Wijmans]; (- -) T70 [de Balmann]; (—·—·) T500 [Ogston]; (···) T500 [Wijmans].*

For the model calculations the osmotic pressure data of Wijmans [1985] for dextran T70 are used:

$$\Delta\Pi = 35.5 C_m + 0.752 C_m^2 + 76.4 \times 10^{-4} C_m^3 \tag{4.9}$$

Diffusivity

Diffusion coefficients of dextran in water are available for 20 °C [Granath et al., 1967]. Corrected for temperature and solvent viscosity the diffusion coefficients for dextranT40, T70 and T250 are 6.0×10^{-11}, 4.6×10^{-11} and 3.1×10^{-11} (extrapolated) m^2/s respectively.

Viscosity

Dynamic viscosity of dextran solutions is correlated with temperature and concentration according to the following relationship [René et al., 1991]:

$$\ln(\mu) = a + b\ln(T-273) \tag{4.10}$$

in which

$a = -5.078 + 3.428 \times 10^{-2} \, C - 1.133 \times 10^{-4} \, C^2 + 2.298 \times 10^{-7} \, C^3$

$b = -5.972 \times 10^{-1} - 2.409 \times 10^{-3} \, C + 1.583 \times 10^{-5} \, C^2 - 4.279 \times 10^{-8} \, C^3$,

with $0 \le C \le 300$ kg/m^3 and $293 \le T \le 313$ K.

Estimations of the viscosity of dextranT40 and T250 solutions are obtained by correcting the viscosity for dextranT70 by means of the viscosity numbers (0.20, 0.27 and 0.47 for T40, T70 and T250 resp. [Schmidt et al., 1985].

Mass transfer coefficient

According to the osmotic pressure model the concentration at the membrane surface varies with the bulk concentration. Therefore the mass transfer coefficient k_m is not equal to the slope of the flux versus $\ln C_b$ plot (eqn. (4.4), $C_p = 0$). The slope of the plot $\partial v / \partial \ln C_b$ should be corrected for the change in the concentration at the membrane surface in order to get a correct value of k_m [Wijmans et al., 1984]:

$$k_m = -\frac{\partial v}{\partial \ln C_b} \left[1 + \frac{R_m k_m}{r \Delta \Pi} \right] \tag{4.11}$$

in which $\Delta \Pi$ is assumed to be equal to (constant)$\times C_m^r$. According to the fit of the osmotic pressure data restricted to the range of the experimental concentration at the membrane surfaces, r equals to 2.7.

The thus determined values of the mass transfer coefficients are compared with coefficients obtained in our laboratory by means of an electrochemical method [Selman et al, 1978] and by heat transfer measurements (see chapter 3). The measurements were performed in cells that resembles the used membrane cell except for the presence of a membrane. In the electrochemical cell the membrane was replaced by a perspex bottom provided with circular nickel electrodes of the same shape as the two permeate sections in the membrane cell (see fig. 4.2). The heat transfer cell was supplied with a copper bottom that was cooled from underneath.The Sherwood relations obtained with these measurements have the following form (chap. 3):

$$Sh = k_m^* d_c/D = A\,Re^P Sc^{0.33}(\eta_b/\eta_w)^{0.14} \qquad Re > 2000$$

in which the Reynolds number $Re = \rho_b n d_s^2/\mu_b$ and the Schmidt number $Sc = \mu_b/\rho_b D$. The coefficient in factor $(\mu_b/\mu_w)^{0.14}$ is obtained from the heat transfer measurements; the coefficient for Sc is taken from literature [Marangozis, 1962]. The values of the other coefficients in the right term of eqn. (4.12) are presented in table 4.1. The cell used for the filtration of dextran is not divided in two permeate sections. Therefore the surface averaged Sherwood relationship is used to calculate the mass transfer coefficient k_m (table 4.1).

	Inner	Outer	Surface averaged
A	0.14	0.29	0.23
p	0.73	0.70	0.71

Table 4.1: *Coefficients for the Sherwood relations for the inner and outer sections and the surface averaged Sherwood relation.*

Silica

Osmotic pressure
Dextran considerably alters the activity coefficient of water due to the strong interaction between dextran and water. Since silica is expected to show little interaction with water in this respect, it is assumed that the silica suspensions behave almost ideally. Calculation of the osmotic pressure for silica with the Van 't Hoff equation for ideal solutions shows that it is negligible (see also Results).

Gel concentration
At the end of each experiment the gel was removed from the membrane cell. To determine the gel concentration and the weight of silica present in the gel layer the gel was weighed before and after drying. The experimental gel concentrations will be presented in table 4.4.

Diffusivity

To calculate the diffusion coefficient of the silica particles the Stokes-Einstein equation is used:

$$D = \frac{kT}{3\pi\eta_{water}d_{par}} \tag{4.13}$$

Viscosity

Viscosities of silica suspensions were measured in the range of shear rates from 1 to 1600 s^{-1} and concentrations from 7 to 100 kg/m^3 by means of a Rheometrics RFS-2. At low concentrations the viscosity was nearly independent of shear rate. Above 40 kg silica/m^3 the viscosity decreased with increasing shear rate up to a factor of 2. All measured viscosities are higher than expected from the volume fraction of particles. Volume fractions calculated from the relative viscosity on the basis of a virial series of the volume fraction of spheres [de Kruif, 1990] are ten times as high as the actual silica volume fractions. This is an indication for the presence of agglomerates. We will come back to this subject later.

The viscosity at the bulk concentration (7 kg/m^3) had a value of 1.1x10^{-3} Pa.s. Viscosities at concentrations of 80 and 100 kg/m^3 seemed to be equal; values ranging from 1x10^{-2} Pa.s. at low shear rates to 0.5x10^{-2} Pa.s. at high shear rates. The equality of the viscosities at the highest concentrations is most likely due to deformation of the agglomerates, so we may expect that viscosity does not increase so much on a further increase of concentration up to the measured gel concentrations in the order of 200 kg silica/m^3. Based on this assumption an estimate is made for the factor $(\mu_b/\mu_w)^{0.14}$ = $(0.1)^{0.14}$=0.7 for use in eqn. (4.12). The value of this factor may be higher for the outer permeate section as a result of the high shear rates near the membrane in this section.

Diameter particles / Mass transfer coefficient

The primary particle diameter of silica as provided by Degussa is equal to 12 nm. However, the degree of agglomeration of the silica in the suspension is unknown, which causes an uncertainty in the particle diameter. Therefore the diameter of silica is used as a fitting parameter for the gel-polarization model. The aim of the fit procedure is to predict correct values for the fluxes and the weight of silica present in the gel layer.

Besides the particle diameter use is also made of k_m as fitting parameter. Due to the

considerable unsteady behaviour during the experiments with silica it is not possible to derive a value for k_m out of a flux vs lnC_b-plot. First estimates of the values for k_{mi} and k_{mo} (the mass transfer coefficients of the inner and outer sections) are calculated from the experimentally determined Sherwood relations (table 4.1). These relations are obtained by an electrochemical method and by heat transfer measurements as described in more detail under *Dextran.*

4.5 Results
To illustrate the flux behaviour under unsteady-state conditions, first the transient permeate fluxes for batch ultrafiltration experiments with dextran will be presented. Henceforth the response of the permeate flux to a sudden pressure change is discussed. The experiments with silica will be described similarly.

Dextran

Permeate flux during batch ultrafiltration
In figure 4.4 the permeate flux is given as a function of time. Three types of dextran (T250, T70 and T40) were ultrafiltered at 200 kPa and a stirrer speed of 90 rpm.
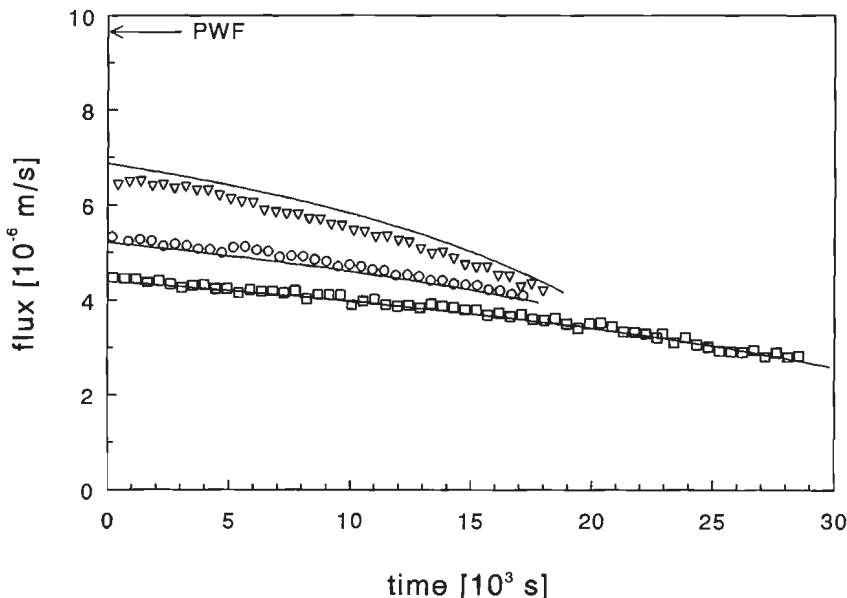
Figure 4.4 *Plot of the flux versus time for dextranT40, T70 and T250. $\Delta P=200$ kPa, $n=90$ rpm. ($\triangledown$) Exp. T40; ($\bigcirc$) Exp. T70; ($\square$) Exp. T250; (——) OPM.*

Experimentally a sudden drop in flux compared to the PWF is observed at the beginning of the filtration of dextran. Afterwards the flux only decreases gradually. The solid lines in figure 4 represent the calculated permeate fluxes according to the osmotic pressure model. Parameters for the model calculations are taken from the data described under Model parameters.

The sudden drop in the flux at the beginning of the filtration of dextran is well described by the osmotic pressure model. According to the model calculations the build-up of the polarization layer takes less than a minute. The osmotic pressure model predicts a strong decline of the permeate flux during the formation of the polarization layer. As a result of the increase of the concentration at the membrane surface the osmotic pressure rises rapidly. A quasi-steady flux is reached which only alters due to changes in the bulk concentration. The change of the bulk concentration during the batch ultrafiltration is slow compared to the rapid formation of the polarization layer. Except for the period necessary to form the polarization layer the flux at each bulk concentration can be considered equal to the corresponding flux in steady situation (eqn. (4.4), $C_p=0$). The experimental permeate fluxes depend on the molecular weight of the dextran. The fluxes calculated with the osmotic pressure model are in good agreement with the experimental fluxes. Lower molecular weight of the solute results in a higher permeate flux, because the back diffusion into the bulk is larger. Due to the higher diffusion coefficient the value for the mass transfer coefficient is higher (table 4.2).

Dextran	n (rpm)	k_m (μm/sec)	k_m^* (μm/sec)
T40	90	2.2	1.8
T70	90	1.6	1.4
T250	90	1.3	1.0

Table 4.2: *Comparison of mass transfer coefficients determined with the flux vs. lnC_b-plot and the surface averaged Sherwood relation.*

Comparison between k_m derived from the flux versus $\ln C_b$ plot and k_m^* calculated with the Sherwood relation shows that k_m is 15-25% higher. It should be noticed that the

values of Schmidt numbers under these conditions are more than an order of magnitude larger compared to the values at the experimental conditions at which the Sherwood relations were determined.

Response of permeate flux to sudden pressure change

An other example of unsteady behaviour of the permeate flux is the response to a sudden pressure change. The pressure was increased from 100 kPa to 200 kPa and after 11000 seconds changed back to 100 kPa. The solute used was dextran T250 (fig. 4.5).
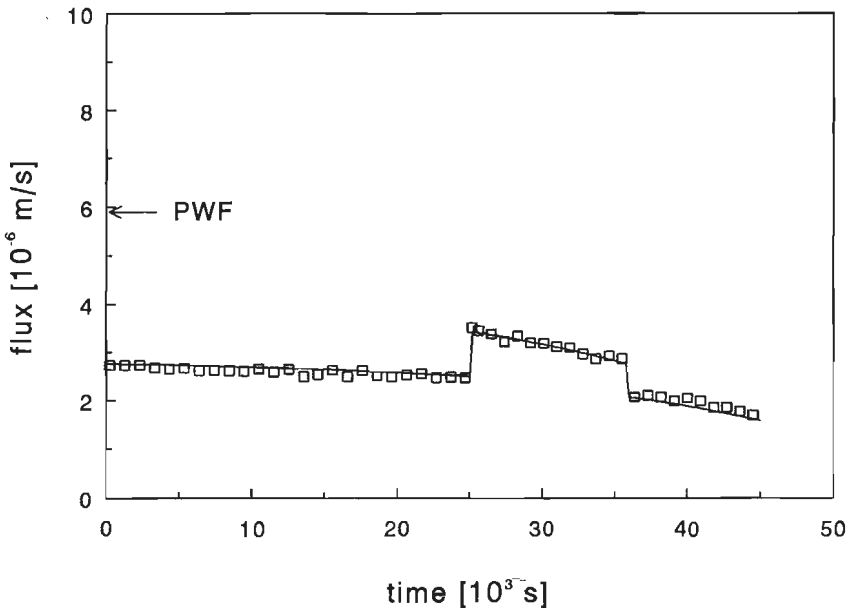
Figure 4.5 *Plot of the flux versus time for dextranT250. n=90 rpm, pressure change: ΔP=100 kPa, 200 kPa, 100 kPa. (□) Exp.; (——) OPM.*

Experimentally it is found that the permeate flux immediately responds to the 100% pressure increase with a 40% increase in permeate flux. This flux behaviour is well predicted by the osmotic pressure model. The doubling of the pressure does not result in a doubling of the permeate flux, because the increase in pressure is partly counter-acted by an increase in osmotic pressure. On account of analogue considerations the decrease of the pressure to 100 kPa does not lead to a 50% decrease of the permeate flux.

At both pressure changes the change of the concentration gradient at the membrane surface is very fast, so almost immediately the quasi-steady permeate flux corresponding to the actual bulk concentration under the new conditions is obtained. The gradual change in flux during the entire experiment is again due to the increase of the bulk concentration with time.

<u>Silica</u>

Permeate flux during batch ultrafiltration

Figure 4.6 shows that for both the inner and outer sections the flux during the filtration of silica decreases gradually, starting from the pure water flux (PWF). A gel layer is observed at the membrane surface. The distribution of the gel layer over the membrane surface is not uniform. At the edge of the membrane the gel thickness is lower than in the middle due to a higher mass transfer coefficient at the edge. Therefore the fluxes in the outer permeate section are higher than in the inner section.
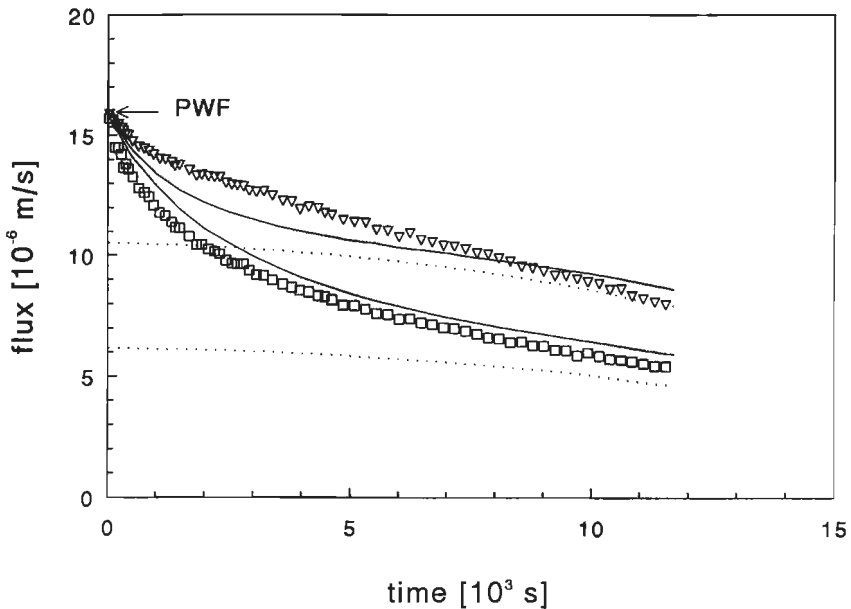
Figure 4.6 *Plot of the flux versus time for silica (Sil4). ΔP=200 kPa, n= 90 rpm. (□) Inner section; (▽) outer section; (——) GPM; (···) quasi-steady flux.*

In figure 4.7 a top view of the gel layer is presented. It shows a fan-shaped pattern of the gel layer. The solid lines represent the highest values for the gel thickness, in

between the gel thickness is lower, superimposed on the already mentioned increase of thickness towards the centre of the membrane.
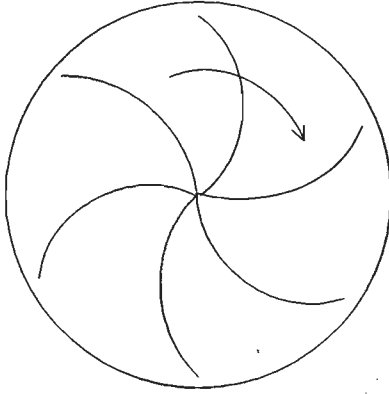
Figure 4.7 *Top view of gel layer. ($\rightarrow$) rotation direction of stirrer.*

No clear relation between the gel concentration and the process parameters is found (see table 4.4). The variation of the gel concentration might be ascribed to variations in the degree of break up of the agglomerates. In experiment Sil6 with only one hour ultrasonic treatment the lowest gel concentration has been determined.

Before the experimental fluxes are compared to the flux calculations with the gel-polarization model a description of the fitting procedure will be given.If the k_m^* values calculated with the Sherwood relations were used model calculations show that it is only possible to predict either correct values for the fluxes or for the weight of silica present in the gel layer but not for both. Therefore it was decided to use silica experiments in which the two permeate fluxes were measured separately (Sil4, Sil5 and Sil6) to fit the mass transfer coefficients, k_{mi} and k_{mo}, for the inner and outer area respectively. The values of the mass transfer coefficients and the particle diameters that give the best fits are presented in table 4.3. Moreover, the values for the mass transfer coefficients calculated with the Sherwood relations k_{mi}^* and k_{mi}^*, are given.

Table 4.3 shows that the electrochemically determined k_{mi}^* and k_{mi}^* are 50-60% smaller than the fitted k_{mi} and k_{mo}. This difference is considerable larger than that for the dextran experiments where the surface averaged k_m^* is 15 to 20% smaller than k_m. The fitted particle diameters have values of 17.5 and 18.5 nm, which is larger than the primary particle diameter of 12 nm. This deviation might be attributed to the presence

of agglomerates but it seems as likely to ascribe it to a compensation for porosity effects in the Kozeny-Carman relation (eqn. (4.8), since porosities of about 90% are extremely high for this relation. The presence of a double layer around the colloidal silica particles can also effect the diameter of the silica particle.The diffusion coefficient used in the Sherwood relation is based on the average value of $d_{par} = 18$ nm taken from table 4.3. As already mentioned by Fane [1984] repulsive forces between the colloidal particles can cause augmented diffusional transport. If a higher value of the diffusion coefficient would be used in the calculation of k^*, the difference between k^* en k becomes smaller. The discussion about the deviations between k^* en k will be extended at the end of this section after all experiments have been dealt with.

Exp.	n (rpm)	k_{mi} (μm/sec)	k_{mi}^* (μm/sec)	k_{mo} (μm/sec)	k_{mo}^* (μm/sec)	d_{par} (nm)
Sil4	90	1.7	0.9	3.1	1.4	18.5
Sil5	90	1.6	0.9	2.8	1.4	17.5
Sil6	90	2.1	0.9	3.5	1.4	17.5

Table 4.3: *Comparison of mass transfer coefficients determined by the fit procedure and by the Sherwood relations for the inner and outer sections.*

The mean values for both k_{mi} and k_{mo} from exp. Sil4, Sil5 and Sil6 are used to fit all experiments and the resulting values of the fitting parameter d_{par} are presented in table 4.4 together with the experimental conditions and results. It is seen that the particle diameters found do not deviate much from the diameters according to the best fits.

The experimental fluxes of experiment Sil4 are compared with the model calculations in which the values of d_{par} and k_m from table 4.3 are used. From figure 4.6 it is seen that the inner permeate flux is rather well described, the outer permeate flux is somewhat underpredicted. This might be explained by the presence of large silica agglomerates (see additional remarks at the end of silica section).
According to the gel-polarization model the permeate flux decreases until quasi-steady flux is reached. The quasi-steady fluxes for the inner and outer permeate section, which only change due to the increasing bulk concentration, are represented by the dotted lines in figure 4.6. The figure shows that the experimental fluxes indeed

during the experiment until the quasi-steady flux is attained.

The long time to reach steady-state is in strong contrast with the time needed during the filtration of dextran. Under the experimental conditions the gradual decrease in unsteady permeate flux clearly indicates the formation of a gel layer.

Exp.	ΔP (kPa)	T (K)	C_0 (kg/m^3)	$C_g{}^b$ (kg/m^3)	M_{sil} (g)	V_{fin} (dm^3)	d_{par} (nm)
Sil1[a]	200	298	2.5	$230 \pm 10\%$	3.11	0.175	13
Sil2[a]	200	298	7	$230 \pm 5\%$	8.21	0.281	17
Sil3[a]	200	318	7	$230 \pm 1\%$	8.75	0.220	15
Sil4	200	298	7	$250 \pm 1\%$	7.06	0.370	19
Sil5	100/200	298	7	$264 \pm 1\%$	5.21	0.555	18
Sil6	200/0/200	298	7	$198 \pm 1\%$	5.86	0.460	16.5

[a]Only one permeate stream.
[b]Density silica $= 2250$ kg/m^3

Table 4.4. *Experimental conditions and results. Values of d_{par} from fit with mean values of k_{mi} and k_{mo} (1.8×10^{-6} and 3×10^{-6} m/s resp.).*

Response of permeate flux to sudden pressure change

To study the influence of the pressure on the permeate flux the pressure was increased from 100 to 200 kPa during the filtration of a silica suspension (Sil5).Experimentally it is found that for both the inner and outer permeate section the sudden pressure increase with 100% immediately results in an 100% increase of the permeate flux (fig. 4.8). This is in agreement with the flux behaviour predicted by the gel-polarization model, since the permeate flux is linear dependent on the pressure for the same gel thickness. The effect of a sudden pressure increase on the permeate flux is strikingly different from the flux behaviour during the ultrafiltration of dextran (see fig. 4.5). In that case no doubling of the flux is observed due to an increase in osmotic pressure (see dextran).Due to the pressure increase the convective flux of silica towards the membrane is higher than the back diffusion flux. So, immediately after the pressure rise the gel thickness will increase until the net silica flux becomes equal to zero

(steady situation). The dotted lines in the figure represent the flux in steady situation at the actual concentration of the bulk solution for the inner and outer permeate section. The decline in the quasi-steady flux is the result of the change in bulk concentration during the experiment. According to the gel-polarization model the steady flux is independent of the pressure (eqn. (4.4), $C_m = C_g$). The gradual decrease in flux towards the quasi-steady flux as predicted by the model is really found experimentally (fig. 4.8). This gradual decrease in flux is a great contrast to the immediate change in flux during the filtration of dextran. In that case only the polarization layer has to adjust itself to the new situation, which according to our calculations takes a few seconds (see dextran).
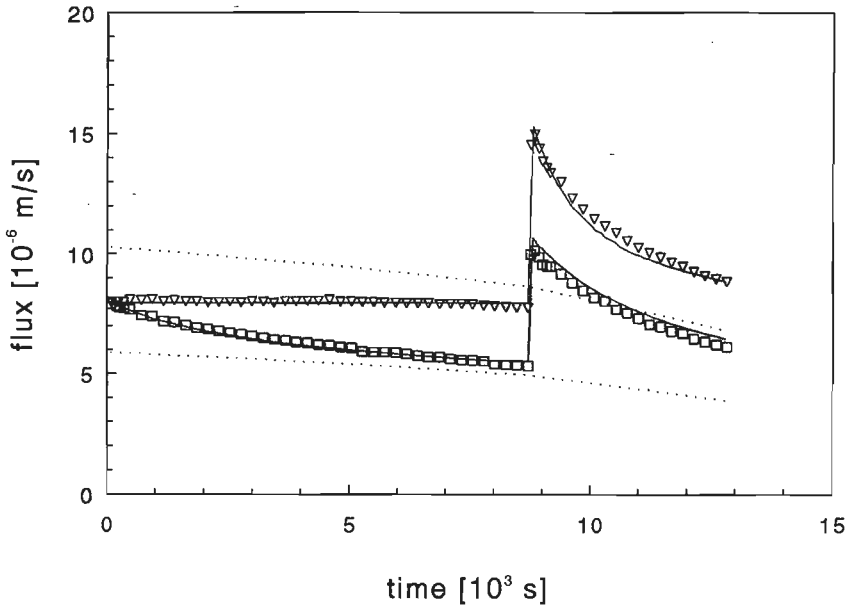
Figure 4.8 *Plot of the flux versus time for silica (Sil5). Pressure change: $\Delta P = 100kPa$, 200 kPa, $n = 90$ rpm. ($\square$) Inner section; ($\triangledown$) outer section; (——) GPM; ($\cdots$) quasi-steady flux.*

During the filtration at 100 kPa the permeate fluxes in the inner and outer permeate section behave different. The flux in the inner permeate section decreases gradually from the PWF towards quasi-steady flux as usual. On the other hand the flux in the outer permeate section is considerably lower than the quasi-steady flux. In this case the flux is not limited by gel formation but determined by the membrane resistance. In other words no gel layer is formed on top of the outer permeate section.

Since the permeate flux in the outer permeate section is only determined by the membrane resistance the flux must be equal to the PWF. According to eqn. (4.4 the value for k_{mo} should at least be larger than $PWF/\ln(C_g/C_b) \approx 2.5 \times 10^{-6}$ m/s. This indicates that the mass transfer coefficient is indeed larger than the one calculated with the Sherwood relation (table 4.3). The fact that the flux equals the PWF confirms that the osmotic pressure of the silica suspension is negligible up to concentrations quite near to the gel concentration.

The absence of a gel layer in spite of the convective transport towards the membrane is a strong evidence for the existence of back diffusion into the bulk solution. A cake layer model without back diffusion is not able to predict that phenomenon. This conclusion is supported by experiment Sil6 in which after 9000 s of filtration the cell was depressurized for almost 21 hours while stirring was continued. When pressure was put on again the permeate flux was almost equal to the PWF, so silica seems to have diffused back into the bulk solution.

Before concluding this section we give some additional remarks about the deviations between k_m and k_m^* as presented in table 4.3. Besides the already mentioned influence of repulsive forces on the diffusion coefficient the presence of agglomerates may also play a role in the deviations between k_m and k_m^*. The presence of agglomerates, that was deducted from the high values found for the suspension viscosities, implies that the actual concentration of the primary particles is lower than the total silica concentration. The fitted values for k_m would become lower - closer to the values of k_m^* - if the concentration of the primary particles would be used in the fitting calculations instead of the silica concentration. The above reasoning only holds if the aggregates do not deposit onto the gel layer. That this may be the case under certain conditions can be concluded from the lack of a change in the flux during the first part of experiment Sil5 at 100 kPa. Since the agglomerates will show far less back diffusion than the primary particles this behaviour must be attributed to lift forces in the non uniform flow field near the membrane. This lift behaviour is typical for larger colloids. Attempts to measure the size of the aggregates by means of light scattering gave an indication of a size of about 500 nm. Fane [1984] showed that capture efficiency for this particle size is low. The deposition of agglomerates is more likely to occur in the inner permeate section due to the comparatively lower shear forces exerted in this region. In experiment Sil4 the outer permeate flux is probably under-predicted because in reality less material is deposited on the membrane due to the lift of the aggregates. If a lower concentration of primary particles is assumed, the shape

of the flux curve can be reasonably well predicted. In the inner section the flux is mainly determined by convective transport due to the low mass transfer coefficient and low shear forces.

Concluding we may say that the concentration lowering of the primary particles might attribute to the deviations between the fitted k_m and the electrochemical determined k_m^* in the silica experiments. Besides this also the irregular shape of the gel layer surface will certainly increase the mass transfer coefficient compared with the one for a flat surface as has been shown for corrugated membranes [van der Waal, 1989].

Unsteady flux behaviour in relation to the presence of a gel layer

The presented results show a clear distinction in the unsteady flux behaviour when only a polarization layer is build up (dextran) and in case also the formation of a gel layer takes place (silica). This difference expresses itself in two ways:

1. The time to reach steady-state is much longer in case a gel layer is formed due to the larger layer thickness compared with the polarization layer.

2. A sudden change in pressure results in a different steady flux due to the change in concentration at the membrane surface in case only a polarization layer is formed. On the other hand after a linear change with pressure the flux gradually decreases to the same steady flux in case a gel layer is present.

For the filtration experiments with dextran and silica a clear discrimination can be made between the presence or absence of a gel layer based on either 1. or 2.. However, the differences are not always as pronounced as in these cases. A restriction which should be made to 1. is the fact that the time to build up the gel layer strongly depends on its permeability. Illustrative in this respect are the results obtained by Chudacek et al [1984]. They measured the time to build up a gel layer of another type of silica: Syton X-30 ($d_{par} = 16$ nm) by means of a droplet counter on the permeate outlet. According to the experimental flux measurements the formation of the gel layer lasts 20 to 60 seconds, depending on bulk concentration and pressure.

If an estimated mass transfer coefficient is used (from the available flux vs $\ln C_b$ plot) the flux during the formation of the gel layer can be well predicted by our model calculations. If we apply our model calculations to the flux vs time curve presented by Chudacek it does not show the slight overprediction of the transient flux as predicted by the model curve of Chudacek. The reason for this difference is that in our model description the change in diffusive flux during the build-up of the gel layer is taken

into account, whereas Chudacek assumed it constant and equal to the diffusive flux in the steady-state situation.

The large difference in time to build up the gel layer for Syton X-30 and Aerosil 200 (used in this work) is a result from the large difference in specific resistances of the gel layers: $5.5-16 \times 10^{14}$ m/kg and $3-5 \times 10^{13}$ m/kg, respectively. The surface-averaged gel layer thickness under steady state conditions is $5.5-18.8 \times 10^{-6}$ m for Syton X-30 and $1-2.5 \times 10^{-3}$ m for Aerosil 200.

The higher specific resistance for Syton X-30 is mainly caused by its higher gel concentration (ca. 900 kg/m^3); the diameters of Syton X-30 and Aerosil 200 are almost equal. If Syton X-30 is filtered under identical conditions as used for Aerosil 200 the time required to form the gel layer would also be about one minute.

Summarized, one can only expect a considerable difference in the times to build up a gel layer and a polarization layer if the specific gel layer resistance is not too high. Therefore no definite answer can be given to the question whether a gel layer is formed or not in case steady-state is reached quickly.
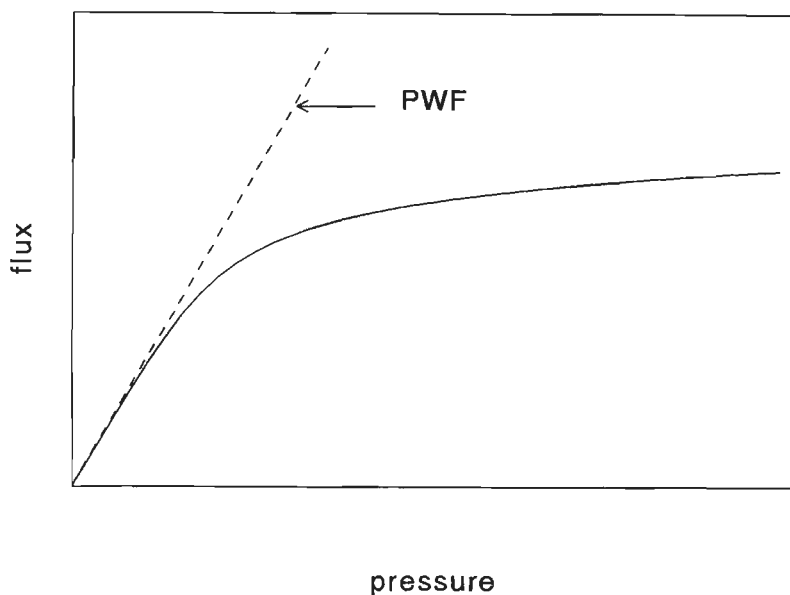

Figure 4.9 *Plot of the flux versus pressure according to osmotic pressure model.*

However, the response of the flux to sudden pressure changes can provide additional information which is indicative of a sole presence of a polarization layer (see 2.). If

the measurements show that the steady-state flux changes due to the change in pressure, it is clear that only a polarization layer is present. However, if the flux has an equal value for both pressures it does not proof the presence of a gel layer. In that case it is still possible that only a polarization layer has been formed. In fig. 4.9 the steady-state flux vs pressure is depicted in case only a polarization layer is formed (osmotic pressure model). At low pressures the flux indeed changes by changing the pressure. But at high pressures the flux turns out to be almost independent of pressure, because the change in osmotic pressure caused by the rise in the concentration at the membrane surface compensates the change in pressure. At which pressure the flux hardly changes with increasing pressure depends on how strong the osmotic pressure varies with the concentration at the membrane surface. The stronger the variation with the concentration at the membrane surface, the lower the pressure at which 'constant' flux is reached.

Summarized, in case only a polarization layer is build up one can just expect a considerable change in flux as a result of a sudden pressure change, if the osmotic pressure does not vary too much with the concentration at the membrane surface.

So far only gel forming species have been considered which cause a negligible osmotic pressure. However, in other systems both osmotic pressure and gel formation may influence the flux. In that case the unsteady-state flux behaviour shows a combined effect. In the beginning of a filtration experiment a rapid drop in flux will occur during the build-up of the polarization layer due to the increase in osmotic pressure. After the gel concentration has been reached a gradual decrease in flux can be observed as a result of gel layer formation (if the permeability of the gel layer is not too high). During a sudden pressure increase the flux will not increase linearly with pressure as described for a gel layer without osmotic pressure, but with a factor $(\Delta P_2 - \Delta\Pi)/(\Delta P_1 - \Delta\Pi)$. Next, a gradual decrease in flux will occur (if the permeability of the gel layer is not too high) until the same steady flux is reached. The increase in pressure does not effect the osmotic pressure since the concentration at the membrane surface stays equal to the gel concentration at the retentate side of the gel layer. This gel concentration is most likely independent of the applied pressure, whereas the gel concentration at the membrane side may increase with increasing pressure due to compression.

In the previous discussion adsorption was not taken into account because according to

PWF measurements dextran and silica did not adsorb on the membrane. If adsorption occurs it can greatly influence the characteristic unsteady-state flux behaviour. Due to adsorption the membrane permeability changes during filtration.

By preadsorption of the membrane the adsorption process may be separated from the filtration [Opong et al., 1991]. Assuming the adsorbed membrane permeability constant during filtration a discrimination between the presence and absence of a gel layer can be made on the grounds as described for the unadsorbed membrane.

4.6 Conclusions

The unsteady flux behaviour during ultrafiltration may differ considerably when either only a polarization layer or also a gel layer is formed as a result of the time needed to build up the layers. In certain situations the difference in unsteady flux can be so pronounced that measurement of the unsteady flux can be used for the discrimination between the presence or absence of a gel layer.

Under the experimental conditions dextran and silica show a clearly different flux behaviour. During the filtration of dextran only a polarization layer is build up, which takes less than a minute, whereas it takes hours before the gel layer of silica is formed. The osmotic pressure model (polarization layer) provides a good description of the flux for the experiments with dextran. If mass transfer coefficients are used which are higher than those electrochemically measured the transient flux for silica can be rather well predicted by the gel-polarization model.

5. PEG/WATER SYSTEMS

5.1 Introduction

In this chapter a detailed study of the flux and rejection behaviour for the binary PEG/water system will be presented. A clear understanding of the behavior of the PEG alone is necessary in order to be able to interpret the influence of another solute on the flux and rejection. After the experimental set-up the flux and observed rejection during PEG filtration will be discussed for various molecular weights of PEG and different types of membranes and membrane modules. The flux and rejection will be modelled in three ways. First, the actual rejection is evaluated from the experimental data by two methods, one based on the mass transfer coefficient in combination with the concentration polarization model, the other based on the osmotic pressure model. Both models have been used in the form presented in chapter 4. Subsequently, the results of the simultaneous modelling of the flux and rejection with the Stefan-Maxwell equations will be discussed. These equations have been described in detail in chapter 2. In the Stefan-Maxwell model the non-ideality of the PEG/water system can be explicitly taken into account. An extension to multicomponent systems is possible by introducing additional equations for the extra components and the interactions between the various components can be taken into account. Finally, the parameters of the Stefan-Maxwell model, which are fitted to the experimental data, are translated to the hindered diffusivities in the hydrodynamic model of hindered transport and compared with known theoretical relationships for these hindered diffusivities (see chap. 2).

5.2 Materials and Methods

Model components

Use was made of different types of poly (ethyleneglycols): PEG1000 (Janssen), PEG3400 (Aldrich) and PEG6000 (Serva). The molecular weights are 1000, 3400 and 6000 Da, respectively. The water used for the experiments was deionized water filtered through the Milli-Q-system of Millipore (resistivity = 18 megaohm-cm).

Membranes

The ultrafiltration experiments in the stirred cell were performed with asymmetric YM5, YM10 and YM30 membranes (Amicon) having a MW cut-off of 5000, 10000 and 30000 Da, respectively. The membrane material is regenerated cellulose. The membranes consist of a very thin (0.1-0.15 μm) dense 'skin' of extremely fine, controlled pore structure which opens to a much thicker (50 to 250 μm), open-celled spongy layer of the same polymer. The structure of the YM10 membrane has been studied by Sheldon [1991a] by thin section transmission electroscopy and freeze-fracture combined with deep-etching. The separating surface of the regenerated cellulose membrane appeared to be composed of closely packed fibres, which had a diameter of around 5.5 nm. Very few distinct circular pores were found, the many pores that were present seem to arise from to the packing of the surface fibres. The pores of the YM10 membrane varied in diameter from approx. 4-10 nm.

The ultrafiltration experiments in the tubular module were performed with WFBX 0121 membranes (Stork-Wafilin) having a molecular weight cut-off of 10000 Da for PEG and 50000 Da for dextran. The membrane material is hydrophilic polysulphone, applied on a composite polyester non-woven carrier. According to the supplier the total thickness of the hydrophilic polysulphone layer is 100-150 μm with a porosity of 0.5. The separating top layer thickness was about 5×10^{-7} m. The polyester carrier consisted of two layers: one layer directly adjacent to the polysulphone layer, with a thickness of 150 μm and a porosity of 0.7 and a second layer of 260 μm and a porosity of 0.5. The internal diameter of the membrane tube is 14.4×10^{-3} m.

Apparatus

Stirred cell

The major part of the flux and rejection measurements were carried out in a stirred batch cell (Amicon, type 2000A). The internal diameter of the cell is 14×10^{-2} m. The bar-like stirrer has a diameter of 12×10^{-2} m. The effective area of the circular membrane is equal to 144×10^{4} m^2 according to Amicon. The volume of the total permeate section between the bottom of the membrane and the liquid outlet has been determined with a displacement experiment and is equal to 27×10^{-6} m^3.

Since electrochemical measurements showed (see chap. 3) that the mass transfer coefficient varies from the centre of the membrane towards the edge, similar cells were built with the possibility to collect the permeate in two separate streams (chap. 4,

fig. 4.2). The membrane area connected with the inner permeate section was 72×10^{-4} m^2, the area connected with the outer section was 88×10^{-4} m^2.

Both cells were pressurized with nitrogen gas and the temperature was controlled by a thermostat. The feed solution was preheated before being added to the cell. The temperature was maintained at 298 K, unless mentioned otherwise. The permeate was collected in a time-based fraction collector to be able to take samples from the various fractions for concentration analysis. The amount of permeate was determined gravimetrically.

Tubular module

Some of the flux and rejection measurements were performed in a tubular cross-flow ultrafiltration module (UF-1, Stork Friesland). The module was pressurized with a centrifugal pump, which also provided the circulation through the module. The system was run in continuous mode, which means that the permeate and concentrate were both returned to the storage vessel. Additional measuring and control equipment were installed in order to obtain accurate information about pressure, flow and temperature in the system. The working temperature of 298 ± 0.1 K was achieved by using a cooling section in the concentrate line together with a temperature controller. The length of the membrane was 1.8 m and the area was 0.08 m^2. To prevent leakage at the entrance and exit of the membrane, the membrane was constrained on both ends by a rubber seal. In order to be able to characterize any entrance or exit effects the permeate was collected in four separate streams (pos. 1-4, 1=entrance, length per position = 0.45 m). The system pressure was measured after position 4. Moreover, the axial pressure drop over the membrane was registered. From this axial pressure drop the transmembrane pressure at the midpoint of the membrane module was calculated. This value was used for the transmembrane pressure.

The permeate was alternately combined and collected in a vessel or collected as separate streams in a fraction collector in order to diminish the necessary capacity for the fraction collector. The liquid hold-up of the total permeate section including the support layer of the membrane was equal to 25×10^{-6} m^3.

Methods

Pure water flux

The pure water flux was used to evaluate the membrane resistance of the clean

membrane. After the working temperature was established the water flux was measured for various pressures, starting from low pressures to high pressures and vice versa. The pressure was both increased and decreased in order to determine possible compressibility effects. Before and after each experiment the pure water flux measurements were repeated for a few pressures in order to check on possible adsorption or deposition on the membrane.

Permeate flux and rejection measurements

The feed solutions were prepared by dissolving weighed quantities of the components in water. Prior to filtration, samples were taken from the bulk solutions for concentration analysis. The bulk concentration was always 10 kg/m^3, unless stated otherwise. After the working temperature was established the system was pressurized. The permeate was collected in fractions as a function of time.

To be sure that all liquid present in the permeate section prior to filtration was removed, permeate samples were taken from two subsequent fractions after 100 ml of permeate was collected. If the pressure was varied during the experiment, the first 100 ml of permeate collected after the pressure jump were not used for concentration analysis. In calculating the rejection of a sample the time lag for the permeate to reach the sample collector after passing through the membrane was taken into account. At the end of the experiment the system was depressurized and a retentate sample was taken.

In the dead-end stirred cell the retentate was concentrated during filtration at constant pressure. In order to be able to measure the influence of pressure at the same concentration, the permeate was returned to the retentate after depressurizing the cell. Subsequently, a bulk sample was taken and a new pressure was set. The same procedure was followed for all pressures.

Concentration analysis

The solute concentration in the samples was determined by HPLC (High Performance Liquid Chromatography). A small Bio-SIL SEC 250 guard column (Biorad) was used since no separation of components was necessary. Deionized water filtered through the Milli-Q-system was used as eluent. The concentrations were determined by a refractive index detector (LKB, 2142). A standard solution with a known quantity PEG was alternately analyzed with the samples. The samples were measured in duplicate and the deviation between both measurements was 1-3%.

5.3 Flux during filtration of PEG solutions

Solutions of PEG of different molecular weight were filtered over various types of membranes (see table 5.1). The flux during the filtration of PEG over a YM5 and YM10 membrane at a stirrer speed of 90 rpm is presented in fig. 5.1.
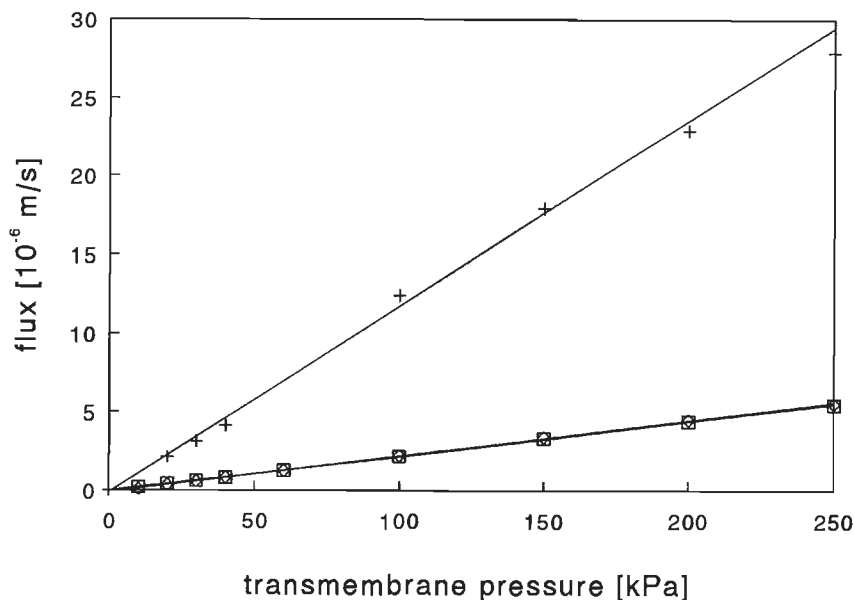
Figure 5.1 *Flux during PEG filtration as a function of the transmembrane pressure for various membranes and different molecular weights of PEG. n=90 rpm. PEG1000, YM5 (□); PEG1000, YM10 (+); PEG3400, YM5 (◇). Stefan-Maxwell fit (——).*

In all cases the flux showed a linear dependence with pressure. The fluxes for the filtration of PEG3400 through the YM30 membrane were measured at 90 and 270 rpm for both inner and outer permeate sections (fig. 5.2). At higher pressures the flux increase is more than proportional. In fig. 5.2 the pure water flux is depicted too. The lower flux of the PEG solution compared to the pure water flux is mainly caused by the osmotic pressure difference between the retentate side and the permeate side of the membrane (the increase in viscosity is low). The difference between the pure water flux and the flux during PEG filtration has the smallest value for 270 rpm in the outer permeate section and the highest for 90 rpm in the inner section. These two conditions correspond to the highest and the lowest value of the mass transfer coefficient, respectively. This dependence on mass transfer coefficient is in agreement with

previous studies in the literature [Nakao, 1981; Wijmans, 1985]. Lentsch [1993] also observed a linear relationship between flux and pressure for the filtration of PEG 20,000 over a 100 kDa membrane. The model curves according to the Stefan-Maxwell equations will be discussed in section 5.5.
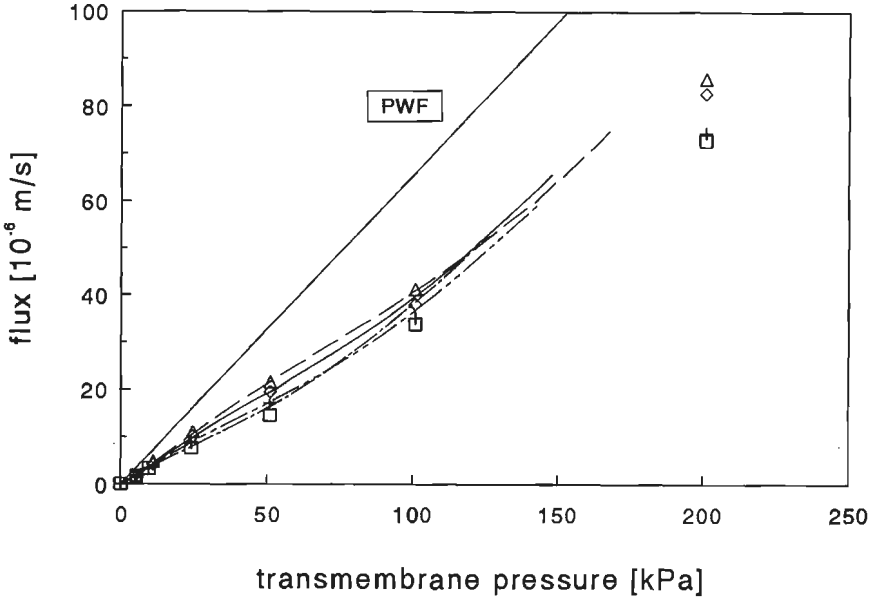
Figure 5.2 *Flux during PEG3400 filtration as a function of the transmembrane pressure for two sections. YM30. Inner: n=90 (□), (—·—·) and 270 rpm (◇), (——); outer: n=90 rpm (+), (—··—) and n=270 rpm (△), (——). Lines represent Stefan-Maxwell fits. PWF=pure water flux.*

The flux during the filtration of PEG3400 on a WFBX 0121 membrane showed a linear dependence of the flux with pressure (see fig. 5.3). Similar to the influence of the mass transfer on the rejection in the stirred cell, the highest flux should be found at the highest circulation velocity (equivalent to the highest mass transfer coefficient). In this case the difference was hardly visible. The relationship between the flux and the pressure will be considered in detail after the rejection of PEG in these experiments has been discussed.
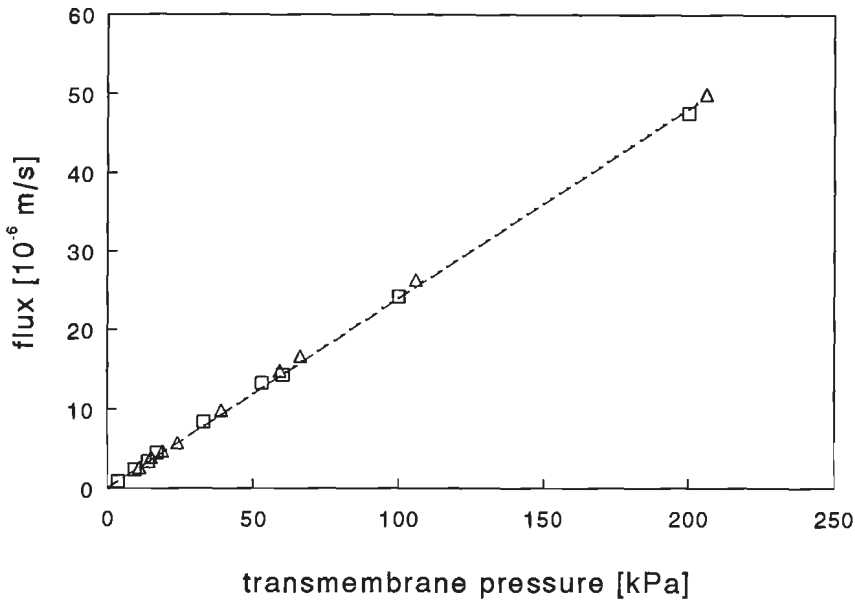
Figure 5.3 *Flux during PEG3400 filtration as a function of the transmembrane pressure for pos. 3. WFBX 0121. $u_{circ}=1.04$ m.s^{-1} ($\square$), (- -); $u_{circ}=1.95$ m.s^{-1} ($\triangle$), ($\cdots$). Lines represent Stefan-Maxwell fits.*

5.4 The PEG rejection during filtration of PEG solutions

In eqns. (5.1a) and (5.1b) the observed and actual rejections are defined.

$$R_o = 1 - \frac{C_p}{C_b} \quad (a) \qquad\qquad R_a = 1 - \frac{C_p}{C_m} \quad (b) \qquad (5.1)$$

The observed rejection represents the fraction of rejected solute based on the bulk concentration and the actual rejection is equal to the fraction of rejected solute based on the concentration at the membrane surface.

The observed rejection is a measured quantity, the actual rejection can only be determined by calculating the concentration at the membrane surface. First the observed rejection will be presented and subsequently the calculated actual rejection is shown.

Observed rejection

In fig. 5.4 the observed rejections are depicted as a function of the flux, which correspond with the flux measurements in fig. 5.2.
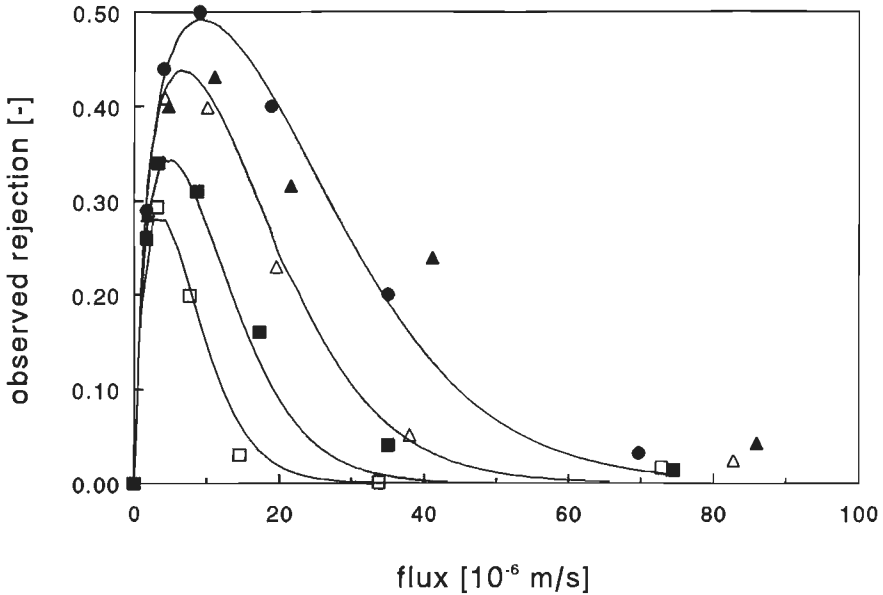
Figure 5.4 *Observed PEG rejection during PEG3400 filtration as a function of the flux for two sections. YM30. n=90 (□) and 270 rpm (▲). Open symbols: inner section; closed symbols: outer section. Stefan-Maxwell fit (——). (○) n=270 rpm, outer, pH=7.4.*

With increasing flux the observed rejection increases and after a maximum value is reached a decrease in rejection is observed. At almost zero flux the diffusive flux in the membrane towards the permeate is predominant and the permeate and bulk concentrations will be equal, i.e. the observed rejection is zero. With increasing flux the diffusive contribution to the flux in the membrane becomes less important compared to the convective contribution to the flux. Therefore the permeate concentration will decrease, which corresponds to an increase in rejection. At higher fluxes the convective transport will become the most important. Due to the convective transport in the polarization layer and the exclusion of PEG by the membrane, the concentration at the membrane surface will rise with increasing pressure, which causes an increase in permeate concentration and therefore a decrease in observed rejection. The highest observed rejection is measured under the highest mass transfer conditions (270 rpm, outer section), because in that case the concentration polarization is the least pronoun-

ced. The same type of relationship between the observed rejection and the flux has been found by Tsapiuk et al. [1990] for PEG filtration, Opong et al. [1991a] for BSA and Mochizuki et al. [1992b] for dextran.

The flux at which the maximum in the observed rejection occurs is analytically derived by Opong et al. [1991a]:

$$v = \frac{k_m}{Pe^*} \ln(1 + Pe^*) \qquad Pe^* = \left(\frac{\phi K_c k_m L}{(\varepsilon/\tau)\phi K_d D_{s,w}} \right) \qquad (5.2)$$

in which Pe^* is the membrane Peclet number based on the mass transfer coefficient. For small Pe^* numbers the flux at maximum rejection is equal to k_m, independent of the membrane properties, while at large Pe^* the maximum occurs at $v < k_m$. This can be seen in fig. 5.5, where the observed rejection of all experiments from table 5.1 (p.109) have been depicted.
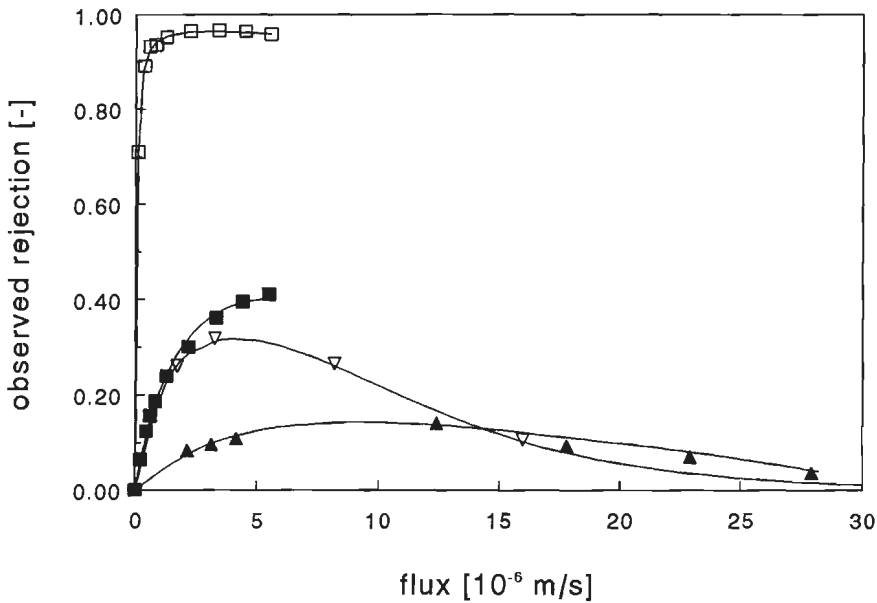
Figure 5.5 *Observed rejection during PEG filtration as a function of the transmembrane pressure for various membranes and different molecular weights of PEG. n=90 rpm. PEG1000, YM5 (♦); PEG1000, YM10 (▲); PEG3400, YM5 (□); PEG3400, YM30 (▽). Stefan-Maxwell fit (——).*

The filtration of PEG3400 through YM5 and YM30 membranes both show a maxi-

mum value at $v \approx 4 \times 10^{-6}$ m/s. The maximum for PEG1000 is reached at a higher flux of $8\text{-}10 \times 10^{-6}$ m/s (YM10). This is in qualitative agreement with the higher mass transfer coefficient for PEG1000 due to the higher diffusion coefficient. The experimental maxima for PEG3400 on YM5 and YM30 correspond well with the flux calculated by eqns. (5.2) with the value for the mass transfer coefficient determined with the Sherwood-relation (see chap. 3) and Pe^* calculated with the parameters presented in table 5.1: 3.8×10^{-6} m/s and 4.3×10^{-6} m/s, respectively. The flux calculated for PEG1000 on YM10 was 7.7×10^{-6} m/s, which is lower than the value that appears on the figure, but no rejection measurements have been carried out in the region of the maximum. The flux during the filtration of PEG1000 on a YM5 membrane was too low to reach a maximum value, even at a pressure of 200 kPa, which is consistent with the calculated value of 5.8×10^{-6} m/s.

The rejection of PEG has also been studied in the tubular module. In fig. 5.6 the observed rejection is depicted as a function of the flux for the four membrane positions (see Methods) at a circulation velocity of 1.95 m/s.
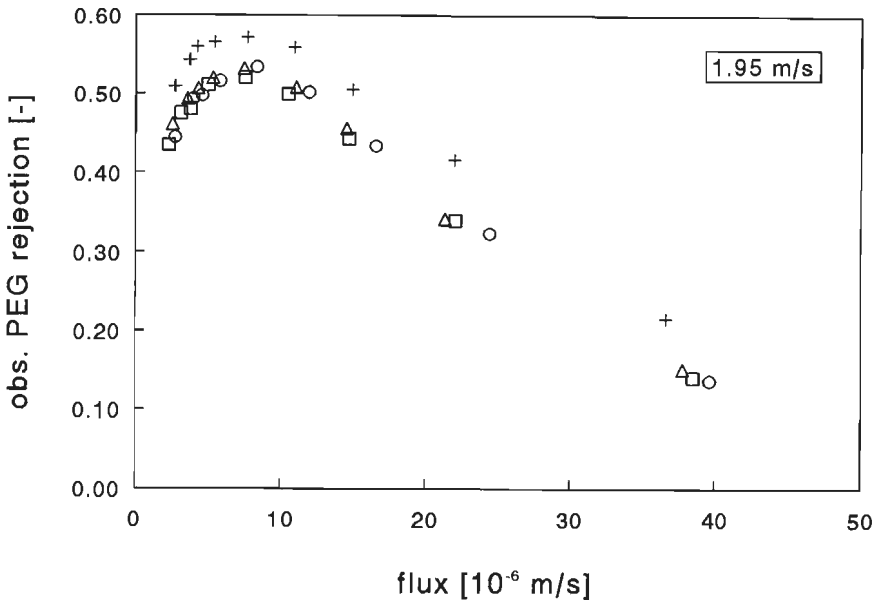
Figure 5.6 *Observed PEG rejection during PEG6000 filtration as a function of the flux for four membrane positions in the tubular membrane WFBX 0121. $u_{circ}=1.95$ m.s^{-1}. Pos. 1: (+); pos. 2: (△); pos. 3: (○); pos. 4: (□).*

The observed rejection of PEG6000 shows the same type of relationship with the flux as in the stirred cell. The rejections for positions 2, 3 and 4 fall onto one curve, the rejection for position 1 is distinctly higher at the same flux. This augmented value at the first position is due to entrance effects. The higher turbulence at the inlet of the module results in a higher mass transfer and therefore a higher observed rejection. This effect has also been observed to a lesser extent for the filtration of a PEG3400 solution. In fig. 5.7 the influence of the variation of the circulation velocity on the observed PEG3400 rejection is shown. Analogous to the stirred cell the highest PEG rejection is observed at the highest mass transfer rate for a circulation velocity of 1.95 m/s.
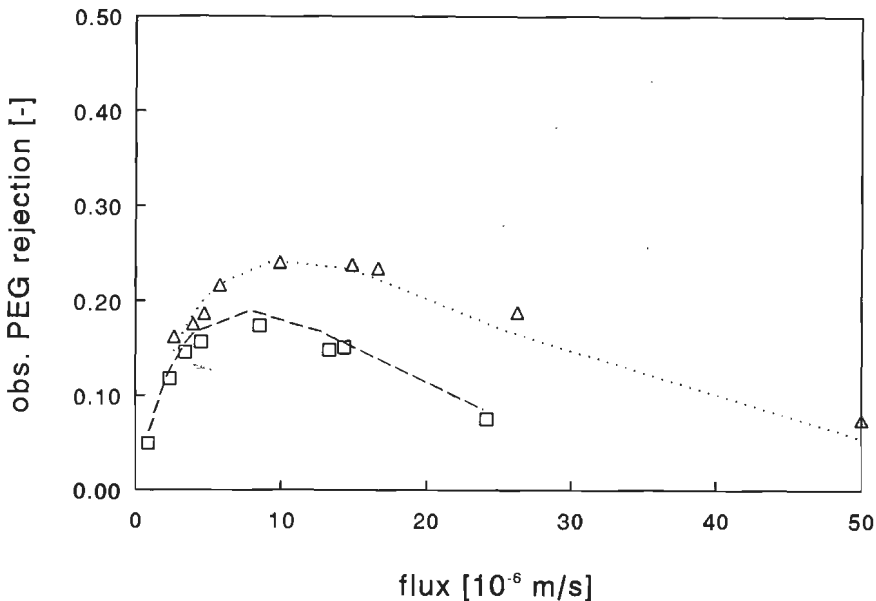
Figure 5.7 *Observed PEG rejection during PEG3400 filtration as a function of the four membrane positions in the tubular membrane WFBX 0121. $u_{circ}=1.04$ $m.s^{-1}$ (□), (- -); $u_{circ}=1.95$ $m.s^{-1}$ (△), (···). Lines represent Stefan-Maxwell fits.*

Actual rejection

The actual rejection can be calculated from the experimental data by two different methods. The first method uses a rearranged form of equation (4.4) derived from the concentration polarization model for the steady-state flux (5.3a):

Deriving the mass transfer coefficient from the Sherwood relation (chap. 3), the concentration at the membrane surface can be calculated from the experimentally

$$C_m = C_p + \left(C_b - C_p\right) e^{\frac{v}{k_m}} \quad \text{(a)} \qquad\qquad v = \frac{\Delta P - \sigma(\pi_m - \pi_p)}{\eta_p R_m} \quad \text{(b)} \quad (5.3)$$

determined flux and permeate concentration. The actual rejection for PEG3400 through the YM30 based on the mass transfer coefficient k_m is depicted in fig. 5.8. An alternative method to determine the concentration at the membrane surface is based on the osmotic pressure difference over the membrane caused by the difference in PEG concentration at the retentate and permeate side of the membrane (eqn. 5.3b). Using the osmotic virial equation (chap. 3) the concentration at the membrane surface can be evaluated from the known flux and permeate concentration if the osmotic reflection coefficient is available. Although there is considerable disagreement in literature concerning the equivalence between the osmotic reflection coefficient σ and the filtration reflection coefficient $R_{a,\infty}$ (reviewed by Opong [1992]) equality is assumed as a first approximation. According to fig. 5.8 $R_{a,\infty} \approx 0.85$ (the actual rejections with a value of almost one are found for unrealistically high values of the concentration at the membrane surfaces, as will be discussed in more detail below). The actual rejections based on the osmotic pressure using an osmotic reflection coefficient equal to 0.85 are depicted in fig. 5.9. The introduction of the osmotic reflection coefficient has only a minor effect on the actual rejection.

The actual rejection shows a rise with flux until a plateau value is reached. The increase in rejection is due to the decreasing importance of the diffusive flux compared to the convective flux in the membrane. The plateau value is reached when the diffusive flux is negligible compared to the convective transport. The plateau value represents that part of the convective flux which is rejected due to geometric exclusion of the solute by the membrane. In contrast to the observed rejection no drop in rejection occurs for higher fluxes. This confirms that the drop in the observed rejection is the result of concentration polarization, which is supported by the fact that the different mass transfer conditions (inner-outer permeate section and the two stirrer speeds) in a range of $k_m = 4\text{-}13 \times 10^{-6}$ m/s do not affect the relationship between the actual rejection and the flux.

The actual rejections according to the two methods coincide for fluxes below 30×10^{-6} m/s, but at higher fluxes the actual rejection calculated from the osmotic pressure reaches a plateau value of 0.85, whereas actual rejections according to the mass transfer coefficient show considerable scattering.
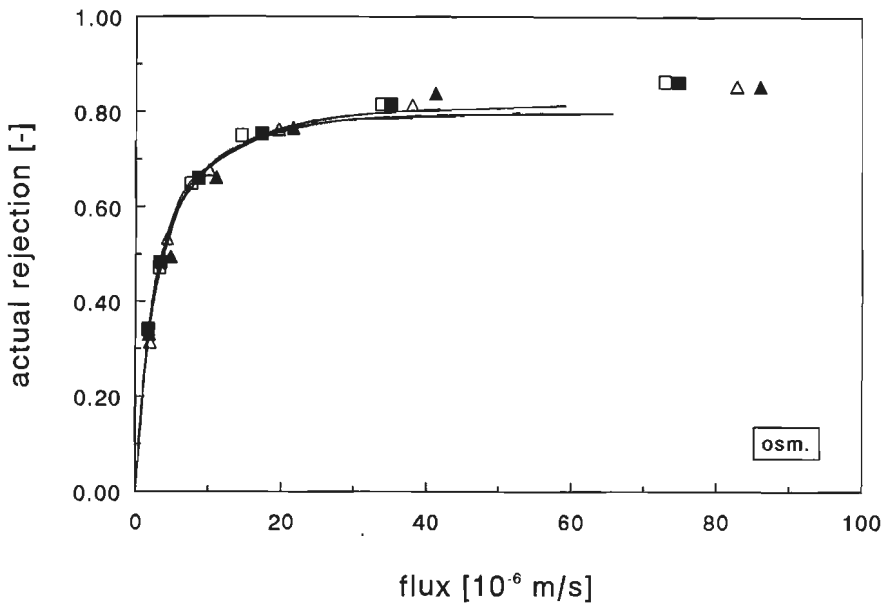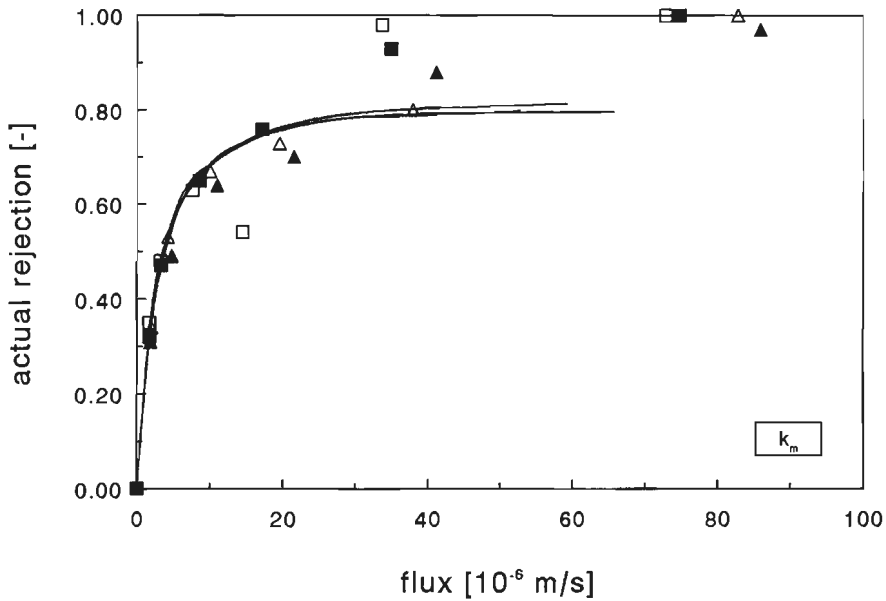
Figure 5.8 *Actual PEG rejection during PEG3400 filtration as a function of the flux for two sections based on the mass transfer coefficient. YM30. Inner: n=90 (□) and 270 rpm (△); Outer: n=90 (♦) and 270 rpm (▲). Lines represent Stefan-Maxwell fits.*
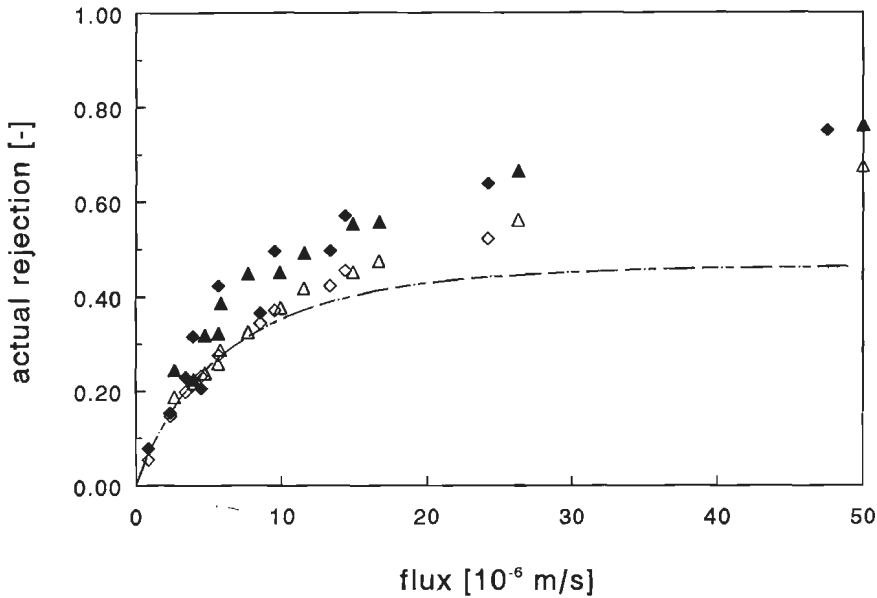**Figure 5.9** *Idem based on the osmotic pressure.*

The scattering in the actual rejections according to the mass transfer coefficient is caused by the very low values of the observed rejection at high fluxes (see fig. 5.4). In that case the difference between the bulk concentration and permeate concentration is very small and a deviation in the concentration analysis will cause a large relatively error in the factor in front of the exponential in eqn. 5.3a. So in the high flux region the actual rejection can be more accurately be determined by using the osmotic pressure model than the mass transfer coefficient.

The actual rejection for the WFBX 0121 membrane in the tubular module has also been evaluated by both methods in fig. 5.10. A value of one is assumed for the osmotic reflection coefficient. The actual rejection based on k_m coincides for the two circulation velocities 1.04 m/s and 1.95 m/s corresponding to a mass transfer coefficients for the PEG3400 of 9.3×10^{-6} m/s and 15×10^{-6} m/s, respectively. In contrast with the actual rejection data in the stirred cell, no scattering is found for the highest fluxes since the observed rejection does not reach very low values and v/k_m is generally lower than that in the stirred cell. The actual rejections based on the osmotic pressure also coincide for the two circulation velocities, but are higher than those calculated according to the mass transfer coefficient.

The rejections show considerable scattering, probably due to the less controllable pressure in the tubular pilot system. Introducing uncertainties in pressure or flux does not shift the actual rejection enough to match the actual rejections found with k_m. The use of a lower value for the osmotic reflection coefficient would only increase the discrepancy between the actual rejection based on the osmotic pressure and that according to the mass transfer coefficient. Since the error of the mass transfer coefficient is about 20%, the influence of a variation of the prefactor in the Sherwood relation has been checked. For variations of more than 10% the actual rejections for the two circulation velocities do not coincide anymore. The absolute value of the actual rejection hardly shifts for a variation of the mass transfer coefficient within 10%. This suggests that the actual rejections based on the osmotic pressure deviate. Since the same behaviour was also observed for PEG3400 it is unlikely that the deviation is the result of deviations in the osmotic virial relation for PEG6000. Although the actual rejections according to the osmotic pressure and mass transfer coefficient do not collapse onto a single curve, the trend in the actual rejection is as was theoretically expected and the rejection values seem to be in accordance with the molecular weight cut-off of 10,000 for PEG.

Figure 5.10 *Actual PEG rejection during PEG3400 filtration as a function the flux based on the mass transfer coefficient* (open symbols) *and the osmotic pressure* (closed symbols). *WFBX 0121.* $u_{circ}=1.04$ $m.s^{-1}$ ($\square$), (——); $u_{circ}=1.95$ $m.s^{-1}$ ($\triangle$), ($\cdots$). *Lines represent Stefan-Maxwell fits.*

Relationship between the flux and the pressure

After the discussion of the observed and actual rejection it is possible to interpret the relationship between flux and pressure in fig. 5.2. The flux during PEG filtration shows an almost linear dependence with pressure and no sign of flux limitation at higher pressures is visible. On the contrary, the slope of the flux vs. pressure rises slightly from 100 kPa to 200 kPa. Flux limitation (discussed in chap. 4) occurs if the osmotic pressure is a strong function of the concentration. In that case a small variation in the concentration at the membrane surface causes a considerable increase in osmotic pressure, which limits the flux. The flux limitation is favoured by a low mass transfer coefficient (see eqn. (5.3a)), since a rise in flux strongly affects the exponent v/k_m and therefore the concentration at the membrane surface. If the membrane rejection is not equal to one, a concentration limitation instead of a flux limitation may occur. At high fluxes the actual rejection reaches a plateau value, which means a constant ratio between C_m/C_p. Moreover, at high fluxes the ratio between C_b/C_p becomes 1 ($R_o=0$). Combining these two conditions leads to a fixed value for the concentration at the membrane surface $C_m = C_b/(1-R_{a,\infty})$ and the

permeate concentration $C_p = C_b$. A constant value for both concentration at the membrane surface and permeate concentration means a constant value of the osmotic pressure. A further rise in pressure will cause an increase in flux, according to a line with a slope equal to $1/(\eta_p R_m)$ and a non-zero intercept of $\Delta\Pi/(\eta_p R_m)$.

For the PEG filtration through YM30 (fig. 5.9) membrane the plateau value of the actual rejection is 0.85. At a bulk concentration of 10 kg/m^3 the limiting concentration at the membrane surface is 64 kg/m^3, which corresponds to an osmotic pressure difference of 86 kPa. The permeate concentration is only equal to the bulk concentration ($R_o = 0$) for the highest pressures (fig. 5.4). For 90 rpm in the inner section the rejection is zero for both 100 and 200 kPa. The rise in flux at these pressures is indeed more than proportional with pressure: from 33.8×10^{-6} m/s to 73×10^{-6} m/s. Further measurements at higher pressures could confirm the rise in flux due to the constant value of the osmotic pressure. However the YM30 membrane cannot be used at higher pressures.

The above-described limitation in the concentration at the membrane surface due to the limitation in the permeate concentration is likely to occur under the following circumstances. First of all, the highest pressures used for the measurements should exceed the osmotic pressure difference over the membrane at the maximum concentration at the membrane surface plus ($\Delta\Pi + v \cdot \eta_p \cdot R_m$): the pressure drop over the membrane . Furthermore, the plateau value in the actual rejection should be reached, which is favoured by a low diffusion coefficient inside the membrane, low membrane porosity and a high value for the tortuosity multiplied by the membrane thickness (high Pe_m number). Finally, the concentration polarization must be so strong that the observed rejection will be zero, which is supported by a low mass transfer coefficient.

5.5 Simultaneous modelling of flux and rejection by the Stefan-Maxwell equations

The filtration of PEG through the various membranes has been modelled by simultaneous description of the flux and the rejection by means of the Stefan-Maxwell equations. A detailed description of the equations and the assumptions is given in chapter 2.

Before the results of the modelling of the PEG filtration will be considered, first the introduction of the thermodynamic activity in the transport equations and its influence on the observed rejection will be discussed. Moreover, the consequences of the assumption of a concentration-independent diffusion coefficient will be evaluated.

Subsequently, the procedure for the modelling of the PEG rejection and flux will be

explained. In the last part of this section the Stefan-Maxwell fits and the values of the fit parameters will be discussed.

Introduction of the thermodynamic activity in the transport equations
The introduction of the thermodynamic activity in the transport equations requires a translation of the Fick diffusion coefficient for PEG in water to the Stefan-Maxwell diffusion coefficient according to the following relationship [Krishna, 1987a]:

$$D_{j,k}^{Fick} = \left[1 + x_j \frac{\partial \ln \gamma_j}{\partial x_j} \right] D_{j,k}^{SM} \qquad (5.4)$$

This equation is developed from comparison of eqn. (2.9) with Fick's Law. In contrast to the Fick diffusion coefficient, no thermodynamic influences are incorporated in the Stefan-Maxwell diffusion coefficient. When we use the thermodynamic models described in chapter 3 the Stefan-Maxwell diffusion coefficient can be calculated from the experimentally measured Fick diffusion coefficient. Both the UNIQUAC model and the LQCA model predict the same values for the thermodynamic factor of PEG (see chapter 3). In fig. 5.11 the calculated Stefan-Maxwell diffusion coefficient is presented together with the measured Fick diffusion coefficient for PEG3400 [van der Linden, 1973].
The Fick diffusion coefficient increases moderately from 1.37×10^{-10} to 1.87×10^{-10} in the mass fraction range shown. This is in contrast with the strong decrease in the Stefan-Maxwell coefficient as a function of the mass fraction of PEG3400. It implies that apart from thermodynamic influences additional concentration effects occur, which cause the lowering of the diffusion coefficient.
Krishna has shown for triethylamine-water [1987b] and methanol-n-hexane [1993] that the Fick diffusion coefficient is a strong function of the concentration, whereas the Stefan-Maxwell diffusion coefficient is much less dependent on the concentration. In our case the opposite situation occurs: the concentration dependence of the Stefan-Maxwell diffusion coefficient is cancelled out by the thermodynamic influences. This example for PEG3400 is an exception to the general rule suggested by Wesselingh and Krishna [1990] that by introducing Stefan-Maxwell diffusion coefficients the concentration dependence of the diffusion coefficient can be diminished. For dextranT70 as much as a tenfold decrease in Stefan-Maxwell diffusion coefficient is calculated at 250 kg/m^3 compared to the diffusion coefficient at infinite dilution.
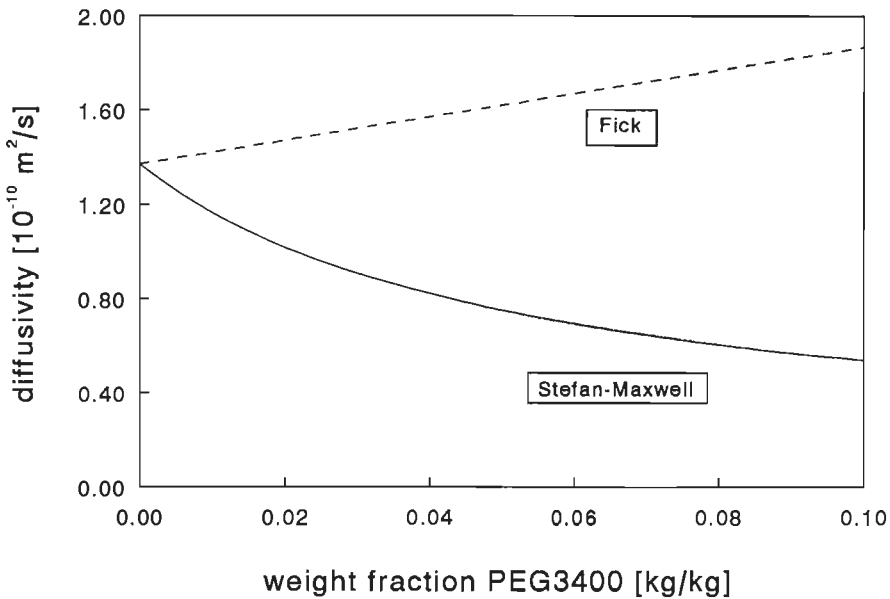
Figure 5.11 *Comparison between the Fick diffusion coefficient and the Stefan-Maxwell diffusion coefficient of PEG3400 in water as a function of the mass fraction.*

In fig. 5.12 the calculated observed PEG rejection is depicted as a function of the flux in four distinct cases: a constant and variable Fick diffusion coefficient in combination with concentration gradients and a constant and variable Stefan-Maxwell diffusion coefficient in combination with activity gradients. Both constant diffusion coefficients have been set equal to the value for the Fick diffusion coefficient in the bulk solution. The variation in the diffusion coefficient has been taken into account by adjusting the values of the diffusion coefficients at each gridpoint in the polarization layer and the membrane to the value which corresponds with the concentration at that point. For the other parameters in the Stefan-Maxwell equation the values for PEG3400/YM30 in the outer section (table 5.1) have been used.

The minor difference in rejection between the results of the variable Fick and the variable Stefan-Maxwell version of the model indicates that the influence of the activity gradient in the membrane is small. The observed rejection for the constant Fick diffusion coefficient is slightly lower, because at higher concentrations the diffusion back to the bulk solution is underestimated compared to the diffusion

according to the Stefan-Maxwell coefficient multiplied by thermodynamic factor (equivalent to D_{Fick}). The discrepancy between the constant and variable version of the Stefan-Maxwell model is small in the low-flux region, but large at high fluxes. In the latter region the concentration polarization is considerable and the effect of an overestimation of the Stefan-Maxwell diffusion coefficient at higher concentrations is clearly visible. The results depicted in fig. 5.12 emphasize that it is an oversimplification to assume that in general the Stefan-Maxwell diffusion coefficients are less concentration dependent than the Fick diffusion coefficients. In this particular case the assumption that the Stefan-Maxwell diffusion coefficient is constant introduces considerably more error than in case a constant Fick diffusion coefficient is assumed.
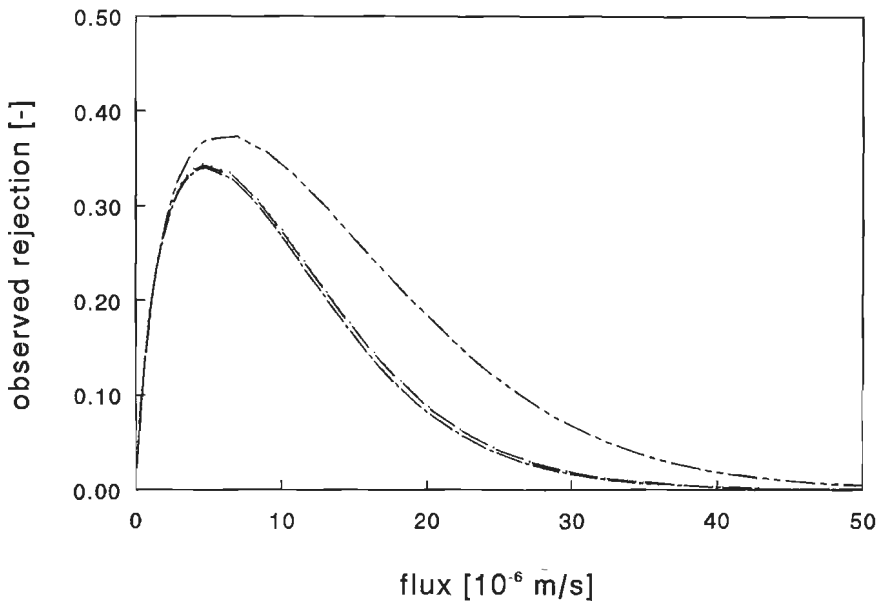
Figure 5.12 *Comparison between the observed rejection calculated for a constant (—·—·) and variable (···) Fick diffusion coefficient based on concentration gradients and for a constant (—··—) and variable (——) Stefan-Maxwell diffusion coefficient based on activity gradients.*

In contrast with the minor influence of the thermodynamic interaction found in our case Zydney [1992] has reported a considerable influence of solute-solute interactions in the polarization layer on the calculation of the actual rejection. This difference is due to the fact that he compares the solute transport in the polarization layer for an infinitely diluted diffusion coefficient (instead of the Fick diffusion coefficient) with the solute transport including thermodynamic and frictional interactions.

Procedure for the modelling of the PEG filtration experiments

In order to model the PEG filtration experiments the various parameters should be evaluated. The Stefan-Maxwell equations contain transport coefficients, the so-called Stefan-Maxwell diffusion coefficients. Furthermore the exclusion of the solute by the membrane is described by the solute partition coefficient and the equations contain some characteristic parameters concerning the membrane: porosity ε, tortuosity τ, pore diameter d_{pore} and membrane thickness L. Finally, the Sherwood relation is incorporated in the model to describe the mass transfer in the polarization layer.

The Stefan-Maxwell diffusion coefficient $D_{s,w}$ has been derived from the Fick diffusion coefficient as described above. The unknown membrane Stefan-Maxwell diffusion coefficients $D_{PEG,m}$ and $D_{w,m}$ and the solute partition coefficient K_{eq} have been fitted to the experimental flux and rejection data. Most of the membrane properties appear solely as a combination in one term: $\varepsilon L/\tau$ (see eqn. (2.30)). We have chosen to fix the membrane thickness as the value provided by the supplier of the membrane and to use ε/τ as one parameter, which as a consequence will express possible deviations in the membrane thickness. By means of the experimentally determined membrane resistance for pure water the quotient of the porosity and tortuosity has been expressed as a function of the diffusion coefficient between solvent and membrane (see eqn. (2.30)). This restraint for the quotient of the porosity and tortuosity has been incorporated in the fit procedure. After some preliminary calculations the pore diameter was set to a value which was in the range provided by the supplier of the membrane. Since the non-constant surface concentration during filtration might alter the mass transfer compared to the one electrochemically measured, the pre-factor A of the Sherwood relation was also fitted to the experimental flux and rejection data.

Discussion of the Stefan-Maxwell fits and the values of the model parameters

In figures 5.1 to 5.5 and 5.7 to 5.10 the model fits according to the Stefan-Maxwell equations have been depicted. The model parameters used for the fits with the Stefan-Maxwell model are presented in table 5.1; their values will be discussed later. The observed rejection, the actual rejection and the flux are described very well. Deviations only occured for the YM30 membrane and the WFBX 0121 membrane for the observed and actual rejection at higher pressures (fluxes). The observed rejection of PEG3400 on the YM30 membrane is well described for fluxes below 40×10^{-6} m.s^{-1} except for the outer section at 270 rpm. In order to show that these values are not

representive for the rejection under those conditions (probably due to problems with the analyses) the observed rejections in a buffer solution of pH=7.4 are provided too. Although these values of the rejection have not been used in the fit, the description is remarkably well. As will be shown in more detail in chapter 8 the observed PEG rejection is not affected by the presence of salts in the buffer solution.

Due to numerical problems occurring during the calculations of the more open YM30 and WFBX0121, which required various adaptations to the computer program, only the first fits can be presented for those membranes.

	PEG1000	PEG1000	PEG3400	PEG3400	PEG3400	PEG3400
	YM10	YM5	YM5	YM30 inner	YM30 outer	WFBX 0121
$D_{s,m} \times 10^9$	6.5	0.59	0.50	0.086	0.44	4.7
$D_{w,m} \times 10^9$	20	7.8	5.8	149	334	7.7
K_{eq}	0.333	0.232	0.00510	0.232	0.190	0.511
A	0.47	0.40	0.20	0.14	0.28	0.026
$\varepsilon/\tau \times 10^2$	1.51	0.571	0.665	2.01	1.43	3.42
$d_{pore} \times 10^9$	4.5	3.2	3.2	8	8	9
$L \times 10^7$	1	1	1	1	1	5
ϕK_c	0.364	0.256	0.0055	0.186	0.167	0.516
ϕK_d	0.320	0.161	0.0040	0.0886	0.144	0.497
$R_m \times 10^{-12}$	8.7-10	50.3	47.6	1.79	1.79	4.5

Table 5.1 Top panel: *Values of the parameters used in the Stefan-Maxwell equations for various types of PEG and membranes. The first five parameters have been fitted (see text).* Second panel: *Values for the hindered diffusivities evaluated from the parameters for the Stefan-Maxwell model.* Bottom panel: *experimental membrane resistance.*

The Stefan-Maxwell equations with the parameters in table 5.1 predict the flux, the observed rejection and the actual rejection for PEG3400 on YM30 very well up to a

flux of 40×10^{-6} m/s. Above that value deviations occur: the calculated rise in flux with pressure is stronger than experimentally observed, the drop in observed rejection is more pronounced and the actual rejection levels off to a lower value than calculated by means of the osmotic pressure model (see above). The discrepancy between the calculated and experimentally measured fluxes and observed rejections can be ascribed to the underprediction of the actual rejection.

The fit procedure has been performed with a selected number of experimental data points. As can be seen from the scattering in fig. 5.8, the calculation of the concentration at the membrane surface is very sensitive to small errors in the flux and the permeate concentration. This causes numerical problems during the calculations with the fit procedure. Therefore only the datapoints which showed a regular behaviour in the actual rejection plot have been taken into account. Because the highest pressures were not incorporated in the fit, the plateau value of the actual rejection is underestimated (0.81 instead of 0.85). This results in a limitation of the permeate concentration at lower fluxes, which explains the stronger decrease in the observed rejection and the overprediction of the flux.

The Stefan-Maxwell model gives a reasonable description of the flux and observed rejection in the tubular module, taking into account the discrepancy in the actual rejection according to the osmotic pressure and the mass transfer coefficient according to the experimental data. The actual rejection is underestimated by the model at the highest fluxes, which is at least partly caused by the fact that only data points below 10×10^{-6} m/s have been used in the fit procedure. The fluxes are still well described at the higher pressures. If more weight is given to the rejection in the objective function the fit of the rejection might improve with a still reasonable description of the flux.

It has been shown that the Stefan-Maxwell model is able to provide a good description of both flux and rejection for various PEG's and membranes. In this paragraph the values the fitted parameters are considered in more detail. The diffusion coefficients between solute/solvent and the membrane are expected to increase with decreasing solute diameter and increasing pore diameter. This trend is indeed visible for the water-membrane diffusion coefficient $D_{w,m}$ in the YM membranes. Although the WFBX membrane has the highest pore diameter, a low value of $D_{w,m}$ was found. This is in contrast with the high value of the PEG-membrane diffusion coefficient $D_{PEG,m}$ in that type of membrane. The correlation coefficients between $D_{w,m}$ and $D_{PEG,m}$ are

in general larger than 0.99, which indicates a strong correlation between these parameters (for WFBX only 0.85). The exclusion coefficient is strongly correlated with the membrane diffusion coefficients for PEG3400 filtration through the YM5 and YM30 membranes; in the other cases the correlation coefficients are about 0.5. The trend in the exclusion coefficient conforms with expectations based on the solute and pore diameter. The pre-factor is the parameter which is the least correlated with the other fit parameters. The pre-factor of the Sherwood relation for the experiments with one permeate collection in the stirred cell shows some variation between the different PEG and membrane systems and deviates from the electrochemically determined value of 0.23. The electrochemically determined pre-factor for the inner section (A=0.14) and the outer section (A=0.29) agree very well with the fitted values for the experiments with separately collected permeate streams. The pre-factor obtained for the third position of the tubular membrane was also in good agreement with the literature value of 0.027. This might indicate that when there are large variations in mass transfer over the membrane surface the surface-averaged flux and rejection are not a good measure for the fit of the parameters in the Stefan-Maxwell equations. Additional research is necessary to confirm this.

The porosity divided by the tortuosity ε/τ has been fitted in combination with $D_{w,m}$ (see above). The value of ε/τ indeed increases for the membranes, which are expected to be more open based on the pure water flux.

Except the pre-factor, which is different for the inner and outer section, all parameters should be equal for the inner and outer section of the YM30 membrane. However, a considerable deviation is found between the two sections. In order to check whether this is the result of the correlation between the parameters, a combined fit for the two sections could be performed with the pre-factors set to the values corresponding to the inner and outer section.

5.6 Comparison with the hydrodynamic model

As mentioned in the previous section the fitted parameters of the Stefan-Maxwell show considerable correlation. The strongest correlation occurs between the diffusion coefficients $D_{PEG,m}$, $D_{w,m}$ and the exclusion coefficient K_{eq}. Those three parameters all influence the transport in the membrane. In chap. 2 besides the Stefan-Maxwell model a hydrodynamic model is also described, which is able to predict the transport coefficient from the relative size of the solute and the pore diameter. By comparing the Stefan-Maxwell model and the hydrodynamic model two equations have been

derived, which express the hydrodynamic coefficients K_d and K_c in terms of the parameters used in the Stefan-Maxwell model (eqns. (2.64) and (2.65), respectively). These equations are only valid for dilute solutions, but the non-ideality of the PEG is low at the concentrations in the membrane. By substituting the fitted parameters into these equations and by multiplying the results by the exclusion coefficient the combined effect of these parameters can be compared with the theoretical relationships for ϕK_c and ϕK_d. The calculated values for these parameters have been presented in table 5.1.
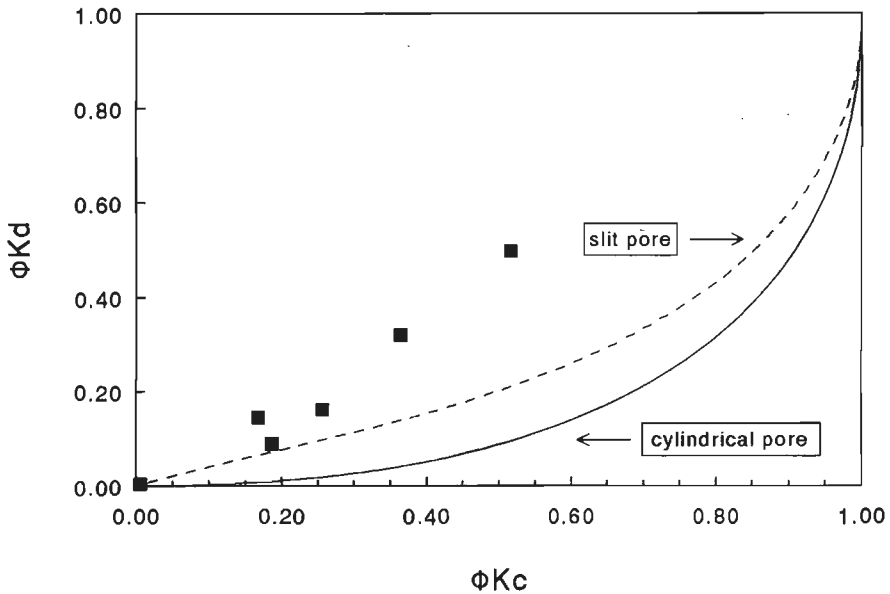
Figure 5.13 *Hindered diffusivity ϕK_d as a function of the asymptotic sieving coefficient ϕK_c evaluated from the fitted parameters of the Stefan-Maxwell equations in comparison with the theoretical curves for spherical solutes in cylindrical and slit pores.*

As described in more detail in chap. 2, relationships between ϕK_c and ϕK_d have been derived for cylindrical pores [Bungay and Brenner, 1973] and slit-shaped pores [Deen, 1987]. These values are depicted in fig. 5.13 together with the calculated values according to the Stefan-Maxwell fit. ϕK_d rises with increasing ϕK_c, as was theoretically expected, however the increase is stronger than predicted. ϕK_d and ϕK_c can also be considered as a function of the ratio of solute radius to pore radius, λ (see fig. 5.14). The values for λ have been calculated from the fitted solute partition coefficient

K_{eq}, using eqn. (2.26).

According to fig. 5.14 the difference between the values for ϕK_c and ϕK_d derived from the fits is much less than the one predicted for both the cylindrical and slit-shaped pores. The values for ϕK_c are lower than predicted by both models. The correction of the underpredicted asymptotic actual rejections $R_{a,\infty}$ would only further decrease the asymptotic sieving coefficient ϕK_c. The ratio between ϕK_c and ϕK_d occurs in combination with $\varepsilon L/\tau$ in the membrane Peclet number (eqn. (2.35) with $v'' = v/(\varepsilon/\tau)$). This ratio could be increased by lowering the value of $\varepsilon L/\tau$. By adjusting the membrane thickness, which was provided by the supplier, a better agreement of ϕK_d with the theoretical values can be achieved. However, a change in $\varepsilon L/\tau$ also directly affects the description of the flux.
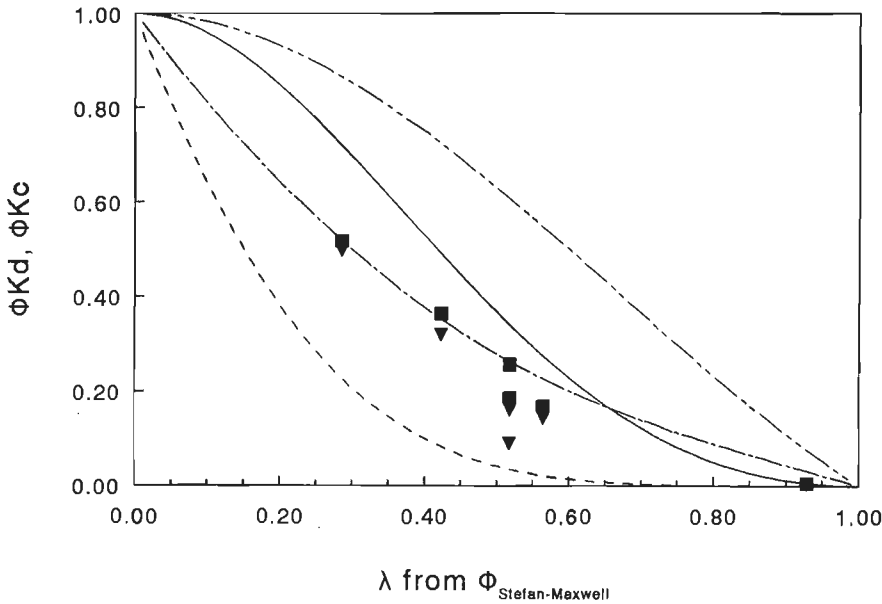

Figure 5.14 *Hindered diffusivity ϕK_d and the asymptotic sieving coefficient ϕK_c evaluated from the fitted parameters of the Stefan-Maxwell equations as a function of λ in comparison with the theoretical curves for spherical solutes in cylindrical and slit pores. Cylindrical: ϕK_c (——) and ϕK_d (———); slit pores: ϕK_c (—··—) and ϕK_d (—·—).*

The discrepancy between the theoretical and fitted values could be caused by the pore size distribution of the membrane. Mochizuki et al. [1993b] have shown for cylindrical pores that the values for ϕK_c and ϕK_d are both considerably larger if the pores are

not uniform. Moreover, they showed that the relationship between ϕK_d and ϕK_c shifts to lower values, which is in disagreement with fig. 5.13. According to Sheldon [1991a] the separating surface of the regenerated cellulose YM membrane appeared to be composed of closely packed fibres. Very few distinct circular pores were found; the pores that were present seemed to arise due to the packing of the surface fibres. It could be possible that the assumption of cylindrical or slit pores is not allowed for these type of membranes.

Another possible explanation could the flexibility of PEG and its non-spherical shape. One would expect that the PEG might have a more elongated configuration in the pore, which would reduce the hydrodynamic interactions and thereby increase K_d. This would cause the ϕK_d data to fall above the theoretical predictions as in fig. 5.13. Further study is necessary to determine to what extent the strong correlation between the Stefan-Maxwell parameters is responsible for the deviations in ϕK_d and ϕK_c.

5.7 Conclusions

The flux during PEG filtration was lower than the pure water flux as a result of the osmotic pressure difference over the membrane. In most cases an almost linear relationship between the flux and the pressure was observed. Filtration of PEG3400 through a YM30 membrane, a more than proportional increase in flux was measured for the highest fluxes. It has been shown that this phenomenon can be attributed to concentration limitation. Concentration limitation occurs for partially rejected components if the observed rejection is lowered to zero due to concentration polarization and the actual rejection has reached its plateau value.

At high fluxes a considerable difference was found between the observed PEG rejection and the actual PEG rejection by the membrane. The observed rejection showed a sometimes very strong decrease at higher fluxes, whereas the actual rejection reached a plateau value. The relationship between the actual rejection and the flux was found to be independent of the mass transfer in the polarization layer, which confirmed that the decrease in observed rejection can be ascribed to concentration polarization, as has been reported for other solutes. The calculation of the actual rejection based on the mass transfer coefficient in the polarization layer or the osmotic pressure showed similar relationships with the flux. The plateau values calculated by both methods agreed fairly well in most cases.

Simulations with the Stefan-Maxwell model have shown that the introduction of the non-ideal behaviour in the equations only slightly influences the flux and PEG

rejection.

In general, the Stefan-Maxwell equations were able to describe the flux and the rejection very well, using fitted values for the diffusion coefficients with the membrane, the exclusion factor and the pre-factor of the Sherwood relation. The strong correlation between some of the parameters sometimes resulted in unrealistic values of the parameters. Comparison of combinations of these parameters with the hindered diffusivity and the asymptotic sieving coefficient in the hydrodynamic model for dilute solutions showed a poor agreement with the theoretical models for cylindrical and slit-shaped pores. If PEG would have an elongated configuration in the pore the agreement would be better. Separate determination of at least some of the parameters which determine the actual rejection by the membrane, will diminish the correlation of the parameters in the fit procedure.

6. PEG/DEXTRAN/WATER SYSTEMS

6.1 Introduction

Few studies have been performed to characterize the mutual influence of components on the rejection in multicomponent systems. Most previous studies have dealt with the formation of a deposit or gel layer on the membrane surface and its effect on the rejection. This will be discussed in more detail in chapter 8. From the Stefan-Maxwell equations it can be seen that even without the formation of a layer on the membrane surface, the transport of the solute can be altered by addition of another component due to friction between the two solutes expressed by the diffusion coefficient $D_{i,j}^{sm}$. The solute transport can also be affected by changes in the thermodynamic behaviour expressed by the thermodynamic factor due to the presence of another component. The possible influence of those phenomena has been studied for combinations of PEG and dextran. As is shown in chap. 4 dextran forms only a polarization layer on the membrane surface, no gel layer formation occurs. The extent of concentration polarization can be considerable. Since PEG and dextran are able to form two-phase systems they are likely to mutually influence their thermodynamic activities to a considerable extent [Kang et al., 1988a].

First the flux and rejection for the binary dextran/water system will be discussed and subsequently the flux and rejection in the ternary system will be evaluated.

6.2 Materials and methods

The method used for the flux and rejection measurements at various pressures during PEG filtration has been explained in chapter 5. The same procedure has been used to characterize the flux and rejection for the binary dextran/water system and the ternary PEG/dextran/water system as a function of pressure and stirrer speed. The concentrations of PEG and dextran were both 10 kg/m^3. The flux and rejection for the ternary system has also been studied by concentration experiments at a constant pressure of 200 kPa. The initial bulk concentration of dextran was varied by adding the appropriate weight of dextran to a solution with an initial PEG concentration of 10 kg/m^3.

The PEG concentrations used for the calculation of the observed PEG rejection in the ternary system have been expressed as kg PEG/(m^3 PEG + water), which excludes the amount of dextran present in the solution. Due to this definition the observed rejection is equal to zero, if all of the PEG that is supplied by convective transport

permeates through the membrane.

All experiments have been performed in stirred cells using YM5, YM10 and YM30 membranes (see chapter 5). The experiments were carried out on YM5 and YM10 membranes in a cell with one combined permeate collection, those on YM30 were performed with separate permeate collection.

As model solutes PEG1000 (Janssen), PEG3400 (Aldrich) and dextranT70 (Sigma Chemical) were used. Information about physical properties is available in chap. 3.

6.3 Flux and rejection in the binary dextran/water system

In this section the flux and rejection during the filtration of the dextran/water system will be discussed to be able to compare them with the data found for the filtration of the ternary PEG/dextran/water systems. The flux and rejection for the binary PEG/water system have already been discussed in chapter 5.

In figs. 6.1 and 6.2 the flux vs. pressure is depicted for the binary dextranT70/water system filtered through a YM30 membrane for 90 and 270 rpm, respectively. The bulk concentration of dextran was 10 kg/m^3 and was kept constant for all pressures. The measurements were performed in the stirred cell with two separate permeate streams (inner/outer). The corresponding observed dextran rejections for both stirrer speeds are depicted in fig. 6.3.

Flux during the filtration of dextran

A remarkable difference between the filtration of PEG and dextran is the flux limitation, which occurs at higher pressures during the filtration of dextran. The experimental flux still rises slightly with increasing pressure, but certainly not linear or more than proportional as is the case for the PEG filtration (see chap. 5). Another feature is the much larger decrease in flux compared to the pure water flux for the filtration of dextran than for PEG. The strong decrease in flux during the filtration of dextran is caused by the high concentration at the membrane surface. Due to this high concentration the osmotic pressure during the dextran filtration is much larger than for the PEG filtration, although the osmotic pressure of dextran is distinctly lower than that of PEG at the same concentration. The high value for the concentration at the membrane surface is partly the result of the high actual rejection of dextran, but the low diffusion coefficient of dextran considerably reduces the rate of back transport leading to the very high concentrations at the membrane surface.
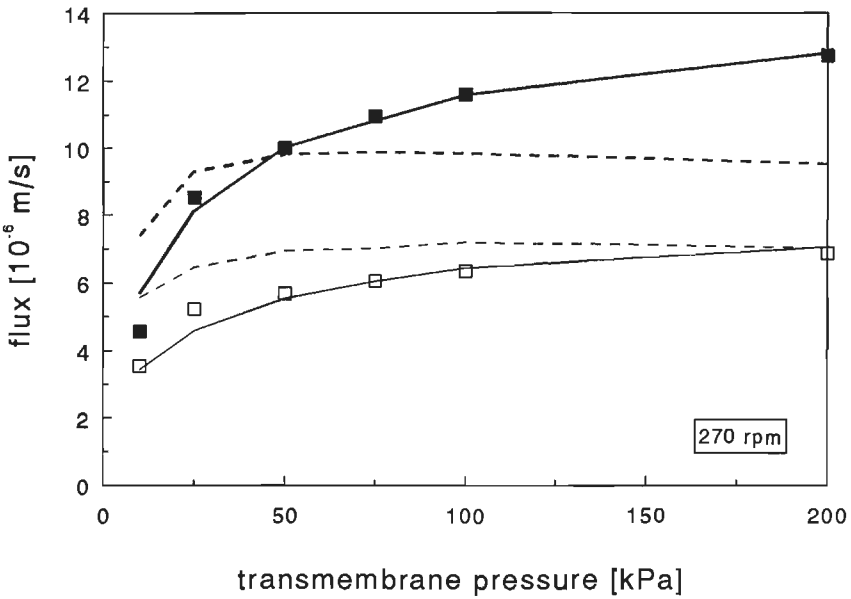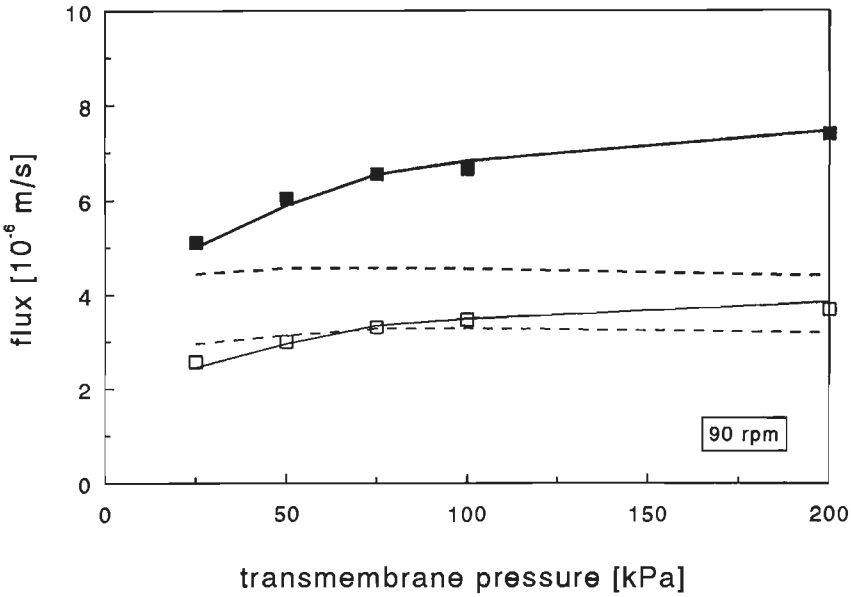
Figure 6.1 *Flux during dextranT70 filtration as a function of the transmembrane pressure for two sections. YM30. n=90 rpm. C_{dex}=10 kg.m^{-3}. Model curves based on fitted average mass transfer coefficients (- -) and coefficients derived from the Sherwood correlation (——).*
Thin lines represent inner section, thick lines represent outer section.
**Figure 6.2** *Idem for n=270 rpm.*

The fact that the fluxes for the outer permeate section are lower than those in the inner permeate section can be ascribed to the higher mass transfer coefficient in the outer section, which has been measured electrochemically (chap. 3). An increase in stirrer speed from 90 rpm to 270 rpm (fig. 6.2) shows an increase in flux. The higher mass transfer coefficient at the higher stirrer speed decreases the concentration at the membrane surface and therefore the osmotic pressure. The curves in figs. 6.1 and 6.2 represent model calculations. The flux during dextran filtration can be well described by a constant average fitted mass transfer coefficient for both stirrer speeds and the inner and outer permeate section. If the mass transfer coefficient is calculated with the electrochemically determined Sherwood relation (chap. 3), the flux is underpredicted at higher pressures, mainly due to the introduction of the viscosity correction $(\eta_b/\eta_w)^{0.14}$. According to a recent study of Rosén et al. [1993] the exponent of the viscosity factor (η_b/η_w) is far less than the value of 0.14 for high Schmidt numbers. They obtain a value of 0.025, which is consistent with our observation that a constant mass transfer coefficient provides a better description of the flux during dextran filtration than a viscosity correction with the power 0.14.

The modelling of the flux during dextran filtration is discussed in more detail in an appendix at the end of this chapter.

Dextran rejection

The observed dextran rejection (fig. 6.3) shows a monotonic decrease with flux, in contrast with the maximum observed for the filtration of PEG (chap. 5). As discussed in more detail in chapter 5 the maximum in the observed rejection occurs at a flux equal to the mass transfer coefficient or even lower, depending on the membrane Peclet number. The exact values of the mass transfer coefficient are given in the appendix, but all of them are below the lowest filtration flux as a result of the low diffusion coefficient of dextranT70. This means that in the entire evaluated flux region the rejection is influenced primarily by concentration polarization. This is affirmed by the higher observed rejection at 270 rpm compared to 90 rpm. The difference in observed rejection in the inner and outer section clearly shows the influence of the variation in local mass transfer coefficient in the stirred cell. The higher observed rejection in the outer section compared to the inner section is in accordance with the higher mass transfer found electrochemically.
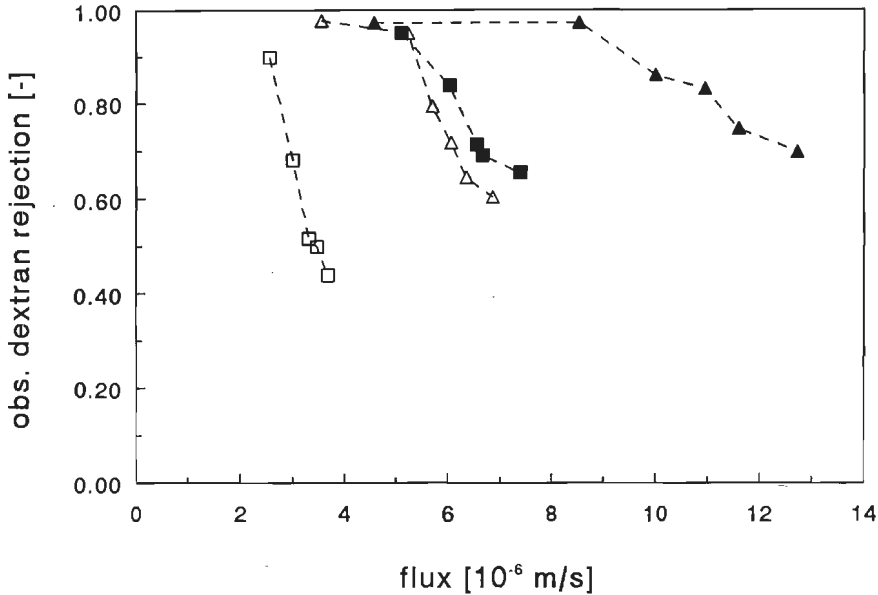
Figure 6.3 *Observed dextranT70 rejection as a function of the flux. Inner section: n=90 rpm (□) and n=270 rpm (△); Outer section: n=90 rpm (■) and n=270 rpm (▲).*

6.4 Flux in ternary system

The flux in the ternary PEG/dextran/water system (fig. 6.4) is mainly determined by the presence of dextran as was to be expected, since the flux for the binary dextran system is much lower than the one for the binary PEG system. The presence of PEG causes a small additional decrease in flux. The osmotic pressure in the ternary PEG/dextran/water system is considerably higher than in the binary dextran/water system (fig. 6.5, the solid lines will be discussed in section 6.5). Due to PEG-dextran interactions the ternary osmotic pressure is higher than the addition of the two binary osmotic pressures. Besides a rise in osmotic pressure the activities of both components are also increased by their mutual presence (figs. 6.6a and 6.6b). This increase causes an increased back-diffusion of PEG and dextran to the bulk solution, which results in a lower concentration at the membrane surface for both components. The combination of both effects is a slight decrease in flux for the filtration conditions used for the experiments depicted in fig. 6.4. In the figure only the data for the outer permeate

section are presented; the results for the inner permeate section are similar.
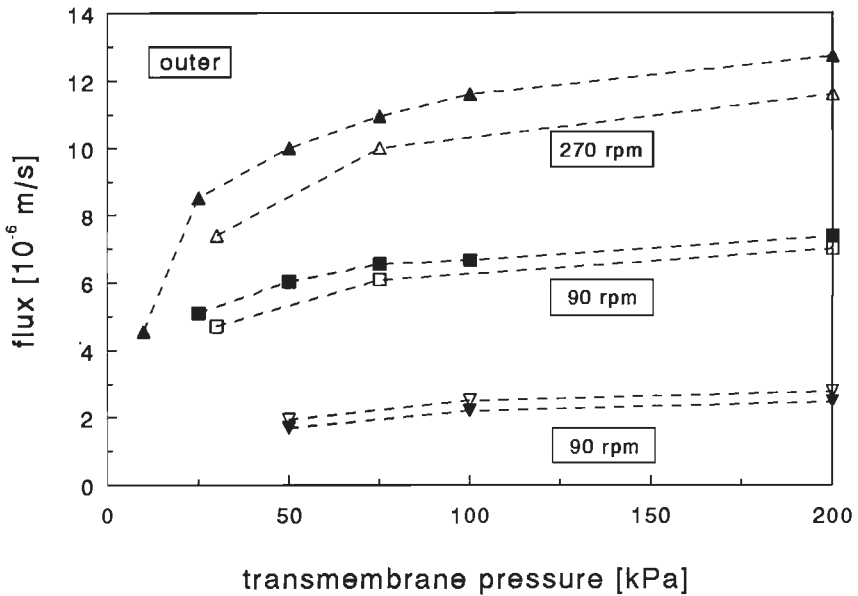
Figure 6.4 *The influence of PEG addition on the flux during dextranT70 filtration as a function of the transmembrane pressure for the outer section. YM30. $C_{dex}=10$ kg.m^{-3}: n=90 (□) and 270 rpm (△); $C_{dex}=50$ kg.m^{-3}: n=90 rpm (▽). Open symbols:* only dextran; *closed symbols:* dextran + PEG, $C_{PEG}=10$ kg.m^{-3}.

The flux was also studied as a function of the dextran concentration. The experiments were performed by concentrating a (PEG)/dextran/water solution in a stirred cell with one permeate stream. In this case a YM5 membrane was used instead of a YM30 membrane as in fig. 6.4. In fig. 6.7 the flux is depicted as a function of the natural logarithm of the bulk concentration of dextran at three different PEG concentrations. The flux decreases by the addition of PEG; the higher the initial PEG concentration, the stronger the decrease. It can be concluded that the addition of PEG to the dextran solution does not change the linearity of the relationship between the flux and $\ln(C_b)$.
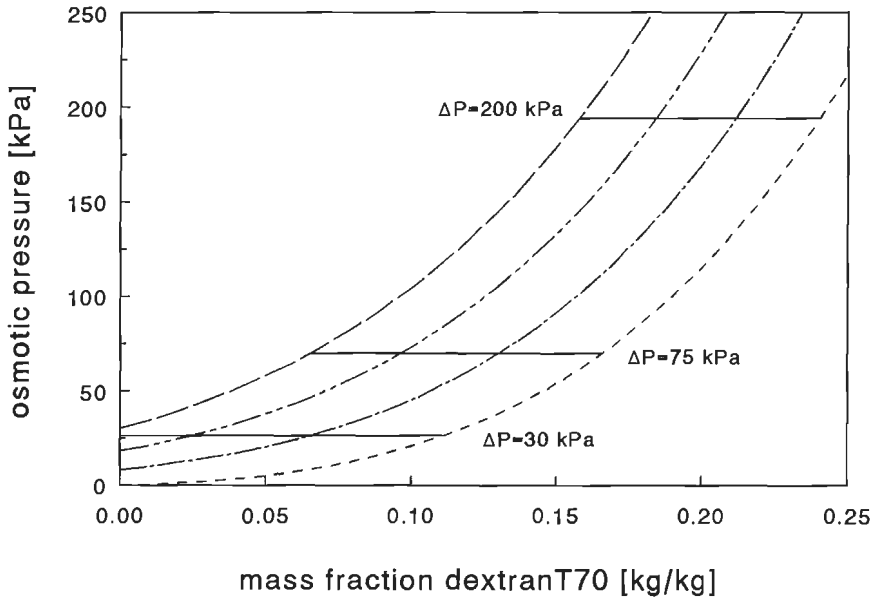
Figure 6.5 *Ternary osmotic pressure as a function of the mass fraction dextranT70 for various PEG3400 mass fractions. Mass fraction PEG: 0 (- -), 0.01 (—·—·), 0.02 (—··—), 0.03 kg.kg⁻¹ (——).*
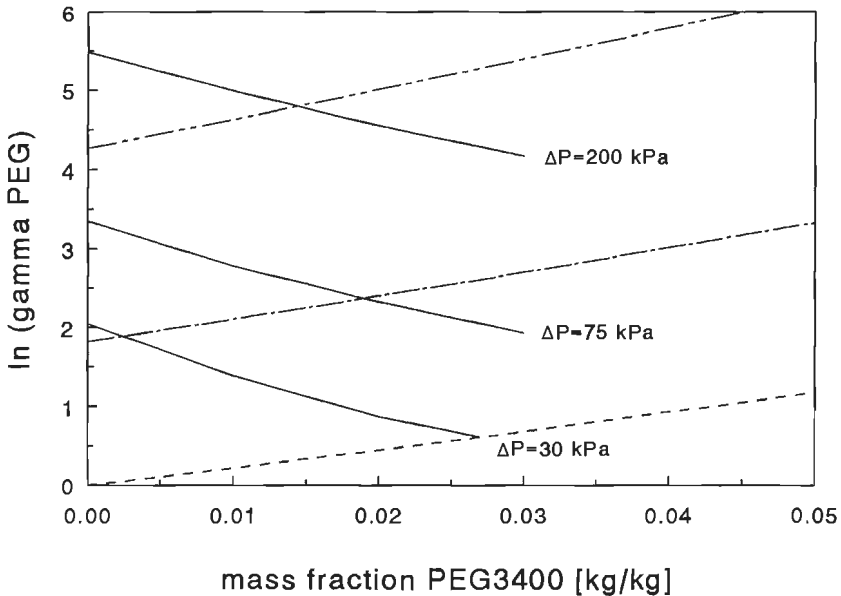
Figure 6.6a *Ternary activity coefficient PEG3400 as a function of the mass fraction PEG for various dextranT70 mass fractions. Mass fraction dextran: 0 (- -), 0.1 (—·—·), 0.2 kg.kg⁻¹ (—··—).*
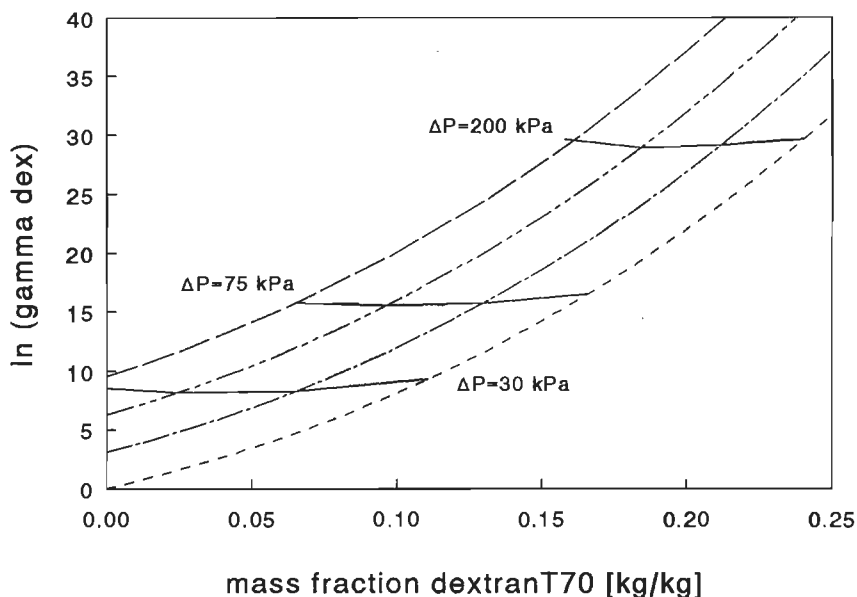
Figure 6.6b *Ternary activity coefficient dextranT70 as a function of the mass fraction dextran for various PEG3400 mass fractions. Mass fraction PEG: 0 (- -), 0.01 (—·—), 0.02 (—··—), 0.03 kg.kg^{-1} (——).*
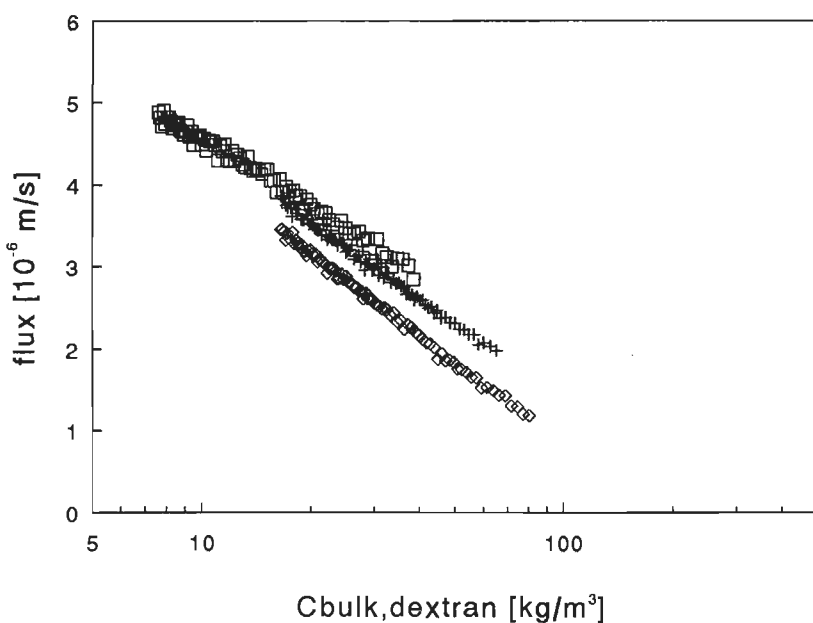
Figure 6.7 *Ternary flux during PEG3400 and dextranT70 filtration as a function of the dextran concentration for various PEG concentrations. YM5. n=90 rpm. C$_{PEG}$: 0 (□), 2 (+), 10 kg.m^{-3} (◇).*

The flux for the binary dextran/water system can be evaluated similarly as described in the previous section. As described in the appendix a constant mass transfer coefficient of 1.52 μm/s can be derived, which provides a good description for the entire dextran/water experiment. According to the Sherwood relation the mass transfer coefficient varies from 1.39 μm/s at the start to 1.23 μm/s at the end of the experiment. The decrease in the mass transfer coefficient is due to the increase in bulk viscosity from $1.09 \times 10^{-3}$ Pa·s to 2.23×10^{-3} Pa·s. The decrease in $(\eta_b/\eta_w)^{0.14}$ is only minor: from 0.664 to 0.649.

6.5 Rejection in ternary system

The rejection in a ternary PEG/dextran/water system has been determined in two types of experiments:

-By concentrating a PEG/dextran/water solution at constant pressure.

-By changing the pressure at constant PEG and dextran concentration.

First the results of the concentration experiments will be discussed.

The rejection has been measured for several combinations of PEG, dextran and membranes. In fig. 6.8 a typical result is given for the system PEG1000/dextranT70 on a YM10 membrane in a stirred cell with one combined permeate section. The observed rejection of PEG is depicted as a function of the flux at a constant pressure of 200 kPa. The variation in flux is due to the rise of the dextran concentration of the solution during the experiment. Starting from the highest flux to the lowest flux the dextran bulk concentration increases from 7 to 250 kg/m^3. The variation in PEG concentration (max. 10%) is relatively small since the rejection has low values.

In the figure the rejection for PEG1000 without the presence of dextran is also given. To obtain comparable values for the flux these rejections have been measured at lower transmembrane pressures. It is very important to compare the observed rejection at the same flux instead of at the same pressure, because the concentration polarization is determined by both the flux and the mass transfer coefficient and the actual rejection is a function of the flux. Comparison of these results with the rejection in the ternary system shows that at high fluxes in the range of 2×10^{-6} to 6×10^{-6} m/s (low dextran concentrations) the rejection increases from 0.1 to 0.2. Decreasing the flux by concentration of the PEG/dextran solution results in a decrease in PEG rejection. At fluxes below 1×10^{-6} m/s the rejection becomes negative. Even values as low as -0.9

have been measured. The rejection is based on concentrations in which only the amount of PEG and water are taken into account.
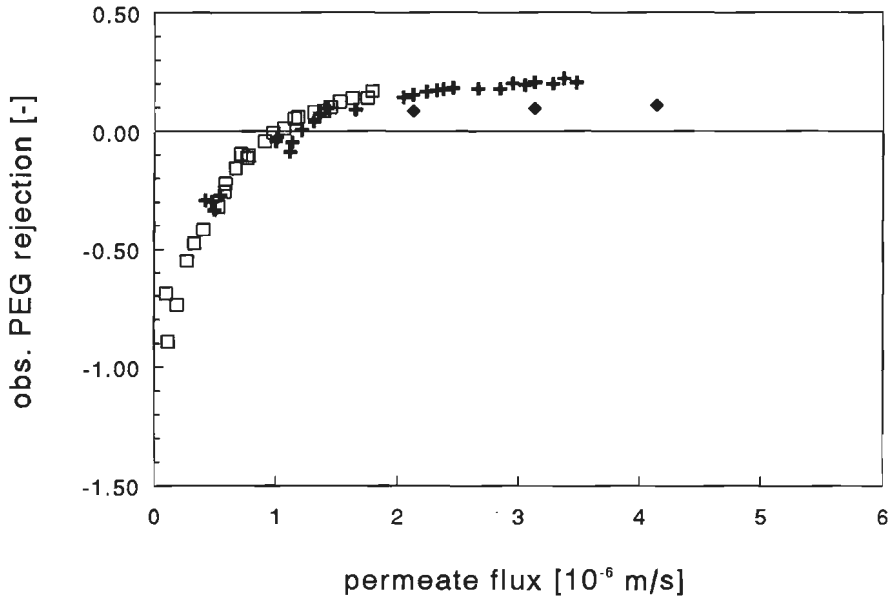
Figure 6.8 *PEG1000 rejection vs. permeate flux for various stirrer speeds in the presence of dextranT70. YM10. $\Delta P = 200$ kPa, $C_{PEG} \approx 10$ kg.m^{-3}, $C_{dex} = 20\text{-}288$ kg.m^{-3}. $n = 90$ (+), 120 rpm ($\square$). PEG1000 rejection without dextran: $\Delta P = 20\text{-}40$ kPa, $n = 90$ rpm ($\blacklozenge$).*

Rejection measurements for PEG1000 with a YM5 membrane also showed a strong decrease in PEG rejection in the presence of dextran compared with the rejection without dextran (fig. 6.9). In this case a decrease in PEG rejection occurs over the entire flux range in contrast with the increase in the rejection, which has been observed at higher fluxes for YM10. In both figs. 6.8 and 6.9 the variation in stirrer speed does not show a clear influence on the relationship between the rejection and the permeate flux.

The decrease in PEG rejection in the presence of dextran has also been found for PEG3400/dextranT70 on the YM5 membrane.
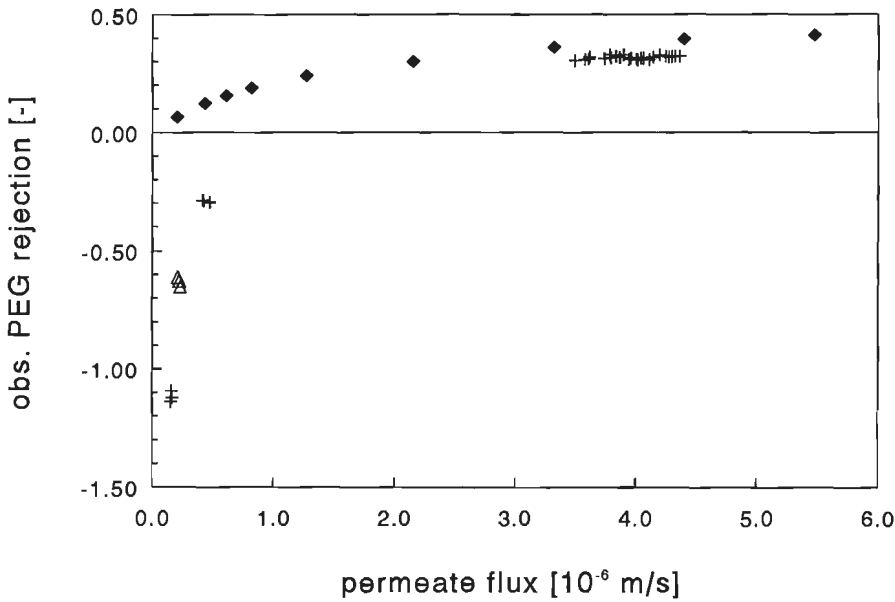
Figure 6.9 *PEG1000 rejection vs. permeate flux for various stirrer speeds in the presence of dextran T70. YM5. ΔP=200 kPa, C_{PEG}=10 kg.m^{-3}, C_{dex}= 7-247 kg.m^{-3}, n=90 (+), 270 rpm (▵). PEG1000 rejection without dextran: ΔP=20-250 kPa, n=90 rpm (♦).*

Negative values for the PEG rejection, which are calculated with concentrations based on kg PEG/(volume PEG + water), imply that the permeate concentration is larger than the bulk concentration. In other words, due to the presence of the dextran the transport of PEG through the membrane is promoted to such extent, that the permeate concentration reaches even higher values than the bulk concentration. According to the film model, the convective transport in the polarization layer is equal to $v \cdot C_b$ at z=0, which is in this case lower than the solute flux in the permeate $v \cdot C_p$. Except convective transport diffusion should also occur in the direction of the membrane in order to explain the high PEG concentrations in the permeate. This means that the presence of dextran should cause an extra driving force for PEG transport through the membrane besides the pressure gradient.

The presence of dextran at the retentate side of the membrane strongly influences the activity coefficient of PEG. Due to the high rejection of dextran the activity coefficient of PEG in the permeate is close to one. Therefore, a large difference in PEG activity exists between both sides of the membrane, which causes a considerable diffusion flux

through the membrane. Especially at low fluxes where diffusion is predominant the influence on the rejection is the most pronounced. Negative rejections can only be achieved if the PEG activity in the bulk solution is higher than in the permeate solution, in spite of the higher PEG concentration in the permeate. The higher the dextran concentrations, the stronger the increase of the diffusive flux through the membrane. In this experiment high dextran concentrations and low fluxes go together, which reinforces the decrease in PEG rejection.
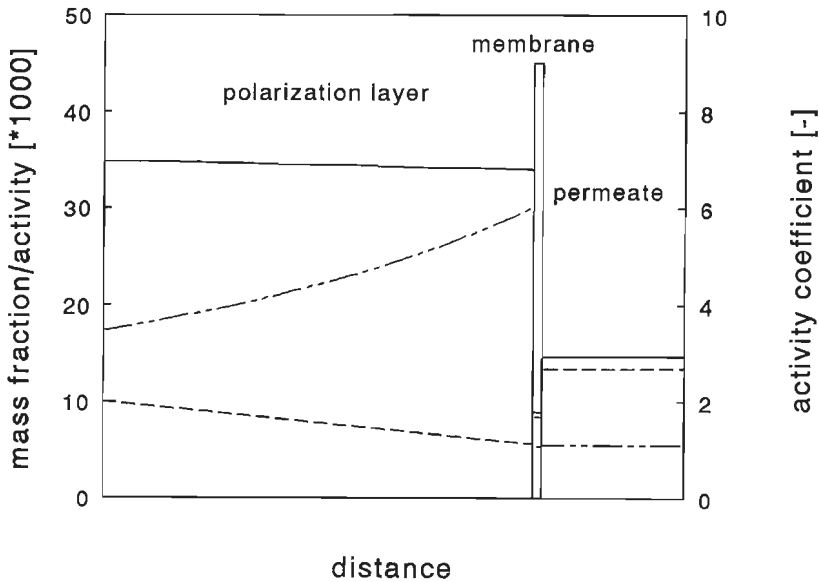
Figure 6.10 *Mass fraction* (- -), *activity* (——) *and activity coefficient* (—··—) *profiles of PEG1000 in polarization layer and membrane at* $v=4.8\times10^{-7}$ *m/s and* $R_o=-0.34$. $C_{dex}=173$ *kg.m^{-3}. YM10. n=90 rpm.* $\Delta P=200$ *kPa.*

To estimate whether the increase in the PEG activity coefficient in the presence of dextran is indeed sufficient to cause a higher activity in the retentate than in the permeate a simplified calculation of the activity profiles has been performed. The conditions used for the calculation are bulk concentrations of 10 kg/m^3 PEG1000 and 173 kg/m^3 dextran, a flux of 4.8×10^{-7} m/s and an observed rejection of -0.34. Those values for the observed rejection and flux have been measured experimentally for these bulk concentrations on the YM10 membrane. As a first estimate it is assumed that the concentration profile of dextran is hardly affected by the low concentrations of

PEG. From the dextran profile in the polarization layer the activity coefficients for PEG can be found. The results of the calculation, which are depicted in fig. 6.10, show that the activity of PEG1000 is indeed higher in the polarization layer than in the permeate, which means an additional driving force due to a difference in thermodynamic activity between both sides of the membrane. The activity profile in the polarization layer has a negative gradient, which indicates a positive diffusion in the direction of the membrane. Since the activity coefficient of PEG increases in the direction towards the membrane due to the higher dextran concentrations near the membrane surface, the gradient in mass fraction is even more negative than that for the PEG activity.

In the experiments discussed above the flux was varied by concentrating the PEG/dextran/water solution. The rejection in the ternary system has also been studied at constant bulk concentrations of PEG6000 and dextranT70 at various pressures. The solutions were filtered through a YM30 membrane, which is more open than the membranes used for the concentration experiments. Therefore, higher fluxes could be reached during filtration. The bulk concentrations of dextran in these experiments were 10 kg/m^3 and 50 kg/m^3. These values were relatively low compared to the highest concentrations reached in the concentrating experiments. In this way the influence of PEG-dextran interactions could also be studied in the high flux region. In figs. 6.11a and 6.11b the PEG rejection is presented as a function of the flux for two dextran concentrations in the inner and outer section, respectively. As a comparison the PEG rejection is also given without dextran present.

Remarkable differences between the PEG rejection in the presence and absence of dextran have been found. The observed PEG rejection in the presence of dextran shows a strong increase with the flux, whereas the PEG rejection in the binary system remains equal or even decreases. The PEG rejections for the two different dextran concentrations do not appear to coincide on one curve as a function of flux as is the case in the concentration experiments at constant pressure. Moreover, the PEG rejections in the inner and outer section are very similar at each pressure for each of the two bulk concentrations, although the flux differs considerably between the two sections. This indicates that the observed PEG rejection is more related to the pressure difference than to the filtration flux. Another feature is the increase of the PEG rejection for the highest pressures compared to the PEG rejection for the binary system at the same flux.
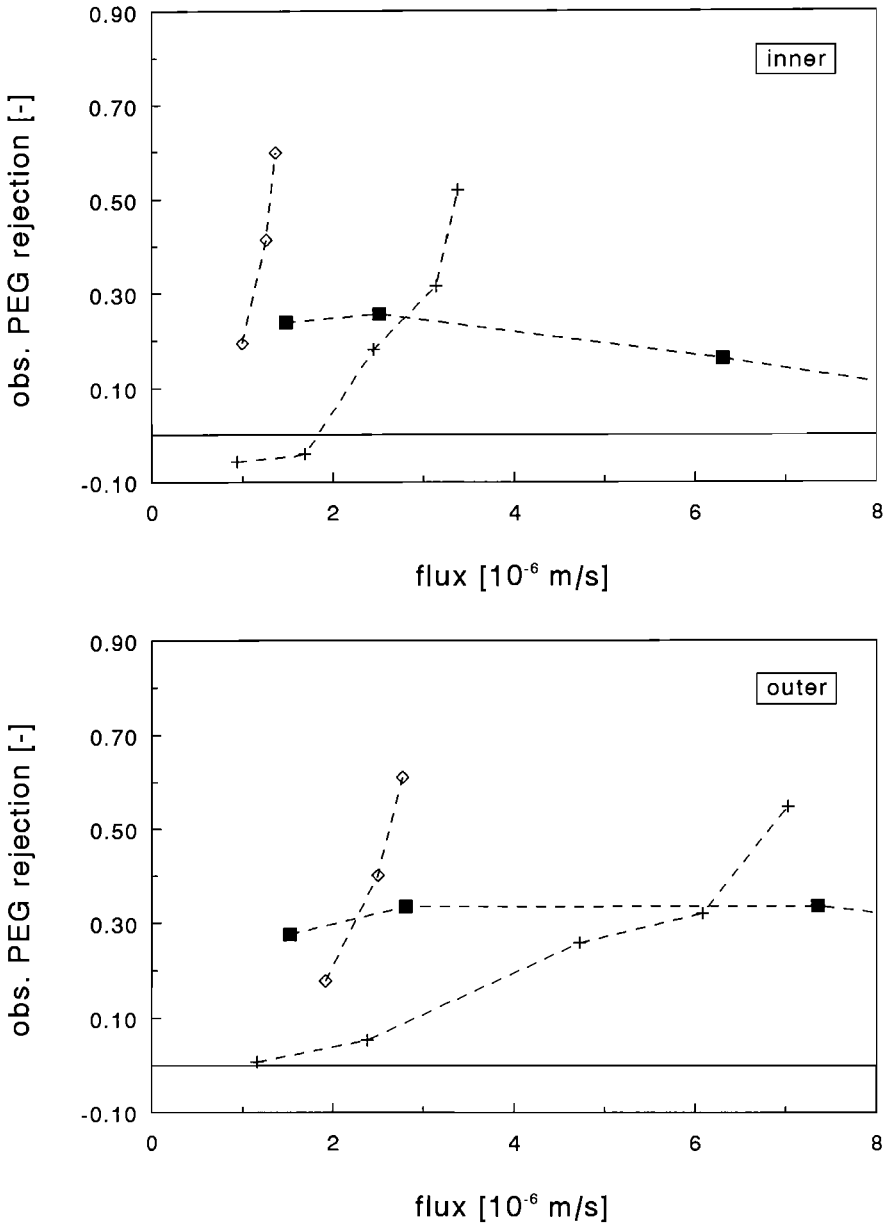
Figure 6.11a *Observed PEG3400 rejection as a function of the flux in the presence of dextran T70 for the inner section. YM30. n=90 rpm. $C_{PEG}=10$ kg.m^{-3}. $C_{dex}=$ 10 kg.m^{-3} (+): $\Delta P=$ 5-200 kPa and $C_{dex}=$ 50 kg.m^{-3} ($\diamond$): $\Delta P=30$-200 kPa.*
PEG1000 rejection without dextran (■): $\Delta P=5$, 10 and 25 kPa.
Figure 6.11b *Idem for the outer section.*

Below, some effects are described which may influence the rejection behaviour in the ternary system. The interaction can take place in the polarization layer, at the membrane surface and in the membrane pores.

Since the pressure seems to be an important factor, the effect of an increase in pressure is evaluated. An increase in pressure causes an increase in dextran concentration at the membrane surface. The difference in the dextran concentration at the membrane surface for the inner and outer permeate section is probably small as was the case for pure dextran (see appendix, table A.1). This would be consistent with the small difference in rejection between the inner and outer permeate section. As we have seen for the concentrating experiments dextran can strongly influence the thermodynamic activity of PEG, especially at high dextran concentrations. Therefore it is interesting to know the value of the dextran concentration at the membrane surface.

In the ternary system it is not possible to derive one value of the dextran concentration at the membrane surface from the osmotic pressure, as could be done for the binary dextran/water system.

However, if the experimental osmotic pressure is derived from the osmotic pressure model (see appendix, eqn. (A.1b) with $\sigma = 1$), a range of combinations of PEG and dextran concentrations can be determined by means of the UNIQUAC model, which all yield that value for the osmotic pressure. The osmotic pressure in the permeate has been neglected compared to the osmotic pressure at the membrane surface. These combinations of PEG and dextran concentrations can be read from fig. 6.5. for the transmembrane pressures of 30, 75 and 200 kPa for a bulk concentration of 10 kg/m^3 dextran and 10 kg/m^3 PEG in the inner permeate section. From fig. 6.5 the concentration at the membrane surface lines are projected into figs. 6.6a and 6.6b.

The values of the activity coefficients of PEG at the membrane surface are considerably higher at 200 kPa, $\gamma_{PEG}^{wt} = 65\text{-}240$, than at 30 kPa, $\gamma_{PEG}^{wt} = 1.8\text{-}7.8$, as a result of the higher dextran concentrations at the membrane surface (fig. 6.6a). The increase in activity coefficient in the presence of dextran would result in an augmented back-diffusion in the polarization layer and at the same time in an increase in the diffusion through the membrane, although the convective transport towards the membrane would not increase. Assuming that the presence of dextran in the pores does not influence the PEG transport too much, this implies that the PEG concentration at the membrane should decrease in the presence of dextran. This is in accordance with the fact that the PEG concentration in the permeate in the presence of dextran has a lower

value compared to that without the presence of dextran (fig. 6.11a). Due to a lowering of the PEG concentration in the polarization layer the convective transport towards the membrane decreases, resulting in a lower net PEG transport through the membrane at equal diffusive transport towards the bulk. If the diffusive transport through the membrane is important, as is the case for 50 kg/m^3 dextran, the activity of PEG at the membrane surface should also not be too high in order to explain the low permeate concentration. A lower activity coefficient of PEG at the membrane implies that less back-diffusion will take place. The lowering in the permeate concentration can only occur if there is still diffusion back to the bulk solution.

The back-diffusion for the experiments on the YM30 membrane seems to be consistent with the increase in PEG rejection found on the YM10 membrane at high fluxes. The enhanced back-diffusion, which is in contrast with the positive diffusion for YM5 and YM10 at low fluxes, is the result of the larger gradient in activity coefficient of PEG in the polarization layer. This larger gradient is due to the much larger difference between the dextran concentration in the bulk and the concentration at the membrane surface than in the experiments on YM5 and YM10. Moreover, the contribution of the diffusive transport through the membrane is lower at the higher fluxes seen with the YM30 membrane. At the lowest pressures, where the activity coefficient of PEG at the membrane surface is much less increased by the presence of dextran and the contribution of a diffusive flux is larger, a decrease in the PEG rejection is also observed for the YM30 membrane.

Besides effects due to the change in thermodynamic activity the PEG transport can also be influenced by friction between dextran and PEG. The increase in dextran concentration with increasing pressure could cause a stronger friction between PEG and dextran in the polarization layer during the transport towards the membrane. This may lead to a higher PEG rejection. The fact that at high fluxes the PEG rejection for the YM10 membrane (fig. 6.8) also increases in the presence of dextran may indicate that the dextran concentration at the membrane surface is important. For the YM5 membrane, where the dextran concentration at the membrane surface is lower due to the lower flux, such an increase was not found.

Increasing the pressure affects the observed rejection of dextran (see fig. 6.12). For example, the rejection of dextran in the outer permeate section (both dextran and PEG concentration equal to 10 kg/m^3) decreases from 0.93 at 30 kPa to 0.62 at 200 kPa. This implies that the permeate concentration rises from 0.7 kg/m^3 to 3.8 kg/m^3. The

higher dextran concentration in the pore might hinder the passage of the PEG molecule through the pore. However, the dextran rejection for 50 kg/m^3 dextran varies only between 0.81 and 0.71 for 50 to 200 kPa, whereas the PEG rejection shows a considerable increase. Also, at a given pressure the dextran rejections differ for the inner and outer sections, whereas the PEG rejections are nearly equal.
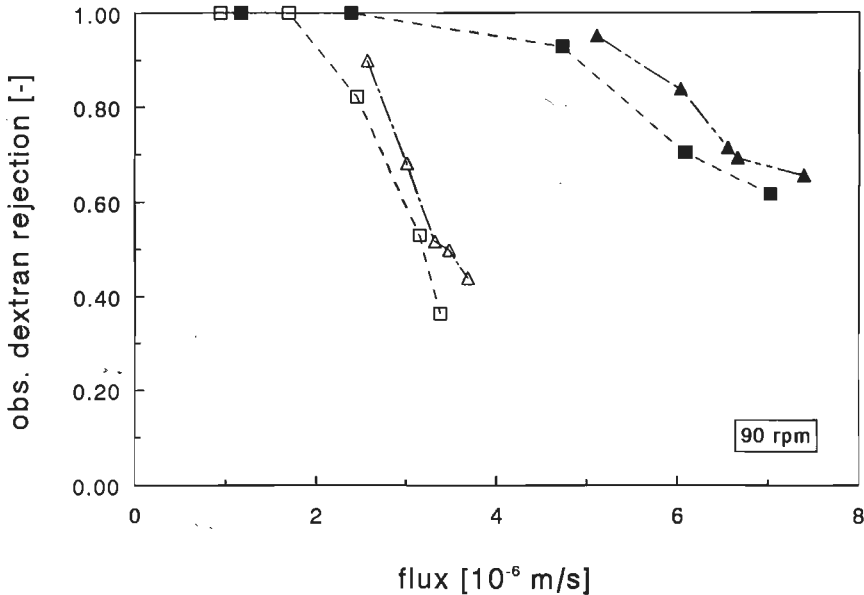
Figure 6.12 *Observed dextranT70 rejection as a function of the flux in the presence of PEG3400 for 90 rpm. YM30. $C_{PEG}=10$ kg.m^{-3}. $C_{dex}= 10$ kg.m^{-3} ($\square$): $\Delta P=5$-200 kPa. DextranT70 rejection without PEG3400 ($\triangle$): $\Delta P=25$-200 kPa.*
Open symbols: *inner section;* closed symbols: *outer section.*

Another possibility could be that demixing of the PEG/dextran/water system in a dextran- rich and a PEG-rich phase occurs at high concentrations at the membrane surfaces. However, the dextran-rich phase would have almost the same composition as the demixing solution and only a small amount of PEG-rich phase would be formed. The permeation of a PEG-rich phase would increase the permeate concentration, which is in contradiction with the experimentally observed increase in rejection.
From the above tentative explanations the increase in PEG activity coefficient and the friction in the polarization layer due to the presence of dextran are in accordance with

the effect of the pressure on the PEG rejection.

The addition of PEG to the dextran solution caused a small decrease in dextran rejection compared to the dextran rejection in the binary system at the same flux (see fig. 6.12). This can be understood as follows. In the presence of PEG the dextran concentration at the membrane surface is lower at the same flux, because the ternary osmotic pressure is higher than the binary pressure (see fig. 6.5). Without the presence of PEG a lowering of the dextran concentration would imply a strong decrease in dextran activity, which would result in an increase in the observed dextran rejection. This lower concentration at the membrane surface is compensated by the increase in activity coefficient of dextran in the presence of PEG. According to the experimental rejection these counteracting effects result in a slight increase in permeate concentration and a minor decrease in the dextran rejection. In fig. 6.6b it can be seen for the lines at equal osmotic pressure that despite the presence of PEG, $\ln(\gamma_{dex}{}^{wt})$ slightly decreases in the presence of PEG due to the lower dextran concentration. Given the uncertainties in the thermodynamic model (originating from the demixing data) one may assume that a small rise in dextran activity coefficient compared to the activity coefficient in the absence of PEG might be possible.

To obtain a quantitative description of the solute transport for the PEG/dextran/water system by means of the Stefan-Maxwell model, additional parameters concerning dextran are necessary. Therefore the rejection and flux for a binary dextran/water system were modelled. Calculations showed that it was not possible to predict both flux and rejection for YM5 and YM10. This is probably due to the fact that the dextran molecules are larger than the average pore diameter. Since dextran does passes the membrane, a pore size distribution of the membrane should be taken into account. The recent results for the filtration of dextran through the YM30 membrane, which are probably less sensitive to the extreme values of the pore size distribution, have not been modelled yet. First a good model description of the binary dextran system should be found before the ternary system can be quantitatively described.

6.6 Conclusions

Solute interaction can strongly influence the rejection of the components during ultrafiltration. Rejection measurements on YM5 and YM10 membranes show a decrease in PEG rejection, if dextran is added to the PEG solution. This effect can be

qualitatively explained by the influence of dextran on the thermodynamic activity of PEG. The strongest decrease in PEG rejection is found for low fluxes, where diffusion is predominant and the dextran concentration is the highest. Under those conditions the rejection of PEG can even become negative, which means that the concentration of PEG in the permeate is higher than in the bulk solution. Due to the additional driving force of the activity gradient, more PEG permeates through the membrane than the amount of PEG transported towards the membrane by pressure-induced convective transport. This phenomenon can be used advantangeously for the simultaneous concentration and purification of solutions.

At high flux conditions for a low resistance membrane the PEG rejection shows an opposite behaviour: a considerable increase in rejection, which might be the result of the much higher activity coefficient of PEG at the membrane surface compared to the one in the bulk solution due to the strong concentration polarization of dextran. The friction between PEG and dextran molecules due to the strong concentration polarization may also contribute to the increase in PEG rejection.

Appendix

Flux during dextran filtration

The flux has been modelled using the relationship for the flux based on concentration polarization (A.1a) (see chap. 4):

$$v = k_m \ \ln \frac{(C_m - C_p)}{(C_b - C_p)} \quad \text{(a)} \qquad\qquad v = \frac{\Delta P - \sigma \Delta \Pi}{\eta_p R_m} \quad \text{(b)} \quad \text{(A.1)}$$

To calculate the flux, the concentration at the membrane surface has been independently derived from the osmotic pressure model (eqn. (A.1b)) in combination with the osmotic virial equation for dextranT70 (eqn. (3.3)). The osmotic reflection coefficient in the osmotic pressure model was assumed to be equal to one, since the value of the asymptotic actual rejection is close to one. For all pressures the osmotic pressures at the permeate side could be neglected compared with the osmotic pressure at the retentate side. Since the osmotic pressures are considerable the concentration at the membrane surface could be accurately determined. Besides the concentration at the membrane surface a value of the mass transfer coefficient was needed as well. The mass transfer coefficient has been evaluated in two ways. The first method was to use equation (A.1b), the calculated concentration at the membrane surface and the measured permeate concentration and fluxes for the calculation of the mass transfer coefficient for each pressure. The values are presented in table 6.1 under $k_m(1)$. The values for the mass transfer coefficient have been averaged for both the inner and outer permeate sections and are 0.922 μm/s and 1.99 μm/s for 90 rpm and 1.83 μm/s and 3.48 μm/s for 270 rpm, respectively. With one exception maximum deviations of $k_m(1)$ remain within 15%. These average values have been used to calculate the flux for a constant fitted mass transfer coefficient by means of equation (A.1a). These fluxes are depicted in figs. 6.1 and 6.2 labelled as "k_m av".

The second method was to calculate the mass transfer coefficient from the Sherwood relation measured by the electrochemical method multiplied by the viscosity correction factor derived from heat transfer measurements (see chap. 3):

$$Sh = A \, Re^p Sc^{0.33} \left(\eta_b / \eta_w \right)^{0.14} \tag{A.2}$$

The coefficients A and p have different values for the inner and outer permeate section.

The concentration at the membrane surface calculated from the osmotic pressure was

used to evaluate the wall viscosity. It is assumed that the diffusion coefficient is constant and equal to the bulk diffusivity. The values for the mass transfer coefficient are presented in table A.1 under $k_m(2)$. According to the Sherwood relation the mass transfer coefficient decreases considerably due to the increase in concentration at the membrane surface with pressure. These mass transfer coefficients have been used to calculate the flux with eqn. (A.1a). The results are depicted in figs. 6.1 and 6.2 for 90 and 270 rpm, respectively.

If we first look at the fluxes with a constant mass transfer coefficient both figs. 6.1 and 6.2 show that the flux can be described well as a function of the applied pressure. As a contrast a large deviation between the calculated and measured fluxes is found for the mass transfer coefficient determined by the Sherwood relation. The difference in experimental fluxes between inner and outer permeate section is larger than predicted by the Sherwood relation. Moreover, the calculated fluxes show a stronger limitation with pressure than the measured fluxes. The limited change in flux is due to the decrease in mass transfer coefficient with increasing concentration at the membrane surface. A higher concentration at the membrane surface causes a higher wall viscosity and results in a lower $(\eta_b/\eta_w)^{0.14}$.

The fact that a constant mass transfer coefficient gives a far better prediction of the relationship between the flux and the pressure suggests that the introduction of $(\eta_b/\eta_w)^{0.14}$ overestimates the influence of the wall viscosity on the mass transfer coefficient. This contradicts the findings of Field et al. [1993], who introduced this viscosity ratio in order to be able to describe the flux data for the filtration of dextranT10. Mochizuki et al. [1992] have described the mass transfer of dextran in a range of 4000 to 750,000 Da without taking a correction for the viscosity into account. Their main interest was the prediction of the actual sieving coefficients for each molecular weight dextran present in the solution. These sieving coefficients have been evaluated using eqn. (A.1b) and the mass transfer coefficient corresponding with each type of dextran. The observed and actual sieving coefficients were described well with a mass transfer coefficient which did not vary with a change in concentration at the membrane surface. They made no attempt to verify the flux by means of the osmotic pressure model or any other model for the average molecular weight dextran properties.

In our case total omission of the viscosity correction would lead to strong overprediction of the mass transfer coefficients.

Inner permeate section							
ΔP kPa	n rpm	v μm/s	C_p kg/m^3	C_m kg/m^3	k_m (1) μm/s	$(\eta_b/\eta_w)^{0.14}$	k_m (2) μm/s
25	90	2.56	1.01	129	0.964	0.722	1.14
50	90	3.00	3.18	173	0.934	0.663	1.04
75	90	3.31	4.84	201	0.910	0.630	0.993
100	90	3.47	5.02	225	0.917	0.605	0.952
200	90	3.68	5.62	289	0.883	0.539	0.849
10	270	3.55	0.22	64	1.89	0.844	2.97
25	270	5.23	0.49	117	2.08	0.741	2.60
50	270	5.69	2.05	169	1.88	0.671	2.36
75	270	6.05	2.81	197	1.84	0.634	2.23
100	270	6.35	3.54	220	1.81	0.609	2.14
200	270	6.86	3.96	286	1.79	0.542	1.90
Outer permeate section							
ΔP kPa	n rpm	v μm/s	C_p kg/m^3	C_m kg/m^3	k_m (1) μm/s	$(\eta_b/\eta_w)^{0.14}$	k_m (2) μm/s
25	90	5.10	0.48	120	2.02	0.737	1.79
50	90	6.03	1.62	166	2.03	0.671	1.63
75	90	6.55	2.86	197	1.98	0.634	1.54
100	90	6.66	3.07	221	1.93	0.609	1.48
200	90	7.39	3.44	286	1.96	0.542	1.32
10	270	4.57	0.27	50	2.80	0.879	4.61
25	270	8.52	0.26	101	3.65	0.769	4.03
50	270	10.00	1.39	155	3.47	0.685	3.59
75	270	10.95	1.68	188	3.52	0.645	3.38
100	270	11.60	2.52	213	3.48	0.617	3.24
200	270	12.73	3.01	281	3.46	0.547	2.87

Table A.1: Experimental data of the filtration of dextranT70 on a YM30 membrane for the inner and outer permeate section and the results of the model calculations of method (1) and (2). $C_{b,dex} = 10$ kg/m^3.

From a comparison of the flux and rejection in the outer section at 90 rpm and the inner section at 270 rpm it can be concluded that besides the viscosity other phenomena influence the mass transfer. The lower flux and rejection in the inner section at 270 rpm contradict with the higher mass transfer coefficient predicted by the electrochemically measured Sherwood relation. According to the mass transfer coefficient derived by method (1) a lower mass transfer coefficient exists in the inner section at 270 rpm compared to the outer section at 90 rpm. For the filtration of PEG3400 on YM30 the difference in mass transfer between the two sections was in accordance with the Sherwood relation (see fig. 5.4).

Part of the decrease in mass transfer coefficient due to the increase of the wall viscosity with higher concentrations at the membrane surfaces could be counteracted by an increase in diffusion coefficient. However, except for the outer section at 90 rpm the mass transfer coefficient is already overestimated by the Sherwood relation. According to Gill et al. [1988] the variation in viscosity is much larger than those in diffusivity for the systems reviewed (BSA, sucrose and dextran).

7. SOLUTE REJECTION IN THE PRESENCE OF SILICA GEL LAYERS

7.1 Introduction

In the previous chapter the influence of the addition of a component was studied without the formation of a gel layer on the membrane surface. This chapter describes how the separation behaviour can be completely changed by the presence of a gel layer on the membrane surface.

First the procedure for the series of experiments will be presented. Then the gel formation during silica filtration will be discussed, followed by the results of the PEG rejection measurements with and without an Aerosil gel layer on the membrane surface. Finally, the rejection of dextran during the filtration of a Ludox/dextran suspension will be discussed and how it is effected by the formation of a Ludox gel layer on the membrane surface.

7.2 Materials and methods

To characterize the influence of a gel layer on the PEG rejection the following procedure has been used:

- Determination of the PEG rejection on the clean membrane as a function of the flux by filtering a 10 kg/m^3 PEG solution at various pressures.
- Formation of a silica gel layer on the membrane by filtering a silica suspension at a constant pressure.
- Determination of the PEG rejection in the presence of the silica gel layer as a function of the flux by filtering a PEG/water solution at various pressures.

The experiments have been performed in the tubular module (for a detailed description: chap. 5). The PEG rejection on a clean membrane has been determined by the same method as described in chapter 5. In order to measure at very low pressures the feed solution was pumped from a feed vessel which was placed below the UF-1 module. In that case the lowest pressures were 2 kPa for a circulation velocity (u) of 1.04 m/s and 11 kPa for $u_{circ} = 1.95$ m/s.

The silica suspension was prepared by diluting a stock suspension with a concentration of 60 kg/m^3. The silica was suspended in the water using a TURRAX mixer. Afterwards the suspension was given an ultrasonic treatment for 20 min. The stock solution was then diluted to 30 kg/m^3. Subsequently, the ultrasonic treatment was repeated several times until the viscosity of the silica suspension did not change anymore.

The silica suspension was filtered at constant pressure and circulation flow rate. Both retentate and permeate were returned to the feed vessel. The flux was followed as a function of time. The filtration was stopped when the stationary flux was reached and the gel layer formation was completed.

After the silica filtration the module was disconnected and the suspension was allowed to flow out of the system. After reconnection the system was carefully filled with water. The first part of the water which had run through the module was not returned to the feed vessel in order to clean the system from 'free' silica which was not incorporated in the gel layer.

A pure water flux was measured to check the condition of the gel layer. Subsequently, the system was filled with a PEG/water solution, the system was pressurized and the flux and rejection were measured as a function of time until a steady-state situation was reached. The PEG rejection measurements were repeated on the same gel layer for various pressures, circulation velocities and two types of PEG of different molecular weight.

After the rejection measurements were performed, the tubular membrane was removed from the module and cut in twelve equal pieces. From each part several samples of the gel layer were taken to determine the thickness of the gel layer and the gel concentration along the entire length of the membrane.

The type of silica used for the experiments is Aerosil 200: non-porous particles with a particle diameter of 12 nm (Degussa). The molecular weights of the two types of PEG are 3400 (Aldrich) and 6000 Da (Serva).

An additional experiment was performed in the stirred batch cell instead of in the tubular module. In this case another type of silica (Ludox HS-40, Dupont) of the same particle diameter as Aerosil was used, which was able to form more concentrated gel layers. DextranT40 was used as a model solute (Sigma Chemical). In contrast with the experiments performed with Aerosil and PEG, the gel layer formation occurred during the simultaneous filtration of Ludox and dextran at a pH value of 6.1 and three different pressures (50, 100 and 200 kPa). The concentrations of Ludox and dextran were 50 kg/m^3 and 10 kg/m^3, respectively. The type of membrane used was YM30, which totally rejected the Ludox particles. Further details about the membrane and module have been given in chap. 5.

The concentration analyses for PEG were performed as described in chapter 5. If the samples contained salt, as was the case for the dextran/Ludox/water systems, they

were analyzed using a Zorbax GF250 column. This column was able to separate dextran and salt.

7.3 Gel formation during silica filtration

After the PEG rejection was measured on the clean membrane (chap. 5), a gel layer was formed on the membrane surface by filtering an Aerosil suspension at 200 kPa and $u_{circ,begin}$ =0.74 m/s. During the experiment the flux and the axial pressure were measured as a function of time. The results have been depicted in fig. 7.1.
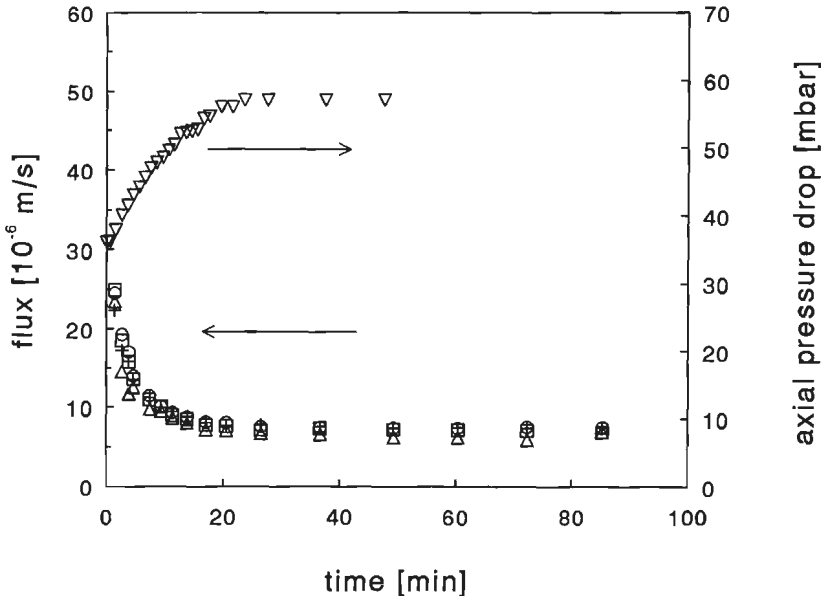
Figure 7.1 *Flux and axial pressure as a function of time during the filtration of a 30 kg/m³ Aerosil suspension at 200 kPa and u_{begin}=0.74 m/s. Flux: pos. 1: (+), pos. 2: (△), pos. 3: (○), pos. 4: (□); axial pressure (▽).*

The flux decreases rapidly with time until after about 20 min. a steady-state flux is reached. The axial pressure shows a strong increase and reaches a plateau value at the same time the steady-state flux is reached. Both phenomena can be explained by the formation of a gel layer on the membrane surface. Both the decrease in flux and the increase in axial pressure are the result of an increasing gel thickness. Due to the thicker gel layer the resistance of the layer increases, causing a drop in flux. Another effect of the increasing gel thickness is a decrease in open cross-section of the tubular membrane, which enhances the circulation velocity. The circulation velocity directly

influences the axial pressure.

The flux during the filtration of Aerosil has been modelled using the gel-polarization model [Blatt et al., 1970]:

$$v = \frac{\Delta P}{\eta(R_m + R_g)} \quad \text{(a)} \qquad\qquad v = k_m \ln\left(\frac{C_g}{C_b}\right) \quad \text{(b)} \qquad (7.1)$$

The osmotic pressure of Aerosil is considered to be negligible. Since Aerosil is expected to show little interaction with water, it is assumed that the Aerosil suspension behaves ideal thermodynamically. Calculation of the osmotic pressure for Aerosil with the Van 't Hoff equation for ideal solutions shows that it is negligible. Equation (7.1b) is only valid under steady-state conditions. A detailed description of the method used for the modelling with the gel-polarization model under unsteady-state conditions has been given in chapter 5.

During the filtration of Aerosil the flux gradually decreases, starting from the pure water flux (PWF), when no gel layer has been formed yet, to the steady-state condition, when the final gel thickness is reached. The final gel thickness is reached when the resistance of the gel layer R_g is so large that the flux in equation (7.1a) is equal to the flux in equation (7.1b). The gel concentration and the final gel thickness were determined experimentally as a function of the distance from the inlet of the tubular module (see Method). The average gel concentration over the entire length of the membrane was equal to 309 kg/m^3 with a standard deviation of 3.4 kg/m^3. The gel thickness was found to be 1.24 mm with a standard deviation of 0.07 mm. However, there was hardly any gel layer over the first 2 to 3 cm of the membrane. This indicates the existence of entrance effects, which alter the mass transfer in the first few centimeters of the tubular membrane.

By means of eqn. (7.1a) the final resistance of the gel layer can be calculated from the steady-state flux: $R_g = 2.84 \times 10^{13}$ m^{-1}. If the gel layer can be considered as a packed bed of particles the resistance R_g can be described with the Carman-Kozeny relation [Kerkhof et al., 1988]:

$$R_g = \frac{170(1-\varepsilon_g)^2}{\varepsilon_g^3 d_{par}^2} \delta_g \qquad (7.2)$$

The gel porosity ε_g is equal to $1 - C_g/\rho_{par} = 0.86$. The final gel resistance according to

eqn. 7.2 is equal to 4.30×10^{13} m^{-1}, using the primary particle diameter of 12 nm provided by the supplier of Aerosil and the experimentally determined gel concentration and thickness. Since the gel concentration and the final gel thickness have been determined with good accuracy it seems reasonable to attribute the difference between the experimental and calculated R_g to the uncertainty in particle diameter. Aerosil has a tendency to agglomerate and it is likely that in spite of the ultrasonic treatment Aerosil has not reached its primary particle diameter. Therefore, the particle diameter was fitted to the experimentally determined final gel thickness, which provides a value of $d_{par} = 15$ nm. From the results of the unsteady-state flux modelling in chapter 5 we also found that a higher particle diameter was necessary to describe the resistance for the same type of Aerosil. In that case the particle diameter had to be adjusted to 17-18 nm. This higher particle diameter together with that lower gel concentration could be ascribed to the less rigorous ultrasonic treatment the suspension was exposed to.

The mass transfer coefficient used for the modelling has been determined from the measured steady-state flux $(7 \times 10^{-6}$ m/s) by means of eqn. (7.1b) and the measured gel and final bulk concentration (28.5 kg/m^3). The final bulk concentration deviates from the initial bulk concentration due to the incorporation of part of the Aerosil in the gel layer. The mass transfer coefficient in the steady-state situation has thus been determined to be equal to $k_{m,ss} = 2.94 \times 10^{-6}$ m/s. Due to the variation in circulation velocity and hydraulic diameter with increasing gel thickness, the mass transfer coefficient is not constant during the entire experiment. These effects have been taken into account by correcting the steady-state mass transfer coefficient with the proportion between the actual Re number at the time of filtration and the Re number in the steady-state situation, Re_{ss}, according to:

$$k_m = k_{m,ss} \cdot \left(\frac{Re}{Re_{ss}} \right)^{0.8} \tag{7.3}$$

This relationship can be derived from the Sieder-Tate Sherwood relation (see chap. 3), assuming that only the circulation velocity and the hydraulic diameter change during the filtration of Aerosil. According to the Sieder-Tate correlation the steady-state mass transfer coefficient should be equal to 3.2×10^{-6} m/s without viscosity correction. The exact viscosity at the wall is not known, but with viscosity correction the mass transfer coefficient is likely to be underestimated.

In fig. 7.2 the average experimental flux has been depicted together with the results of the model calculation. It can be seen that the model description with the above-

mentioned parameters gives an excellent description of the average flux. Application of a constant value of the mass transfer coefficient resulted in a poorer fit. This indicates that the assumptions of negligble osmotic pressure and increasing mass transfer coefficient are valid. Moreover, it shows that the unsteady-state gel-polarization model can describe the flux in both a stirred filtration cell (chap. 5) and a cross-flow tubular membrane.
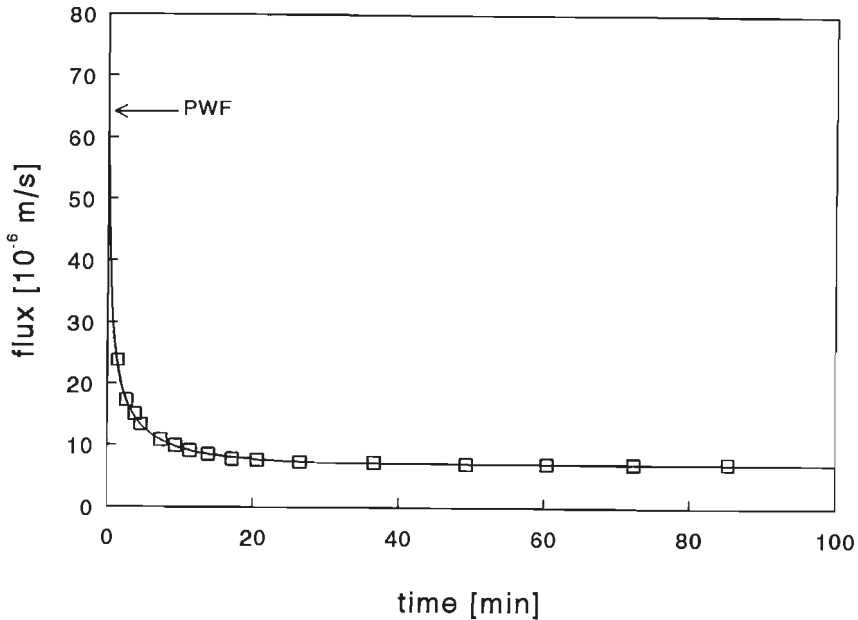
Figure 7.2 *Experimental and model flux as a function of time during the filtration of a 30 kg/m³ Aerosil suspension at 200 kPa and $u_{begin} = 0.74$ m/s. PWF=pure water flux.*

7.4 PEG rejection in the presence of an Aerosil gel layer

After the Aerosil layer was brought onto the membrane surface and the PWF was measured, a PEG solution was filtered through the membrane + gel layer. In table 7.1 the steady-state flux and the observed rejection are presented for PEG3400 and PEG6000 at various pressures and a circulation velocity of 1.51 m/s in the presence of a gel layer. Moreover, the observed rejection on a clean membrane is given at the same flux, v_{ss}, as the steady-state flux in the presence of the gel layer. The pressures in table 7.1 correspond to the rejection measurements in the presence of a gel layer. It is very important to compare the observed rejection at the same flux instead of at the same pressure, because the concentration profile in the polarization layer is determined

by the flux and the mass transfer coefficient and the actual rejection is a function of the flux (see chap. 5). The mass transfer coefficient is determined by the circulation velocity and the hydraulic diameter. Since k_m depends only slightly on the hydraulic diameter $(d_h^{-0.2})$, the mass transfer coefficient is determined by the circulation velocity. The rejection without a gel layer is depicted for a circulation velocity of 1.04 m/s. For both PEG3400 and PEG6000 the value of the PEG rejection is also available for 1.95 m/s at the highest flux. The value for the PEG rejection at a circulation velocity of 1.51 m/s (equal to the circulation velocity in the presence of a gel layer) will be higher than the value for 1.04 m/s, but lower than the value for 1.95 m/s. As an example the PEG6000 rejection both in the presence and absence of a gel layer is shown in fig. 7.3. In both table 7.1 and fig. 7.3 the presented rejections only hold for position 2, 3 and 4 of the membrane module. The behaviour of the rejection at position 1 will be discussed later.
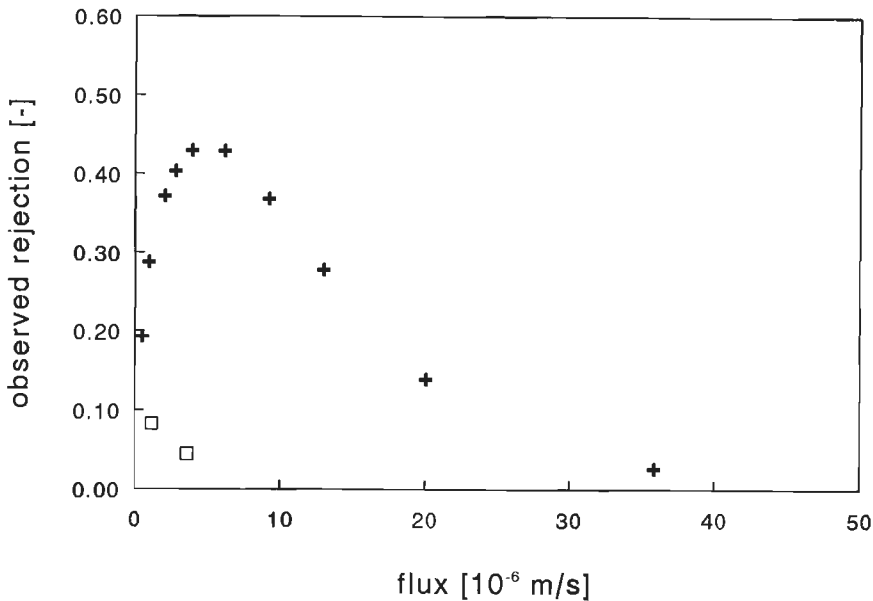
Figure 7.3 *PEG6000 rejection in the presence (□) and absence (+) of an Aerosil gel layer.* $u_{circ}=1.04$ m/s without gel and 1.51 m/s with gel. $C_{PEG}=10$ kg/m^3.

From table 7.1 and fig. 7.3 it can be concluded that the observed rejection in the presence of a gel layer is almost equal to zero. Especially for both experiments with PEG6000 and the experiment with PEG3400 at a pressure of 107 kPa it can be clearly

seen that the observed rejection in the presence of a gel layer is considerably lower than the rejection on a clean membrane. This means that due to the presence of a silica gel layer on the membrane surface the separation behaviour is completely changed. A normally partly rejected PEG solution almost totally permeates through the membrane if a gel layer is present.

Membrane with gel layer				Clean membrane	
component	pressure	v_{ss}	R_o^{gel} $u_{circ} = 1.51m/s$	$R_o^{\dagger}$ $u_{circ} = 1.04m/s$	$R_o^{\dagger}$ $u_{circ} = 1.95m/s$
	[kPa]	$[10^{-6}m/s]$	[-]	[-]	[-]
PEG3400	36	1.00	0.021	0.07	----
PEG3400	55	1.30	0.062	0.06	----
PEG3400	107	4.00	0.012	0.16	0.19
PEG6000	36	1.18	0.083	0.30	----
PEG6000	103	3.60	0.045	0.41	0.49

† at same flux as membrane with gel layer

Table 7.1 *Experimental flux and rejection during the filtration of PEG in the presence and absence of a gel layer.*

The fact that the PEG rejection drops to almost zero in the presence of a gel layer can be understood if the following conditions are fulfilled:

1. The Aerosil layer shows hardly any exclusion for PEG3400 and PEG6000.

2. The thick Aerosil layer causes a strong decrease in back-diffusion of PEG to the bulk solution.

In order to explain how these two conditions lead to a drop in PEG rejection to almost zero, the transient behaviour will be discussed from the start of the experiment until steady-state is reached.

At time $t=0$ the pore volume of the gel layer is filled with water. From $t=0$ the PEG solution displaces the hold-up of water, which results in a build-up of a PEG concentration profile. Analogous to the differential equation for the concentration build-up in a polarization layer the following equation can be derived for a gel layer:

$$\varepsilon_g \frac{\partial C}{\partial t} = -v \left[\frac{\partial C}{\partial z} \right] + \frac{\varepsilon_g}{\tau_g} D \left[\frac{\partial^2 C}{\partial z^2} \right] \qquad (4)$$

Initial and boundary conditions:

$t=0$: $0 \leq z \leq \delta_g$ $C=0$

$t>0$: $z=0$ $C=C_b$

      $z=\delta_g$ $v \cdot C = (\varepsilon_g/\tau_g) \cdot D \cdot (\partial C/\partial z) + v \cdot C_p$

ε_g =   porosity gel layer (correction for the volume in which the component is present) [m^3/m^3]

τ_g =   tortuosity (correction for the path length covered in the gel layer) [-]

δ_g =   gel layer thickness [m]

C_p =   permeate concentration [kg/m^3]

in which $C_p = (1 - R_a) \cdot C_{z=\delta g}$ and R_a is the actual rejection of the membrane itself as a function of the flux. For the boundary condition at $t>0$ and $z=0$ it is assumed that
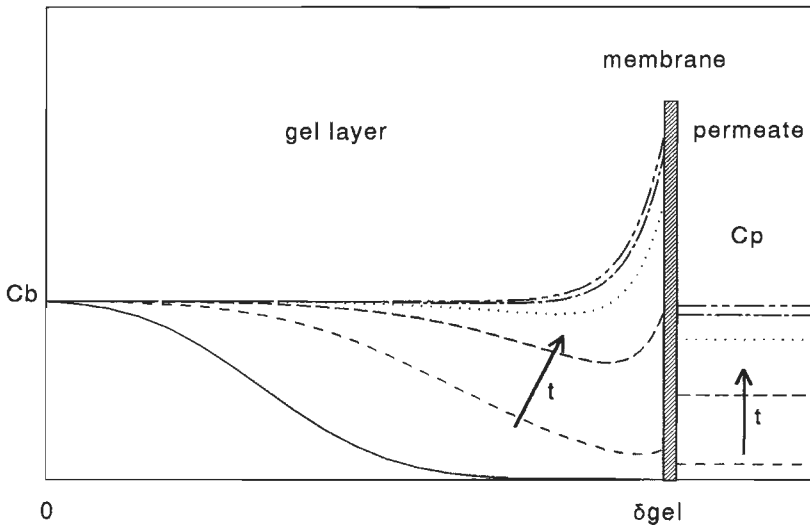

Figure 7.4 *Concentration profiles of PEG in gel layer and permeate as a function of time during the filtration of a PEG solution over an Aerosil layer initially filled with water.*

the concentration is equal to the bulk concentration, which implies that the gel layer exhibits no exclusion for PEG and that the gel layer is thick. This assumption introduces an inaccuracy in the beginning, because high concentration gradients exist at the start of the experiment when the gel layer is filled with only water. At longer periods of filtration this assumption is reasonable. For thinner gel layers the transport in the polarization layer adjacent to the gel layer should be taken into account.

By means of equation (7.4) the concentration profiles in the gel layer can be calculated numerically as a function of time. An example is presented in fig. 7.4.

At first PEG has not penetrated into the entire gel layer and the PEG concentration remains zero in the righthand side of the gel layer. The immediate consequence is that the permeate still consists only of water. The second profile shows that PEG has fully penetrated into the gel layer but the concentration at the membrane surface is still very low. Therefore the permeate concentration has hardly increased. With increasing time the concentration in the entire gel layer and at the membrane surface increases, which causes an increase in permeate concentration until steady-state is reached.

If the gel layer is sufficiently thick, the steady-state permeate concentration will not be determined by the rejection of the membrane, but will instead be governed by the extent of solute exclusion by the gel layer. If the gel layer is sufficiently open that PEG exclusion is negligible, the steady-state permeate concentration is determined by the extent to which the solute diffuses back to the bulk solution through the gel layer. In the presence of a gel layer the back-diffusion will diminish and the concentration at the membrane surface and therefore also the permeate concentration can reach very high values. For a thick gel layer the diffusive flux will approach zero near $z=0$. In that case the permeate concentration will be equal to the bulk concentration, because for negligible back-diffusion the convective transport to the membrane $v \cdot C_b$ can be considered equal to the solute flux in the permeate $v \cdot C_p$. The concentration at the membrane surface has then reached a value of $C_b/(1-R_a)$. If the bulk and permeate concentration have the same value, the observed rejection R_o is equal to zero. The observed rejection is only zero, if the gel layer does not show any exclusion for the solute <u>and</u> the back-diffusion is negligible. In general, the back-diffusion can be neglected if the Pe-number in the gel layer, $v\delta_g/(\varepsilon D/\tau)$, is much larger than 1.

In fig. 7.5 the calculated observed PEG rejection is shown as a function of the gel layer thickness for an open Aerosil layer on the membrane surface. With increasing

gel thickness the rejection drops from 0.5 when no gel layer is present to zero for a gel thickness of more than 0.55 mm. This decrease in rejection is the consequence of the diminishing back-diffusion in the layer. According to these calculations the observed PEG rejection in the presence of an 1.24 mm Aerosil gel layer should be zero. The fact that the measured rejections (table 7.1) were slightly higher than zero could be ascribed to some extent of exclusion by the gel layer.
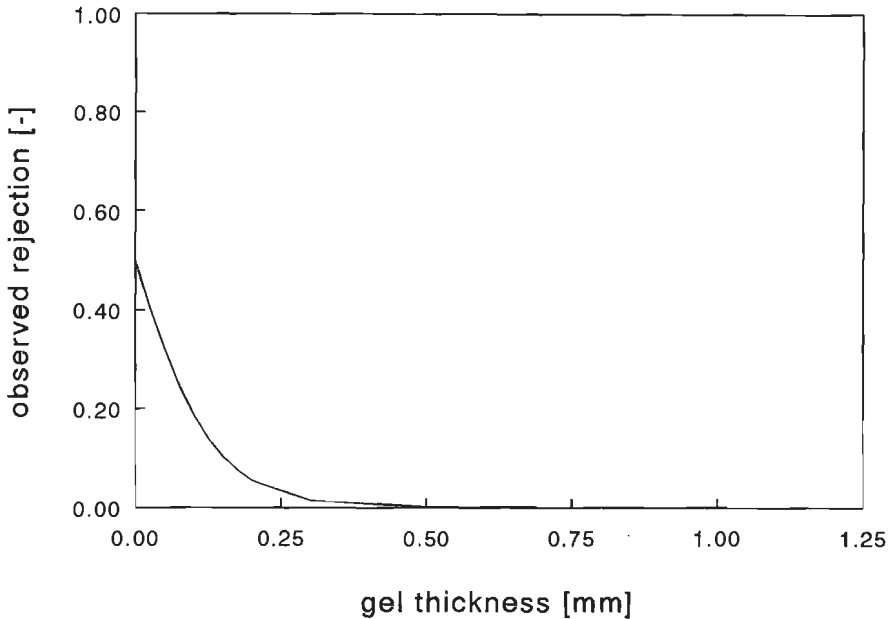
Figure 7.5 *Calculated PEG rejection as a function of the thickness of an Aerosil gel layer with no exclusion.*

In fig. 7.6 the experimentally measured permeate concentration of PEG3400 is depicted as a function of time for the four membrane positions, when an Aerosil layer of 1.24 mm thickness was present on the membrane.

The permeate concentrations at positions 2, 3 and 4 clearly show the increase in concentration with time starting from zero to the same steady-state value as follows from fig. 7.4. The permeate concentration at position 1 is higher in the beginning but reaches a lower steady-state value. This can be explained by the absence of a gel layer on the first few centimetres near the membrane inlet. Due to the absence of the gel layer, the water hold-up is only that of the membrane itself and its support layer and

the PEG solution has to displace less water compared to the other positions. Therefore the permeate concentration starts to increase much earlier. Part of position 1 keeps a rejection for PEG, because it is not covered by a gel layer. Thus the end value of the permeate concentration stays below that of positions 2, 3 and 4. The same deviation has also been observed for the other experiments.
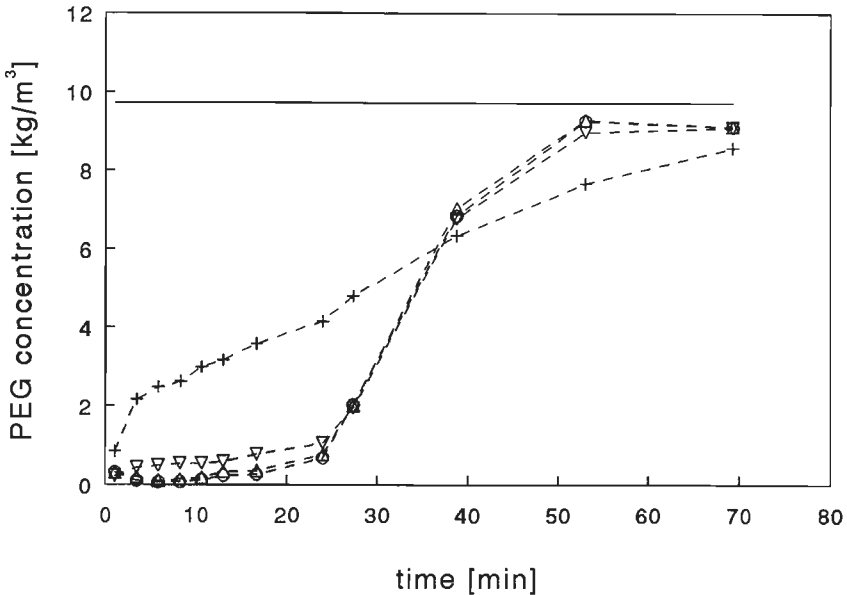
Figure 7.6 *Permeate concentration of PEG3400 in the presence of an Aerosil gel layer as a function of time after switching from water to PEG solution for four membrane positions.* u_{circ}=1.51 m/s, ΔP=55 kPa. $C_{p,PEG}$: pos. 1: (+), pos. 2: (△), pos. 3: (○), pos. 4: (▽); $C_{b,PEG}$: (——)

Calculations with equation (7.4) have shown that the experimental time to reach steady-state is much longer than theoretically expected. The incorporation of the hold-up of the support layer of the membrane into the model was not sufficient to explain the difference in time. The delay in reaching steady-state can be explained if PEG is adsorbed at the Aerosil layer. In that case the PEG is adsorbed at the gel particles while it starts to permeate through the layer and it takes longer to reach steady-state. The possible adsorption of PEG on silica particles has been reported by Killman

[1985]. Some adsorption experiments have been performed to verify the occurrence of adsorption for our type of PEG and silica, which indeed was the case. The loading was of the same order of magnitude as to be expected from the delay in reaching a steady-state value for the PEG rejection (see appendix).

The PEG adsorption on the silica layer had no affect on the permeability of the gel layer, since no change in pure water flux was found before and after performing the PEG rejection measurements.

7.5 Dextran rejection during the simultaneous filtration of Ludox and dextran

To study the rejection by a tighter gel layer, another type of silica (Ludox) was used, which still was in suspension at 500 kg/m^3, which is higher than the gel concentration for Aerosil. Since Ludox formed a weak gel layer, it was not possible to replace the Ludox suspension by a PEG solution without destruction of the gel layer. Therefore it was necessary to filter PEG and Ludox simultaneously. As was also the case for Aerosil, PEG showed a considerable adsorption on the Ludox particles. Since PEG and Ludox needed to be filtered simultaneously, a lot more surface area of silica was available for adsorption than when the PEG solution was filtered through an already existing gel layer in which only a relatively small amount of silica was present. The adsorption of PEG caused a considerable drop in bulk concentration of PEG and the PEG concentration could not be determined very accurately in the presence of Ludox. Therefore dextranT40 was used instead of PEG, because it hardly adsorbed on the Ludox particles.

The dextran rejection is presented in fig. 7.7 with and without Ludox present in the solution.

The observed dextran rejection without Ludox is equal to 0.90 at the lowest fluxes and decreases with increasing fluxes due to concentration polarization. The decrease is stronger for the inner permeate section because the mass transfer coefficient is lower and therefore the degree of polarization is stronger.

The flux during the filtration of dextran/Ludox decreases very rapidly and within a few minutes steady-state is reached. After filtration a thin, weak gel layer is visible on the membrane surface, but no sample could be taken to determine the gel concentration. Separately performed centrifugation experiments have shown that the gel concentration of thin weak Ludox layers is about 700 kg/m^3.

The influence of the presence of a Ludox gel layer is found by comparing the dextran rejection with and without Ludox at the same flux (see also table 7.2).
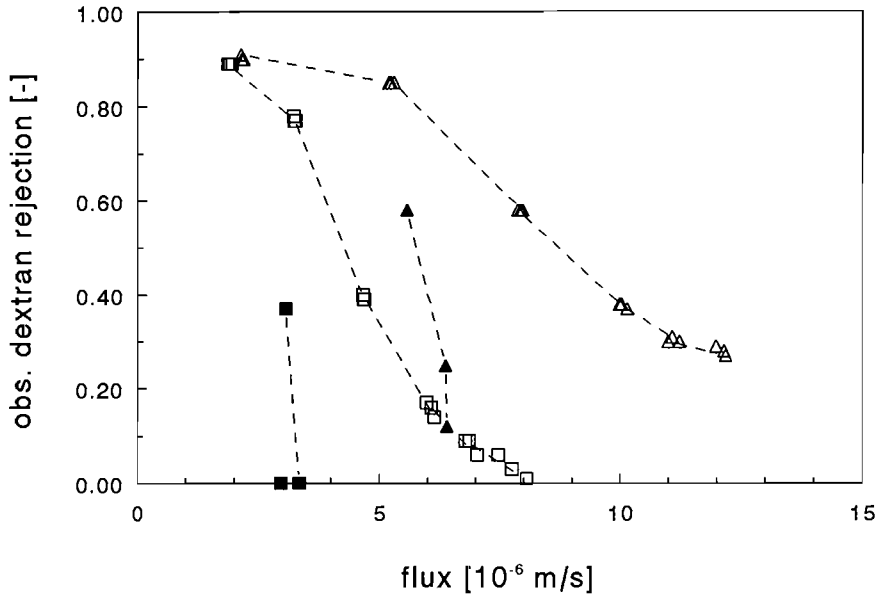
Figure 7.7 *DextranT40 rejection in the presence and absence of Ludox. 90 rpm.* $C_{dex}=10$ kg/m^3. Open symbols: *only dextran;* closed symbols: *dextran + Ludox,* $C_{Ludox}=50$ $kg.m^{-3}$. *Inner section:* ($\square$); *outer section* ($\triangle$).

dextranT40/Ludox					Clean membrane	
pressure	v_{ss} inner	v_{ss} outer	R_o^{gel} inner	R_o^{gel} outer	$R_o^{\dagger}$ inner	$R_o^{\dagger}$ outer
[kPa]	$[10^{-6}m/s]$	$[10^{-6}m/s]$	[-]	[-]	[-]	[-]
50	3.06	5.57	0.37	0.58	0.78	0.83
100	3.35	6.38	0.00	0.25	0.77	0.70
200	2.96	6.41	0.00	0.12	0.79	0.69

†at same flux as for dextran/Ludox.

Table 7.2 *Experimental flux and rejection during the filtration of dextranT40 in the presence and absence of Ludox.*

The pressures in table 7.2 correspond with the rejections in the presence of Ludox. It can be seen that for both the inner and outer permeate section the dextran rejection

drops in the presence of Ludox. The dextran rejection decreases with increasing pressure. This is the result of the increase in gel layer thickness on the membrane surface as a function of pressure, which diminishes the back-diffusion in the Ludox gel layer (see discussion for PEG and Aerosil). In the inner section at 100 and 200 kPa the dextran rejection even drops to zero, which is much lower than the values of 0.77 and 0.79 for the clean membrane. The fact that the rejection drops to zero indicates that dextranT40 is not excluded by the Ludox gel layer.

We have also performed the same type of experiments with the higher molecular weight dextranT250. Due to the low diffusion coefficient of dextranT250 the concentration polarization of dextranT250 is considerably higher than for dextranT40. As result the osmotic pressure is so high that Ludox is not able to form a gel layer anymore. In that case the observed rejection of dextranT250 remains unaltered in the presence of Ludox.

7.6 Conclusions

Under the experimental conditions a gel layer can be formed at the membrane surface by filtering a suspension of silica particles. The flux as a function of time during the filtration can be described well with the gel-polarization model for unsteady-state conditions.

In the presence of an Aerosil gel layer of 1.24 mm thickness and a porosity of 0.86, the observed rejection for PEG3400 and PEG6000 drops to almost zero. This phenomenon can be explained by assuming that the present gel layer does not show any exclusion for PEG. Due to the thickness of the gel layer, the diffusion back to the bulk solution is strongly decreased, which results in a total permeation of the bulk solution through the membrane, when the Pe-number in the gel layer is equal to one.

The same type of effects has been found during the simultaneous filtration of dextranT40 and Ludox. It is shown that the increase of the gel layer thickness causes a decrease in rejection due to the diminishing back-diffusion.

In general, if one of the components in the filtration solution forms an open gel layer on the membrane surface, which shows no exclusion for the solute, the rejection of the solute can be lowered considerably compared to rejection of the solute by the clean membrane. If the gel layer is thick enough to prevent all diffusion of solute from the layer back to the bulk solution, the rejection will become zero and total permeation of the solute will occur. The formation of an open gel layer, although unfavourable due

to the loss in flux, can be used advantageously in the simultaneous concentration and purification of a gel-forming solute. For purification the rejection of contaminants should be as low as possible. By carefully optimizing the layer thickness, total permeation of the contaminants can be achieved with a minimal loss in flux due to the presence of a gel layer. If on the other hand both solutes need to be retained, gel layer formation should be avoided by, for example, lowering the trans membrane pressure, increasing the mass transfer coefficient, or back-flushing.

Appendix

PEG adsorption on silica particles

The permeate concentration of PEG in the presence of an Aerosil layer has been measured as a function of time after switching from water to PEG solution. From the experimental curves the virtual water hold-up has been calculated. The experimental value of 253 ml is much higher than the hold-up of 100 ml calculated from the porosities in the gel layer and support layer and the volume of the permeate section. In an experiment to displace the PEG by water, which has been performed immediately after the measurment shown in fig. 7.5, the calculated virtual hold-up was only 105 ml. This value is close to the expected hold-up. All these effects can be explained if PEG is adsorbed within the Aerosil layer. In that case the PEG is adsorbed at the gel particles when it starts to permeate through the layer and it takes longer to reach steady-state. The virtual hold-up of 105 ml indicates that only little PEG desorbs due to the replacement of the PEG solution in the gel layer with water. Adsorption experiments have been performed to justify this explanation. Due to separation problems with the HPLC analyses of samples which contain both Aerosil and PEG, only a rough estimation of the adsorption of PEG on Aerosil could be made. For a concentration of 20 kg/m^3 the loading is equal to 90 mg/g of Aerosil. In literature adsorption-isotherms have been measured for several PEG molecules varying in molecular weight from 86,000 to 996,000 Da and silica particles of 140 nm [Killman, 1985]. From these isotherms it can be concluded that the plateau value for the adsorption of PEG is independent of the molecular weight of PEG. This plateau value is reached at very low equilibrium concentrations of PEG ($<5\times10^{-3}$ kg/m^3). To obtain a rough estimation it is assumed that the plateau value can be used for our system, although the molecular weight of the PEG used for our experiments is lower and the particle diameter of silica is only 12 nm. The plateau value given by Killman is equal to 0.6 mg/m^2. Based on this value the maximum loading for Aerosil 200 with a specific surface area of 200 g/m^2 would be 120 mg/g Aerosil. This value is 30% higher than determined by the adsorption experiments. Both loadings are higher than the loading which can be calculated from the difference in the virtual hold-up (253 ml) and the hold-up based on porosities (100 ml): 56 mg/g of Aerosil. This might be ascribed to the fact that the PEG has incomplete access to the total surface area of the Aerosil, within the gellayer.

8. PEG/BSA/WATER SYSTEMS

8.1 Introduction

Ultrafiltration is often used for process liquids which contain proteins in the solution. During the filtration of proteins several phenomena can occur influencing the flux and/or the rejection of other solutes present in these solutions: osmotic pressure, adsorption on the membrane surface, deposition on the membrane surface and compression of the deposition layer. Numerous studies have been performed to characterize the flux decline during the filtration of BSA. Opong and Zydney [1991] have reviewed most previous studies of the flux decline during protein filtration. They have added an extensive study on protein filtration, which described separately the influence of each of the above-mentioned phenomena on the flux during ultrafiltration. It was found that all phenomena made significant contributions to the decline in flux.

A smaller amount of studies has dealt with the influence of protein on the rejection behaviour of other solutes [Nakao, 1982; Kimura, 1985; Meireles, 1991; Mochizuki, 1992a, 1993a]. All of them report an increase in rejection of the accompanying solutes compared to the rejection without protein present (discussed in more detail by Mochizuki and Zydney, [1993]). Mochizuki and Zydney have characterized the rejection behaviour of protein adsorbed membranes [1993a] and the influence of the presence of a deposited BSA layer on the membrane surface [1993b] using polydisperse dextrans with the dextran molecular weight distribution evaluated using gel permeation chromatography. They used microfiltration membranes, which without treatment with proteins showed no rejection for the dextran molecules. According to their measurements both the actual rejection of dextran and the hydraulic resistance of the deposit is minimum at the isoelectic point (pH=4.7). These effects on hydraulic permeability and actual rejection are consistent, but they contrast with the maximum in hydraulic resistance at the isoelectric point found by Suki et al. [1984].

Three investigations have been performed with a combination of PEG and BSA in the system. Busby and Ingham [1980a, 1980b] have studied the separation of PEG and BSA solutions by means of diafiltration. They concluded from a two-step flux decline over a 10^6-fold range in BSA concentration that both adsorption and concentration polarization occurred for polysulfone PM30 membranes (Amicon). The PEG rejection was increased due to the presence of BSA. This increase was ascribed to the irreversible adsorption on the membrane, because an overnight treatment with trypsin was

necessary to restore the flux and the rejection to the value which prevailed prior to the exposure of the membrane to BSA. For the regenerated cellulose membrane (YM30) only one flux decline was found indicating reversible concentration polarization. The flux was not affected by the protein filtration, however the PEG rejection showed an increase from of 0.2 to 0.4 after BSA filtration and this effect was reversed by trypsin treatment. According to Ingham and Busby this suggests a higher sensitivity of the rejection to adsorption than the flux. Optical density measurements used for determining the amount of BSA present on an Amicon XP-50 hollow fiber unit showed an increase in both the irreversible and reversible amount of BSA with increasing pressure. The irreversible amount of BSA strongly depended on the pH, whereas the reversible amount of BSA (due to concentration polarization) was much less pH-dependent.

Papamichael and Kula [1987] have also studied the separation of PEG and BSA by a YM5 and a YM10 membrane using both diafiltration and ultrafiltration. In the diafiltration mode the convective flux was kept constant using a pressure-independent syringe pump. Increasing the BSA concentration from 0 to 10 wt% at a flux of 0.28×10^{-6} m/s caused an increase in the observed PEG rejection from 0.3 to 0.58 at 0.2 wt% followed by a drop in rejection to 0.18 at 5-10 wt%. At higher fluxes a maximum in the rejection was also observed, but the PEG rejection remained higher than the value for the case where no BSA was present. This indicated that the rejection could be lower or higher than the PEG rejection without BSA, depending on the circumstances. The authors attributed the lowering of the PEG rejection to the stripping of water bonded to the PEG molecule by BSA, in that way reducing the effective size of the PEG molecule. The increase in rejection was not explained.

In a recent study, Lentsch [1993] observed an increase in PEG20,000 rejection on polysulphone membranes when BSA was adsorbed to the membrane, and after the filtration of 10 kg/m^3 BSA solution through the membrane the rise in rejection was even higher.

The objective of the present study is to determine the influence of BSA on the PEG rejection. An attempt is made to consider the influence of adsorption and deposition separately according to the procedure followed by Opong [1991], which was also used by Mochizuki in his recent study on dextran sieving by BSA deposits. The influence of the pH on the rejection of PEG is tested. Moreover, PEG and BSA were filtered simultaneously to study possible effects of the presence of BSA on the thermodynamic activity of PEG. BSA and PEG are known to mutually influence their thermodynamic

activity as shown by Atha et al. [1981] and Knoll et al. [1983]. The PEG activity increased in the presence of BSA. The decrease in rejection found by Papamichael and Kula suggests that this might influence the rejection of the PEG, as we have shown in chapter 6 for PEG and dextran.

8.2 Materials and methods

Preparation of solutions

The filtration experiments have been performed at two pH values, 7.4 and 4.5. The ionic strength of the solution was chosen equal to 0.15 $kmol.m^{-3}$. For those pH and ionic strength values Vilker [1981] has determined the osmotic pressure of the BSA solution (see chap. 3). The isoelectric point of BSA is pH=4.7 at the ionic strength of 0.15 $kmol·m^{-3}$ [Opong, 1991b].

To obtain a buffer solution with pH=7.4 and an ionic strength of 0.15 $kmol·m^{-3}$ the following quantities were dissolved in water: 5.509 kg/m^3 $Na_2HPO_4·2H_2O$, 1.108 kg/m^3 KH_2PO_4, 2.457 kg/m^3 NaCl. Two types of solutions were used for pH=4.5. The first one was an acetate buffer solution containing 5.675 kg/m^3 CH_3COONa, 3.500 kg/m^3 CH_3COOH and 0.500 kg/m^3 NaCl. Because the seal which separated the two permeate sections was poorly resistent to the acetate buffer, an alternative composition of the solution was chosen. The second solution for pH=4.5 was made by acidification of a 0.15 M NaCl solution with an HCl solution.

PEG3400 (Aldrich) and the protein Bovine Serum Albumine, BSA, (Sigma Chemicals, Fraction V) were used as model solutes. PEG and/or BSA were dissolved in the NaCl solution before HCl was added. No evidence was found that BSA behaved differently for the two types of solutions with an equal pH value of 4.5 and an equal ionic strength of 0.15 $kmol·m^{-3}$. All solutions were protected from bacterial growth by adding 0.5 kg/m^3 NaN_3 and storage at 4 °C.

Procedure

Several phenomena can occur during protein filtration: adsorption on the membrane surface or inside pore, deposition on the membrane surface, compression of the deposition layer, and osmotic pressure of the protein. To characterize the influence of these phenomena on the PEG rejection a procedure analogous to that of Opong [1991] was used. The procedure described below was performed on one single membrane for each pH value:

- The pure water flux and the saline flux were measured as a function of pressure.
- The PEG rejection on the clean membrane was determined as a function of the flux by varying the pressure. The rejection was measured for PEG in an aqueous solution and PEG in the saline solution.
- The membrane was soaked in a BSA solution of the same concentration and pH as the one which was used in the filtration experiments for approximately 24 hours at 4 °C. Afterwards the membrane was carefully rinsed with a saline solution of equal pH. After the membrane was mounted in the cell, the resistance was evaluated to check on possible adsorption by measuring the saline flux at various pressures. Also the PEG rejection was again determined by filtering PEG in the saline solution.
- A BSA solution of 10 kg/m^3 was filtered at a constant pressure of 200 kPa for 160 min. Afterwards the BSA solution was removed from the cell and the cell was rinsed 3 times with at least 200 ml of saline solution of equal pH to be sure no free BSA was left. To check on possible protein deposition and the compressibility of this layer the resistance was evaluated by measuring the saline flux at one or two pressures as a function of time. Immediately afterwards the PEG rejection was measured.
- To conclude this series of experiments the PEG rejection with BSA present in the solution was determined by filtering a PEG/BSA solution at a constant pressure of 200 kPa.

The resistances of the membranes used for the two pH values differed by 40%, which complicates the comparison between the the results at these two pH values. Therefore additional measurements were performed with a shortened procedure on membranes of which the resistance was within 5%. The separate adsorption and deposition of BSA were skipped and immediately after characterizing the clean membrane a PEG/BSA solution was filtered at a range of pressures and a constant bulk concentration. The effect of possible adsorption and deposition was checked <u>after</u> the experiment by the saline flux and the PEG rejection in a saline solution. The filtration of BSA at a constant pressure of 200 kPa was also repeated.

For the concentration analysis of the salt containing samples a Zorbax GF-250 column was used. In that case a saline solution of pH=7.4 of the same composition as described under *Preparation of solutions* was chosen as eluent, because BSA would not elute from the column if water was used. The UV-analysis of the permeate concentration of BSA (at 280 nm) showed that the membranes were fully retentive for BSA. The pH of the permeate remained unchanged throughout the experiment.

The experiments were performed in the stirred cell with two separate permeate streams (for a detailed description: chap. 5). The PEG rejection on a clean membrane was determined by the same method as described in chapter 5. The physical properties of the model components can be found in chapter 3.
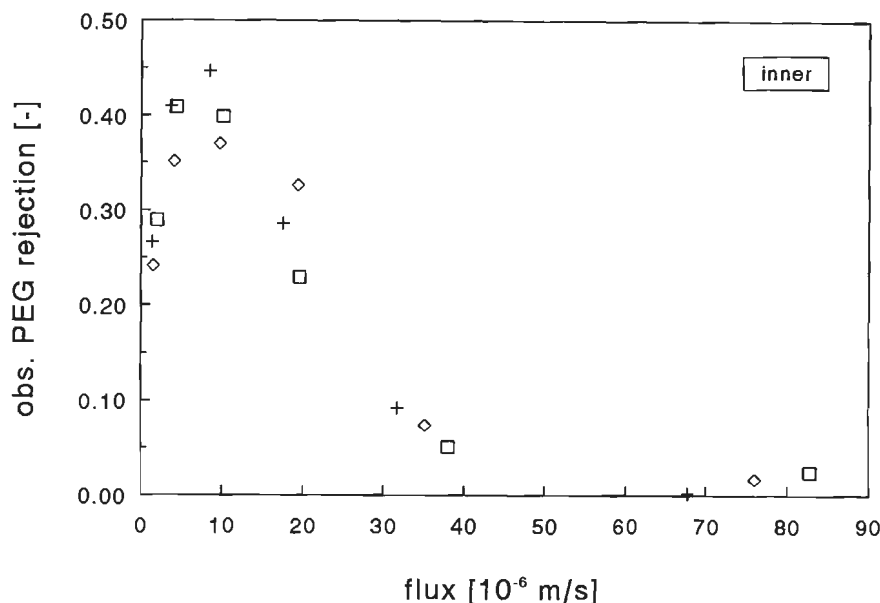
Figure 8.1 *The observed PEG rejection as a function of the flux for three different solvents on a clean membrane. n=270 rpm. Inner section. Solvent: water (□); pH=7.4 (+); pH=4.5 (◇).*

8.3 Influence of the presence of salt on the PEG rejection

Before the PEG rejections were measured in the aqueous and saline solutions the possible influence of the saline solutions on the membrane resistance was determined. The membrane resistance for pH=7.4 and pH=4.5 were equal, although the fluxes are, respectively, 2% and 1% lower than the one determined for pure water, due to the higher viscosities of the saline solutions. This means that the swelling of the membrane remains unaltered by the saline solutions. Moreover, it indicates that the salts are not rejected by the membrane, otherwise the rejected salts would have caused a more pronounced decrease in flux due to their osmotic pressure.

The observed PEG rejections for the aqueous solution and the two saline solutions at a stirrer speed of 270 rpm are depicted in fig. 8.1 for the inner permeate section. The

figure shows that the observed rejections all show the same relationship between rejection and flux. Therefore it is concluded that the PEG rejection is not influenced by the presence of the salts in the saline solutions or the pH value of the solution. The rejection in the outer section showed a comparable picture.

8.4 Influence of BSA adsorption on the PEG rejection

The adsorption of BSA on the membrane was performed with a 10 kg/m^3 BSA solution of the same pH as the solutions used for the subsequent measurements. After the membrane was soaked in the BSA solution the resistance was measured with a saline solution of the same pH. For both pH=7.4 and pH=4.5 the increase in resistance is 2-3%. There is no significant difference in resistance between both pH values. From these measurements it can be concluded that the adsorption of BSA has minimal effect on the resistance of the regenerated cellulose membrane. Sheldon [1991b] measured the combined effect of adsorption and deposition on YM10 membranes and determined an increase in resistance of 4.5% at pH=7.0. The effect of adsorption alone is likely to be less than 4.5%, which suggests a low adsorption on YM membranes. This corresponds to our measurements. Opong et al. [1991b] found an increase in resistance of 18% for a polyethersulphone membrane of the same MW cut-off (30 kDa) and a 30% lower clean membrane resistance compared to the YM30 membrane. According to Matthiasson [1983] the amount of BSA adsorption depends on the membrane material. For the adsorption from a 10 kg/m^3 BSA solution on 20 kDa membranes he found 30-40 mg BSA/m^2 for polysulfone membranes and 0.5 mg BSA/m^2 for cellulose acetate. This indicates that a considerable difference in adsorption can exist between different membrane types. For both the polysulfone and cellulose acetate membranes Matthiason reports an increase in adsorption with decreasing pH value starting from pH=7. Above the isoelectric point only a slight increase is found, below that point the adsorption increases strongly with decreasing pH. The difference in adsorption on our membranes between pH=7.4 and pH=4.5 is probably too low to detect this difference by the saline flux measurements.
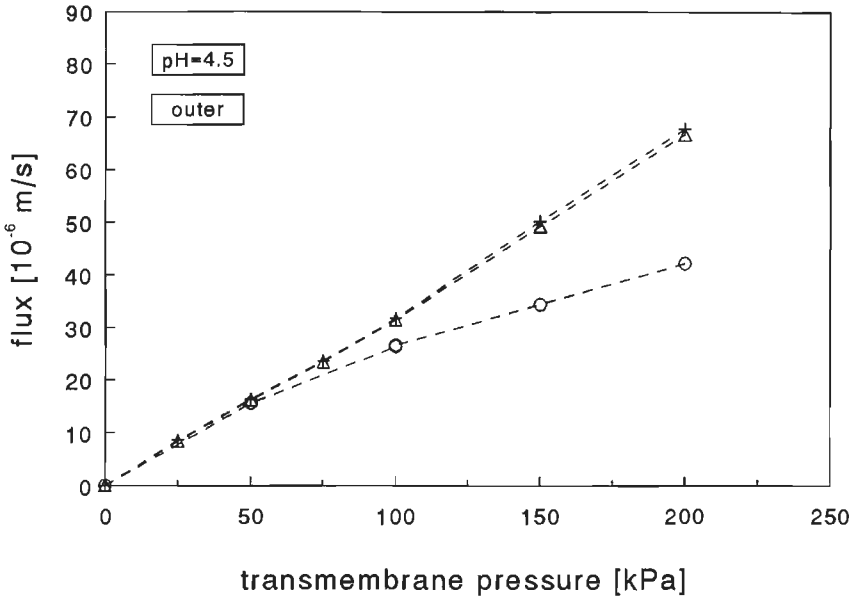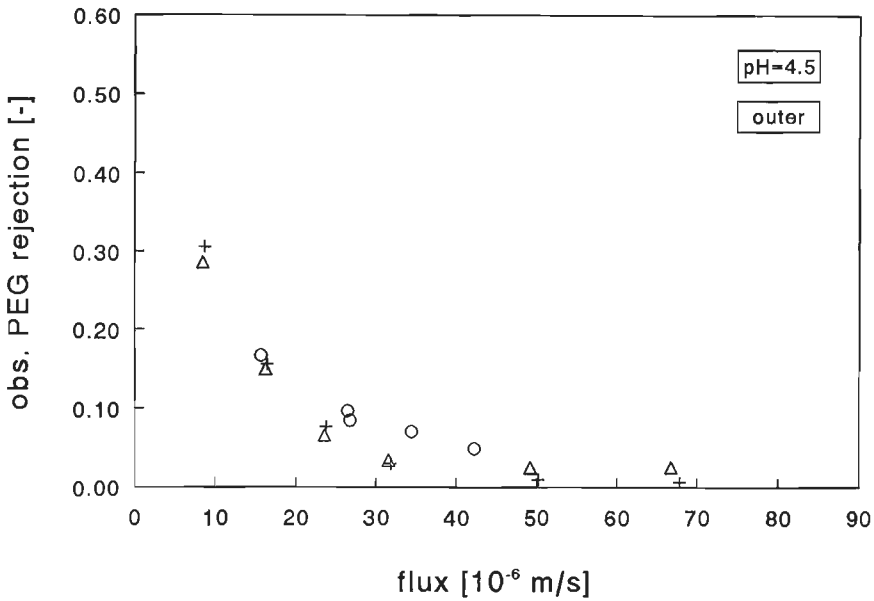
Figure 8.2 *Observed PEG3400 rejection as a function of the flux for a clean membrane (+), a pre-adsorbed membrane (△) and after the filtration of a 10 kg.m⁻³ BSA solution (○). n=90 rpm. pH=4.5. Outer section.*

Figure 8.3 *Flux as a function of the transmembrane pressure for the same experiments.*

To determine whether the influence of the BSA adsorption on the PEG rejection is more pronounced than on the membrane resistance, PEG in saline solutions was filtered through the adsorbed membranes. For both pH values no significant changes in PEG rejection were found for the adsorbed membrane. Also the flux during the PEG filtration was hardly effected by the adsorption. This is illustrated by the figures 8.2 and 8.3 for the pH value of 4.5. The data points labelled after deposition will be discussed later below.

8.5 Filtration of BSA solutions

A 10 kg/m^3 BSA solution was filtered at 200 kPa and a stirrer speed of 90 rpm for both pH=7.4 and pH=4.5. The flux as a function of the logarithm of the bulk concentration is depicted in figures 8.4 and 8.5. For both pH values a linear decrease in flux vs. logarithm of the bulk concentration was observed in the inner and outer permeate sections. The flux in the outer section is in both cases higher than in the inner section, which affirms that a higher mass transfer coefficient promotes a higher flux.

No slow decrease in flux was observed at the start of the experiments, as was the case during Aerosil filtration: the quasi-steady flux was reached immediately comparable to the filtration of dextran (see chap. 4). This indicates that either only a polarization layer is formed or both a polarization layer and a thin high resistant deposit layer are formed. In case only a polarization layer is formed the flux is totally determined by the osmotic pressure. Vilker [1984] measured the osmotic pressure of BSA at pH=7.4 and 4.5 (see chap. 3). As is shown in fig. 3.3 the osmotic pressure at pH=7.4 is considerably higher than at pH=4.5. In figures 8.4 and 8.5 the model curves are depicted, calculated with the osmotic pressure model and the osmotic virial equation derived by Vilker taking concentration polarization into account. The mass transfer coefficients were determined from the slope of the flux vs. lnC_b according to the method of Wijmans (see chap. 4). The calculated flux for pH=7.4 slightly overestimates the flux, for pH=4.5 the discrepancy between the calculated and experimental fluxes is much larger. According to the osmotic pressure model a linear decrease in flux means that the concentration at the membrane surface hardly changes anymore with increasing bulk concentration. In that case the extrapolation of the flux to zero would give the concentration at the membrane surface at which the osmotic pressure is equal to the applied pressure (200 kPa).
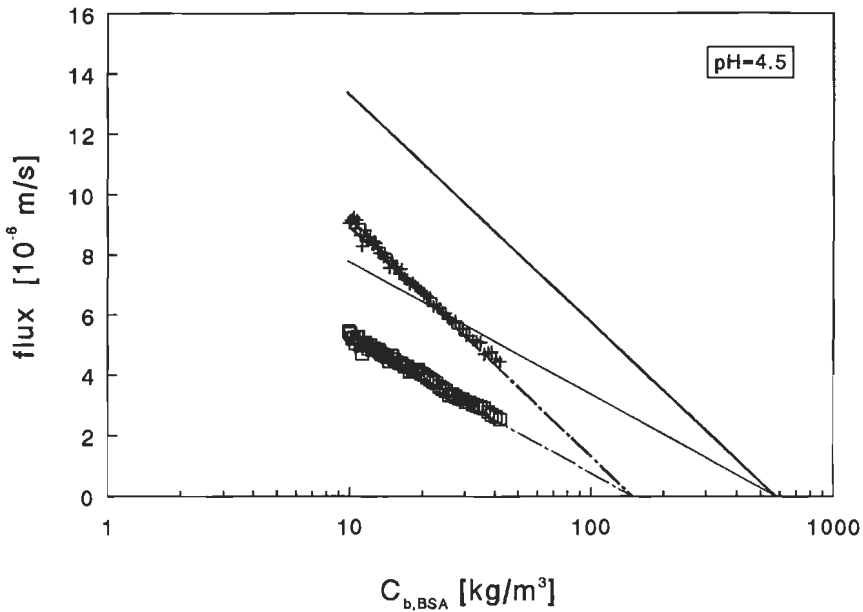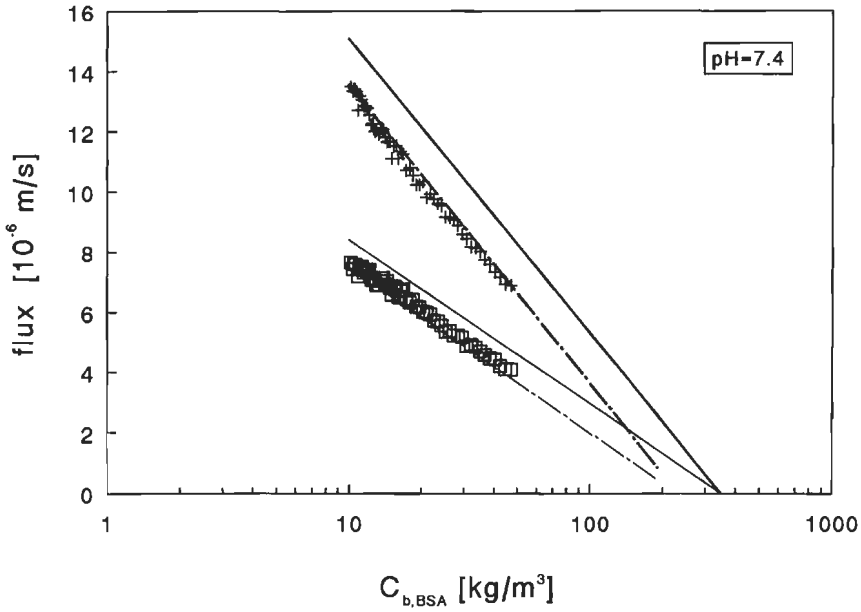
Figure 8.4 *Flux during BSA filtration as a function of the bulk concentration for a clean membrane. n=90 rpm. ΔP=200 kPa. pH=7.4. Inner section: (□), outer section (+). Lines represent the osmotic pressure model (——) and the gel-combination model (—·—·); thin: inner,* thick: *outer.*

Figure 8.5 *Idem for pH=4.5.*

For pH=4.5 the calculated fluxes in fig. 8.4 intersect at a bulk concentration of 584 kg/m^3, where the osmotic pressure is 200 kPa according to the relation of Vilker. Extrapolation of the experimental fluxes suggests that the concentration at which an osmotic pressure of 200 kPa is reached, is equal to the considerably lower value of 150 kg/m^3. The calculated osmotic pressure for 150 kg/m^3 is only 6 kPa. Although we did not measure the osmotic pressure of BSA ourselves but derived it from literature, it seems very doubtful that such a large difference in osmotic pressure could exist for two types of BSA.

Measurements of the saline flux after the filtration of BSA showed that some deposition of BSA had occurred during the filtration of BSA (detailed discussion follows in the next section). Therefore we used the gel-combination model (eqn. (4.7)) to model the fluxes during BSA filtration, which takes both gel layer formation and osmotic pressure into account. In that case it is assumed that the concentration at the membrane surface rises up to the value at which deposition of the protein occurs. The flux is determined by the osmotic pressure corresponding with the concentration at the interface between the deposit layer and the polarization layer and the hydraulic resistance of the deposit layer. The concentration at the interface is derived from the extrapolation of the flux vs. lnC_b plot to zero flux (see above).

As shown in figs. 8.4 and 8.5 the fluxes are described very well by the gel-combination model. This should be expected, of course, because the mass transfer coefficient and the concentration at the interface are derived from the flux vs. lnC_b plot itself. The mass transfer coefficients derived from the plot and those calculated with the Sherwood relation (chap. 3) are depicted in table 8.1. The variation in the mass transfer coefficients from the Sherwood relation reflects the difference in diffusion coefficient due to the change in concentration. Except for the outer section for pH=7.4, the agreement between the mass transfer coefficient determined from the experiment and the Sherwood relation is quite good. The enhanced value of the mass transfer coefficient might be the result of a potential gradient in the polarization layer due to the faster back-diffusion of the co-ions in the polarization layer compared to the protein diffusion [Wesselingh et al., 1993]. The gradient would have the largest value at pH=7.4, because of the higher charge on the protein molecule in comparison to pH=4.5. A simplified calculation to estimate the influence on the mass transfer coefficient has shown that an increase of 15-20% can be expected under our circumstances. This can only explain part of the deviation between the experimental between the experimental mass transfer coefficient and the one determined with the Sherwood

relation.

The concentration at which the protein layer deposits is higher at pH=7.4 than at pH=4.5, 240 kg/m^3 and 150 kg/m^3, respectively. This corresponds with the lower solubility of BSA at pH=4.5 than at pH=7.4. However we were able to dissolve at least 400 kg/m^3 of BSA at pH=7.4. According to the model deposition takes place at a lower concentration. The combined effect of osmotic pressure and deposition in the steady-state of the filtration of BSA has also been modelled by Opong [1991] and Palecek [1993]. They found an excellent agreement between the experimental and modelled fluxes. The resistance of the deposited layer was derived from the saline flux after the BSA filtration. This was combined with membrane resistance to an effective membrane resistance. The osmotic pressure model and the concentration polarization model were solved simultaneously using the effective membrane resistance. This method implies that the concentration at the interface of the deposit layer and polarization layer is independent of the concentration at which the protein deposits. The highest interface concentration they found was about 75 kg/m^3, which is also considerably lower than the solubility limit. This might suggest that the deposit is a different 'phase' with some type of phase equilibrium condition between the concentration in the deposit and that in the solution. It is also possible that the deposit forms by initial depostion of BSA aggregates with the deposited layer formed by the 'reaction' with these 'nucleii'. Occuring to Opong [1991c] this mechanism was valid for microfiltration.

	pH=7.4		pH=4.5	
	k_m inner (μm/s)	k_m outer (μm/s)	k_m inner (μm/s)	k_m outer (μm/s)
flux vs. lnC_b plot	2.4	4.3	1.9	3.3
Sherwood relation	2.1-2.2	3.3-3.4	2.0-2.3	3.1-3.5

Table 8.1 *Comparison between the mass transfer coefficient derived from the experimental flux vs. lnC_b plot and those calculated according to the electrochemically determined Sherwood relation.*

8.6 Influence of BSA deposition on the PEG rejection

The influence of BSA deposition on the PEG rejection will be discussed for the

measurements after the filtration of the PEG/BSA solution using the shortened procedure. The effect of the deposition of BSA was also studied after the BSA filtration in the extensive procedure, but the resistances of the clean membranes used for pH=7.4 and 4.5 differed 40%, which complicates the comparison between the two pH values. The resistance of the membranes used in the shortened procedure was within 5%.

After the filtration of a 10 kg/m^3 solution of both BSA and PEG the membrane was checked on possible protein deposition and its influence on the PEG rejection. According to saline fluxes measured directly after the BSA filtration experiment the membrane resistance has increased in both permeate sections for pH=7.4: 2-5% for the inner section and 3-6% for the outer section. The membrane resistance depended on the pressure and increased with increasing pressure from 25 to 200 kPa. The rise in membrane resistance at pH=4.5 also increased with pressure and was equal to 3-11% for the inner permeate section and 2-7% for the outer section.


From the membrane resistance measurements it can be concluded that at both pH values protein was deposited on the membrane. The dependence of pressure indicated that the deposition layer was compressible. The deposition at pH=4.5 caused the strongest decrease in flux. This is in accordance with the measurements of Opong [1991c], who showed that the saline flux through a BSA deposit formed at pH=7.4 and a ionic strength of 0.15 kmol·m^{-3} is considerably higher than the flux through a deposit formed at pH=4.5 and the same ionic strength. These measurements were performed on a polysulfone membrane. Suki et al. [1984] have measured the amount of BSA deposited on a YM30 membrane from an aqueous solution and reported a higher amount of deposition at pH=4.5 compared to at pH=7.4.

To determine the influence of the deposition on the PEG rejection a PEG solution of the same pH was filtered through the BSA deposit. The PEG rejection as a function of the flux in fig. 8.6a and the fluxes with the corresponding pressures during the PEG filtration in fig. 8.6b are depicted for pH=7.4. Figures 8.7a and 8.7b show the results for pH=4.5. At low fluxes (low pressures) no influence of the BSA deposit was found for both pH values. At high fluxes still no signicant change in PEG rejection was measured for pH=7.4, but a slight increase in observed rejection could be determined for pH=4.5. The flux as a function of pressure provides a clearer evidence of the occurrence of an increase in rejection. At 100 and 200 kPa a strong decrease in flux is measured for pH=4.5 compared to the flux from a PEG solution without the presence

of a BSA deposit. This decrease is stronger than would be expected from the change in membrane resistance due to the presence of the deposit as discussed earlier. The additional lowering of the flux is due to an increase in osmotic pressure as a result of the higher rejection of PEG. The higher rejection of PEG causes a rise in the concentration at the membrane surface and therefore an increase in the osmotic pressure. Calculations with the osmotic pressure model confirm that the fluxes are in the range of what would be expected on basis of the observed rejections. The flux measurements support the augmented PEG rejection at the highest pressures for pH=4.5. Although no significant change in PEG rejection was found for pH=7.4 it seems reasonable to conclude from the flux measurements that at 200 kPa the deposit caused a slight increase in the PEG rejection.

The fact that the difference in PEG rejection with and without a BSA deposit depends on the pressure suggests that the deposit layer is compressed at higher pressures. This is in accordance with the results from the membrane resistance measurements with the saline solutions.

We will now discuss the influence of the pH on the rejection and make a comparison with literature data. Comparing the influence of the deposit for the two pH values it is clear that the deposit at pH=4.5 has a stronger effect on the flux and the PEG rejection. The flux is determined by both the compactness and the thickness of the deposit layer. The rejection, however, is mainly determined by the compactness of the layer. The higher PEG rejection at pH=4.5 compared to that at pH=7.4 indicates that the BSA deposit is expected to be more compact at pH=4.5. Opong et al. [1991b] have measured the resistance of a BSA deposit (deposited at pH=7.0) as a function of pH by filtering saline solutions of various pH values through the deposit. They found a minimum in resistance at the isoelectric point, which means that the BSA deposit has the most open structure for a pH value of 4.7. Mochizuki et al. [1993] showed that dextran was less rejected by BSA deposits at pH=4.7 than by deposits at higher and lower pH. Both investigations indicate that the compactness of the BSA deposit at pH=4.5 is lower than at pH=7.4. This behaviour is exactly the opposite of what would be expected from our rejection measurements. However, recent measurements in the research group of Zydney [1993] have shown that transient effects occur if solutions of different pH values are filtered through the BSA layer which has been deposited at pH=7.0. When a solution of pH=4.7 is filtered through the deposit the permeability shows a quick rise and seems to reach steady-state in a short time.
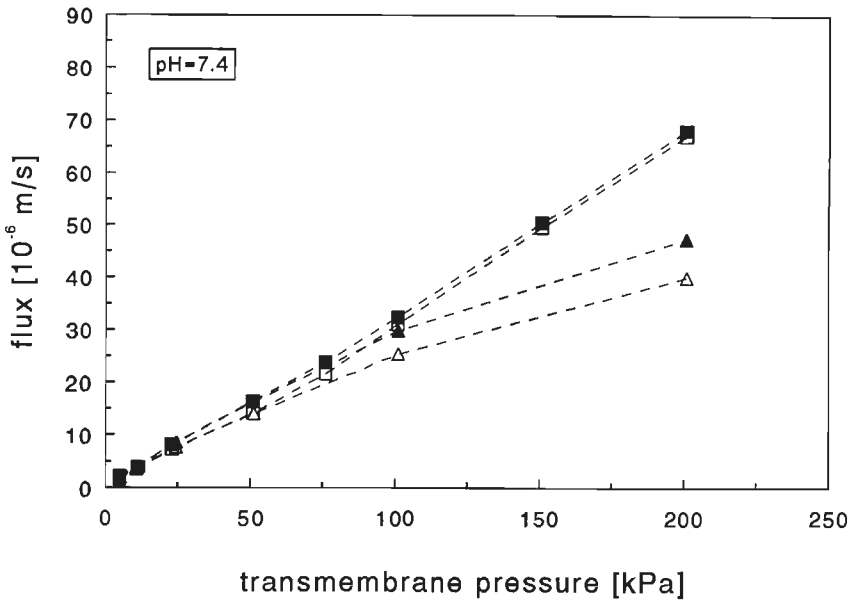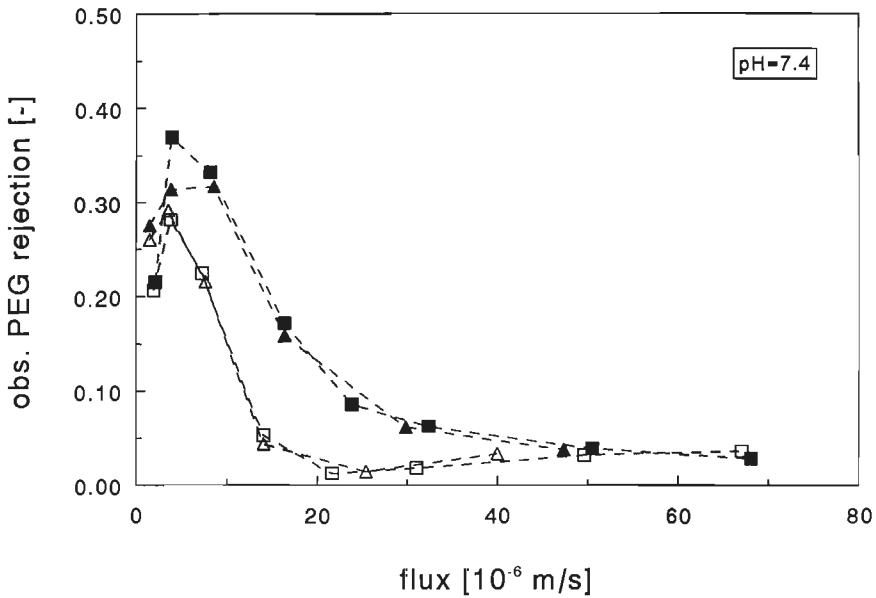
Figure 8.6a *Observed PEG3400 rejection as a function of the flux on a clean membrane* (□) *and after the filtration of a 10 kg.m⁻³ BSA + 10 kg.m⁻³ PEG solution* (△). *n=90 rpm. pH=7.4.* Open symbols: *inner section*; closed symbols: *outer section*.

Figure 8.6b *Flux as a function of the transmembrane pressure for the same experiments.*
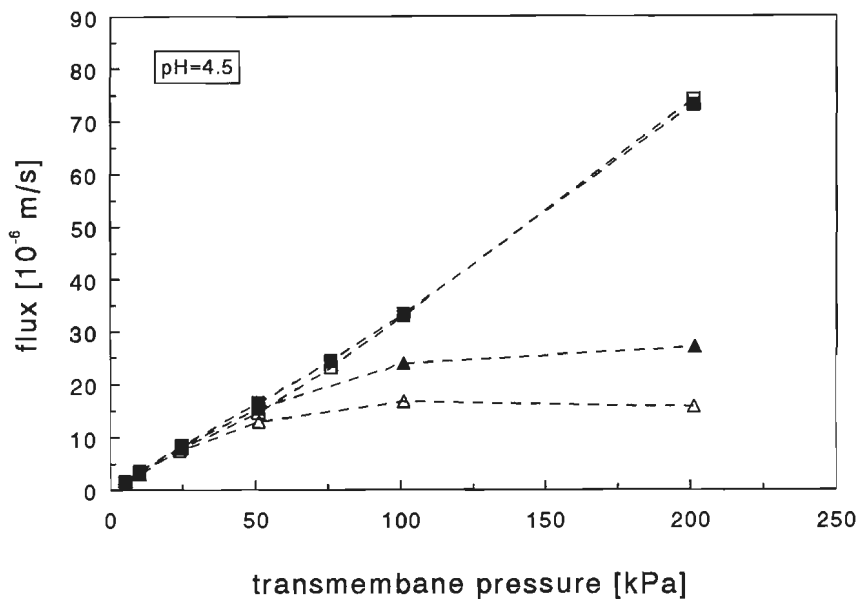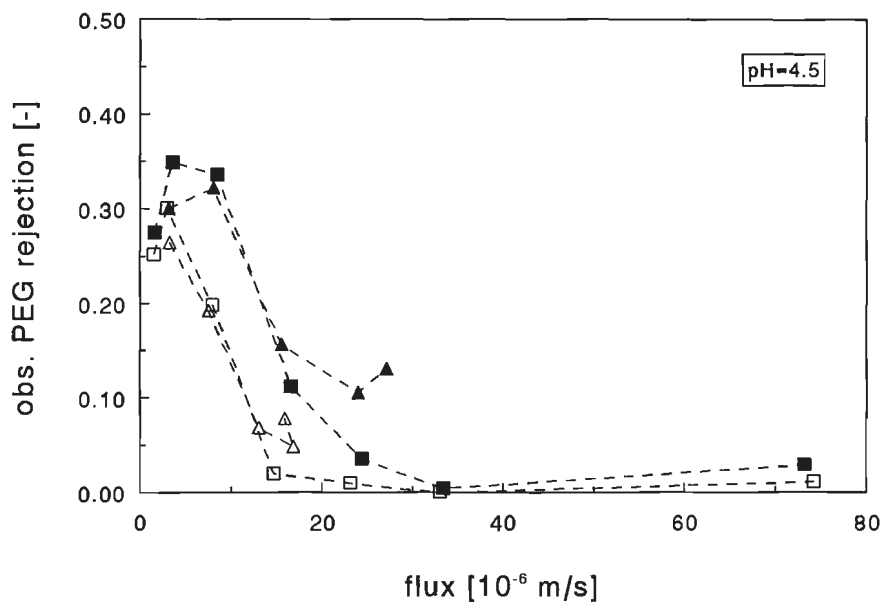
Figure 8.7a *Observed PEG3400 rejection as a function of the flux on a clean membrane* (□) *and* <u>*after*</u> *the filtration of a 10 kg.m^{-3} BSA + 10 kg.m^{-3} PEG solution* (△). *n=90 rpm. pH=4.5.* Open symbols: *inner section*; closed symbols: *outer section*.

Figure 8.7b *Flux as a function of the transmembrane pressure for the same experiments.*

However, measurements over a much longer period (12 hours) showed that eventually the permeability will decrease again and at steady-state a lower permeability is reached compared to the permeability at pH=7.4. The slow transient behaviour is likely to be the result of the slow reorientation of the BSA molecules trapped in the deposit compared to the rapid change of conformation of BSA molecules in bulk solution. The permeability measurements of Opong and the sieving measurements of Mochizuki were performed after filtering a solution of a certain pH value for less than one hour, when steady-state had not yet been reached. Since our rejection measurements have been carried out for the same pH values at which the deposits were actually formed, no transient behaviour due to pH changes was involved. Therefore we measured a more compact layer at pH=4.5 than at pH=7.4 in accordance with the steady-state values found by Zydney. At the isoelectric point (pH=4.7) the BSA molecules have no net charge and are capable of forming more closely packed layers than at higher and lower pH values due to the absence of electrostatic repulsion. Suki et al. [1984] derived a specific hydraulic resistance for BSA deposits as a function of pH from unstirred filtration measurements and indeed found the highest resistance at the isoelectric point, which is in accordance with our rejection measurements. However, the specific resistances should be treated with some caution since they have been derived from the filtration data without accounting for the osmotic pressure at the various pH values. Since the osmotic pressure of BSA is the lowest at the isoelectric point, the specific resistance is likely to be underestimated by a greater extent at the low and high pH values than at the isoelectric point.

8.7 Influence of BSA on the PEG rejection during the filtration of PEG/BSA solutions

To be able to compare the PEG rejection for the two pH values, the PEG/BSA filtration experiments using the shortened procedure are discussed. The figures 8.8a and 8.8b show the PEG rejection with and without the presence of BSA in the solution at pH=7.4 for the inner and outer permeate section, respectively. The results for pH=4.5 are given in figures 8.9a and 8.9b. The corresponding fluxes for the filtration of PEG/BSA are presented in figure 8.10 for both pH values.

Only a minor change in PEG rejection due to the presence of BSA was found at pH=7.4. Initially, no clear trend can be observed in the difference in PEG rejection with and without BSA. However, for pH=4.5 a strong increase in PEG rejection was measured for both the inner and outer permeate sections. The rise in PEG rejection

started from 25 kPa in the inner permeate section and 50 kPa in the outer section. The PEG rejection increased from 0.23 to 0.81 in the inner section and from 0.3 to 0.76 in the outer section. The increase in PEG rejection coincides with the pressure range at which the flux remains constant or even slightly decreases (see fig. 8.10). Returning to the values for pH=7.4 it can be noticed that for the inner permeate section the flux limitation occurs at 100 kPa. At pH=7.4 an increase in PEG rejection was found as well, but less pronounced than at pH=4.5.

Since the rise in PEG rejection occurs at almost equal fluxes, the cause of the increase should be pressure related instead of flux related. The fact that the PEG rejection in the inner and outer permeate sections have similar values, although the fluxes differ more than 50%, also points in the direction that the rise in rejection is pressure related. The sharp change from a gradual increasing flux with pressure to a constant or even a slightly decreasing flux (fig. 8.10) indicates the formation of a BSA deposit on the membrane surface at higher pressures. This is also confirmed by the saline flux and PEG rejection measurements after the PEG/BSA filtration experiments at 200 kPa (see previous section). Since the formation of the BSA deposit and the rise in PEG rejection coincide, the former is likely to cause the latter. The thickness of the BSA deposit grows with increasing pressure. Although the thickness of the deposit has some influence on the rejection by that layer, the rejection of a component is mainly determined by its exclusion and therefore by the compactness of the deposit. This suggests that the compactness of the deposit layer changes with pressure, in other words the deposit is compressible. This explanation is supported by the fact that the differences between the saline flux and PEG rejection measurements before and after the PEG/BSA experiment were the most pronounced at the highest pressures (see previous section). In those experiments only a PEG solution was filtered through the already present BSA deposit, which means that the thickness of the BSA deposit does not increase with higher pressures as in the PEG/BSA filtration. Thus, in that case the stronger effects at higher pressures can only be ascribed to the compressibility of the deposit. Compressibility of BSA deposits has also been reported by Opong [1991b] and Chudacek [1984].
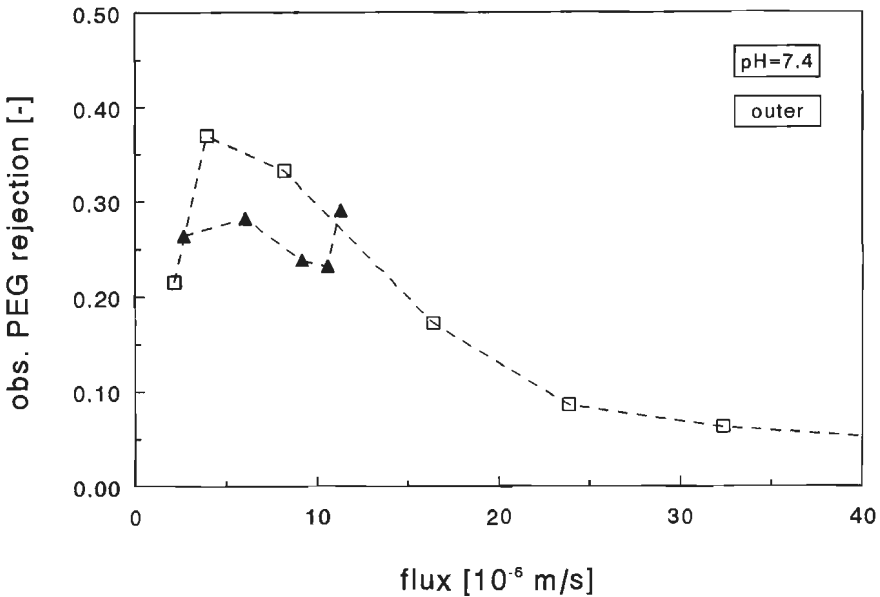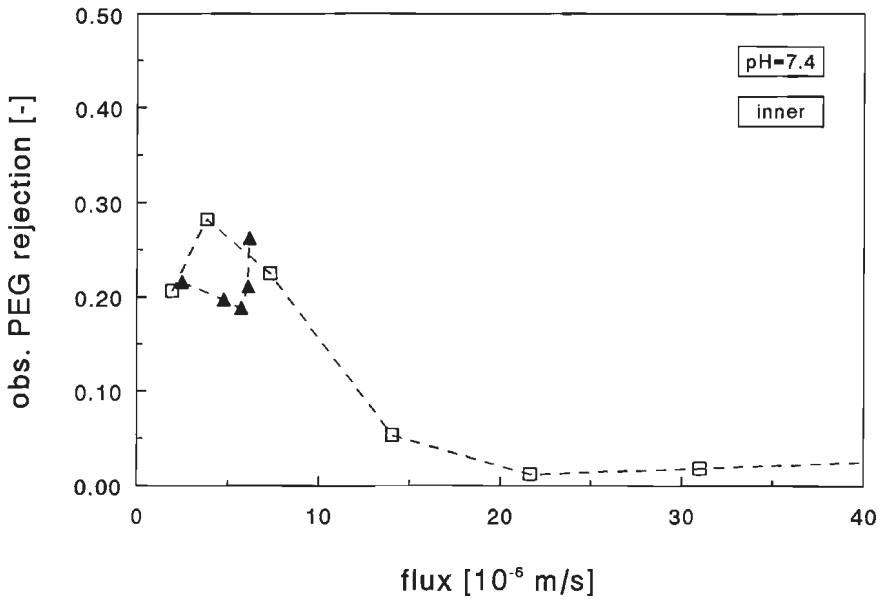
Figure 8.8a *Observed PEG3400 rejection as a function of the flux on a clean membrane* (□) *and* <u>*during*</u> *the filtration of a 10 kg.m^{-3} BSA + 10 kg.m^{-3} PEG solution* (▲). *n=90 rpm. pH=7.4. Inner section.*

Figure 8.8b *Idem for the outer section.*
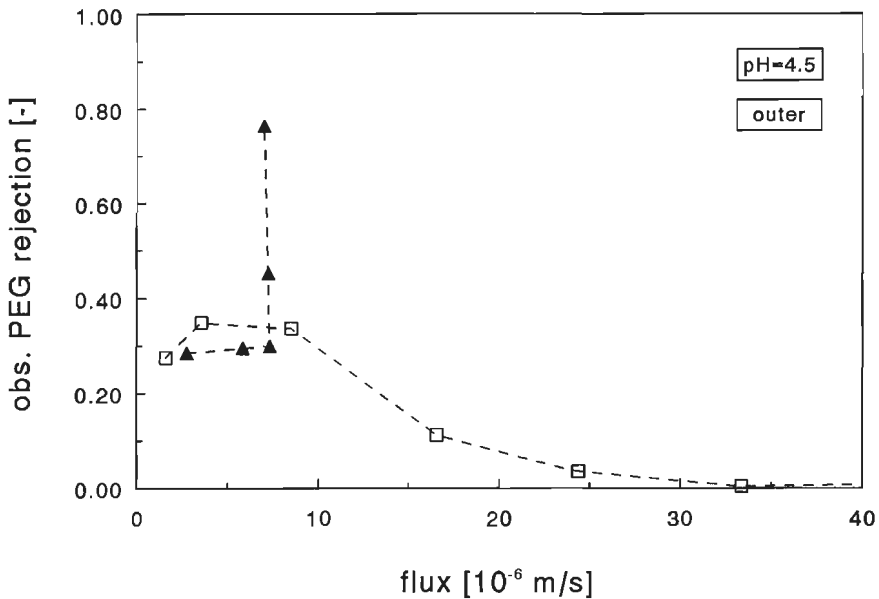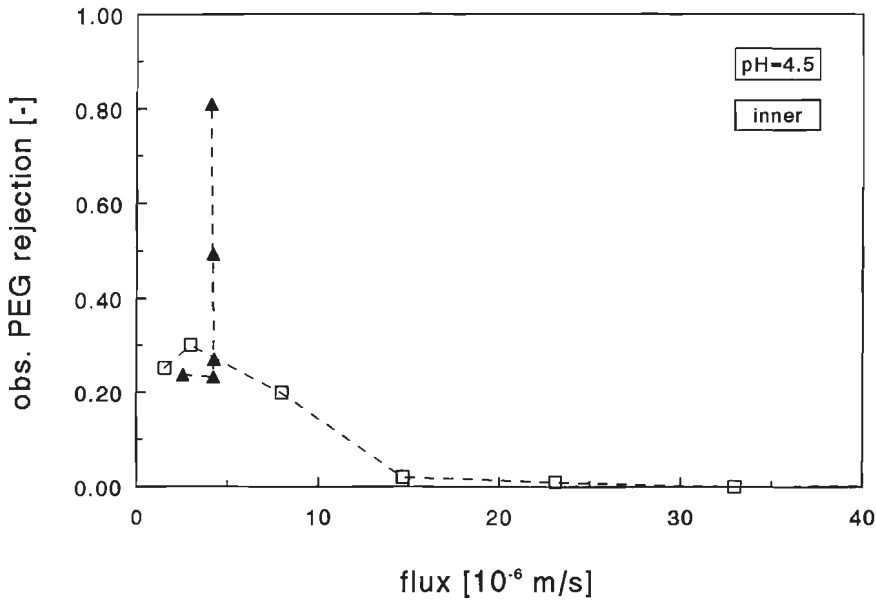
Figure 8.9a *Observed PEG3400 rejection as a function of the flux on a clean membrane (□) and <u>during</u> the filtration of a 10 kg.m⁻³ BSA + 10 kg.m⁻³ PEG solution (▲). n=90 rpm. pH=4.5. Inner section.*

Figure 8.9b *Idem for the outer section.*

Comparing the PEG rejections at pH=4.5 and 7.4 the rejection of PEG is much more strongly affected at pH=4.5. This confirms the results found after deposition and is due to the higher compactness of the deposit layer at pH=4.5 than the one at pH= 7.4. No significant difference in PEG rejection was measured between the PEG/BSA filtration after a BSA layer was deposited in a preceeding BSA filtration and the direct PEG/BSA filtration in the shortened procedure.
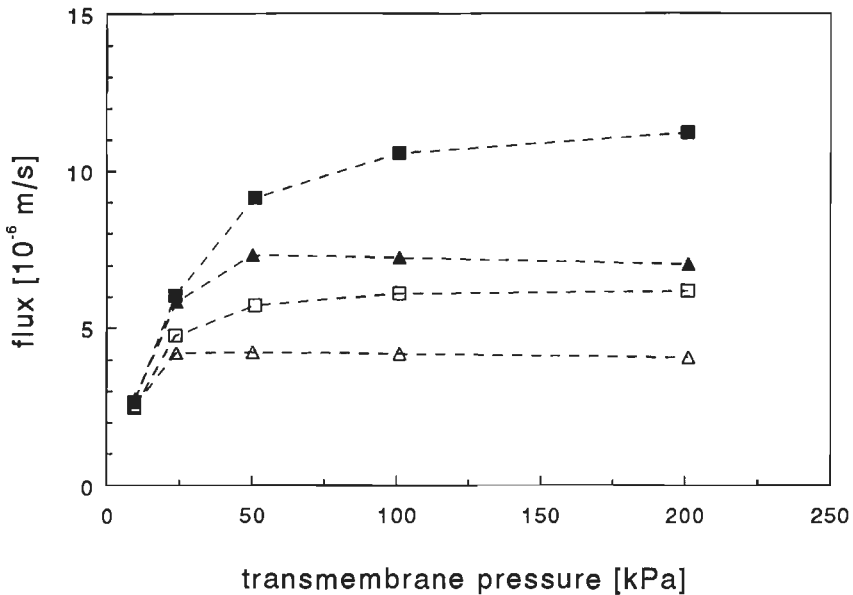
Figure 8.10 *Flux <u>during</u> the filtration of a 10 kg.m^{-3} BSA + 10 kg.m^{-3} PEG3400 solution as a function of the transmembrane pressure for pH=7.4 (□) and pH=4.5 (△). n=90 rpm.* Open symbols: *inner section*; closed symbols: *outer section.*

The fact that the effects on the PEG rejection are more pronounced during the PEG/BSA filtration than when measured for the deposition layer alone after the PEG/BSA filtration could indicate that part of the deposit does not remain on the membrane surface after rinsing. The protein deposit has no strong bonding with the membrane since the membrane resistance recovered its old value after the PEG rejection measurements with the deposit have been performed. This is in contrast with the findings of Opong [1991b] and Mochizuki [1993] who could perform several

experiments with a deposit layer without change of resistance. Sheldon et al. [1991b] examined replicas of BSA fouled membranes after freeze-fracture and deep-etching and found differences in the nature of the protein layer formed on the separating surface of the polysulfone membrane (PM10) and a regenerated cellulose membrane (YM10). The latter is made of the same material as the membranes used for our study. The protein at the YM10 surface had a similar appearance as the BSA molecules in the solution: a more or less globular structure ($4 \times 4 \times 15$nm). On the other hand, the protein molecules on the polysulfone membranes were long and filamentous and seemed to have unfolded due to the hydrophobic nature of the polysulfone membranes. Since the membranes used by Opong and Mochizuki were made of polyethersulphone it is possible that the protein layers on their membranes differed in structure and persistence from the protein layers on our membranes.
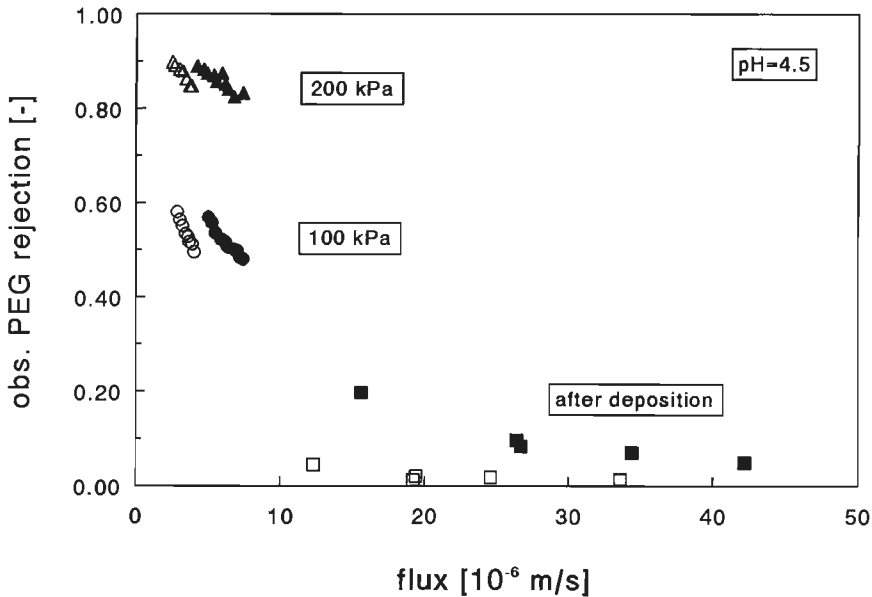
Figure 8.11 *Observed PEG3400 rejection as a function of the flux* <u>*after*</u> *the filtration of a 10 kg.m^{-3} BSA solution (□) and* <u>*during*</u> *the filtration of a 10 kg.m^{-3} BSA + 10 kg.m^{-3} PEG3400 solution at 100 (○) and 200 kPa (△). n=90 rpm. pH=4.5.*
Open symbols: *inner section*; closed symbols: *outer section.*

To study the possible influence of the change in thermodynamic activity of PEG in the presence of BSA on the rejection behaviour, BSA and PEG were filtered at a constant

pressure of 100 and 200 kPa. The BSA concentration was increased from 10 kg/m^3 to 30 kg/m^3.

The observed PEG rejection has been depicted vs. the flux in fig. 8.11 together with the PEG rejections measured after deposition at pH=4.5, but prior to the PEG and BSA filtration. It is not possible to compare the rejections at equal flux, because the PEG rejection after deposition has not been measured at low enough pressures.

However, we have shown in fig. 8.7a for the same type of membrane that the maximum value of the PEG rejection in the presence of a deposit layer is equal to 0.35. Taking this into account it means that the PEG rejection in the presence of BSA is larger than the one without BSA over the whole BSA concentration range. The PEG rejection at 100 kPa is lower than at 200 kPa, confirming the results in figs. 8.9a and 8.9b. The PEG rejection increased with increasing BSA concentration, most likely reflecting the decrease in flux at higher BSA concentrations. No sign of change in rejection behaviour due to thermodynamic interactions have been observed. Further study at higher BSA concentrations and lower fluxes might reveal some influence of the mutual interaction. The thermodynamic activities of PEG and BSA should be modelled to obtain quantitative information on the extent of the interaction.

8.8 Conclusions

The adsorption of BSA on the YM30 membrane prior to filtration has no significant influence on the flux or PEG rejection for PEG3400 solutions at both pH=7.4 and 4.5.

During PEG and BSA filtration no deposit layer is formed for the lowest pressures. The deposit formation at pH=7.4 occurs at higher pressures than the one at pH=4.5. The protein deposits have no irreversible bonding with the membrane, although it takes some time before the value of the flux is restored to that prior to BSA filtration.

Formation of deposit layers during BSA filtration increases the rejection of PEG3400. The rise in rejection from 0.25 to 0.8 is the most pronounced at the highest pressures due to the compressibility of the BSA deposit on the membrane. PEG rejection measurements have shown that the BSA deposits formed at pH=4.5 are more compact than those at pH=7.4. This is probably due to the closer packing of the BSA molecules at pH=4.5 compared to pH=7.4 because of the lower electrostatic repulsions near the isoelectric point.

Under the experimental conditions examined in this study, PEG-BSA interactions do not seem to influence the rejection of PEG.

9. CONCLUSIONS

The filtration behaviour of PEG has been studied on several membranes for two types of membrane modules. The partially rejected PEG showed a maximum in the observed rejection due to concentration polarization. The flux was lowered as a result of osmotic pressure. In most cases an almost linear relationship between the flux and the pressure was observed. At the highest fluxes a more than linear increase in flux was measured, which was ascribed to concentration limitation. Concentration-limitation occurs for partially rejecting membranes if the observed rejection is lowered to zero due to concentration polarization and the actual rejection has reached its plateau value.

The mass transport during ultrafiltration has been modelled by applying the Stefan-Maxwell equations for the transport in both the polarization layer and the membrane. The mass transfer in the polarization layer was based on the stagnant film model. By evaluating the pressure and concentration profiles the flux and the rejection could be simultaneously described.
The Stefan-Maxwell model has been used to simultaneously describe the flux and rejection behaviour during PEG filtration. To obtain a good description the diffusion coefficient of PEG and water with the membrane, the exclusion coefficient and the pre-factor of the Sherwood relation have been fitted to the experimental flux and rejection data. A good fit of both rejection and flux could be achieved for a set of experiments with a particular solute and membrane. A strong correlation was found between the two diffusion coefficients and the exclusion coefficient, which resulted in a physically unrealistic dependence on the membrane and solute properties. The introduction of the thermodynamic activities in the equations had only a minor effect on the calculated flux and rejection.

The mass transfer coefficient for the stirred cell, in which most of the experiments have been performed, has been determined by heat transfer and electrochemical measurements. The local mass transfer coefficient was found to increase with the distance from the centre of the membrane. The influence of the variation of the local mass transfer coefficient on the filtration behaviour has been evaluated by separate collection of the permeate streams from the inner circle of the membrane and the outer ring. Filtration measurements indeed showed a different flux and rejection behaviour

for both sections in accordance with the difference in mass transfer coefficient.

To evaluate the possible formation of a gel layer on the membrane surface during filtration, the unsteady flux behaviour and the response of the flux to a sudden pressure change were studied. From the combined interpretation of these phenomena it was possible to conclude that the filtration of dextran is determined by the osmotic pressure, whereas the decrease in flux during silica filtration is caused by gel formation. Although no unsteady flux behaviour was observed for BSA the response of the flux to a pressure change indicated that at low pressure the flux was determined by the osmotic pressure, while at higher pressures it was also influenced by the formation of a deposit layer.

The effect of changes in the thermodynamic activity on the solute rejection has been studied by the combined filtration of PEG and dextran. The thermodynamic activities of PEG and dextran have been modelled with the UNIQUAC model and the Linearized Quasi-Chemical Approxmation. Rejection measurements showed a decrease in the observed PEG rejection when dextran was added to the solution under conditions where the dextran was mainly retained by the membrane. At high dextran concentrations and low fluxes the PEG rejection even became negative, implying a higher PEG concentration in the permeate than in the bulk solution. This is the result of the additional driving force (besides the pressure difference) for PEG transport through the membrane due to the increased thermodynamic activity of PEG in the presence of dextran. For a more open membrane the PEG rejection was found to increase in the presence of dextran.

The change in solute rejection due to the presence of an open gel layer on the membrane surface has been evaluated using silica sols in combination with PEG or dextran. In the presence of a silica gel layer a decrease in the solute rejection was observed. The thicker the gel layer, the stronger decrease in rejection was found. A thick, open silica gel layer showing no exclusion for the permeating solutes caused the observed solute rejection to drop to zero. By means of a model it was proven that due to the thickness of the gel layer the diffusion back to the bulk solution strongly diminishes, which resulted in a total permeation of the normally partly rejected bulk solution through the membrane.

The solute rejection in the presence of proteins has been studied using PEG and BSA as model solutes. BSA adsorption, by simply soaking the regenerated cellulose membrane in the protein solution, was so low that the solute rejection was not affected. Filtration of BSA caused protein deposition on the membrane surface at higher pressures, which resulted in an increase in the observed PEG rejection. The rejection increased with increasing pressure indicating the compressibility of the deposit layer. Rejection measurements at different pH values showed that the most compact BSA deposit was formed close to the isoelectric point.

General implications

This thesis provides an insight into phenomena which may alter the solute rejection during the ultrafiltration of multicomponent systems in comparison with binary systems. Three major aspects and their influence on the solute rejection have been investigated: the change in thermodynamic activity due to the presence of other components, the presence/formation of an open gel layer on the membrane surface, and the presence of protein in the solution.

The presence of a rejected component, which strongly increases the thermodynamic activity of other permeable components, can promote the transport of these components through the membrane. The effect will be the most pronounced under the conditions where the diffusive flux through the membrane contributes considerably to the flux and the composition of the solution is favourable for a strong increase in thermodynamic activity. Opposite effects in solute rejection can be expected if the thermodynamic activity of a solute is decreased in the presence of other components.

If one of the components in the filtration solution forms an open gel layer on the membrane surface, which shows no exclusion for the solute, the rejection of the solute can be lowered considerably compared to rejection of the solute by the clean membrane. If the gel layer is thick enough to prevent all diffusion of solute from the layer back to the bulk solution, the rejection will become zero and total permeation of the solute will occur. The formation of an open gel layer, although unfavourable due to the loss in flux, can be used advanteously for the simultaneous concentration and purification of a gel forming solute. For purification the rejection of contaminants should be as low as possible. By carefully optimizing the layer thickness, total permeation of the contaminants may be achieved with a minimal loss in flux due to the

presence of a gel layer. In order to retain the solute in the retentate, gel layer formation should be prevented.

Proteins tend to form compact deposit layers on the membrane surface, which increase the rejection of other solutes. To filter at low pressures might prevent protein deposition and lower the compression of the protein deposit, resulting in a smaller increase in the solute rejection. Altering the pH value can influence the formation of the deposition layer and the compactness of the deposit. If it is the objective to retain the lower molecular solutes in the retentate, the compression of the BSA layer at higher pressures can be used in a positive sense to increase the rejection of the solutes.

Summarizing, the introduction of other components in the filtration solution may completely alter the separation behaviour compared to binary systems. The insights gained in this thesis can be used to interpret the rejection behaviour in multicomponent systems. Interesting possibilities exist to use these multicomponent phenomena to improve the separation characteristics.

REFERENCES

Abrams, D.S. and J.M. Prausnitz, *AIChE J., ***1975,** *21*, 116.

Amu, Th. C., The unperturbed molecular dimensions of poly(ethylene oxide) in aqueous solutions from intrinsic viscosity measurements and the evaluation of the theta temperature, *Polymer* **1982,** *23*, 1775.

Anderson, J.L. and J.A. Quinn, Restricted transport in small pores. A model for steric exclusion and hindered particle motion, *Biophys. J.* **1974,** *14*, 130.

Atha, D.H. and K.C. Ingham, Mechanism of precipitation of proteins by polyethylene glycols, *J. Biol. Chem.* **1981,** *256*, 12108.

Balmann, H. de and R. Nobrega, The deformation of dextran molecules. Causes and consequences in ultrafiltration, *J. Membrane Sci.* **1989,** *40*, 311.

Bearman, R.J. and J.G. Kirkwood, Statistical mechanics of transport processes. XI. Equations of transport in multicomponent systems, *J. Chem. Phys.* **1958,** *28*, 136.

Berg, G. van den, Concentration polarization in ultrafiltration, PhD thesis, Twente University of Technology, Enschede, The Netherlands, **1988.**

Bhattacharjee, C. and P.K. Bhattacharya, Prediction of limiting flux in ultrafiltration of kraft black liquor, *J. Membrane Sci.* **1992,** *72*, 137.

Bhattacharjee, S. and P.K. Bhattacharya, Flux decline behaviour with low molecular weight solutes during ultrafiltration in an unstirred batch cell, *J. Membrane Sci.* **1992,** *72*, 149.

Blatt, W.F., A. Dravid, A.S. Michaels and L.M. Nelson, Solute polarization and cake formation in membrane ultrafiltration: causes, consequences and control techniques, in: *Membrane Science and Technology*, ed. J.E. Flinn, Plenum Press, New York, NY, **1970,** 74.

Bozzano, A.G. and C.E. Glatz, Separation of proteins from polyelectrolytes by ultrafiltration, *J. Membrane Sci.* **1991,** *55*, 199.

Bungay, P.M. and H. Brenner, The motion of a closely fitting sphere in a fluid filled tube, *Int. J. Multiph. Flow,* **1973,** *1*, 25.

Busby, T.F. and K.C. Ingham, Separation of macromolecules by ultrafiltration: removal of poly(ethylene glycol) from human albumin, *J. Biochem. Biophys. Methods* **1980,** *2*, 191.

Chudacek, M.W. and A.G. Fane, The dynamics of polarisation in unstirred and stirred ultrafiltration, *J. Membrane Sci.* **1984**, *21*, 145.

Clifton, M.J., *PhD Thesis*, Université Paul Sabatier, Toulouse, France, **1982**.

Colton, C.K. and K.A. Smith, Mass transfer to a rotating fluid. II. Transport from the base of an agitated cylindrical tank, *AIChE J.*, **1972**, *18*, 958.

Connemann, M., Untersuchungen zur Thermodynamik wässriger zweiphasiger Polymersysteme und Bestimmung von Proteinverteilungskoeffizienten in diesen Extraktionssystemen, *Fortschr.-Ber. VDI Reihe 3, nr. 293,* VDI-verlag, Düsseldorf, **1992**.

Cooney, D.O., *Biomedical Engineering Principles: An Introduction to Fluid, Heat and Mass Transport Processes,* Marcel-Dekker, New York, **1976**.

Deen, W.M., Hindered transport of large molecules in liquid-filled pores, *AIChE J.* **1987**, *33*, 1409.

Fane, A.G., C.J.D. Fell and A.G. Waters, Ultrafiltration of protein solutions through permeable membranes. The effect of adsorption and solution environment, *J. Membrane Sci.* **1983a**, *16*, 211.

Fane, A.G. Factors affecting flux and rejection in ultrafiltration, *J. Sep. Proc. Technol.*, **1983b**, *4*, 15.

Fane, A.G., Ultrafiltration of suspensions, *J. Membrane Sci.* **1984**, *20*, 249.

Field, R.W. and P. Aimar, Ideal limiting fluxes in ultrafiltration: comparison of various theoretical relationships, *J. Membrane Sci.* **1993**, *80*, 107.

Flory, P.J., *Principals of polymer chemistry*, Cornell University Press, Ithaca, NY, **1953**.

Fredenslund, A, J. Gmehling and P. Rasmussen, *Vapor-liquid equilibria using UNIFAC*, Elsevier: Amsterdam, **1977**.

Frolov, Yu.G., V.V. Ceskin, N.A. Shabanova, I.A. Donelskii, V.V. Kandaryuk and A.I. Pavlov, Concentration of silica sols by ultrafiltration and properties of polymer membranes, translated from: *Kolloidn. Zh.* **1978**, *40*, 393.

Gekas, V., G. Trägårdh, P. Aimar and V. Sanchez, Diffusive flows in ultrafiltration and their effect on membrane retention properties, *J. Membrane Sci.* **1993**, *80*, 73.

Giddings, J.C., E. Kucera, C.P Russell and M.N. Myers, Statistical theory for the equilibrium distribution of rigid molecules in inert porous networks, *J. Phys. Chem.*

1968, *72,* 4397.

Gill, W.N., D.E. Wiley, C.J.D. Fell and A.G. Fane, Effect of viscosity on concentration polarisation in ultrafiltration, *J. Membrane Sci.* **1988,** *34,* 1563.

Goldsmith, R.L., Macromolecular ultrafiltration with microporous membranes, *Ind. Eng. Chem., Fundam.* **1971,** *10,* 113.

Granath, K.A. and B.E. Kvist, Molecular weight distribution analysis by gel chromatography on Sephadex, *J. Chromatogr.* **1967,** *28,* 69.

Guggenheim, E.A. *Mixtures,* **1952,** Clarendon Press, Oxford.

Happel, J. and H. Brenner, *Low Reynolds Number Hydrodynamics,* **1983,** Nijhoff, The Hague.

Ingham, K.C., T.F. Busby, Y. Sahlestrom and F. Castino, Separation of macromolecules by ultrafiltration: influence of protein adsorption, protein-protein interactions and cocnentration polarization, *Proceedings of the symposium on ultrafiltration membranes and applications,* Washington DC, sept 9-14, ed. A.R. Cooper, **1979.**

Jackson, R., *Transport in porous catalysts,* Elsevier, Amsterdam, **1977.**

Jonsson, G. Boundary layer phenomena during ultrafiltration of dextran and whey protein solutions, *Desalination* **1984,** *51,* 61.

Kang, C.H. and S.I. Sandler, Phase behavior of aqueous two-polymer systems, *Fluid Phase Equilib.* **1987,** *38,* 245.

Kang, C.H. and S.I. Sandler, A thermodynamic model for two-phase aqueous polymer systems, *Biotechnol. Bioeng.* **1988a,** *32,* 1158.

Kang, C.H. and S.I. Sandler, Effects of polydispersivity on the phase behavior of aqueous two-phase polymer systems, *Macromolecules* **1988b,** *21,* 3088.

Kaufmann, T.G. and E.F. Leonard, Mechanism of interfacial mass transfer in membrane transport, *AIChE J..* **1968,** *14,* 421.

Keller, K.H., E.R. Canales and S.I. Yum, Tracer and mutual diffusion coeffients of proteins, *J. Phys. Chem.* **1971,** *75,* 379.

Kerkhof, P.J.A.M. and G.H. Schoutens, Membrane processing of industrial enzymes, in: *Preconcentration and drying of food materials,* ed. S. Bruin, Elsevier, Amsterdam, **1988,** 87.

Killmann, E., *Chem. Ing. Techn.* **1964,** *4*, 36.

Killmann, E., H. Maier, P. Kaniut and N. Gütling, Photon correlation spectrometric measurements of the hydrodynamic layer thicknesses of adsorbed polyethylene oxides on precipitated silica, *Colloids and surfaces*, **1985,** *15*, 261.

Kimura, S., T. Ohtani and A. Watanabe, *ACS Symp. Series* **1985,** *281*, 35.

King, R.S., H.W. Blanch and J.M. Prausnitz, Molecular thermodynamics of aqueous two-phase systems for bioseparations, *AIChE J.* **1988,** *34*, 1585.

Knoll, D. and J. Hermans, Polymer-protein interactions, *J. Biol. Chem.* **1983,** *258*, 5710.

Kozinski, A.A. and E.N. Lightfoot, Ultrafiltration of proteins in stagnation flow, *AIChE J.*. **1971,** *17*, 81.

Kozinski, A.A. and E.N. Lightfoot, Protein ultrafiltration: a general example of boundary layer filtration, *AIChE J.*. **1972,** *18*, 1030.

Krishna, R. and G.L. Standart, A multicomponent film model incorporating a general matrix method of solution to the Maxwell-Stefan equations, *AIChE J.*. **1976,** *22*, 383.

Krishna, R., A unified theory of separation processes based on irreversible thermodynamics, *Chem. Eng. Comm.* **1987a,** *59*, 33.

Krishna, R., A simplified procedure for the solution of the Dusty Gas Model equations for steady-state transport in non-reacting systems, *Chem. Engng. J.*. **1987b,** *35*, 75.

Krishna, R., Problems and pitfalls in the use of the Fick formulation for intraparticle diffusion, *Chem. Engng. Sci.* **1993,** *48*, 845.

Kruif, C.G. de, The rheology of colloidal dispersions in relation to their microstructure, in: *Hydrodynamics of dispersed media*, eds. J.P. Hulin et al, Elsevier, Amsterdam, **1990,** 79.

Lee, J.C. and L.L.Y. Lee, Preferential solvent interactions between proteins and polyethylene glycols, *J. Biol. Chem.* **1981,** *256*, 625.

Lentsch, S., P. Aimar, J. Orozco, Enhanced separation of albumin-poly(ethylene glycol) by combination of ultrafiltration and electrophoresis, *J. Membrane Sci.* **1993,** *80*, 221.

Lightfoot, E.N., *Transport Phenomena and Living Systems*, Wiley & Sons, New York, **1974.**

Linden, J.M. van der, *De diffusie van polyethyleenglycol in water*, PhD thesis, Rijksuniversiteit Leiden, **1973**.

Lonsdale, H.K., The growth of membrane technology, *J. Membrane Sci.* **1982,** *10*, 81.

Madden, W.G., *J. Chem. Phys.* **1990,** *92*, 2055.

Malone, D.M. and J.L. Anderson, Diffusional boundary-layer resistance for membranes with low porosity, *AIChE J.*. **1977,** *23*, 177.

Marangozis, J. and A.I. Johnson, Mass transfer with and without chemical reaction, *Can. J. Chem. Eng.* **1962,** *39*, 231.

Mason, E.A. and L.A. Viehland, Statistical-mechanical theory of membrane transport for multicomponent systems: Passive transport through open membranes, *J. Chem. Phys.* **1978,** *68*, 3562.

Mason, E.A. and L.F. del Castillo, The role of viscous flow in theories of membrane transport, *J. Membrane Sci.* **1985,** *23*, 199.

Mason, E.A. and H.K. Lonsdale, Statistical-mechanical theory of membrane transport, *J. Membrane Sci.* **1990,** *51*, 1.

Matthiasson, E., The role of macromolecular adsorption in fouling of ultrafiltration membranes. *J. Membrane Sci.* **1983,** *16*, 23.

Meireles, M., P. Aimar and V. Sanchez, Effects of protein fouling on the apparent pore size distribution of sieving membranes, *J. Membrane Sci.* **1991,** *56*, 13.

Mitchell, B.D. and W.M. Deen, Effect of concentration on the rejection coefficients of rigid macromolecules in track-etch membranes, *J. Colloid Interface Sci.* **1986,** *113*, 132.

Mochizuki, S. and A.L. Zydney, Effect of protein adsorption on the transport characteristics of asymmetric ultrafiltration membranes, *Biotechnol. Prog.* **1992a,** *8*, 553.

Mochizuki, S. and A.L. Zydney, Dextran transport through asymmetric ultrafiltration membranes: Comparison with hydrodynamic models, *J. Membrane Sci.* **1992b,** *68*, 21.

Mochizuki, S. and A.L. Zydney, Sieving characteristics of albumin deposits formed during microfiltration, *J. Colloid Interface Sci.* **1993a,** *158*, 136.

Mochizuki, S. and A.L. Zydney, Theoretical analysis of pore size distribution effects

on membrane transport, **1993b**.

Nakao, S, S. Yumoto and S. Kimura, *J. Chem. Eng. Jpn.* **1982,** *15,* 463.

Nilsson, J.L., Protein fouling of UF membranes: causes and consequences, *J. Membrane Sci.* **1990,** *52,* 121.

Ogston, A.G. and N. Preston, Macromolecular compression of dextran, *Biochem. J.* **1979,** *183,* 311.

Opong, W.S. and A.L. Zydney, Diffusive and convective protein transport through asymmetric membranes, *AIChE J..* **1991a,** *37,* 1497.

Opong, W.S. and A.L. Zydney, Hydraulic permeability of protein layers deposited during ultrafiltration, *J. Colloid Interface Sci.* **1991b,** *142,* 41.

Opong, W.S., Protein transport and deposition during size-selective membrane filtration, PhD thesis, University of Delaware, Wilmington, USA, **1991c.**

Opong, W.S. and A.L. Zydney, Effect of membrane structure and protein concentration on the osmotic reflection coefficient, *J. Membrane Sci.* **1992,** *72,* 277.

Palecek, S.P., S. Mochizuki and A.L. Zydney, Effect of ionic environment on BSA filtration and the properties of BSA deposits, *Desalination* **1993,** *90,* 147.

Papamichael, N. and M.R. Kula, A hydrodynamic study of the retention of polyethylene glycols by cellulose acetate membranes in the absence and presence of proteins, *J. Membrane Sci.* **1987,** *30,* 259.

Phillies, G.D.J., G.B. Benedek and N.A. Mazer, Diffusion in protein solutions at high concentrations: A study by quasielastic light scattering spectroscopy, *J. Chem. Phys.* **1976,** *65,* 1883.

Press, W.H., B.P. Flannery, S.A. Teukolsky, W.T. Vetterling, *Numerical recipes in Pascal*, Cambridge University, Cambridge, **1983.**

Probstein, R.F., W.F. Leung and Y. Alliance, Determination of diffusivity and gel concentration in macromolecular solutions by ultrafiltration, *J. Phys. Chem.* **1979,** *83,* 1228.

René F. and M. Lalande, Momentum and mass transfer during ultrafiltration of dextran with tubular mineral membranes in turbulent flow regime, *J. Membrane Sci.* **1991,** *56,* 29.

Renkin, E., Filtration, diffusion and molecular sieving through porous cellulose membranes, *J. Gen. Physiol.* **1954,** *38,* 225.

Robertson, B.C. and A.L. Zydney, Stefan-Maxwell analysis of protien transport in porous membranes, *Sep. Sci. Technol.* **1988,** *23,* 1799.

Rosén, Ch. and Ch. Trägårdh, Computer simulations of mass transfer in the concentration boundary layer over ultrafiltration membranes, *J. Membrane Sci.* **1993,** *85,* 139.

Selman, J.R. and C.W. Tobias, Mass transfer measurements by the limiting-current technique, *Adv. Chem. Eng., Vol. 10,* Academic Press, New York, NY, **1978,** 211.

Schmidt, M. and W. Burchard, Moleküleigenschaften in verdünnten Lösungen, in: *Polysaccharide,* ed. W. Burchard, Springer-Verlag, Berlin, **1985,** 154.

Sheldon, J.M., The fine structure of ultrafiltration membranes. I. Clean membranes, *J. Membrane Sci.* **1991a,** *62,* 75.

Sheldon, J.M., The fine structure of ultrafiltration membranes. II. Protein fouled membranes, *J. Membrane Sci.* **1991b,** *62,* 87.

Sieder, E.N. and G.E. Tate, *Ind. Engng. Chem.* **1936,** *28,* 1429.

Smith, K.A., C.K. Colton, E.W. Merrill and L.B. Evans, Convective transport in a batch dialyzer: determination of true membrane permeability from a single measurement, *Chem. Eng. Progr. Symp. Ser.,* **1968,** *64,* 45.

Smith, K.A. and C.K. Colton, Mass transfer to a rotating fluid. II. Transport from a stationary disk to a fluid in Bödewalt flow., *AIChE J.,* **1972,** *18,* 949.

Spiegler, K.S., Diffusion of gases across porous media, *Ind. Eng. Chem., Fundam.* **1966,** *5,* 529.

Stakic, M., S. Milonjic, V. Pavasovic and Z. Ilic, Ultrafiltration of silica sols, *Collect. Czech. Chem. Commun.* **1989,** *54,* 91.

Standart, G.L., R. Taylor and R. Krishna, The Maxwell-Stefan formulation of irreversible thermodynamics for simultaneous heat and mass transfer, *Chem. Eng. Comm.* **1979,** *3,* 277.

Stork Friesland, *New developments in the application of the membrane filtration in the food industry* **1983/1984,** and personal communications.

Strathmann, H., Untersuchungen zur Konzentrationsüberhöhung bei der Membranfiltration. II. Konzentrationsüberhöhung bei der Filtration von makromolekularen Lösungen, *Chemie Ing.-Techn.* **1973,** *45,* 825.

Suki, A.G., A.G. Fane and C.J.D. Fell, Flux decline in protein ultrafiltration, *J.*

Membrane Sci. **1984,** *21*, 269.

Svensson, H., *Acta Chem. Scand.* **1950,** *4*, 399.

Tam, C.M. and A.Y. Tremblay, Membrane pore characterization-comparison between single and multicomponent solute probe techniques, *J. Membrane Sci.* **1991,** *57*, 271.

Thomas, D.K. and A. Charlesby, Viscosity relationship in solutions of polyethylene glycols, *J. Polymer Sci.* **1960,** *42*, 195.

Tremblay, A.Y., Finely porous models and radially averaged friction factors, *J. Appl. Poly. Sci.* **1992,** *45*, 159.

Trettin, D.R. and Doshi, M.R., Pressure independent ultrafiltration - is it gel limited or osmotic pressure limited? in: *Synthetic membranes, A.C.S. Symp. Ser. no. 154, Vol II, American Chemical Society*, ed. A.F. Turbak, Washington, DC, **1981,** 373.

Tsapiuk, E.A., M.T. Bryk, V.M. Kochkodan and E.E. Danilenko, Separation of aqueous solutions of nonionic organic solutes by ultrafiltration, *J. Membrane Sci.* **1990,** *48*, 1.

Vilker, V.L., Colton, C.K. Colton, K.A. Smith and D.L. Green, The osmotic pressure of concentrated protein and lipoprotein solutions and its significance to ultrafiltration, *J. Membrane Sci.* **1984,** *20*, 63.

Waal, M.J. van der, S. Stevanovic and I.G. Rácz, Mass transfer in corrugated-plate membrane modules. II. Ultrafiltration experiments, *J. Membrane Sci.* **1989,** *40*, 261.

Wesselingh, J.A. and R. Krishna, *Mass transfer*, Ellis Horwood, Chichester, **1990**.

Wesselingh, J.A. and P. Vonk, submitted to *J. Membrane Sci.*

Wijmans, J.G., S. Nakao and C.A. Smolders, Flux limitation in ultrafiltration: osmotic pressure model and gel layer model, *J. Membrane Sci.* **1984,** *20*, 115.

Wijmans, J.G., S. Nakao, J.W.A. van den Berg, F.R. Toelstra and C.A. Smolders, Hydrodynamic resistance of concentration polarization boundary layers in ultrafiltration, *J. Membrane Sci.* **1985,** *22*, 117.

Zydney, A.L., Concentration effects on membrane sieving: development of a stagnant film model incorporating the effects of solute-solute interactions, *J. Membrane Sci.* **1992,** *68*, 183.

Zydney, A.L., Personal communication, **1993**.

LIST OF SYMBOLS

a_j	thermodynamic activity component j at reference T and P	[-]
A	pre-factor in mass and heat transfer correlations	
A_j	virial coefficient, j = 1, 2, 3	[Pa.m^{3j}.kg^{-j}]
A_{jk}	interaction parameter between components j and k	[K]
b_{jk}	interaction parameter between components j and k	[K]
B_o	permeability	[m^2]
c_{heat}	specific heat	[J.kg^{-1}.K^{-1}]
c_j	molar concentration component j	[mol.m^{-3}]
c_t	total molar concentration	[mol.m^{-3}]
C	solute/particle concentration	[kg.m^{-3}]
C_0	initial bulk concentration	[kg.m^{-3}]
d	diameter	[m]
d_j	total driving force on component j	[m^{-1}]
D	Fick diffusion coefficient in bulk solution	[m^2.s^{-1}]
$D_{j,k}{}^{sm}$	Stefan-Maxwell diffusion coefficient of j-k pair	[m^2.s^{-1}]
$D_{j,m}$	Stefan-Maxwell "membrane" diffusion coefficient component j (eqn. 2.6)	[m^2.s^{-1}]
D_∞	diffusion coefficient of solute in free solution	[m^2.s^{-1}]
D_1	lumped diffusivity (eqn. 2.54)	[m^2.s^{-1}]
D_2	lumped diffusivity (eqn. 2.55)	[m^2.s^{-1}]
$E_{j,m}$	augmented "membrane" diffusion coefficient of component j	[m^2.s^{-1}]
$E_{j,k}$	augmented diffusion coefficient of pair j-k	[m^2.s^{-1}]
F	Faraday's constant	[C.mol^{-1}]
g_j	total body force per mass of component j	[N.kg^{-1}]
GCM	Gel-Combination Model	
GPM	Gel-Polarization Model	
I_{lim}	limiting current	[A]
K_c	hindrance factor for convection	[-]
K_d	hindrance factor for diffusion	[-]
K_{eq}	equilibrium partition coefficient	[-]
k_m	mass transfer coefficient	[m.s^{-1}]
L	membrane thickness	[m]
m_{PEG}	molality PEG	[mol.(kg solvent)$^{-1}$]
m_j	relative chain length compared to solvent	[-]
M_j	molecular weight	[g.mol^{-1}]
$M_{n,j}$	number-averaged molecular weight	[g.mol^{-1}]

M_{sil}	mass of silica in gel layer	[kg]
n	stirrer speed	[s^{-1}]
n_e	number of electrons	[-]
n_φ	total number lattice sites	[-]
N_j	molar flux with respect to stationary coordinates	[mol.m^{-2}.s^{-1}]
n_{comp}	number of components	
Nu	Nusselt number	[-]
OPM	Osmotic Pressure Model	
p	exponent Reynolds number	[-]
P	pressure	[Pa]
P_{heat}	power submitted by heat elements	[J.s^{-1}]
ΔP	transmembrane pressure	[Pa]
Pe	Peclet number	[-]
Pr	Prandtl number	[-]
PWF	pure water flux	[m.s^{-1}]
q	exponent viscosity correction	[-]
$q_j{}'$	surface area parameter	[mol.g^{-1}]
r_j	total friction force on component j	[m^{-1}]
$r_j{}'$	volume parameter	[mol.g^{-1}]
r_p	radius of cylindrical pore	[m]
R	molar gas constant	[J.mol^{-1}.K^{-1}]
R_a	actual rejection	[-]
$R_{a,\infty}$	filtration reflection coefficient	[-]
R_o	observed rejection	[-]
R_m	membrane resistance	[m^{-1}]
R_g	gel layer resistance	[m^{-1}]
Re	Reynolds number	[-]
S	surface	[m^2]
S_a	actual sieving coefficient	[-]
S_∞	asymptotic sieving coefficient	[-]
Sc	Schmidt number	[-]
Sh	Sherwood number	[-]
t	time	[s]
T	temperature	[K]
u_{circ}	circulation velocity in tubular membrane	[m.s^{-1}]
u_j	specific velocity of component j	[m.s^{-1}]
u_{jk}	interaction energy	[J.mol^{-1}]
v	solution velocity, flux	[m.s^{-1}]

V_j	partial molar volume component j	$[m^3.mol^{-1}]$
V_{fin}	final retentate volume	$[m^3]$
w_j	mass fraction	$[kg.kg^{-1}]$
x_j	mole fraction of component j	$[mol.mol^{-1}]$
z	coordination number in UNIQUAC and LQCA	$[-]$
z	coordinate perpendicular to the membrane surface	$[m]$
Z_j	number of charges on component j	$[-]$

Greek

α	heat transfer coefficient	$[W.m^{-2}.K^{-1}]$
α_j	correction term for connectivity	$[-]$
γ_j	activity coefficient component j based on mole fractions	$[mol.mol^{-1}]$
γ_j^{wt}	activity coefficient component j based on mass fractions	$[kg.kg^{-1}]$
δ	thickness	$[m]$
ε	porosity	$[m^3.m^{-3}]$
η	viscosity of the solution	$[Pa.s]$
$[\eta]$	intrinsic viscosity	$[m^3.kg^{-1}]$
$\theta_j{}'$	surface area fraction	$[m^2.m^{-2}]$
λ	quotient of the solute radius and the pore radius	$[-]$
λ_{therm}	thermal conductivity	$[W.m^{-1}.K^{-1}]$
μ_j	chemical potential	$[J.mol^{-1}]$
ν_j	specific volume component j	$[m^3.kg^{-1}]$
σ	osmotic reflection coefficient	$[-]$
ρ_j	mass concentration component j	$[kg.m^{-3}]$
ρ_{tot}	total density	$[kg.m^{-3}]$
τ	tortuosity	$[-]$
ϕ	solute equilibrium partition coefficient	$[-]$
ϕ_j	volume fraction of component j	$[m^3.m^{-3}]$
$\phi_j{}'$	volume fraction in UNIQUAC	$[m^3.m^{-3}]$
Φ	electrical potential	$[V]$
ω_j	mass fraction of component j	$[kg.kg^{-1}]$

Subscript

| b | bulk |

begin	start of experiment
c	cell
e	external phase
Fick	diffusion coefficient according to Fick's law
g	gel
h	hydraulic
i	inner permeate section
L	interface between membrane and permeate ('), pore entrance (")
m	membrane
o	outer permeate section
par	particle
p	permeate
per	permeate
pol	polarization layer
pore	pore
ret	retentate
s	solute
s	stirrer in combination with diameter d
sp	specific
ss	steady-state
w	water
w	wall in combination with viscosity η:
	-membrane for OPM
	-gel layer surface for GPM
T,P	constant temperature and pressure
0	interface between polarization layer and membrane ('), pore exit (")

Superscript

$'$	homogeneous description inside the membrane (see § 2.21)
$''$	heterogenous description inside the pore (see § 2.21)
d	diffusive
gel	gel layer
m	at membrane surface
p	permeate
v	viscous
*	calculated by the Sherwood relation

CURRICULUM VITAE

De auteur werd op 13 juli 1965 geboren te Eindhoven. In 1983 behaalde ze het Gymnasium-β diploma aan het Van der Putt-lyceum te Eindhoven. Aansluitend studeerde ze Scheikundige Technologie aan de Technische Universiteit te Eindhoven. Het afstudeerwerk op het gebied van continue omkristallisatie werd verricht bij Philips Lighting Maarheeze onder leiding van prof.dr.ir. D. Thoenes van de vakgroep Fysische Technologie. In 1988 slaagde ze cum laude voor het ingenieursexamen. Van 1989 tot 1993 was ze werkzaam als promovendus in de vakgroep Chemische Proceskunde. Het in dit proefschrift beschreven onderzoek werd uitgevoerd in de groep van prof.dr.ir. P.J.A.M. Kerkhof.

Sinds 1 maart 1994 is ze werkzaam bij AKZO Research Laboratories te Arnhem.

Stellingen behorende bij het proefschrift van C.W. van Oers

1. Een open gellaag op een membraanoppervlak kan een totale permeatie veroorzaken van een andere stof, die zonder gellaag gedeeltelijk door het membraan zou worden tegengehouden.
    Dit proefschrift; hoofdstuk 7

2. De verhoging van de thermodynamische activiteit van een component door het toevoegen van een tweede component kan het transport door het membraan zodanig bevorderen, dat de concentratie in het filtraat hoger wordt dan in het retentaat.
    Dit proefschrift; hoofdstuk 6

3. De algemene regel, dat het introduceren van Stefan-Maxwell diffusiecoëfficiënten de concentratieafhankelijkheid van de diffusiecoëffiënten vermindert, blijkt minder algemeen dan Wesselingh en Krishna in hun boek voorstellen.
    J.A. Wesselingh and J.R. Krishna, *Mass transfer*, Ellis Horwood, Chichester, **1990**.
    Dit proefschrift, hoofdstuk 5

4. Balakrishnan et al. schrijven de door hen gemeten transmissie van meer dan 100% toe aan een constante electroforetische flux in de polarisatielaag. Het is waarschijnlijker dat deze het gevolg is van een Donnan effect aan het membraanoppervlak.
    M. Balakrishnan, G.P. Agrawal and C.L. Cooney, Study of protein transmission through ultrafiltration membranes, *J. Membrane Sci.*, **1993**, *85*, 111.

5. Door de aanname van een constante wandtemperatuur hebben Andrews en Fonta de temperatuursgradiënten in de continu doorstroomde electroforese cel overschat en daarmee ook de nadelige invloed van de vrije convectie op de scheiding.
    G.F. Andrews and J.-P. Fonta, The engineering of continuous electrophoresis, *Electrophoresis*, **1985**, *6*, 483.

6. Een niet-lineair vaste-stof-deformatie model kan het droge stofgehalte als functie van de druk bij het persen van compressibele, poreuze media nauwkeuriger voorspellen dan het Terzaghi-Voigt model.
    M.P. Shirato, T. Murase, M. Iwata and S. Nakatsuka, The Terzaghi-Voight combined model for constant-pressure consolidation of filter cakes and homogeneous semi-solid materials, *Chem. Engng. Sci.*, **1986**, *41*, 3213.

7. Voor de berekening van de coalescentie tussen een geleidende druppel en een bulkfase wordt ten onrechte geen onderscheid gemaakt tussen de kracht voor de afplatting van de druppel en die voor het leegstromen van de film.

   A.H. Brown and C. Hanson, The effect of oscillating electric fields on the coalescence of liquid drops, *Chem. Engng. Sci.*, **1968**, *23*, 841.

8. Bij het beoordelen van wetenschappelijk onderzoek wordt het predikaat 'moeilijk/onbegrijpelijk' vaak ten onrechte verward met 'goed'.

9. De bereidheid tot het gebruik van modelstoffen bij onderzoek is een graadmeter voor het fundamentele gehalte van het onderzoek binnen een bedrijf.

10. Om de functie van zwangerschapsverlof en/of ouderschapsverlof te waarborgen, zou het opnemen van een dergelijk verlof door een AIO aanleiding moeten zijn tot het verlengen van zijn/haar aanstellingsduur.

11. Zonder flexibele werktijden is het bevorderen van het reizen buiten de spits d.m.v. het extra verhogen van de prijs van de NS-jaarkaarten dé manier om de reiziger in de auto te krijgen.

12. De discussie over de hoogte van de uitkeringen, die met name in tijden van grote werkloosheid wordt gevoerd, zou juist op z'n plaats zijn bij een grote vraag naar arbeidskrachten.

13. De opmerking dat je na je promotie eindelijk 'echt' aan het werk gaat, doet op z'n zachtst gezegd enige afbreuk aan de geleverde inspanning.